Tiered Approach to Detect Nanomaterials in Food and Environmental Matrices

by

Jared Schoepf

A Dissertation Presented in Partial Fulfillment
of the Requirements for the Degree
Doctor of Philosophy

Approved June 2017 for the
Graduate Supervisory Committee:

Paul Westerhoff, Chair
Lenore Dai
Kiril Hristovski
Pierre Herckes
Mary Laura Lind

ARIZONA STATE UNIVERSITY

May 2018

ABSTRACT

Nanomaterials (NMs), implemented into a plethora of consumer products, are a potential new class of pollutants with unknown hazards to the environment. Exposure assessment is necessary for hazard assessment, life cycle analysis, and environmental monitoring. Current nanomaterial detection techniques on complex matrices are expensive and time intensive, requiring weeks of sample preparation and detection by specialized equipment, limiting the feasibility of large-scale monitoring of NMs. A need exists to develop a rapid pre-screening technique to detect, within minutes, nanomaterials in complex matrices. The goal of this dissertation is to develop a tiered process to detect and characterize nanomaterials in consumer products and environmental samples. The approach is accomplished through a two tier rapid screening process to screen likely presence/absence of elements present in common nanomaterials at environmentally relevant concentrations followed by a more intensive three tier characterization process, if nanomaterials are likely to occur. The focus is on SiO_2 and TiO_2 nanomaterials with additional work performed on hydroxyapatite ($Ca_5(PO_4)_3(OH)$). The five step tiered process is as follows: 1) screen for elements in the sample by laser induced breakdown spectroscopy (LIBS) and X-ray fluorescence (XRF), 2) extract nanomaterials from the sample and screen for extracted elements by LIBS and XRF, 3) confirm presence and elemental composition of nanomaterials by transmission electron microscopy paired with energy dispersive X-ray spectroscopy, 4) quantify the elemental composition of the sample by inductively coupled plasma – mass spectrometry, and 5) identify mineral phase of crystalline material by X-ray diffraction. This dissertation found LIBS to be an accurate method to detect Si and Ti in food matrices (tier one approach) with strong

agreement with the product label, detecting Si and Ti in 93% and 89% of the samples labeled as containing each material, respectively. In addition XRF identified Ti, Si, and Ca in 100% of food samples TEM-confirmed to contain Ti, Si, and Ca respectively. As a tier two approach, LIBS on the 0.2 μm filter identified nano silicon in 42% of samples confirmed by TEM to contain nano Si and 67% of TEM-confirmed samples to contain Ti. XRF identified Si, Ti, and Ca loaded on to a 0.1 μm filter and Ti in the surfactant rich phase of CPE of water and water with NOM.

ACKNOWLEDGMENTS

First, I would like to thank my advisor Dr. Paul Westerhoff, for all of his support, mentorship, and guidance throughout my graduate program. His support and guidance has provided myself with immense knowledge, enabling success in my research and professional career. My committee, Dr. Lenore Dai, Dr. Mary Laura Lind, Dr. Kiril Hristovski, and Dr. Pierre Herckes have been crucial in providing guidance and direction. Specifically, I would like to thank Dr. Lenore Dai who was a key advisor in my undergraduate research career, providing the solid foundation to start my graduate program. I thank Dr. Mary Laura Lind for her support and guidance in my undergraduate and graduate course work, facilitating strong core chemical engineering skills. I would like to thank Dr. Kiril Hristovski, and Dr. Pierre Herckes, both providing expert guidance in group meetings and pushing me to achieve exemplar experimentation development and writing skills. Additionally I would like to thank Dr. Scott Shrake for his career guidance, mentorship, and support which have resulted in me obtaining my first appointment. I would like to thank my lab group Kyle Doudrick, Robert Reed, David Hanigan, Yu Yang, James Faust, Heather Stancl, Natalia Fischer, Xiangyu Bi, Yuqiang Bi, Justin Kidd, Natalia Hoogesteign, Onur Apul, Arjunkrishna Venkatesan, Mac Gifford, Anjali Mulchandani, and Heuidae Lee for their motivation and moral support throughout my graduate program. I would like to thank all of my friends, Taylor Barker, Michael Machas, Tim Duarte, Danny Herschel, Lindsay Fleming, Jaime Balesteri, Melina Machas, Amelia Bourke, Joel Stauffer, Sebastian Hussein, Steven Denke, Varendra Silva, Abhishek Dharan, Justin Jordan, Yifei Xu, Patrick Brown, Ben Weinfeld, Kyle McConn,

and Adam Turnock for their support throughout my college career. Finally, I would like to thank my family for their love and support, without them I would not be here today.

The research herein has been funded by the US Environmental Protection Agency through the STAR program (RD83558001) and the National Science Foundation through the Nano-Enabled Water Treatment Technologies Nanosystems Engineering Research Center (EEC-1449500) and CBET 1336542. Assistance from Ian Illuminati and Jeremy Tager from Friends of the Earth and Austin Wilson from As You Sow is appreciated.

TABLE OF CONTENTS

LIST OF TABLES

Table Page

LIST OF FIGURES

Figure Page

Figure Page

Figure Page

CHAPTER 1

INTRODUCTION

The development of manufacturing procedures to engineer and synthesize materials from the bottom up rather than the top down (e.g. grinding, and milling) has created a new class of materials (i.e. nanomaterials). Nanomaterials are characterized by their size (one dimension less than 100 nm) and their high surface area to volume ratio resulting in novel properties such as higher reactivity, refractivity, as well as improved anticaking and pigment properties compared to their bulk micron-sized counterparts [2, 3]. The novel properties have allowed nanotechnology to become a promising opportunity to develop new materials and commercial products [4-6]. Nanomaterials (NMs) have been implemented across a range of industries such as titanium dioxide for water purification and consumer products (e.g. sunscreen and food) [7, 8], silicon dioxide as an anticaking agent in food products [9], silver and copper nanoparticles as antimicrobials (e.g. coated textiles, filters, and food storage) [10, 11], zinc oxide for absorbance of UV for applications such as sunscreen [12], and hydroxyapatite as a calcium source in toothpaste and supplements [13]. However, currently there are no labeling requirements for NMs in any consumer products and no easy method to test for NM presence, absence, or quantity.

Nanomaterial's beneficial characteristics are improving consumer products and industry processes; however, NMs have been identified as a new class of pollutants due to release during product use and disposal [14, 15]. The unknown environmental behavior (e.g. morphology, size, and surface characteristic changes of NMs due to their interaction with plants and animals, exposure to UV sunlight, and heat from burning) of NMs has

raised regulatory and health concerns [15-23]. The National Institute of Environmental Health and Sciences (NIEHS) recognizes the benefit of NMs; however, highlights the problem "little is known about the human and environmental risks". The National Nanotechnology Initiative (NNI) Environmental, Health, and Safety Research Strategy is to "Develop measurement tools to detect and identify engineered nanoscale materials in products and relevant matrices" [24]. The European Food Safety Authority has outlined a framework for essential tests to approve the application of NMs in food products; however, outlines gaps in characterization and detection methods [25]. These gaps exist in part due to the difficulty in detecting NMs in complex matrices (heterogeneous samples with low mass percent nanomaterial content such as consumer products, biological tissues, soils, water, etc.) as they transform from pristine materials (changing size, morphology, and surface characteristics) to materials with new properties through product use and end-of-life phases [26-34].

Current techniques to detect and characterize NMs in complex matrices require extensive pretreatment, fixation of particles, and specialized equipment [32-37]. For example, acid digestion with oxidants and microwave treatment are required prior to inductively coupled plasma – mass spectrometry (ICP-MS) analysis to quantify elemental composition of the bulk sample. Although ICP-MS has the ability to quantify the bulk mass concentration of elements in the part per trillion range, this technique is not nano specific. As emerging techniques, single particle ICP-MS (spICP-MS) and field flow fractionation ICP-MS (FFF-ICP-MS) have been employed to overcome the analytical limitations of conventional ICP-MS for inorganic nanomaterials in liquid solutions, but spICP-MS exhibits minimum detection particle diameter values above 100 nanometers

for SiO_2 and TiO_2 [38] and FFF cannot determine particle morphology (rod, sphere, etc.). Additionally both spICP-MS and FFF-ICP-MS require weeks from point of sample collection to final processed data, each being costly with high technical training requirements. Better nanomaterial characterization may be achieved via electron microscopy techniques such as transmission electron microscopy (TEM) or scanning electron microscopy (SEM) paired with elemental analysis by energy-dispersive X-ray spectroscopy (EDX), but lengthy and expensive sample preparation techniques are required such as dehydration or fixation of small samples [39]. Electron microscopy techniques excel at size and morphology characterization of nanomaterials, but exhibit nanomaterial quantification limitations, especially in heterogeneous matrices [39]. Heterogeneous dispersions of nanomaterials, which are characterized with relatively low percentages of total content, like complex food and environmental matrices, frequently render nanomaterial detection and characterization a time consuming, difficult, and expensive process [26, 40]. Additionally, sample preparation for TEM potentially alters the state (e.g. size, morphology, aggregation, and surface characteristics) of the nanomaterials [41]. Ultimately, challenges determining the presence of NMs rather than nanomaterial artifacts from sample preparation have proven difficult to overcome.

Tiered approaches have been developed for NM hazard assessment in the workplace (e.g. aerosols) and the environment [42, 43] applying decision flowcharts to facilitate action plans if NM exposure to humans or the environment is suspected. Both approaches mention the need for additional toxicity and exposure assessment data. Hazard assessment depends upon the NM toxicity and exposure conditions. Many ecotoxicity studies have investigated risks [44-51]; however, limited exposure

assessments have resulted in the use of acute toxicity assays at unrealistically high NM concentrations. A need exists to obtain real-world exposure levels to aid in toxicology testing and life-cycle assessment.

Dissertation Objectives and Hypotheses

No single analytical technique exists to comprehensively characterize nanomaterials. Complete characterization of a nanomaterial is prohibitively expensive and time intensive resulting in small sample sizes, applications not sufficient for large sample size applications such as NM monitoring. A tiered approach is proposed to comprehensively characterize nanomaterials while reducing the cost of sample analysis through the elimination of samples deemed free of nanomaterials through an inexpensive pre-screening process. The order of each tier is structured to eliminate samples systematically to reduce sample preparation, analysis costs, and time, accomplished by stopping at the tier which identifies the absence of nanomaterials. A sample completing all tiers aims to characterize the nanomaterials based on key characteristics (e.g. concentration, particle size, particle coating, mineral phase, morphology, and aggregation state) used in toxicology testing [52].

The overarching goal of this research is to develop of a tiered nanomaterial detection framework that first rapidly detects nanomaterial presence in complex matrices, followed by the characterization of occurrence, morphology, and elemental composition of NMs in consumer products and environmental samples.

The specific objectives for the tiered approach include:

1. Rapidly (<10 minutes) detect elemental composition of sample (tier 1)

2. Extract nanomaterials from the sample and rapidly detect elemental composition of extracted, nano-sized partition (tier 2)
3. Characterize the nanomaterial size, morphology, aggregation state, surface coating, and elemental composition (tier 3)
4. Quantify elemental composition of the bulk sample using standard methods (tier 4)
5. Identify mineral phase of crystalline nanomaterials (tier 5)

To accomplish the goal and objectives, the framework for a multiple line of evidence based tiered screening approach is developed involving laser induced breakdown spectroscopy (LIBS) and X-ray fluorescence (XRF) to rapidly inform NM occurrence in various matrices with TEM, SEM, ICP-MS, X-ray diffraction (XRD) to characterize size, morphology, crystallinity, surface and coating, quantify bulk elemental composition, and identify phase composition of nanomaterials. The hypotheses of each tier and analytical device are:

1. Portable LIBS and XRF instruments can detect, at concentrations above 50 ppm, specific elements (Ti, Si, and Ca) present in nanomaterials (TiO_2, SiO_2, and hydroxyapatite ($Ca_5(PO_4)_3(OH)$) contained in solid food and water matrices.
2. Physical filtration and cloud point extraction processes separate and concentrate nanomaterials (TiO_2, SiO_2, and hydroxyapatite ($Ca_5(PO_4)_3(OH)$) from the food and water samples and improves by 50X the LIBS and XRF detection limits of Ti, Si, and Ca elements.
3. Artifact-free detection of size, morphology and composition of nanomaterials (TiO_2, SiO_2, and hydroxyapatite ($Ca_5(PO_4)_3(OH)$) in food and water samples can

be achieved through reproducible suspension and centrifugation preparation techniques.

4. A five step tiered analysis scheme can reduce the time and need from presence/absence screening through mineral characterization of TiO2, SiO2 or $Ca_5(PO_4)_3(OH)$ in solid food and liquid water matrices.

Tiered Approach Flow Chart

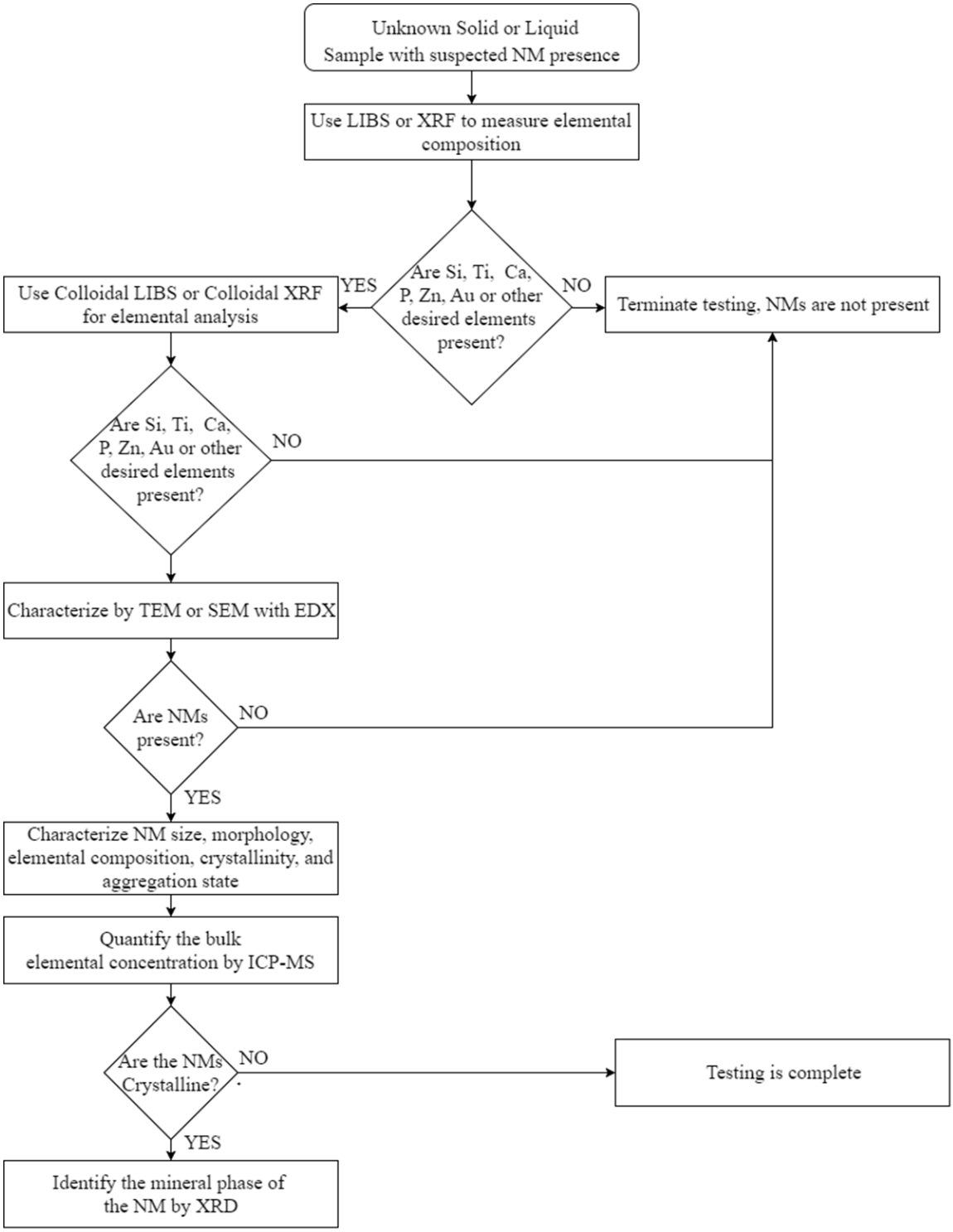

Figure 1.1: Tiered Approach Framework

The tiered analytical approach is comprised of five tiers, eliminating samples if they do not pass a tier due to the absence of desired elements suspected to exist as nanomaterials. An example of not passing a tier is when screening a sample, suspected to contain SiO_2, and finding the absence of Si in the sample. Eliminating samples in tier one or two reduces the number of samples requiring expensive and time intensive TEM, SEM, ICP-MS, and XRD (tiers three, four, and five). A sample containing micron-sized SiO_2 would pass tier one as Si would be detected in the bulk sample; however, would be eliminated at tier 2 as Si would not be detected on the surface of a filter for colloidal-LIBS eliminating the need for TEM, ICP-MS, and XRD. Additionally, if a sample passes tiers one, two, and three; however, TEM identifies amorphous nanomaterials, tier five can be eliminated. Figure 1.1 outlines the tiered approach.

The first tier employs XRF or LIBS to analyze the elemental composition of each sample. Tier one is developed through the analysis of 60+ consumer products (food products, infant formula, and vitamin supplements, products with global distribution and a potential source of NM release into the environment) screening initially for the presence of Si, Ti, Ca, and P. Analysis of infant formulas by TEM (Chapter 3) identified calcium phosphate nanomaterials in food, adding Ca and P elements to the desired list of elements for screening in tier one, resulting in the need and creation of tier five. The hypothesis for tier one is Portable LIBS and XRF instruments can detect, at concentrations above 50 ppm, specific elements (Ti, Si, and Ca) present in nanomaterials (TiO_2, SiO_2, and hydroxyapatite ($Ca_5(PO_4)_3(OH)$) contained in solid food and water matrices.

The goal of detection limits of nanomaterials above 50 µg/g (50 parts per million) in solid and liquid samples is based on a comprehensive review of the toxicity of a variety of nanomaterials [53] where several nanomaterials (e.g. TiO_2, CeO_2, and Al_2O_3) have been found to cause 50% of terrestrial and aquatic species to exhibit sensitivity (e.g. lethal concentration, half maximum effect concentration, median lethal dose, lowest observed effect concentration, no observed effect concentration, and half maximum inhibitory concentration) to the nanomaterials [53]. Additional basis of the 50 µg/g was based on FDA regulations and suspected concentration of nanomaterial in liquid such as stomach fluid after digestion of food. The solid matrix goal was compared to FDA food product label regulation where less than 50 ppm of an ingredient, suspected as a trace or incidental concentration, does not require food product labelling – FDA Code of Regulations 21 CFR 101.100(a)(3)). To calculate the liquid sample goal based on FDA food labelling regulation, a food serving size of 100 grams was used for calculations based on investigation of common food ingredient labels. Using the FDA food labeling regulation of 50 ppm concentration of a material, a serving size of 100 g, and 100 mL as the average volume of a pocket of stomach fluid in large intestine [54], eating 100 g of a food product equates to a liquid concentration of 50 µg of a nanomaterial per L of stomach fluid as the lower limit.

Tier two employs a filtration technique to rapidly determine the presence of nanomaterials through elemental analysis by XRF and LIBS. Filtration and cloud point extraction have been employed as an extraction method to concentrate the nanomaterials and lower detection limits of the analytical instruments. A two stage filtration technique was developed to physically remove large particles (8 µm filter), followed by a 0.1 or 0.2

μm filter to trap colloidal particles on the surface while dissolved organics and ions pass through the filter. The surface of the 0.1 or 0.2 μm filter is analyzed by XRF and LIBS to identify elements present on the filter. Cloud point extraction (CPE), an extraction technique, employs the use of a surfactant solution to separate into an immiscible surfactant-rich and surfactant free phase [55]. At particular temperatures, the surfactant assembles into micelles, which interact and concentrates analytes into a surfactant-rich phase. Centrifugation is used to separate the phases, concentrating the analytes [56]. The detection and confirmation of desired elements on the filter surface, or in the concentrated surfactant phase passes samples to tier three. The hypothesis for tier 2, physical filtration and cloud point extraction processes separate and concentrate nanomaterials (TiO_2, SiO_2, and hydroxyapatite ($Ca_5(PO_4)_3(OH)$) from the food and water samples and improves by 50X the LIBS and XRF detection limits of Ti, Si, and Ca elements, has a detection benchmark of 1 μg/g in solid and liquid samples. The benchmark is based on the threshold where less than 1% of terrestrial and aquatic species exhibit sensitivity (e.g. lethal concentration, half maximum effect concentration, median lethal dose, lowest observed effect concentration, no observed effect concentration, and half maximum inhibitory concentration) to a variety of nanomaterials including titanium dioxide, cerium oxide, aluminum oxide, and zinc oxide [53]. The benchmark is used as a metric of success to validate the tiered approach as a framework for a global nanomaterial monitoring.

Tier three uses electron microscopy to validate the findings in tier one and two, providing confirmation and characterization of the nanomaterials. Transmission electron microscopy characterizes nanomaterials in terms of particle size, morphology,

crystallinity, and elemental composition. Transmission electron microscopy is considered the standard for characterization of nanomaterials; however, TEM only identifies the size and elemental composition of the nanomaterials rather than the quantity in the bulk sample. TEM protocols were developed through analysis of reference nanomaterials (SiO_2 and TiO_2) and food products. TEM and SEM expertise was further developed through the analysis of fresh fruits and produce, infant formula, sunscreen (TiO_2, ZnO, and hydroxyapatite ($Ca_5(PO_4)_3(OH)$), environmental matrices, textiles, fiber optics, chemical mechanical planarization (CMP) slurry, adhesives, and polymer coatings.

Tier four quantifies the bulk elemental composition of the sample to the part per trillion region by ICP-MS. Once TEM confirms nanomaterials are present concurrently with elemental composition, ICP-MS quantifies the bulk concentration of elements present. Initial research used ICP-MS to quantify the concentration of Si and Ti in wastewater effluent (Nogales, AZ). Complicated sample preparation and nanomaterial detection fueled the development for a tiered analytical approach.

Tier five identifies the crystalline phase of the nanomaterial by X-ray diffraction (XRD). If TEM finds crystalline nanoparticles, XRD is employed to identify the mineral phase of the nanomaterial (e.g. crystalline or amorphous SiO_2, rutile or anatase TiO_2, as well as mineral phase of calcium phosphate, calcite, monetite, or hydroxyapatite). XRD provides the final tier to the analytical approach, completing the characterization of nanomaterials in complex matrices.

The tiered approach focuses on food products, infant formula, vitamins, and environmental samples based on their direct human contact and the highest potential for release into the environment. Silicon dioxide (SiO_2) and titanium dioxide (TiO_2)

nanomaterials were selected for the development of the tiered approach as they are the most common nanomaterial additives in food products [8, 54, 57, 58] and are characterized in our previous work [54, 57, 58]. Both SiO_2 and TiO_2 food grade additives are approved for food applications as texturizers and color pigments; however, these additives have been found to contain nano-scale primary particles [59, 60], a cause for environmental and human health concerns [61, 62]. Calcium phosphate nanomaterials, suspected present in powdered infant formulas, were investigated due to concerns raised in the European Union (EU) on nano-needle-shaped hydroxyapatite (HA) in products intended for human use [63]. Calcium is an essential element for all biological organisms, and is widely used in human food supplements. Infant formula is intended to be the sole nutrition source for infants for the first 12 months. Although regulations (e.g. 21 CFR 107.100 in the USA) stipulate the elements required in the infant formula, they lack guidance on the type or size of the compounds used to provide the nutrients.

Once the tiered approach was developed based on food products, the tiered approach was applied to a variety of additional nanomaterials. The nanomaterials (SiO_2, TiO_2, and HA) were analyzed in an organic matrix (natural organic matter in water), and simulated biological fluids (sweat and saliva) to validate the method and develop calibration curves for use in human exposure assessment and a global monitoring program.

Dissertation Roadmap

This dissertation develops the tiered analytical approach using LIBS and XRF on food products, infant formula, supplements, and environmental matrixes to prescreen the presence of elements (e.g. Si, Ti) suspected to be present as nanomaterials (e.g. SiO_2,

TiO_2). Extraction techniques, filtration and cloud point extraction, are applied to concentrate and extract nanomaterials from the bulk. TEM, ICP-MS, and XRD are employed to characterize the nanomaterials in terms of size, morphology, particle elemental composition, bulk sample elemental composition, and mineral phase of extracted nanomaterials. With the projected increased use of nanomaterials, LIBS and XRF can be used to rapidly assess the presence or absence of nanomaterials near real-time, allowing for human exposure assessment and global monitoring of nanomaterials. A rapid technique is essential as a pre-screening tool to reduce samples sizes for monitoring nanomaterials across various matrices and to determine the exposure to humans in consumer products and manufacturing facilities. This research has applications in the manufacturing industry, U.S. Food and Drug Administration (FDA), environmental agencies, and academic research facilities to prescreen and characterize NMs in complex matrices.

Overview of Chapters

The overarching goal of this research is the development of a tiered nanoparticle detection framework that first rapidly detects nanomaterial presence in complex matrices, followed by the characterization of occurrence, morphology, and composition. The dissertation is organized into chapters which work toward the fulfillment of the goal to develop a rapid tiered approach to detect nanomaterials. Each chapter builds upon the tiered approach through the additional of analytical instruments and sample preparation methods. The dissertation is organized as follows:

- **Chapter 2** develops the initial tiered approach through the application of LIBS on food products and the use of filtration to concentrate nanomaterials.

- **Chapter 3** consists of characterizing nanomaterials in infant formula by TEM with the key finding of the presence of nano needle-like hydroxyapatite in infant formula. The presence of HA resulted in the need to add XRD to the tiered approach to identify the mineral phase of crystalline nanomaterials.
- **Chapter 4** implements XRF into the tiered approach and outlines a complete analysis of the validity of XRF to quantify elemental composition of food products, vitamin supplements, and infant formula
- **Chapter 5** investigates CPE and filtration to concentrate nanomaterials for detection by XRF. Calibration curves of TiO_2, SiO_2, and HA, are developed in the following matrices: water, water with natural organic matter, simulated saliva, simulated sweat, cotton swab with simulated saliva, cotton swab with simulated sweat.
- **Chapter 6** provides lessons learned from TEM sample preparation and analysis, then summarizes key findings from papers I co-authored by providing TEM imaging capabilities. An extensive Appendix is referenced with TEM images of each product tested, along with other characterization details.
- **Chapter 7** is a synthesis chapter summarizing the key findings of each chapter and merges the conclusions from each individual chapters.
- **Chapter 8** provides final conclusions and recommendations for future research.

CHAPTER 2

Towards Rapid Assessment of Nanomaterial Additives in Foods Using Laser Induced Breakdown Spectroscopy

Jared J. Schoepf[1], Pierre Herckes[2], Kiril Hristovski[3], Paul Westerhoff[4]*

* Corresponding Author: p.westerhoff@asu.edu; 480-965-2885; Arizona State University, School of Sustainable Engineering and the Built Environment, Box 3005, Tempe, AZ 85287

1 - Arizona State University, School for Engineering of Matter, Transport, and Energy, Tempe, AZ 85287

2 - Arizona State University, School of Molecular Sciences, Box 1604, Tempe, AZ 85287

3 - Arizona State University, The Polytechnic School, Box 2180, Mesa, AZ 85212

4 - Arizona State University, School of Sustainable Engineering and the Built Environment, Box 3005, Tempe, AZ 85287

ABSTRACT

Application of Laser Induced Breakdown Spectroscopy (LIBS) as a rapid nanomaterial screening tool was investigated by comparing its performance with conventionally accepted tools for nanomaterial detection, namely transmission electron microscopy (TEM) and inductively coupled plasma - mass spectrometry (ICP-MS). TEM and ICP-MS require hours to days of sample preparation, and the techniques are considered more expensive and require more advanced analytical expertise than LIBS equipment. LIBS, ICP-MS, and TEM were used to detect SiO_2 and TiO_2 in food-grade additives (6 SiO_2 additives and 3 TiO_2 additives) plus 28 food products from the United States of America and Australia. With minimum sample preparation and within a few minutes, LIBS detected silicon or titanium in 92% of foods labeled as containing SiO_2 or TiO_2 additives. Efforts to rapidly differentiate between nano, bulk, or diffusely distributed elements in foods remains an ongoing challenge. A tiered approach using LIBS as an initial rapid screening technique will aid human exposure assessments and demonstrates potential as a technique with applications for swabs, fabrics, biological fluids, and tissues.

2.1 INTRODUCTION

In recent years, silica- and titania-based nanomaterials have found extensive application in food products due to their unique optical and surface area enhancement properties. Silicon dioxide (SiO_2) is added to foods as an anticaking (hygroscopic) agent, for flow control, or to enhance texture [9]. Amorphous nano-SiO_2 is synthesized using either a wet chemical process to form a gel or a pyrolysis process to form a dry fumed powder [64]. Titanium dioxide (TiO_2) is used as a white pigment, anti-caking, or texture additive in food and is most commonly produced by acid treatment of ilmenite ore [64]. Both SiO_2 and TiO_2 food-grade additives are approved for food applications; however, these additives have been found to contain nano-scale primary particles [59, 60]. Many other nanomaterials are currently, or will likely be, used in the food industry [65-70]. Presence of SiO_2, TiO_2, and other nanomaterials in foods, workplaces, humans, and ecosystems has elevated environmental and health concerns among the population [17, 40, 71-76]. As stricter standards for toxicity dose and biological interaction develop, nanoparticle detection becomes more urgent. While SiO_2, TiO_2 and other nanomaterial exposure assessments have been made [60, 74, 77-79], the techniques are severely limited by high costs and lengthy sample preparation times. These limitations impose barriers to scaling detection methods to industrially- and medically-relevant conditions [26-34].

Analytical techniques to detect TiO_2, SiO_2, and other nanomaterials in foods often require extensive sample preparation and/or specialized equipment [32-37]. For example, acid digestion with oxidants and microwave treatment are needed prior to inductively coupled plasma mass spectrometry (ICP-MS). Although ICP-MS has the ability to

quantify the bulk mass concentration of elements sensitive to parts per trillion, this technique is not nano specific. As emerging techniques, single particle ICP-MS (spICP-MS) or field flow fractionation ICP-MS (FFF-ICP-MS) have been overcome the analytical limitations of conventional ICP-MS for inorganic nanomaterials in liquid solutions, but these techniques exhibit minimum detection particle diameter values above 100 nanometers for both SiO_2 and TiO_2 [38]. Better nanomaterial characterization may be achieved via electron microscopy techniques such as transmission electron microscopy (TEM) or scanning electron microscopy (SEM) paired with elemental analysis by energy-dispersive X-ray spectroscopy (EDX), but lengthy and expensive sample preparation techniques are required such as dehydration or fixation of small samples [39]. Electron microscopy techniques excel at size and morphology characterization of nanomaterials, but they exhibit nanomaterial quantification limitations, especially in heterogeneous matrices. The goal of this study is to explore the suitability of a rapid analytical technique, laser induced breakdown spectroscopy (LIBS), as a pre-screening method that requires minimal sample preparation for elements commonly used in nanomaterials (e.g., Si, Ti). LIBS has the potential to be utilized prior to more sophisticated pretreatment or analytical instrumentation (e.g., FFF-ICP-MS, TEM) in a multi-tiered analytical approach.

Portable and lab-based LIBS have been used to detect elements in a wide range of fields including environmental monitoring [80-88], forensics and homeland security [89, 90], planetary and space exploration [91-105], aerosols [85, 106, 107], jewelry and mining [108, 109], and metals and alloy processing or recycling [110-117]. However, to the extent of the authors' knowledge, there are no reports that apply LIBS for

nanoparticle detection in food products. LIBS is an atomic emission technique that uses a laser to create a high temperature (10^4 to 10^7 °C) spark or plasma on a sample, consequently atomizing, exciting, and ionizing several micrograms of the material [80]. Initially, the ablated material breaks down into ionic and atomic species. As the plasma cools, the excited atoms and ions relax to a lower energy state by emitting photons that are characteristic of the elements present in the sample. The atomic emission line is detected by a charge-coupled device (CCD) spectrometer. The wavelength and intensity of each emitted photon allow for a qualitative and semi-quantitative analysis in the low parts per million range [118]. LIBS requires only a few micrograms of sample and minimal sample preparation (e.g., cutting a sample to fit into the sampling chamber, or pellet pressing of powder samples) to determine multi-elemental composition of solids and gases [80]. By using filtration methods to trap particles on a filter, LIBS can identify the composition of micron-scale materials in gas and atmospheric samples, but challenges for analyzing nanomaterial presence still exist [106, 119].

We hypothesize that a portable LIBS system can be used to screen Si- and Ti-based nanomaterials in food with comparable accuracy to ICP-MS. The size and portability of the LIBS instrumentation differentiates it from laboratory-based analytical tools (ICP-MS and TEM), thereby facilitating rapid analysis regardless of location.

Because SiO_2 and TiO_2 are some of the most common nanomaterial additives in food, they were selected for evaluating LIBS as a pre-screening tool in developing a multi-tiered analytical method. Our objective was to detect the presence or absence of nanomaterials at a threshold of 0.005% (50 ppm) in solid and liquid food, which is the threshold where nanomaterials have been found to cause 50% median lethal

concentration to terrestrial and aquatic organisms [120]. To develop our multi-tiered approach, LIBS, ICP-MS, and electron microscopy methodologies were first developed by adding pristine, reference SiO_2 and TiO_2 food-grade materials to common food ingredients (e.g., flour, sugar, baking soda, and salt) at different loading ratios. The methods were developed before analyzing foods procured from the United States of America (USA) and Australia with labels that contained information related to the presence of silica or titania. Several easy sample preparation techniques were applied to food samples prior to LIBS to differentiate nano-scale or colloidal from larger bulk-scale materials. A statistical analysis method was then used to process data from the portable LIBS system.

A four-step, multiple lines of evidence approach was used to screen and verify nanomaterial presence in complex food matrices: 1) screen for Si and/or Ti elemental presence in the sample by LIBS, 2) extract nano-scale from bulk-scale and screen for Si and/or Ti elemental presence in the nano-scale fraction by LIBS, 3) confirm presence of nano-scale objects by TEM, and 4) confirm quantity of target elements (Si and Ti) by ICP-MS. To test the validity of the four-tier process, the most accepted nanomaterial detection method (TEM) was performed first, followed by the new LIBS method. Viability of LIBS is demonstrated by a high degree of positive nanomaterial detection and low level of false negatives and false positives.

2.2 MATERIALS AND METHODS

Simple Food Ingredients

Three food ingredients, flour, sugar, and baking soda (labeled as sample ID numbers S1-S3), were purchased in the USA and labeled as a nanomaterial blank. Food

ingredients were mixed to create a nanomaterial "blank" combined food matrix (S4) containing flour (38 wt/wt %), sugar (61 wt/wt %), and baking soda (1 wt/wt %), a representative ratio of ingredients in common food products. Table 1 contains the complete sample list.

Pristine Food-Grade SiO_2 and TiO_2 Materials

Six pristine (99% pure) SiO_2 samples, identified as food-grade (European Union food code E551), were procured from Chinese vendors and characterized extensively in a previous study [121]. Five samples (S5-S9) were powders, and one sample (S10) was a 1-mm diameter gel bead. Three pristine food-grade (European Union food code E171) TiO_2 powder samples (S11-S13) were procured from USA and Chinese vendors and characterized in a previous study [59]. Table 1 contains the complete sample list.

Food Products

Food products labeled as containing silicon dioxide or titanium dioxide were purchased in 2014 and 2015. Food products purchased in Australia (S14-S27) included candy, powder sauce/gravy mixes, powder flavor mixes, frosting, non-dairy creamer powder, cappuccino powder, and salad dressing. Food products purchased in the USA (S28-S41) included hot chocolate powder mix, corn muffin mix, powder flavor mixes, cappuccino powder, vitamin and probiotic supplement capsules, artificial sweetener, gelatin powder, toothpaste, cake mix, and cereal. Table 2 contains the complete sample list.

LIBS Sample Preparation & Instrumentation

LIBS analysis of solid samples (denoted Bulk-LIBS) required samples to be cut to fit within the 6 cm^2 LIBS sampling chamber. Powder samples were pressed into an 8-mm

diameter by 4-mm thick pellet (Japan Pellet Press) to increase uniformity and consistency of measurements.

Colloidal-LIBS, a method developed to differentiate nano from bulk materials, required solid and powder samples (0.15 g) to be dispersed in water (5 mL) and filtered to separate dissolved from colloidal materials. Gel and solid samples were added to ultrapure water (18.2 MΩ cm, Nanopure Infinity, Barnstead) and shaken for 2 minutes or until well dispersed and then further sonicated (Branson ultrasonic bath - 80 Watts/L) for 30 minutes. Samples (~5 mL) were first filtered using an 8-µm pore sized cellulose paper filter (Whatman 2 - Cellulose Paper Filter) to remove large particulate matter and then filtered using a 0.2 µm nylon filter (Magma Nylon Membrane Filter) to capture nanoparticles or nanoparticle aggregates for analysis [122]. The 0.2-µm filter was air dried at room temperature for 15 minutes before analyzing its surface by LIBS. We hypothesized that passing water samples through 0.2-µm filters could retain enough colloids on the filter surface to reach detectable levels while passing dissolved organic material and inorganic ions through the filter. The concentration of solids in water and the volume of sample filtered were designed to avoid cake filtration on the membrane surfaces.

A portable LIBS system (PortaLIBS2000, Stellarnet) was used with a 25-mJ, 1064-nm, pulsed Nd-YAG laser coupled to a CCD scanner. The configuration is shown in Figure SI.2.1. The instrument produces a digital reading with wavelength spectrum from 190 nm to 800 nm on the x-axis and intensity (counts) on the y-axis. The persistent peaks at 211 nm, 251 nm, and 288 nm indicated the presence of Si, and the persistent peaks at 323 nm and 334 nm indicated the presence of Ti. Samples were analyzed via a

5x replication approach consisting of 5 separate hits of the LIBS laser onto the sample. Elemental analysis was statistically evaluated using the signal to noise ratio (S/N). Assuming a Gaussian distribution, an S/N of 3 represents 3 standard deviations from the background noise, which corresponds to a 99.7% confidence interval that a peak is present.

ICP-MS Sample Preparation & Instrumentation

Solid food samples (~0.25 g) were added to 8 mL concentrated nitric acid (70%) and 2 mL hydrofluoric acid (47-51%) (Ultra-Trace Metal Grade, JT Baker) and microwave digested. During microwave digestion, the temperature was initially increased to 150 °C over 15 minutes, and then increased to 180 °C over another 15 minute period. Once 180 °C was reached, the temperature was kept constant for 20 minutes before cooling the samples to room temperature. To remove hydrofluoric acid from solution after digestion, the digested sample was reacted with 10 mL boric acid (4.5% w/v). The remaining liquid was analyzed for elemental composition by ICP-MS (Thermo Fisher X-Series II). The detection limits of ^{28}Si and ^{47}Ti in food products were 50 ppb (ng/g of food) and 0.75 ppb (ng/g of food), respectively.

TEM and Energy-Dispersive X-ray (EDX) Spectroscopy

Food samples (~0.125 g) were suspended in 40 mL ultrapure water, sonicated for 30 minutes, and then centrifuged at F = 14,000 G for 15 minutes to dissolve and separate organics from particulate matter. The organics-rich supernatant was poured off, leaving a particulate composed pellet at the bottom of the centrifuge tube. The pellet was re-suspended in 20 mL ultrapure water and sonicated for 5 minutes to re-disperse the particles. A 20-µL aliquot of the mixture was pipetted onto a Ted Pella carbon type B,

200 mesh copper TEM grid and allowed to dry overnight prior to TEM/EDX analysis (Philips CM200). Mean particle diameter was measured manually with ImageJ software on 250 particles.

2.3 RESULTS

TEM Characterization of SiO_2 and TiO_2

Figure 2.1 compares TEM images of reference food-grade additives to materials extracted from food product samples and illustrates similarities in size and aggregation state of SiO_2 or TiO_2 particles. Detailed discussion about the reference food-grade SiO_2 and TiO_2 additives is provided in our previous work [57, 121]. The key observation is that the reference TiO_2 food-grade materials and the TiO_2 extracted from food products contained similar TiO_2 size distributions with 20% to 30% of the primary particles exhibiting sizes < 100 nm (nanomaterials) based upon particle number counting. The reference food-grade SiO_2 material contained similar particle size distributions as material extracted from food products with primary SiO_2 particles of 10 to 20 nm in diameter and agglomerates ranging between 1,000 and 1,800 nm. TEM images presented in Figure 2.1 are illustrative of the morphology detected in all of the food samples; TEM images of additional food samples are shown in Figures SI.2.2 and SI.2.3. Table 2.1 summarizes TEM/EDX observations for these blank food ingredients (S1-S4) and reference food-grade additives (S5-S13). The blank food ingredients and combined complex food matrix (S4) did not contain SiO_2 or TiO_2.

Table 2.2 summarizes the size and composition of colloids detected by TEM/EDX in the food product samples (S14-S41). The average primary SiO_2 particle size was between 10 and 33 nm, with all particulate matter present as larger SiO_2 agglomerates. In

contrast, the average TiO_2 particle size was > 100 nm (Table 2.2)—except for S38 (toothpaste) at 37 nm—with all particulate matter present as larger TiO_2 agglomerates. The size distribution of TiO_2 particles in the food samples was consistent with our previously-published data [57], showing ~20% to 40% of the primary TiO_2 particles were < 100 nm in at least one dimension. TEM/EDX analysis of the food products (*n*=28) showed that they contained SiO_2 (*n*=18), TiO_2 (*n*=8), neither (*n*=3), or both (*n*=1). One sample (S15; hard candy) contained both SiO_2 and TiO_2. Neither SiO_2 nor TiO_2 was detected in three food samples (S36, S39, and S40; gelatin powder, cake mix, and cereal, respectively).

The food product ingredient labels contained information on material content, which is also summarized in Table 2.2. Of the 15 samples labeled as containing Si-based ingredients, TEM/EDX confirmed the presence of SiO_2 in 14 products. Overall, 17 samples were identified as containing SiO_2 by TEM/EDX compared with 15 that were labeled as containing Si-based solids. All 9 samples identified as containing TiO_2 by TEM/EDX were also labeled as containing Ti-based solids.

Quantification by ICP-MS of SiO_2 and TiO_2 in Food Products

ICP-MS does not differentiate between ionic, nano, or larger particle forms initially present in the food product. ICP-MS quantified the Si and Ti concentration in each product after digestion. Tables 2.1 and 2.2 summarize Si and Ti concentrations as determined via ICP-MS for blank food ingredients, combined complex food matrix, reference food-grade materials, and digested food products samples. Silicon concentrations ranged from non-detect (<50 ppb) to 189,000 ppm (18.9 wt%), and titanium concentrations ranged from non-detect (<0.75ppb) to 3,000 ppm (0.3 wt%).

Bulk-LIBS Analysis on Pure SiO_2 and TiO_2 Food-grade Additives and Food Products

Figure 2.2 shows LIBS spectra of representative samples for reference food-grade nanomaterials and real food products. Each element has multiple emission peaks. The highest intensity persistent peaks (288 nm for Si and 323 nm for Ti), corresponding with the largest S/N ratios, were chosen for the remainder of the analysis. There was no signal interference from either of the two elements at these wavelengths.

Detection Action Plots (DAPs) were developed for LIBS S/N ratios associated with each pulse analysis of a sample (Figure 2.3). Each pulse takes just a few seconds to obtain, and five replicate analyses from each sample were conducted at different locations on the sample. The stacked bars are greyscale shaded to indicate relative confidence in the emission peak being above the background noise (S/N values of 1, 2, and 3 represent 67%, 95%, and 99.7% confidence intervals, respectively). DAPs were then developed for Si and Ti on all food samples. First, analysis was conducted on solid food samples. Second, food samples were dispersed in water, pre-filtered with an 8-μm pore size filter, and passed through a 0.2-μm filter. The surface of the 0.2-μm filter samples was analyzed by LIBS for Colloidal-LIBS analysis.

As summarized in Table 2.1, all reference food-grade samples (S5-S13) resulted in S/N>3 by LIBS analysis for either Si or Ti. None of the blank food ingredients (S1-S4) had detectable Si or Ti according to the LIBS (Table 2.1). For the blank food ingredients, the DAP (Figure 2.3) illustrates that neither Si nor Ti emission peaks were detected by LIBS. In contrast, Si (S5-S10) or Ti (S11-S13) was detected in the reference food-grade materials with high confidence (S/N>3 for all 5 replicates). The “Bulk-LIBS” column in

Table 2.1 designates DAPs as "+" or "-" based upon presence (+) for an S/N above 3 and absence (-) for an S/N below 3. The high S/N obtained from the control samples demonstrates LIBS' ability to discriminate between food materials containing Si and Ti without any interferences from common bulk food ingredients.

Figure 2.4 presents DAPs for Si detection in Australian foods for solid samples (Bulk-LIBS; top plot) and filtered samples (Colloidal-LIBS; bottom plot). For many solid samples (e.g., S21, S23, and S24 in the top plot), LIBS pulses either detected Si consistently at a high confidence level (S/N>3) in the replicate samples or did not detect Si (e.g., S/N<1) in any replicate samples. Other samples (e.g., S14 and S15 in the top plot) had varying S/N values across the solid sample surface during the five LIBS discrete measurements. Figure 2.5 shows DAPs for Ti on the same Australian food samples as Figure 2.4. Some foods (e.g., S16, S18, S22, and S27 in the top plot) exhibit uniform responses by LIBS with high confidence (S/N>3) that Ti is present in the solid samples. Finally, several samples have consistently low S/N in replicate samples, indicating with high confidence that Ti is absent from these foods. LIBS results from the solid samples are summarized in the "Bulk-LIBS" columns of Table 2.2.

Colloidal-LIBS Analysis on Filters of Water-Dispersed Food Samples

Colloidal-LIBS results are shown in DAP plots in Figures 2.4, 2.5, SI.2.4, and SI.2.5 (lower plot) and can be readily compared against the Bulk-LIBS analysis of the solid samples (upper plot). The detection frequency of Si with S/N>3 was lower in the Colloidal-LIBS mode than direct Bulk-LIBS analysis on the solid food samples. This was consistent for both the Australian foods (Figures 2.4 and 2.5) and USA foods (Figure SI.2.4), with only 33% samples detecting the presence (S/N>3) of Si on the surface of the

0.2-μm filters compared to Bulk-LIBS detecting Si on the solid sample. These samples are indicated by a "+" in the Colloidal-LIBS column of Table 2.2.

The detection of Ti for both the Colloidal-LIBS and LIBS analysis on the Australian solid foods (Figure 2.5) agreed in 58% of samples, but there was less agreement for USA foods (Figure SI.2.5). Again, samples are indicated by a "+" in the Colloidal-LIBS column of Table 2.2 for the positive detection of Ti.

2.4 COMPARISON OF DETECTION METHODS

Data on the 28 food samples indicate the presence of SiO_2 and TiO_2 based upon the food product package label or analysis using TEM, ICP-MS, Bulk-LIBS, and Colloidal-LIBS. TEM detected nano Si in 17 samples and nano Ti in 9 samples. Figure 2.6 compares the TEM results to each method: ICP-MS, Bulk-LIBS, and Colloidal-LIBS. TEM is considered the best—though most costly—method for detecting the presence/absence of nanoparticles in samples. Comparing the food product package label information to TEM, one sample (a toothpaste product, S38) was labeled as containing SiO_2, but TEM did not detect SiO_2, representing a "false positive" for food labeling information. TEM detected SiO_2 in three samples (S15, S24, and S37) not labeled as containing Si-materials, and these would be considered "false negative" for reliance upon food labeling alone. In all cases, any sample labeled as containing Ti-solids also had detectable TiO_2 by TEM/EDX analysis. Thus there were no "false positives" or "false negatives" between TEM/EDX and product labels for Ti-containing solids. Figure 2.6 was developed to compare the agreement and false positive or false negative detection of SiO_2 and TiO_2 for the experimental methods. False positive is defined where TEM did not

detect Si or Ti while the other analytical method did detect presence of Si or Ti, and false negative is the absence of Si or Ti by TEM but presence by the other method.

For all food samples labeled on the package as containing Si materials, ICP-MS detected Si. Silicon was also detected by ICP-MS in three samples where TEM confirmed presence of SiO_2 even though not labeled as containing Si on the food packaging (false negative for the food package label). Only one sample (S15) had confirmed SiO_2 by TEM and LIBS but was not detected by ICP-MS, which was the only false negative by ICP-MS. The S15 sample is a two-layer candy. SiO_2 was detected in the thin, hard, outer candy layer by TEM but not in the inner chewy candy. We believe that silica represents only a small mass of the overall candy product and was likely below the ICP-MS detection limit of 50 ppb (ng/g) for Si. Eight samples had detectable Si by ICP-MS, six of which were not labeled as containing Si-materials and all eight of which did not have TEM-confirmed SiO_2. Therefore, these samples were false nanomaterial positives by ICP-MS. These samples likely had Si-containing chemicals such as calcium silicate rather than SiO_2. Relying upon ICP-MS alone for the presence or absence of nanoparticles would have resulted in 8 out of 24 samples (33%) as “false-positives” results for the presence of nanoparticles, confirming the use of TEM as the gold standard for nanomaterial detection.

For all food samples labeled as containing Ti-materials, Ti was detected by ICP-MS (Table 2.2). Most of these samples contained more than 100 ppm of Ti. Food samples without Ti materials on the label had detectable, but lower Ti concentrations (Table 2.2). Sample S15 contained a low Ti concentration but contained detectable TiO_2 particles by TEM/EDX. This sample was composed of a hard outer layer and softer inner layer. It is

likely that TiO_2 was only present in the outer layer, which resulted in a low Ti concentration of 38 ppm upon acid digestion and ICP-MS analysis. All TiO_2-containing samples fit into two groups as samples with less than 50 ppm Ti (suspected as a trace or incidental concentration not requiring food product labeling per US Food and Drug Administration Code of Regulations 21 CFR 101.100(a)(3)) or samples with 50 to 100 ppm Ti. Overall, relying upon ICP-MS for the presence or absence of nanoparticles (based upon confirmed TEM detection of TiO_2) led to only 1 false positive (S15) if a 100 ppm Ti threshold was applied, but a higher number of false positives if a lower threshold (i.e., any detectable Ti) was used to define a substance as containing nanomaterials.

Comparing LIBS to the package label, LIBS identified silicon in 14 of 15 samples, with the last sample labeled as requiring further analysis due to a signal to noise between 2 and 3 (95% confidence level). LIBS found 4 samples with silicon that were not listed on the label. US food manufactures are not required to label trace or incidental concentration of ingredients according to the US Food and Drug Administration, and Australia Food Standard 1.2.4 does not require labeling of ingredients below 5% that do "not perform a technological function in the final food." The 4 food products were deemed below this limit by the food manufactures and confirmed by ICP-MS. Comparing LIBS to the package label for titanium, LIBS correctly identified titanium in 8 of the 9 samples according to their package label. LIBS was unable to detect titanium in a liquid (salad dressing), which has been proven difficult for LIBS [123]. LIBS found 6 samples with titanium that were not labeled to contain titanium by the food manufacturer. These samples were deemed below the concentration limit by the food manufactures and confirmed by ICP-MS.

Comparing LIBS to ICP-MS data, LIBS identified 17 of 24 samples with silicon. There were 7 samples that LIBS did not find silicon present. The first sample was a liquid sample (salad dressing), and the 6 remaining samples had concentrations between 78 and 6,429 ppm, which were determined to be below the LIBS detection limit. ICP-MS found all 28 food samples to contain titanium. LIBS detected Ti in 13 of the 28 samples. Of the 15 samples where Ti was not detected, one was a liquid (salad dressing), and the other 14 had between 3 and 50 ppm, which were below the LIBS detection limit.

Colloidal-LIBS detected Si in one sample where Bulk-LIBS found none and detected Ti in one sample (the liquid sample) that Bulk-LIBS found none. However, both were confirmed to have Si and Ti, respectively, by TEM. Therefore the absence by Bulk-LIBS was a false negative in both samples.

Colloidal-LIBS concentrates and dries particles on the filter, increasing the detection of small particulate matter and allowing liquids to be analyzed. Colloidal-LIBS detected nano silicon in 7 out of 17 samples confirmed by TEM to contain nano Si. The nano SiO_2 found by TEM averaged less than 50 nm, which may be too small for the 0.2-μm filter to capture efficiently. Additionally, some samples had SiO_2 found by TEM as larger agglomerates that could be retained on the 8-μm pre-filter. LIBS of the 8-μm filters found 4 of the 10 false negative samples having Si present, confirming this hypothesis. Colloidal-LIBS found 1 additional sample with Si that TEM did not detect. LIBS has a wide laser allowing for a larger section of the sample to be analyzed compared to the small electron beam of TEM.

Colloidal-LIBS found 6 out of 9 TEM-confirmed samples to contain nano Ti. Of the 3 samples that Colloidal-LIBS missed (false negatives), the Ti concentrations were

146, 548, and 3,061 ppm. Titania may have passed through the filter or the Ti concentration was below the detection limit of LIBS. Analysis of the 8-μm filter found no Ti, supporting the hypothesis that Ti passed through the filter. Colloidal-LIBS found 2 samples with nano-sized Ti present that TEM did not find. Again, LIBS has a wider laser beam allowing for a 200-μm section of the sample to be analyzed compared to a smaller section with TEM.

In this study, LIBS was an accurate method to detect Si and Ti in food matrices and agreed strongly with the product label, detecting Si and Ti in 93% and 89% of the samples labeled as containing each material, respectively. LIBS also detected Si and Ti in samples that were not marked on the label but were confirmed to have Si and Ti present by ICP-MS. Due to the limited sample preparation and minimal time requirements, LIBS allows for high throughput of samples compared to ICP-MS. Colloidal-LIBS compared to TEM allowed detection of nano Ti. However, additional research is needed for the detection of nano Si. Silicon dioxide may pass through the filter, so using a smaller filter may remove more nano Si and increase the presence and detection of Si on the filter.

The development of Bulk-LIBS and Colloidal-LIBS methodologies allows for a tiered analytical approach (Figure 2.7) using Bulk-LIBS and Colloidal-LIBS as pre-screening techniques followed by standard techniques (TEM and ICP-MS) to fully characterize the sample. Tier one answers the question "What elements are present?" by implementing Bulk-LIBS to identify the presence or absence of elements (e.g., Si or Ti) suspected to be present as nanomaterials (e.g., SiO_2 or TiO_2). Samples without elements suspected to be present as nanomaterials are not further analyzed while samples with suspected elements continue to tier two. Tier two proposes the question "Are colloidal or

nanomaterials present?" Colloidal-LIBS identifies the presence or absence of elements suspected to be present as nanomaterials. If absent of elements suspected to be present as nanomaterials, the sample analysis is complete. If the suspected elements are detected (e.g. Si or Ti), tier three (TEM) is completed for particle sizing, morphology, and composition, and tier four (ICP-MS) is completed for elemental composition of the bulk sample. Through the use of a tiered analytical approach, samples are pre-screened for elemental composition, reducing the number of samples requiring analysis by expensive and time intensive TEM and ICP-MS analysis.

2.5 CONCLUSIONS

LIBS was demonstrated as a feasible technique to determine the presence or absence of silicon, titanium, nano particulates containing silicon, and nano particulates containing titanium in both solid food samples and filtered aqueous samples. Advantages of LIBS are: (a) rapid detection of Si and Ti; (b) rapid detection of Si and Ti containing nanomaterials; and (c) reduced pre-treatment and analysis costs per sample. The present techniques, Bulk-LIBS and Colloidal-LIBS, lends themselves to analysis of additional food matrices as a screening technique for nanomaterials in food products.

Using a tiered approach (Figure 2.7), LIBS can reduce the number of samples that require TEM, resulting in higher sample throughput and lower costs. LIBS DAPs provide an initial screening of elements that could be nanomaterials. This would be a tier one analysis, or first line of evidence that nanomaterials may exist. Colloidal-LIBS would be a second line of evidence that could be quickly performed. If additional evidence is needed, then TEM could be applied. If element-specific concentrations are needed, then ICP-MS could be applied.

Although ICP-MS had the best detection of Si or Ti in the sample, ICP-MS does not provide presence or absence of nanomaterials, rather purely the concentration of Si and Ti in the sample. The silica and titania present may be agglomerates or micrometer-sized particles, and it is difficult to say if nanomaterials are present rather than larger, micrometer-sized particles. While detection limits of ICP-MS are much lower than LIBS, it is difficult to compare "detection limits" of mass concentration from ICP-MS versus TEM. TEM only provides "presence or absence" and perhaps relative abundance. TEM analysis on food samples with very low nanomaterial content can be very time consuming, and it is difficult to prove absence as nanoparticles could be present but below TEM detection capabilities. Single particle ICP-MS currently has minimum size detection limits for Si > 200 nm [38], which is much larger than the primary particles and agglomerates have. This size limit confounds detection issues across multiple dwell times, making them difficult to detect and quantify. Likewise, the Ti minimum size limit for spICP-MS is > 100 nm [38].

With the projected increased use of nanomaterials, a rapid analysis technique is essential to monitoring nanomaterials across various matrices to determine the exposure to humans in consumer products, manufacturing facilities, and the environment. Combining LIBS with the filtration method, the nanomaterial presence in both solid and liquid samples can be determined in near real-time and at lower cost than other elemental analysis techniques. The rapid results when monitoring for presence of nanomaterials allows researchers to develop a strategic analysis plan for further, in-depth analysis and characterization of nanomaterials. A promising application is in real-time health exposure

assessment for industrial workers where saliva and mucus can be dispersed in water and analyzed for a real-time exposure.

2.6 ACKNOWLEDGMENTS

Partial funding was provided from the US Environmental Protection Agency through the STAR program (RD83558001) and the National Science Foundation (CBET 1336542). We gratefully acknowledge the use of the facilities within the LeRoy Eyring Center for Solid State Science at Arizona State University.

Table 2.1. Summary of Measurements for Food Ingredient and Pure Food-grade Additives (* Letters A through E designate samples from different vendors; ND means not detected; "=" means not appropriate; "+" indicates Si or Ti was detected by LIBS or TEM/EDX)

Sample Type and ID	Silica-Based Measurements			Titania-Based Measurements		
	Bulk-LIBS	Colloidal-LIBS	TEM/EDX	Bulk-LIBS	Colloidal-LIBS	TEM/EDX
Food Ingredients						
Flour (S1)	ND	ND	ND	ND	ND	ND
Sugar (S2)	ND	ND	ND	ND	ND	ND
Baking powder (S3)	ND	ND	ND	ND	ND	ND
Combined matrix (S4)	ND	ND	ND	ND	ND	ND
Food-grade Additives*						
E551-A (S5)	+	+	+	-	-	-
E551-B (S6)	+	+	+	-	-	-
E551-C (S7)	+	+	+	-	-	-
E551-D (S8)	+	+	+	-	-	-
E551-E (S9)	+	+	+	-	-	-
SiO2 Gel (S10)	+	+	=	-	-	=
E171-A (S11)	-	-	-	+	+	+
E171-B (S12)	-	-	-	+	+	+
E171-C (S13)	-	-	-	+	+	+

Table 2.2. Summary of Measurements for Manufactured Food Products; ND means not detected; "+" indicates Si or Ti was detected by LIBS; Label* refers to the package product label)

	Silica-Based Measurements					Titania-Based Measurements				
	Label*	Bulk-LIBS	Colloidal-LIBS	TEM/EDX (Avg. Diam., nm)	ICP-MS (μg/g)	Label*	Bulk-LIBS	Colloidal-LIBS	TEM/EDX (Avg. Diam., nm)	ICP-MS (μg/g)
Australian Foods										
S14) Soft Candy	-	-	-	-	-	+	+	-	102	548
S15) Hard Candy	-	+	-	32	-	+	+	+	176	38
S16) Mint Candy	-	-	-	-	-	+	+	+	150	211
S17) Gum	-	-	-	-	150	+	+	+	130	262
S18) Hard Candy	-	-	-	-	78	+	+	+	123	1,044
S19) White Sauce	+	+	-	10	234	-	-	-	-	9
S20) Meat Gravy	+	+	-	15	305	-	-	-	-	5
S21) Taco Seasoning	+	+	+	21	2,697	-	-	-	-	12
S22) Frosting	-	-	-	-	-	+	+	+	148	2,435
S23) Non-dairy Creamer powder	+	+	-	24	944	-	-	-	-	8
S24) Cappuccino powder	-	-	-	15	648	-	+	-	-	9
S25) Chicken Salt	+	+	+	21	2,694	-	-	-	-	14
S26) Caesar Dressing	-	-	-	-	1,584	+	-	+	115	993
S27) Gum	-	+	-	-	4,076	+	+	-	105	3,061
USA Foods										
S28) Hot Chocolate	+	+	-	22	4,535	-	-	-	-	29

Mix										
S29) Corn Muffin Mix	+	+	-	19	4,833	-	-	-	-	40
S30) Taco Seasoning	+	+	+	25	1,328	-	-	-	-	3
S31) Hazelnut Cappuccino	+	+	+	18	5,759	-	-	-	-	28
S32) Vitamin B12 Supplement	+	+	+	20	16,195	-	+	+	-	33
S33) Artificial Sweetener	+	-	+	33	6,429	-	-	-	-	39
S34) Cappuccino	+	+	-	18	8,304	-	+	-	-	31
S35) Vitamin D3 supplement	+	+	-	18	1,576	-	+	-	-	3
S36) Gelatin powder	-	+	-	-	5,421	-	+	+	-	81
S37) Milk Chocolate Cocoa Mix	-	+	-	26	5,154	-	-	-	-	36
S38) Toothpaste	+	+	+	-	189,038	+	+	-	37	146
S39) Cake Mix	-	-	-	-	5,301	-	-	-	-	42
S40) Cereal	-	-	-	-	1,881	-	-	-	-	17
S41) Probiotic	+	+	-	19	16,337	-	-	-	-	50

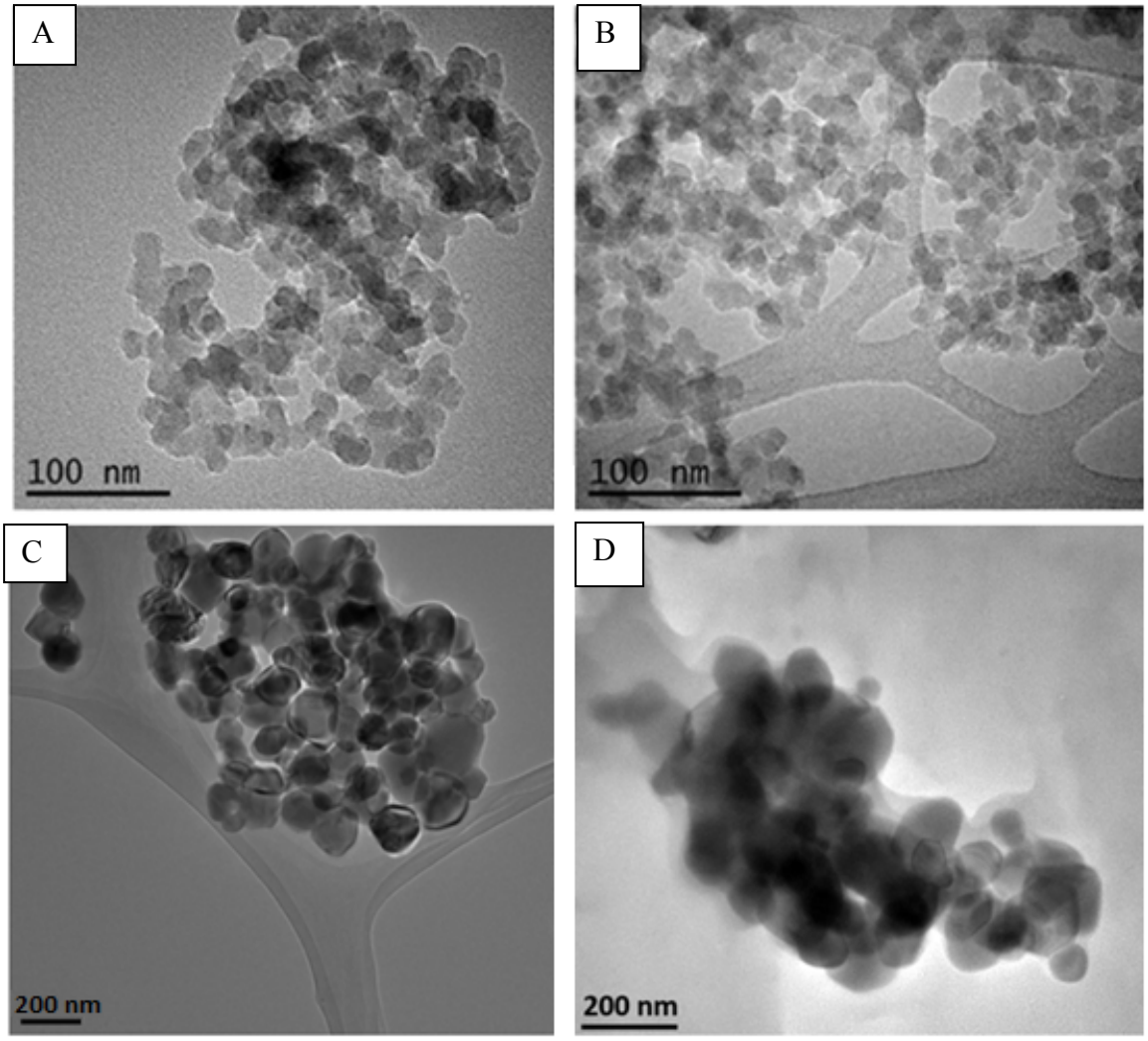

Figure 2.1. TEM images of (A) reference food-grade SiO_2 powder (S5), (B) SiO_2 in food product (S19), (C) reference food-grade TiO_2 powder (S11), and (D) TiO_2 in food product (S14).

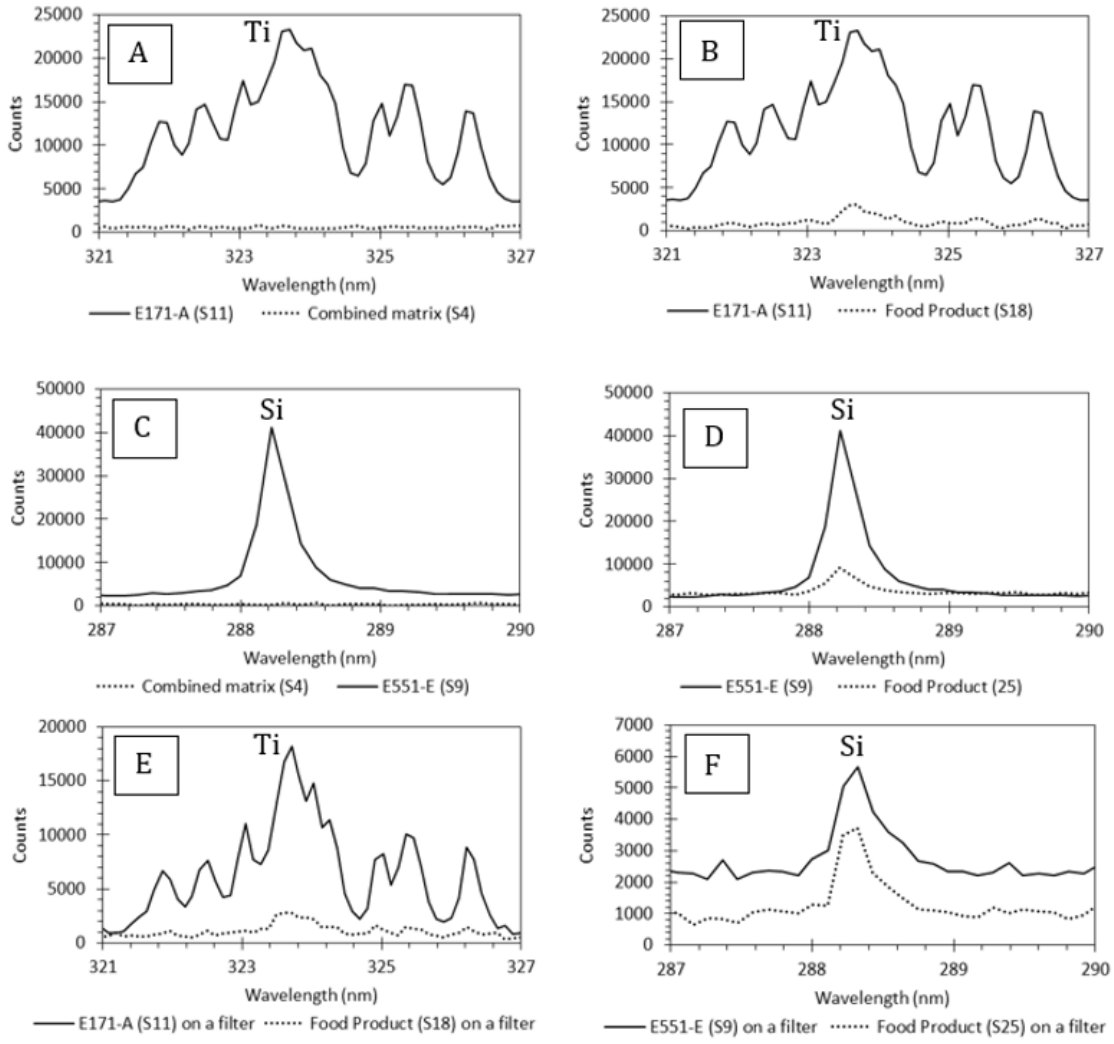

Figure 2.2. LIBS spectra for (A) reference food-grade TiO_2 (S11) and the combined matrix (S4), (B) reference food-grade TiO_2 (S11) and TiO_2 in food product (S25), (C) reference food-grade SiO_2 (S9) and combined matrix (S4), (D) reference food-grade SiO_2 (S9) and SiO_2 in food product (S19), (E) reference food-grade TiO_2 (S11) on a filter and TiO_2 from a food product (S25) on a filter, and (F) reference food-grade SiO_2 (S9) on a filter and SiO_2 from a food product (S19) on a filter.

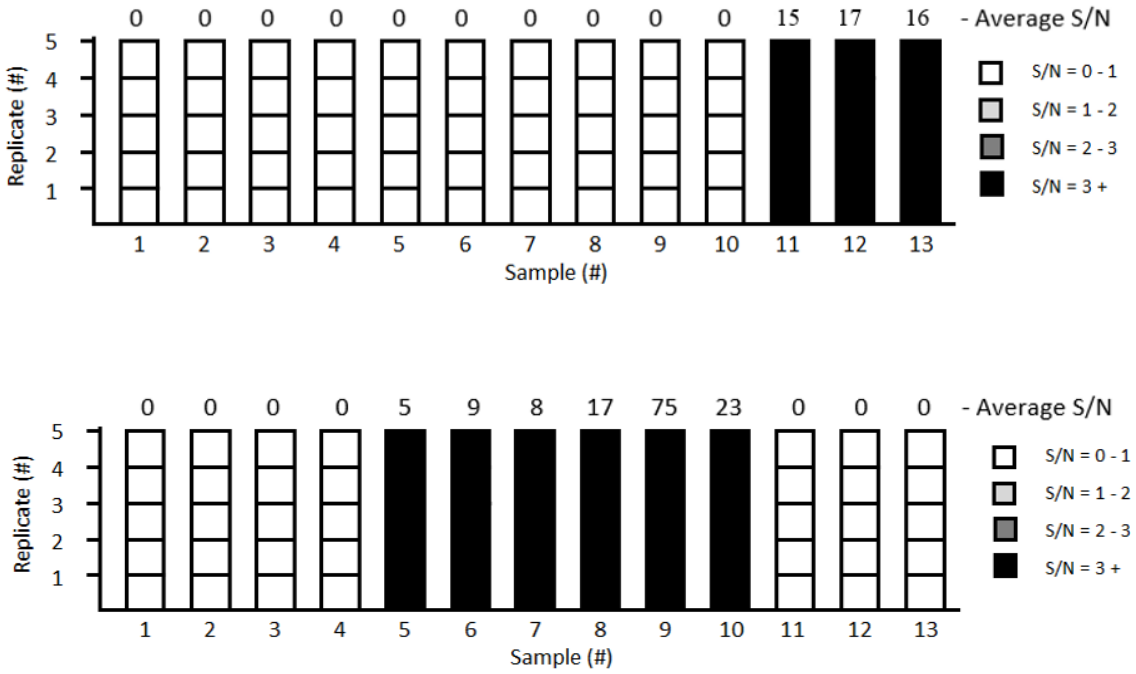

Figure 2.3. DAPs for five replicate LIBS pulse analyses of food ingredients (S1-S4) and reference SiO_2 (S5-S10) or TiO_2 (S11-S13) food-grade materials. Upper plot is for LIBS detection of Si at 288 nm, and lower plot is for Ti at 323 nm. Greyscale shade coding represents S/N for each pulse. Numbers above each bar is the average S/N value for the five replicate analyses.

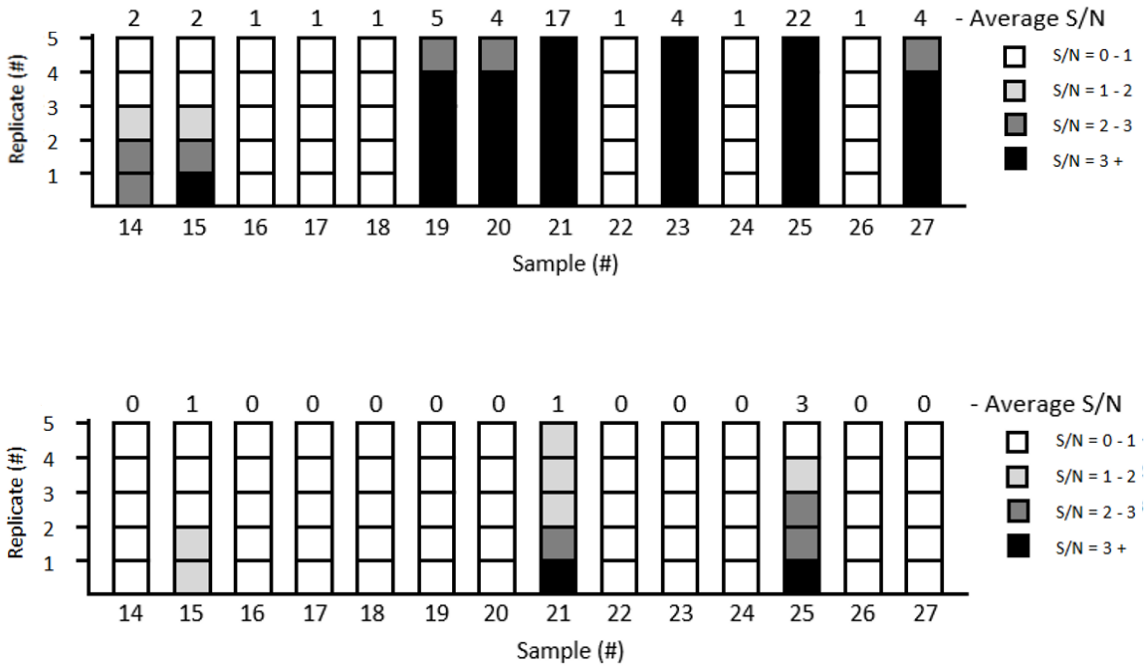

Figure 2.4. DAPs for five replicate LIBS pulse analyses on Australian foods for Si at 288 nm in solid food samples (upper plot, Bulk-LIBS) and captured on a 0.2-µm filter after dispersion in water and with 8-µm pre-filtration (lower plot, Colloidal-LIBS).

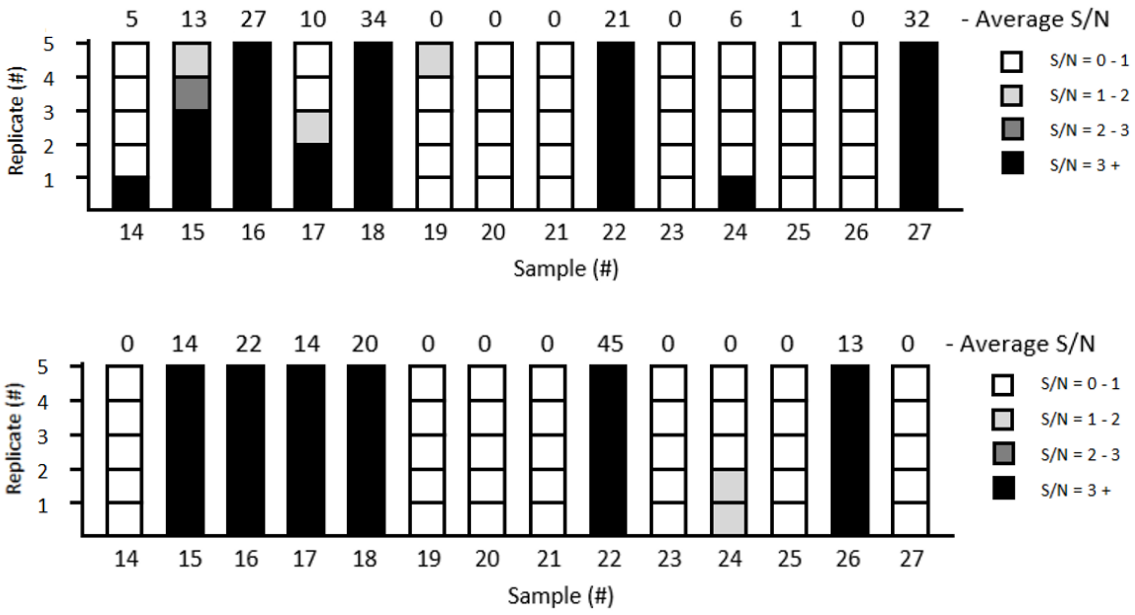

Figure 2.5. DAPs for five replicate LIBS pulse analysis on Australian foods for Ti at 323 nm in solid food samples (upper plot, Bulk-LIBS) and captured on a 0.2-μm filter after dispersion in water and with 8-μm pre-filtration (lower plot, Colloidal-LIBS).

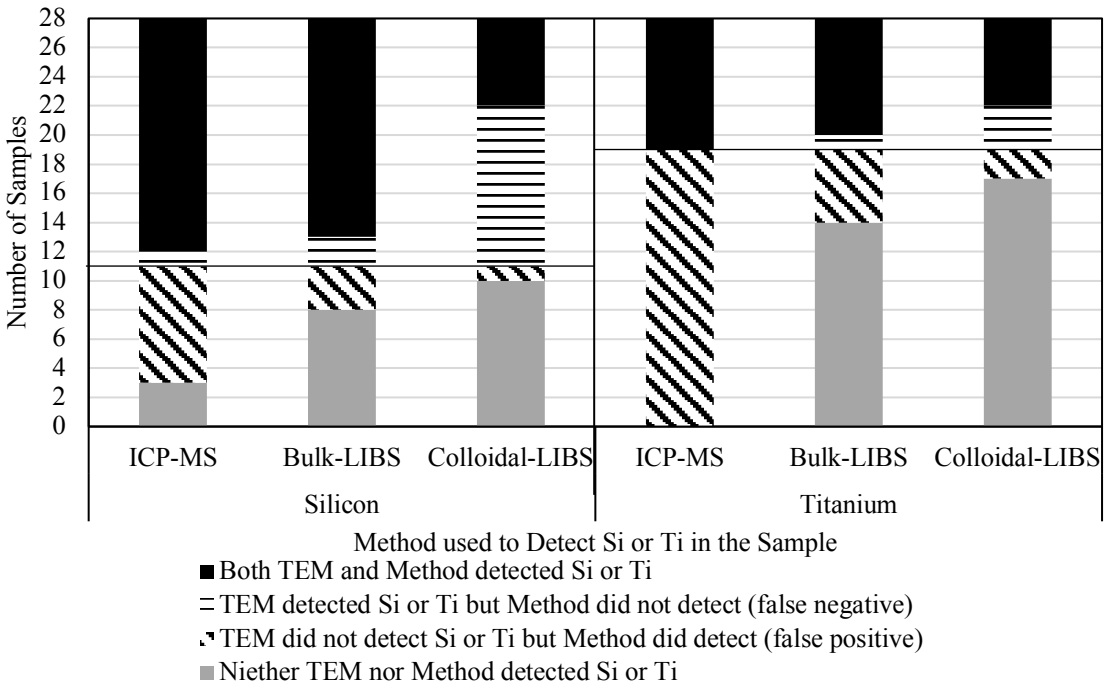

Figure 2.6. Comparisons ICP-MS, Bulk-LIBS, and Colloidal-LIBS to TEM for Si or Ti in the 28 food products from the USA and Australia. Grey denotes neither method detected Si nor Ti, black denotes both methods detected Si or Ti. Horizontal line section denotes false negative where TEM detected Si or Ti but the other method (ICP-MS, Bulk-LIBS, or Colloidal-LIBS) did not. Slashed line denotes false positive where the method (ICP-MS, Bulk-LIBS, or Colloidal-LIBS) detected Si or Ti while TEM did not.

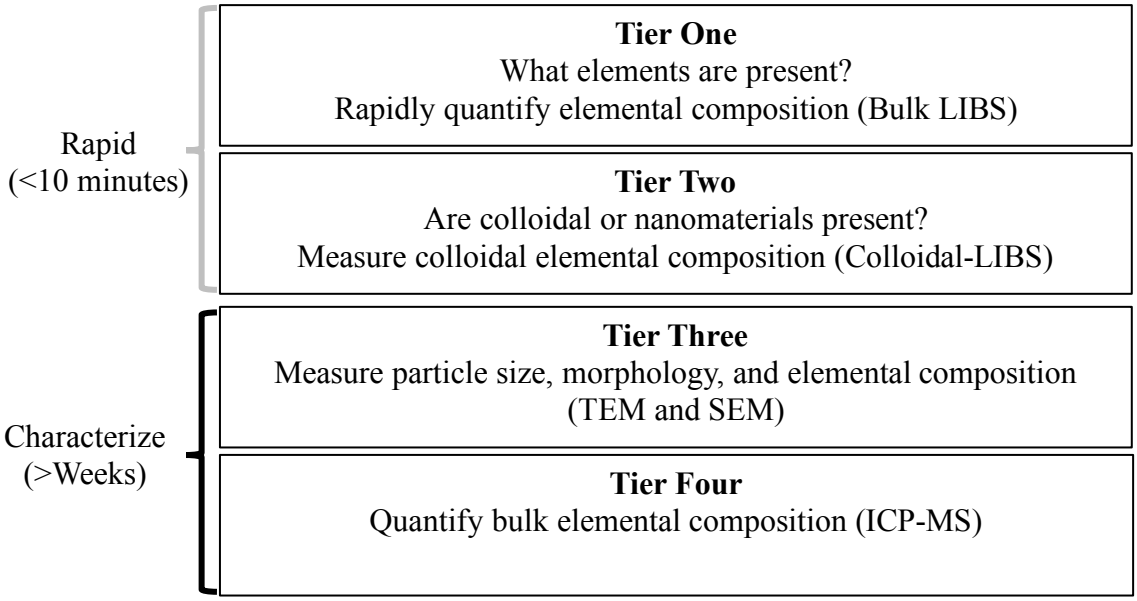

Figure 2.7. Multi-tiered approach for detecting and characterizing nanomaterials in complex matrices.

2.6 SUPPLEMENTAL INFORMATION

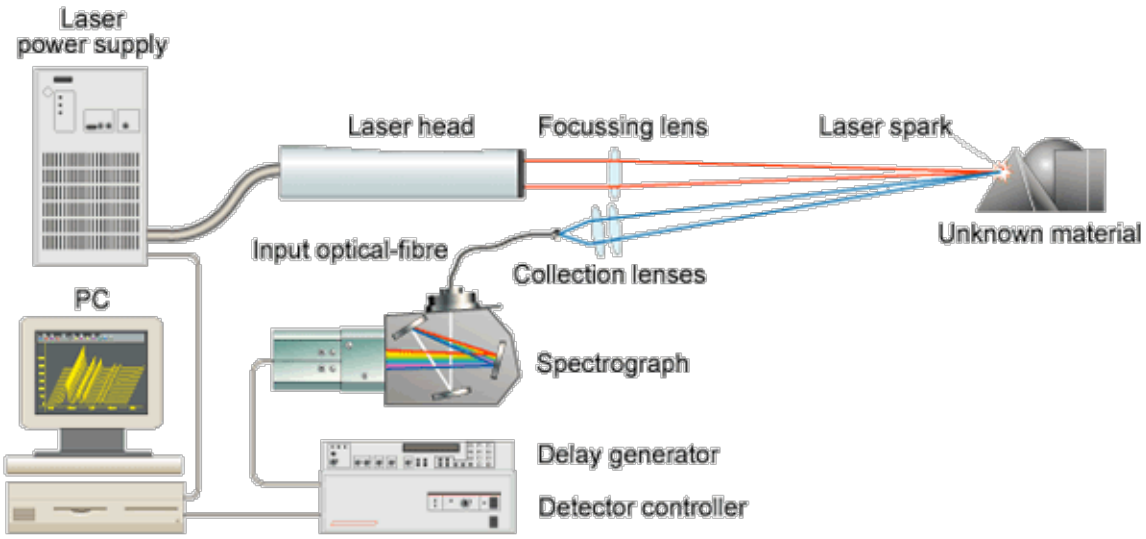

Figure SI.2.1. Diagram of a Laser-Induced Breakdown Spectroscopy (LIBS) system. Graphic courtesy of Applied Photonics Ltd, www.appliedphotonics.co.uk; used with written permission.

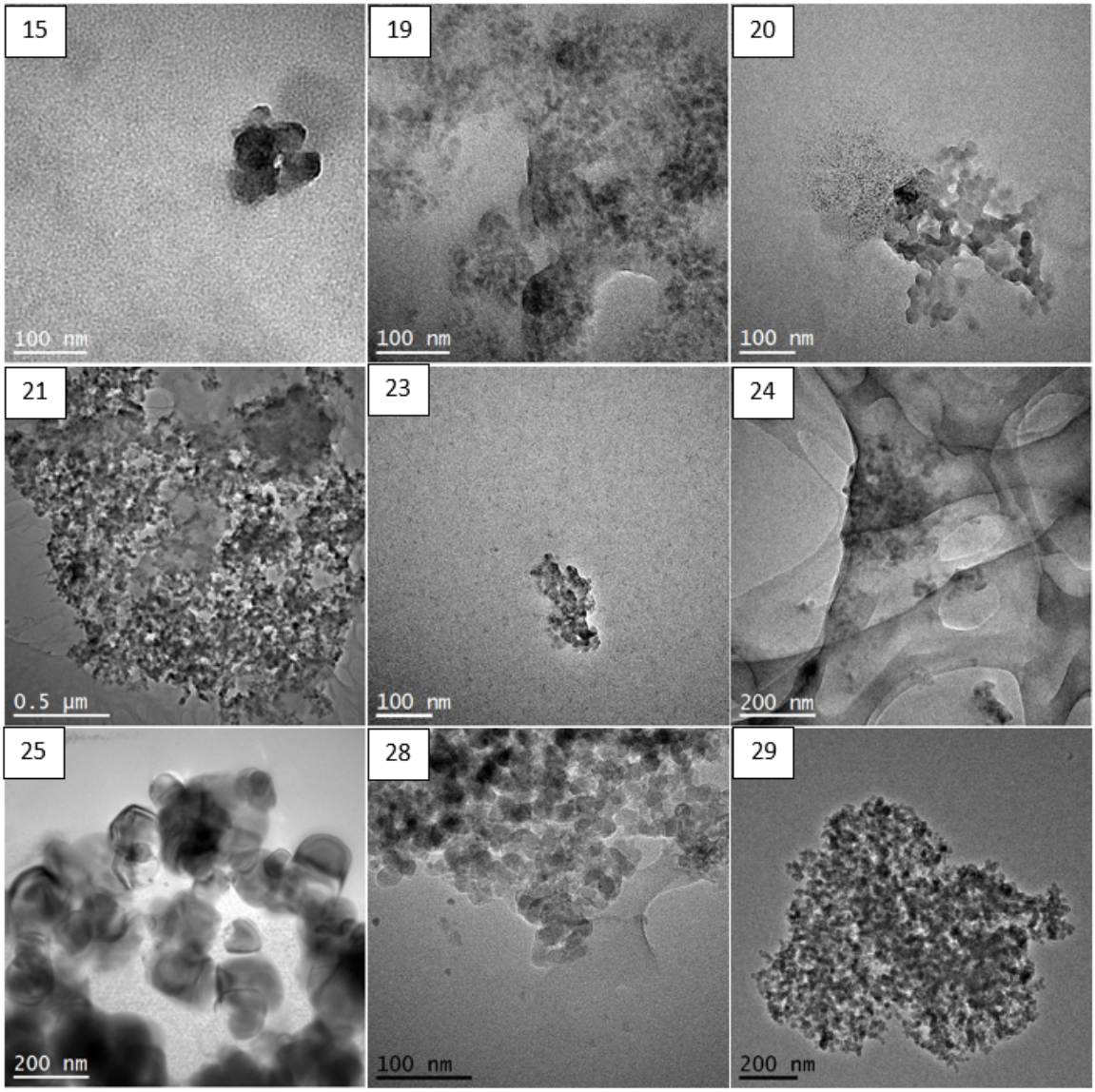

Figure SI.2.2. Transmission electron microscopy of food products containing silicon dioxide

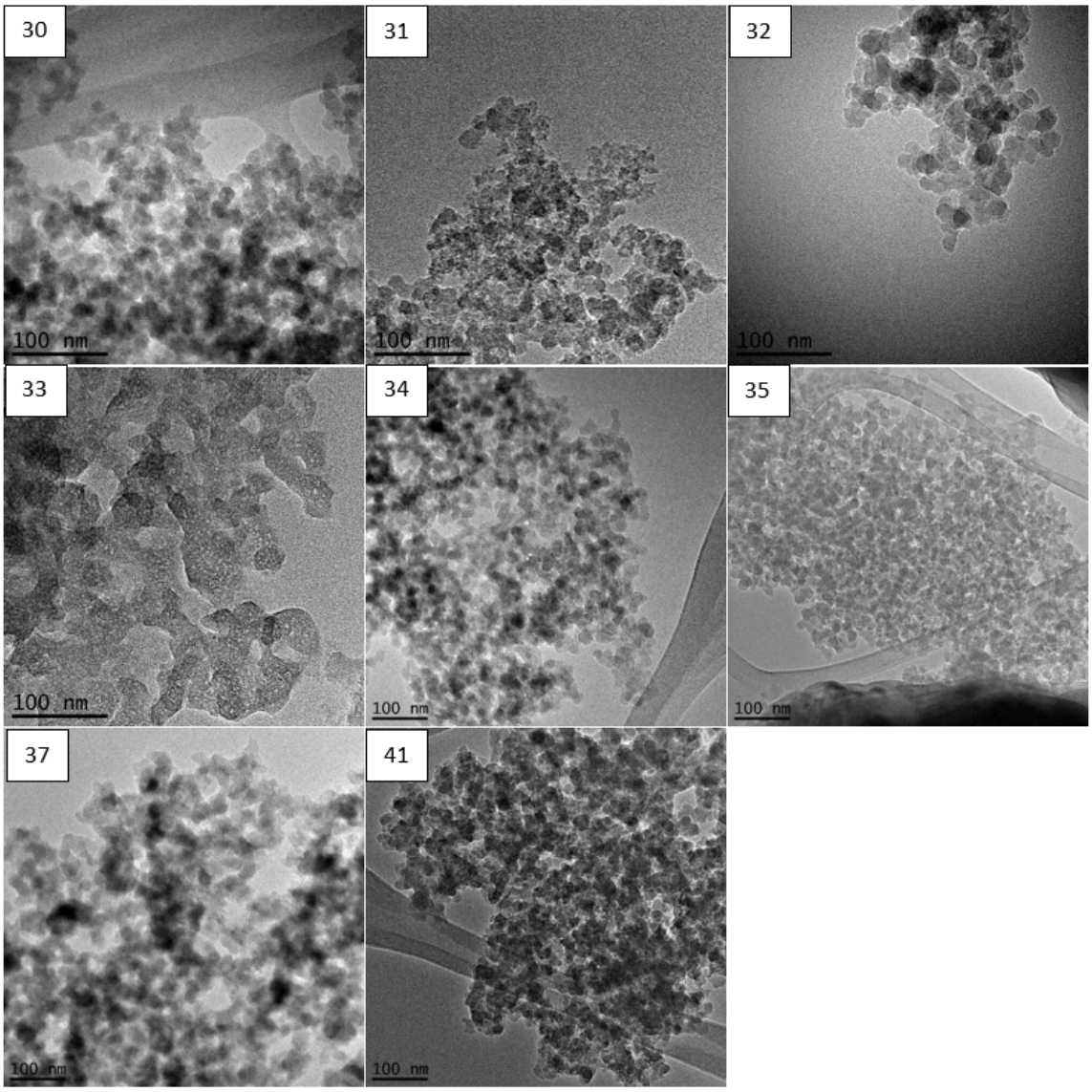

Figure SI.2.2 (continued): Transmission electron microscopy of food products containing silicon dioxide

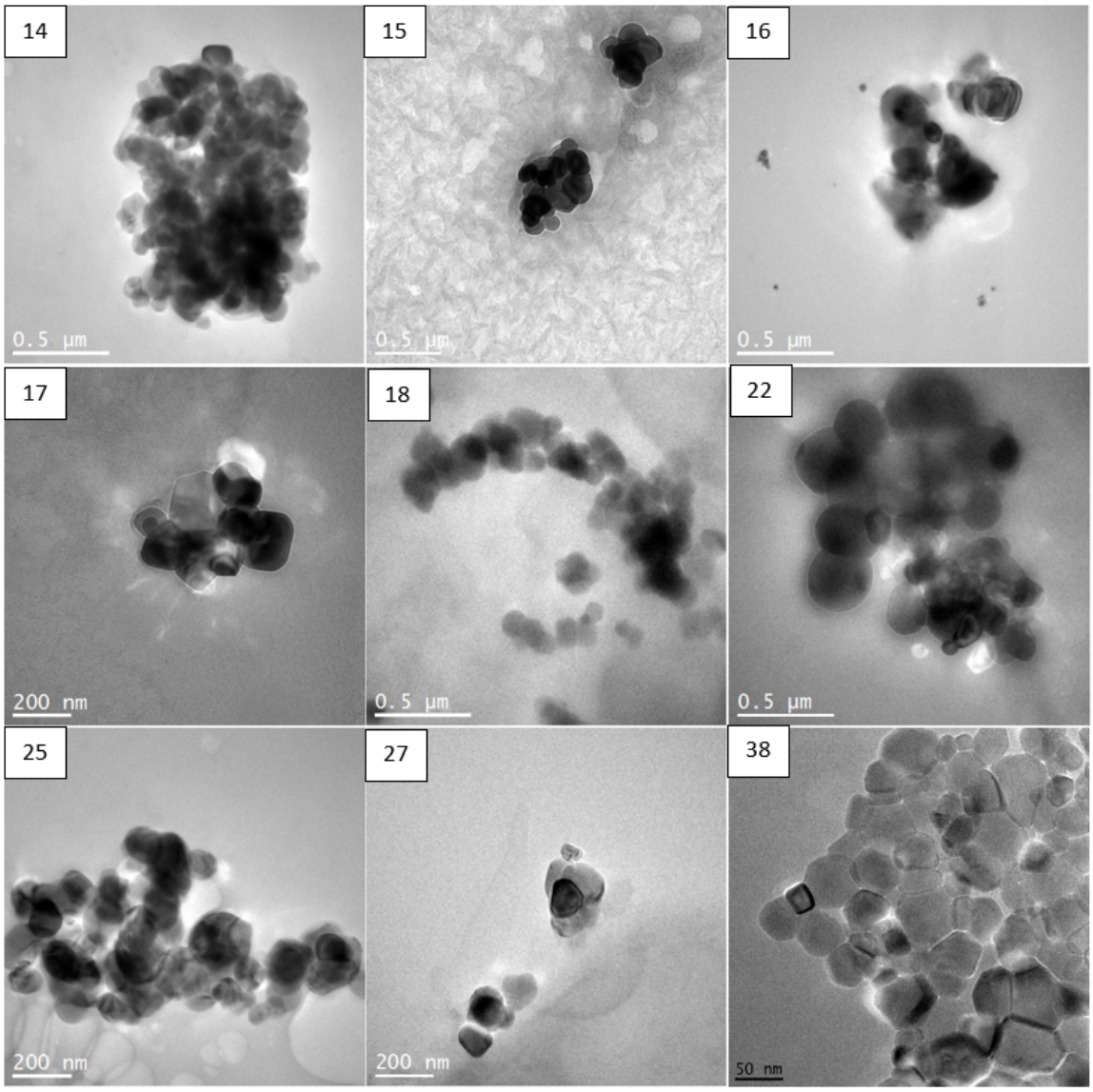

Figure SI.2.3. Transmission electron microscopy of food products containing titanium dioxide

Figure SI.2.4 shows DAPs for Si in USA food products. Some samples are fairly uniform (i.e., each of the five pulses yielded the same S/N), including samples 30, 32, 34, 35, 38, and 41 with S/N>3, sample 33 had one replicate near the detection limit, while all others had S/N<1. These groups represent high confidence. Other samples had S/N values that differed when analyzing different locations on the food samples. Samples 39 and 40 were absent of Si.

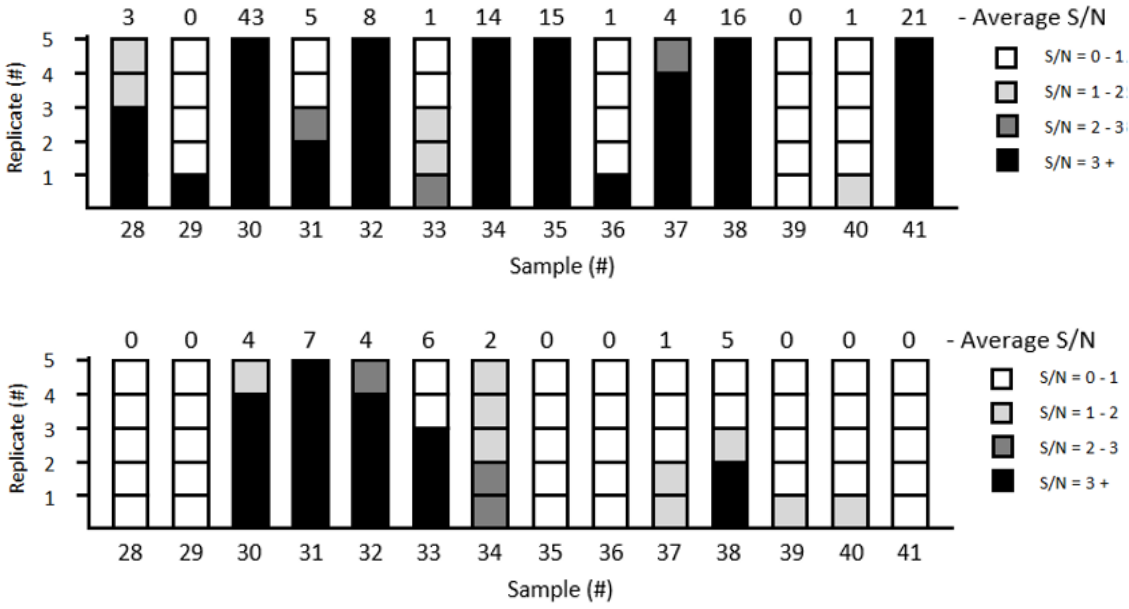

Figure SI.2.4. DAPs for five replicate LIBS pulse analyses on USA foods for Si at 288 nm in solid food samples (upper plot, Bulk-LIBS) and captured on a 0.2-µm filter after dispersion in water and with 8-µm pre-filtration (lower plot, Colloidal-LIBS).

Figure SI.2.5 shows DAPs for Ti in USA food products. Some samples are fairly uniform (i.e., each of the five pulses yielded the same S/N), including samples 35 and 36 with S/N>3, sample 32 had one replicate near the detection limit, while all others had S/N<1. These groups represent high confidence. Other samples had S/N values that differed when analyzing different locations on the food samples. Remaining samples were absent of Ti.

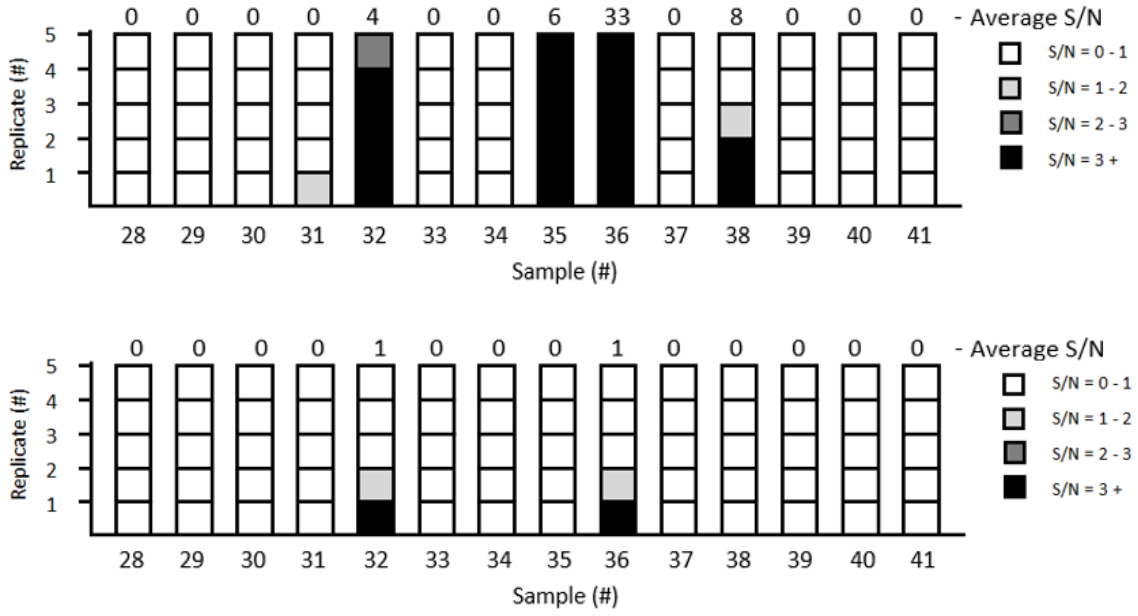

Figure SI.2.5. DAPs for five replicate LIBS pulse analyses on USA foods for Ti at 323 nm in solid food samples (upper plot, Bulk-LIBS) and captured on a 0.2-µm filter after dispersion in water and with 8-µm pre-filtration lower plot, Colloidal-LIBS).

CHAPTER 3

DETECTION AND DISSOLUTION OF NEEDLE-LIKE HYDROXYAPATITE NANOMATERIALS IN INFANT FORMULA

Jared J. Schoepf[1], Yuqiang Bi[1], Justin Kidd[1], Pierre Herckes[2], Kiril Hristovski[1], Paul Westerhoff[1]*

* Corresponding Author: p.westerhoff@asu.edu; 480-965-2885;

1- Arizona State University, School of Sustainable Engineering and the Built Environment, Box 3005, Tempe, AZ 85287-3005

2- Arizona State University, School of Molecular Sciences, Box 1604, Tempe, AZ 85287-1604

ABSTRACT

The unknowns surrounding presence, composition and transformations during the use phase of nanomaterials (NMs) in consumer products raises potential human and environmental health concerns and public discourse. This research developed evidence and confirmatory analytical methods to determine the presence and composition of ENPs in a consumer product with a complex organic matrix (six different infant formula samples). Nano-scale crystalline needle-shaped hydroxyapatite (HA; appx. 25 nm x 150 nm) primary particles, present as aggregates (0.3-2 μm), were detected in half the samples. This is the first report of these NMs in infant formula. Dissolution experiments with needle-shaped HA were conducted to assess potential transformations of nano-HA particles. Rapid and complete dissolution of needle-shaped HA occurred only under lower pH conditions present in simulated biological fluids (acidic gastric fluids), but not in simulated drinking water (near-neutral pH). Other non-nanosized HA minerals exhibited less dissolution under the same low pH conditions. This work demonstrates the occurrence of nanomaterials in the food supply of a sensitive population (infants) and the need to consider transformations in nanomaterials that occur during use, which result in different exposures between pristine/as-produced ENPs and nanomaterials after passing through the human gut.

Keywords: nanomaterials, calcium phosphate, water, digestion

3.1 INTRODUCTION

Many minerals exist in both natural and nanomaterial (NM) forms. While the occurrence of naturally occurring nanoparticles (e.g., hematite, hydroxyapatite) is well recognized in natural systems, the environmental behavior of ENPs raises new regulatory and health concerns. These concerns primarily stem from existing knowledge gaps in understanding the ENP risks, which could be summarized in two categories: (1) discovering where ENPs are used in commerce and hence might enter the environment, and (2) elucidating ENP transformations from pristine materials, to synthesis in the lab or factory, and through use and end-of-life phases. We and others have previously shown that silicon- and titanium-oxide ENPs exist in foods, are ingested by humans, and pass through wastewater treatment plants, which results in their release to surface waters and terrestrial systems where sewage solids are land applied [124-131]. These two ENPs undergo little dissolution (i.e., transformation) during this process, which differs from antimicrobials like silver, copper, or zinc nanomaterials [132-135].

Calcium phosphate minerals are an example of solids present in nature and used in environmental remediation/treatment processes [136-141] and human nutritional supplements. Intentional formation of calcium phosphate is used to immobilize heavy metals in soil [142, 143], remove fluoride from water to protect public health, [144] or remove phosphate from wastewaters to limit the eutrophication potential of wastewater discharges [140]. Calcium phosphate, also referred as tricalcium phosphate (TCP), is used as a leavening agent in foods, a polishing material in toothpaste, an antioxidant activity promoter and texture stabilizer in canned vegetables, a firming agent or to avoid formation of clumps in food. Hydroxyapatite (HA; $Ca_5(PO_4)_3$ or $Ca_5(PO_4)_3(OH)$) is a

common form of calcium phosphate. Many people take calcium supplements, including calcium carbonate, calcium citrate and hydroxyapatite forms, but the literature is mixed on which form leads to greater bioavailable calcium for health bone development [145, 146]. In other applications, nano-forms of calcium minerals have raised concern. For example, the European Union Scientific Committee on Consumer Safety 2015 opinion on nano-HA states that the safety of its use in oral and cosmetic products cannot be currently decided due to limitations in available data, including the exact size, shape and crystallinity of the nano-HA, but that the available information indicates nano-HA in needle form is potentially toxic when used in dermally-applied cosmetic products [63].

Calcium is an essential element for all biological organisms, and is widely used in human food supplements. For example, infant formula is intended to be the sole nutrition source for infants for the first 12 months. Although regulations (e.g. 21 CFR 107.100 in the USA) stipulate the elements required in the infant formula, they lack guidance on the type or size of the compounds used to provide the nutrients. Regulations refer to HA as generally regarded as safe (GRAS); however, new bottom up manufacturing processes that create nanomaterials compared to top down processes create new concerns if the GRAS status applies. Given potential toxicity concerns raised in the EU on nano-needle-shaped hydroxyapatite in products intended for human use, the need for infants to have calcium and other elements (P, Fe) in their diets, and potential transformations for HA under different pH conditions, we undertook a study to separate and identify HA and other nanomaterials in powdered infant formulas. This challenging work with infant formulas that contain salts, sparingly soluble minerals, fats and other components is a

precursor to understanding the occurrence and role of nano-scale HA minerals in complex environmental matrices (soil, biota, and water).

To identify initially unknown nanomaterials in infant formula, samples were separated by centrifugation after dispersing powders in water and then analyzed by transmission electron microscopy (TEM) with energy dispersive X-ray spectroscopy (EDX) and X-ray diffraction (XRD). Findings from these samples were compared against reference calcium phosphate materials. We focused on HA because it was found in three out of six samples, although it has not yet been widely considered by the health and safety exposure community as a risk in the food supply system. Within a complex food matrix, HA nanoparticles are difficult to be detected using conventional analytical paradigms. A secondary focus was the dissolution of HA in synthetic biological fluids to explore potential transformation in human body of these nano- and micron-sized minerals. Because the intended function of calcium phosphate in infant formula is to promote nutrient uptake, we used aqueous matrices representing simple drinking water and simulated gastric fluids. Understanding nanomaterial transformations during their intended use emerges as a critical discussion and conclusion point around the benefits of using nanotechnology (e.g., rapid dissolution of HA to deliver calcium and phosphate ions).

3.2 MATERIALS AND METHODS

Chemicals

Six infant formulas from different companies (Gerber, Similac, Enfamil, and Well Beginnings) were purchased in the United States and identified, for confidentiality, as S1-S6. Samples S1-S5 were dry powders, and S6 was a liquid concentrate. Dry powders and

a liquid concentrate were chosen to compare suspected different additives used for each product. Three reference powder samples of food-grade calcium phosphate, labeled as hydroxyapatite, were procured from three different vendors. Samples R1 (American Elemental) and R2 (Hebei Shunye Import and Export Limited Company) were labeled as 99% pure and containing needle-like nano-HA. Sample R3 (NOW Foods) was an HA supplement provided in a gelatin pill capsule; only the contents of an opened capsule were used in analysis and dissolution tests.

Electron Microscopy Analysis

Infant formula (0.15 grams) samples S1-6 and HA reference samples R1-3 were suspended in 40 mL ultrapure water (18.2 MΩ cm, Nanopure Infinity, Barnstead) and sonicated (80 Watts/L, Branson Ultrasonic Bath, Emerson) for 30 minutes to disperse particles. This mass to liquid ratio was used to parallel work other food samples analyzed by our group. [54, 57]. Additional electron microscopy experiments were conducted at solid to liquid ratios based upon recommended sample preparation on the infant formula packaging, and showed no dependence of outcomes on solid to liquid ratios. Other detailed control and validation experiments are summarized in Table SI.3.4 and described in the Results section. Step-by-step description of sample preparation of electron microscopy samples are summarized in Figures. SI.3.2 through SI.3.4. Briefly, samples in 50 mL vials were centrifuged at F = 14,000 G for 15 min. The organics-rich supernatant was poured off, leaving a pellet of particulate matter at the bottom of the centrifuge tube. The pellet was re-suspended in 20 mL ultrapure water and inverted by hand for 30 s, then 50 μL volumes were pipetted onto a copper/lacey carbon transmission electron microscopy (TEM) grid and allowed to air-dry overnight. Microscopy was performed on

a Philips CM200 HR-TEM with energy dispersive X-ray spectroscopy (EDX). To confirm HA was not an artifact from sample preparation, a pure powder reference sample of HA was procured, deposited on a SEM stub (Figure SI.3.3) and directly analyzed as a powder by scanning electron microscopy (SEM; FEG XL30 ESEM with EDX system) with energy dispersive spectroscopy. Mean particle diameter, particle size distributions, and cumulative distribution below 100 nm were determined by manually measuring the particles sizes of 250 particles from the images using ImageJ software and conducting statistical analysis.

Sample Preparation for Confirmation and Quantification of Hydroxyapatite

Figure SI.3.6 provides a step-by-step description of sample preparation. To determine the relative amount of hydroxyapatite nanoparticles in infant formula, 10 g of each formula sample (six in total) was weighed into 50 mL centrifuge tubes with 40 mL of ultrapure water (18.2 MΩ cm, Nanopure Infinity, Barnstead). The mixed samples were then centrifuged for 20 min at F = 14.000 G to separate lighter components. The pellet collected at the bottom of centrifuges was washed three additional times with UP water. The washed pellet was freeze-dried under vacuum for 48 h (FreeZone Freeze Dry System, Labconco), weighed, and compared with the weight of starting material to calculate the relative concentration of collected minerals. The mineral phases of pellets and reference powders were prepared (Figure SI.3.7) and analyzed using powder X-ray diffraction (pXRD) using a Siemens D5000 diffractometer with a monochromated Cu–Kα radiation at 40 kV and 30 mA. Each sample was scanned at 2θ values from 10° to 70° to collect diffractograms, which were compared with the diffraction patterns of standard materials in ICDD database.

Dissolution Experiments using Hydroxyapatite in Aqueous Media

Ultrapure water and simulated biological fluids were used to examine the dissolution potential of the two reference HA and calcium bioavailability after ingestion. A detailed procedure is outlined in Figure SI.3.1. A Fed-State Gastric Fluid (Fed-SGF, pH 5.0) and a Fasted-State Gastric Fluid (Fast-SGF, pH ~1.6) were prepared following recipes reported previously [147] and detailed in Table SI.3.1. For HA dissolution, 40 mL of the media was placed in 50 mL plastic centrifuge vials followed by the addition of 8 mg of reference HA to achieve a final concentration of 200 mg/L. The HA concentration was chosen to represent the serving size of HA per serving of infant formula. Immediately after mixing HA with simulated media, the suspensions were placed on a rotational shaker (45 rpm). The fed-state gastric fluid and fasted-state gastric fluid were rotated for 2 h to mimic the average contact time of food in the human stomach [148]. Within 5 min of the completion of mixing, 15 mL of each suspension was filtered through 30 kDa centrifugal ultrafilters (NMWL = 30 K Da, ultracel regenerated cellulose, EMD Millipore) at F = 4000 G for 12 min. A HA dose of 200 mg/L was added to the aqueous chemistry described in Table SI.3.1. The solution collected for each filtered sample was diluted in 2% nitric acid and analyzed for dissolved calcium and phosphorous concentrations by inductively coupled plasma mass spectrometry (ICP-MS, X-Series-II, Thermo Scientific). Control experiments were performed to understand potential impact of matrix effects (DI water, 1 mM NaHCO3, biological fluids) on permeation of dissolved Ca2+ through the ultrafilter or matrix effects due to calcium precipitation. Details and results provided in Supplemental Information (Table SI.3.2)

concluded that there were no matrix effects in DI water, 1 mM NaHCO3, or gastric fluids (pH 1.6 or 5.0), and N90% of the spiked Ca2+ was recovered.

3.3 RESULTS AND DISCUSSION

Presence of Nanomaterials in Powder Formulas

Detecting nanomaterials in complex matrices is a challenge [26, 27, 40]. Initially, powder formula samples were analyzed by scanning electron microscopy (SEM), but the amount of organic material prevented meaningful imaging from carbon contamination (see Table SI.3.4), the deposition of carbonaceous material by the electron beam from cracking of carbon-carbon bonds present on the sample and carbon residual within the vacuum of the sampling chamber of the microscope [149]. To overcome these issues and achieve high quality TEM images and meaningful elemental analysis of solids, infant formula samples were added to water and then followed protocols described in the Methods section. Results are discussed in two parts. First, the observed results show needle-like HA is present in some infant formula samples. Second, experiments demonstrate such structures are not artifacts of sample preparation.

TEM images in Figure 3.1 are representative of multiple (typically N10) images taken across several TEM grids of each sample. All six infant formula samples contained Ca and P as determined by EDX (Table 3.1), suggesting the presence of Ca-containing minerals. In addition, SiO2 nanoparticles were found to be present in one sample (S4) and had similar size (~7 nm) and shape with this nanomaterial in other foods [121]. Titanium and oxygen containing material was detected in the liquid formula (S6) and was consistent with TiO_2 nanomaterials in foods reported in the literature [8, 57]. Previous

studies in food samples discuss occurrence and characterization of SiO_2 and TiO^2 materials [8, 57, 58].

The three most prevalent elements in colloids detected on the TEM grids were calcium, phosphorous and oxygen, and these were associated with the colloidal materials having two general shapes (needle-like or spherical). Figure SI.3.8 shows representative TEM with EDX spectra for these colloidal materials and additional TEM images of the samples. S1, S2, and S3 samples contained needle-like shaped particles 10– 30 nm in width and 100–300 nm in length, creating impressions of dendritic networks. The size and shape of HA in S3 were nearly identical to the needle-like hydroxyapatite reference (R1 and R2) samples (Figure 3.1). Additional TEM of the three reference materials are shown in Figure SI.3.9. Samples R1 and R2 containing nearly exclusively needle-like shaped HA whereas sample R3 contains only a few needle-like structures but mostly other micro-crystalline HA structures. This mineral phase, however, was not observed in S1 and S2, although TEM characterization suggested its presence. XRD data for each sample and reference material are presented in Figure 3.2. Initial XRD performed on the entire powdered infant formula samples exhibited a broad peak due to all the salts and organic materials. Therefore, XRD analysis for the infant formula samples were conducted on a purified pellet (Figure 3.2 for S1–S6), but it was feasible to conduct XRD directly without sample pretreatment for the three reference HA. Figure SI.3.10 shows XRD diffraction pattern confirming the presence of a single phase hydroxyapatite ($Ca_5(PO_4)_3(OH)$) in the three reference materials. The two needle-like hydroxyapatite reference samples (R1 and R2) have sharper diffraction peaks compared to the spherical counterpart which contains only a few needle-like structures but mostly other micro-

crystalline HA structures (R3), suggesting larger crystallite sizes of R1 and R2 than R3. The micro-crystalline R3 sample was found to have similar morphology within S5, both displaying spherical shapes. Of the six infant formula samples (S1–S6) in Figure 3.2, one or both forms of calcium was observed (calcite or calcium hydroxyapatite). XRD analysis unambiguously confirmed the presence of hydroxyapatite in S3 based upon library matches (Figure 3.2). Samples S5 appeared to be mostly calcium hydroxyapatite, whereas other samples appear to contain a mixture of calcite and calcium hydroxyapatite. In S5 sample, however, the calcium phosphate was dispersed in larger aggregates composed of organics and calcium material and mainly composed of monetite minerals ($CaHPO_4$) based upon XRD analysis. Together, TEM and XRD analyses provide evidence that needle-shaped Ca-containing nanomaterials are present in 3 out of 6 infant formulas (S1, S2, and S3), likely in the form of HA or HA/calcite mixture. To assess the quantity of nano-scale needle-like HA in the samples, materials were separated from the rest of formula constituents via repeated sonication, centrifugation, and washing (Figure SI.3.6). The minimum concentration of HA in S3 was estimated to be ~0.4 wt% based on the mass of insoluble pellet. The HA mass recovered in pellets from samples S1 and S6 was 0.1 wt%, and even less mass was recovered from the other samples. The presence of needle-like HA in the infant formula was unexpected. Therefore, an extensive array of experiments was performed using S3 and R1 to confirm their presence in the samples and demonstrate they were not artifacts of sample preparation. Complete details are provided in Supplemental Information text and summarized in Table SI.3.4. First, to assess the potential for artifacts or transformations in nanomaterial morphology and size experienced in sample preparation, hydroxyapatite reference materials were purchased

and analyzed using the same sample preparation as the infant formulas (sonication, centrifugation, decantation, and resuspended (following steps in Figure SI.3.2). During the same sample preparation, the needle-like and spherical reference materials maintained their size and morphology through the process, concluding sample preparation did not alter the nanomaterials in the infant formula. SEM analysis directly on the infant formula powder was not able to detect needle-like HA because of the presence of salts and organics in the powder, where HA accounts for b0.4% of the dry mass of powder. Therefore, dispersion of the powder in water and separation of solids was necessary (see discussion related to Figure SI.3.12–3.17). Second, the infant formula (S3) was prepare at a higher solids to liquid ratio (6 g instead of 0.15 g in 40 mL of water) to represent the recommend ratio to prepare the infant formula as described on the package label. The samples were mixed by hand but not sonicated. Liquid was then either pipetted (20 mL) directly onto a TEM grid or centrifuged (4050 G for 4 h) onto a TEM grid placed in the bottom of the centrifuge vial. In both cases, TEM analysis of the grids detected nano needle-like HA (Table SI.3.4). Thus, neither the solid-to-liquid ratio nor method of preparing the TEM grid lead to artifacts in needle-like HA detection. Third, evidence exists that needle-like HA could form due to sonication [1, 3, 150]. To demonstrate that sonication did induce needle-like HA formation experiments on dispersed S3 were performed. Sample S3 was prepared for TEM analysis following our original method (Figure SI.3.2) that included sonication, compared against the sample procedure without sonication. Figure SI.3.11 shows nearly identical TEM images from these comparative experiments. Nano needle-like HA is present both with and without sonication. Thus, this confirms that sonication of the infant formula added to water under the conditions applied

herein does not lead to artifacts related to needle-like HA formation. Upon further inspection of the literature on needle-like HA synthesis, conditions (sonication power of 300 watts for 3 h and 333 °K) required to produce needlelike HA during sonication do not exist during our preparation of sample S3 (Figure SI.3.2 where sonication power 80 watts for 30 min and 300 °K).

Fourth, additional experiments were conducted to confirm our sample pretreatment did not in-situ produce needle-like HA due to the presence of dissolved calcium and phosphorous in the presence of other salts or organic macromolecules that might be present in infant formula. Sample S3 was dispersed in water and needle-like HA centrifuged out, into a pellet, following our original methodology. To the supernatant, absent of needle-like HA pellet, which still contains macromolecules and other inorganics, calcium and phosphorus ions were added to the supernatant at a 1.67 mol ratio (the optimum ratio for HA synthesis [1] and then bath sonicated. Subsequent centrifugation and TEM inspection did not detect HA on the TEM grid. Thus, neither sonication alone nor sonication in the presence of other inorganic/organic components present in the infant formulas could produce nano needle-like HA artifacts, under the sample preparation conditions used in our work.

Dissolution Potential for Hydroxyapatite as a Function of pH in Biologically Relevant Media

High surface area or high aspect ratio of nanomaterials can increase the rate of mineral dissolution and result in the release of soluble ions [134, 151, 152]. While dissolution of nanomaterials can result in toxic responses for some metals (e.g., silver, zinc, copper) for other ENPs, we hypothesized that a beneficial reason of adding needle-

like HA nanomaterials to the infant formula may be to increase dissolution potential of the mineral phase and bioavailability of calcium and phosphate. Therefore, dissolution experiments for the reference needle-like (R1) and spherical (R3) hydroxyapatite materials were conducted in simulated drinking waters and biological fluids. The dissolution potential of HA in each matrix was based upon permeation of calcium ion through the 30 kDa ultrafilter. The HA nanomaterials have larger radii than the pore size of 30 kDa filters (~2 nm), allowing for the size exclusion of HA ions and colloidal HA [153]. Controlled experiments described in Supplemental Information confirm that matrix effects do not influence Ca^{2+} permeation across these ultrafilters under the operating conditions tested.

Figure 3.3 shows that dissolution of hydroxyapatite occurs in the two gastric fluids, while <6% of the HA dissolves in 1 mM NaHCO3 and permeates the ultrafilters. In the pH 5.0 gastric fluid, N60% of needle-like HA (R1) and <50% of the spherical HA (R3) dissolves. At pH 1.6, similar levels of needle-like HA (R1) dissolution occurs but a higher amount of dissolution occurs for spherical HA (R3). Similar patterns in UF permeation of phosphate during these tests were also observed (Figure SI.3.18). Visual observations during the experiments indicate more rapid changes for R1 than R3 samples. Both samples were white and cloudy initially, but R1 became clear in b1 min whereas the change in visibility took 1–2 h for R3 (see supplemental information Figure SI.3.19–3.20). The two hour period is physiologically relevant for the contact time for food and acidic gastric fluids [148]. These visual observations may indicate disaggregation or dissolution. Measurement of dynamic light scattering after each dissolution test indicated a significant decrease in mean diameters for the needle-like HA reference material

(Figure SI.3.19), which could indicate either disaggregation or dissolution. Overall, the quantitative data for calcium and phosphorous, as indicators of HA, presented in Figure 3.3 were supportive of qualitative visual observations.

Attempts were made to differentiate ionic from colloidal forms of Ca and P using single-particle ICP-MS, which is a powerful tool for analysis of many nanoparticles in aqueous media [130, 154-158]. However, the minimum detection of Ca and P elements and associated mineral forms were more than several hundred nanometers due to the response factors of the ICP-MS [26]. This highlights an important research need to improve sensitivity of spICP-MS for materials like HA.

Thermodynamic chemical equilibrium modeling (Visual MINTEQ (ver. 3.1)) predicts complete dissolution of HA in either gastric fluid (Figure SI.3.22). The discrepancies between model predictions and experimental observations (Figure 3.3) indicate that the dissolution of HA in the simulated gastric fluids may have kinetic limitations or differences in solubility products for different aspect ratio HA or presence of non-crystalline forms of calcium phosphate solids. In comparison to two other calcium minerals (i.e., calcite, monetite) identified in infant formula, hydroxyapatite has the lowest solubility at pH N 5.4 (Figure SI.3.22). However, in both gastric fluids, all calcium minerals are predicted to dissolve completely at equilibrium with a serving concentration of 2 mM Ca in infant formula. Future research is needed to quantify the rates of dissolution for these two different HA morphologies.

The calcium bioavailability of different minerals cannot be concluded until additional kinetic studies are performed. However, the comparison between R1 (needle-like) and R3 (spherical) samples of HA (confirmed by XRD) suggest a priori assumptions

about thermodynamic stability constants may not be appropriate for different shapes of HA. The dissolution mechanisms of calcium phosphate nanomaterials with respect to shape are not well understood. However, dissolution of high aspect ratio (i.e. needle-shaped) metal oxide nanoparticles have been reported to dissolve preferentially from each of the two ends [159]. Numerous methodologies exist to synthesize calcium phosphate, including those to produce needle-like nanostructures [1, 150], and it appears these different shapes could impact ability to dissolve in the acid biological fluids.

3.4 HUMAN EXPOSURE IMPACT FINDINGS

TEM detected the presence of nanoparticles in all six samples. Results show that hydroxyapatite was detected in multiple samples at levels on the order of <0.1 to ~0.4 wt%. Other samples contained calcite, monetite, silica dioxide, and titanium dioxide at lower levels. Most attention was placed on hydroxyapatite because the presence of calcium nanomaterials in infant formula has not been reported previously. In the authors opinion, hydroxyapatite (needle-like structure) may be intentionally used in infant formula because of its rapid (almost instantaneous) dissolution potential in gastric fluids at and below pH 5. However, further research is needed to prove this hypothesis. Previous research suggests hydroxyapatite dissolution provides favorable stoichiometric ratios of bioavailable Ca and P [160-162]. Slower dissolution of spherical hydroxyapatite may not provide as much nutritional benefit. Additional techniques are needed to measure needle-like particles as FFF-ICP-MS, and spICP-MS measure particle size, but not morphology resulting in difficulty interpreting results for needle-like materials.

Others have reported the global production of many types of NMs, yet these reports exclude needle-like hydroxyapatite [53, 139, 163] while one report quantifies the

amount of HA in the USA entering the environment from the use in toothpaste to be between 18 and 19 metric tons per year in 2013 [164]. The 2013 global market for infant formula was approximately $41 Billion (US dollar), and growing rapidly in Asia and other markets [165]. Based upon the prevalence of the material in infant formula alone, the global annual production is likely to be on the order of carbon nanotubes, in the range of thousands of metric tons per year (see Supplemental Information).

The dissolution potential of needle-like HA under mildly acidic conditions raises a number of issues for assessing the impact of these types of nanomaterials. First, the US EPA Toxic Substances Control Act (Section 8 rule for nanomaterials) may exclude, from being classified as nanomaterials, substances which dissociate completely in water. The needle-like HA examined here would be difficult to classify, because it did not rapidly dissolve in water at near neutral pH, but did dissolve rapidly under mildly acidic conditions where it was intended to be used (i.e., digestive tract). Further proposed rule changes would exclude substances from being classified as nanomaterials which do not exhibit new properties when their size falls in the range of 1–100 nm. For HA it appears that the needle-like shape is intended to increase the rate of dissolution in acidic conditions, and this needle-like structure is specifically synthesized by controlled chemical and heating conditions through a new bottom up manufacturing process compared to standard top down processes. Therefore, needle-like HA could pose a challenge to proposed classification systems under this rule for ENPs in the USA.

Second, evaluating the toxicity in mammalian cell culture of needlelike hydroxyapatite may give very different results from in vivo administration, where acidic conditions in gastro-intestinal tracts would apparently rapidly transform (i.e., dissolution)

the size of this HA engineered nanoparticle. Calcium ions are absorbed by the small intestine by passive diffusion and active transport [166, 167], but recrystallization of HA may occur. If there is a high concentration of phosphate and calcium ions in the small intestine under alkaline conditions, you can get precipitation of HA [168]. This could impact the effects of HA on the gut microbiome because they would be exposed to non-dissolved (i.e., near pristine) forms of the ENP. Thus working with ENPs like needle-like HA raises challenges to appropriately track dosimetry throughout toxicological testing [169-171].

Finally, elements in other nanomaterials (silver, copper, zinc, cadmium, etc.) can dissolve out of nanomaterials based upon variable environmental conditions. Whereas redox conditions in solution can control the ionic release (Ag^{+}, Cu^{2+}, Zn^{2+}, etc.) from these ENPs, dissolution of calcium and phosphate ions from HA appears to be controlled by its pH-dependent solubility rather than redox conditions in water. The needle-like HA structure may have different KSP values compared against other calcium phosphate forms, or may just influence the relative dissolution kinetics. Fortunately, calcium and phosphorous are not toxic like other metals.

3.5 ACKNOWLEDGMENTS

Funding was provided from the US Environmental Protection Agency through the STAR program (RD83558001) and the National Science Foundation through the Nano-Enabled Water Treatment Technologies Nanosystems Engineering Research Center (EEC-1449500) and CBET 1336542. Assistance from Ian Illuminati from Friends of the Earth is appreciated. We gratefully acknowledge the use of the facilities within the LeRoy Eyring Center for Solid State Science at Arizona State University.

Table 3.1. Sample and reference material characteristics from label information, TEM/SEM*, and EDX**.

Sample ID	Manufacturer Brand / Product ID #				
	Product & Label Information	**Elements detected****	**Likely nano-scale minerals / elements**	**Dimension of primary particles***	**Dimension of aggregates***
S1	*Powder formula* (120 mgCa; 66 mgP; 1.8 mgFe)	Ca, P, O	Nano needle-like HA	13nm (width) by 110nm (length)	320 – 1,627 nm
S2	*Powder formula* (82 mgCa; 44 mgP; 1.9 mgFe)	Ca, P, Si, and O	Nano needle-like HA	28 ± 5 nm (width) by 160 ± 30 nm (length)	391 – 1,026 nm
S3	*Powder formula* (67 mgCa; 38 mgP; 1.5 mgFe)	Ca, P, and O	Nano needle-like HA	28 ± 7 nm (width) by 237 ± 119 nm (length)	211 – 1,722 nm
S4	*Powder formula* (82 mgCa; 110 mgP; 1.9 mgFe)	Si, O, Ca, P, and K	Nano SiO_2	Spherical diameter: 7 ± 1 nm	None
S5	*Powder formula* (72 mgCa; 40 mgP; 1.5 mgFe)	Ca, P Ti, Al, Si, S, K,	Spherical nano Ca, P *unknown*	30 – 35 nm 10 – 30 nm	1000 – 2000 nm 1000 – 2000 nm
S6	*Liquid Formula* (78 mgCa; NA mgP; 1.8 mgFe)	Ca, O	Nano TiO_2 Nano Ca, O particles	16 – 530 nm 590 ± 126 nm	None 1,184 – 2,647 nm
R1	Hydroxyapatite reference (American Elements Inc.)	Ca, P, O	Nano needle-like HA	30 ± 5 nm (width) by 131 ± 25 nm (length)	141 – 1,786 nm
R2	Hydroxyapatite reference (Chinese supplier)	Ca, P, O	Nano needle-like HA	30 ± 6 nm (width) by 126 ± 28 nm (length)	220 – 1,322 nm
R3	Hydroxyapatite dietary supplement (NOW, Australia)	Ca, P, O	Spherical HA	Diameter: 20 ± 5 nm	225 – 837 nm

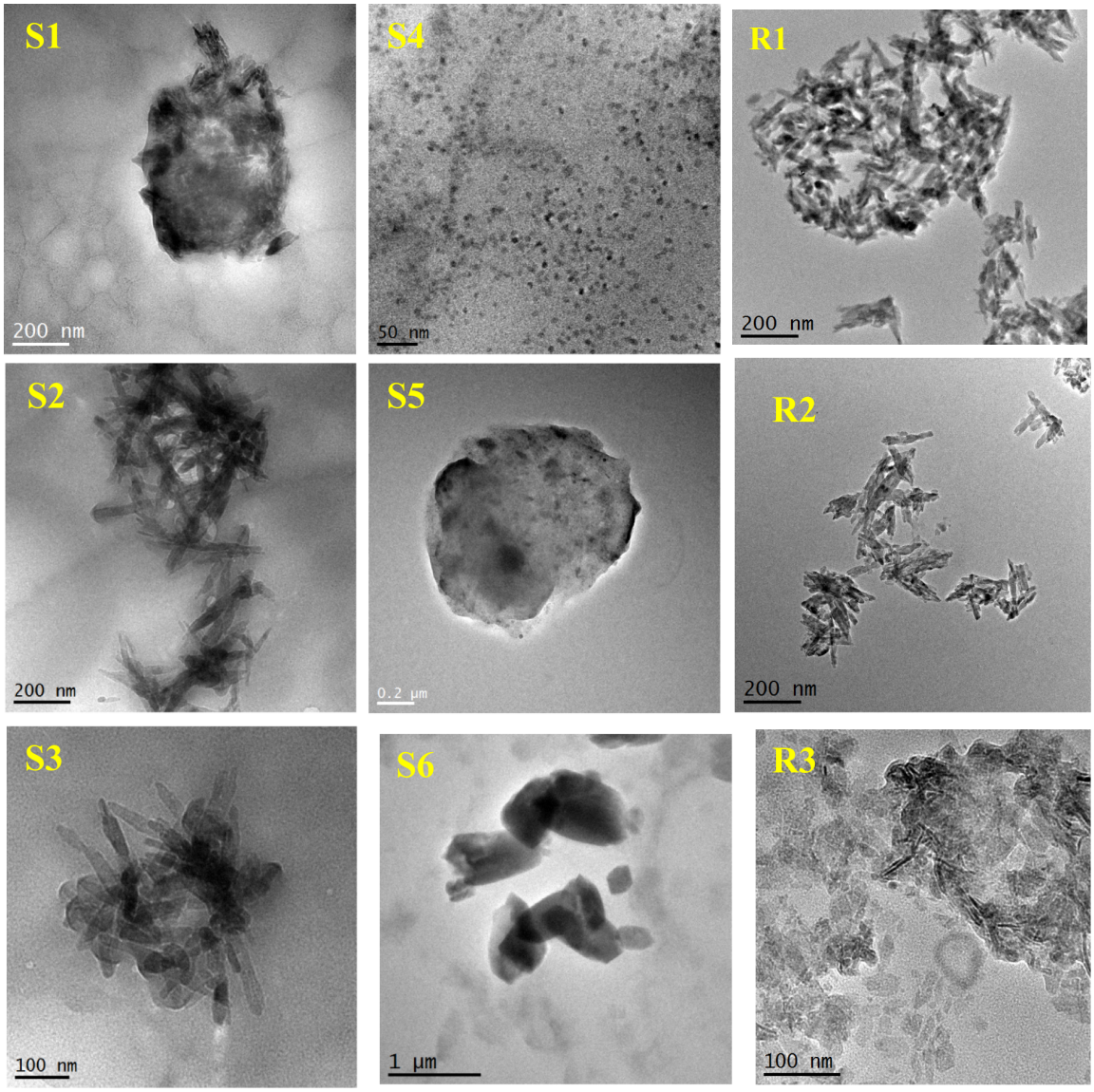

Figure 3.1. Transmission electron micrographs of particles separated from infant formulas (S1-S6) and reference samples (R1-R3). EDX results summarized in Table 3.1.

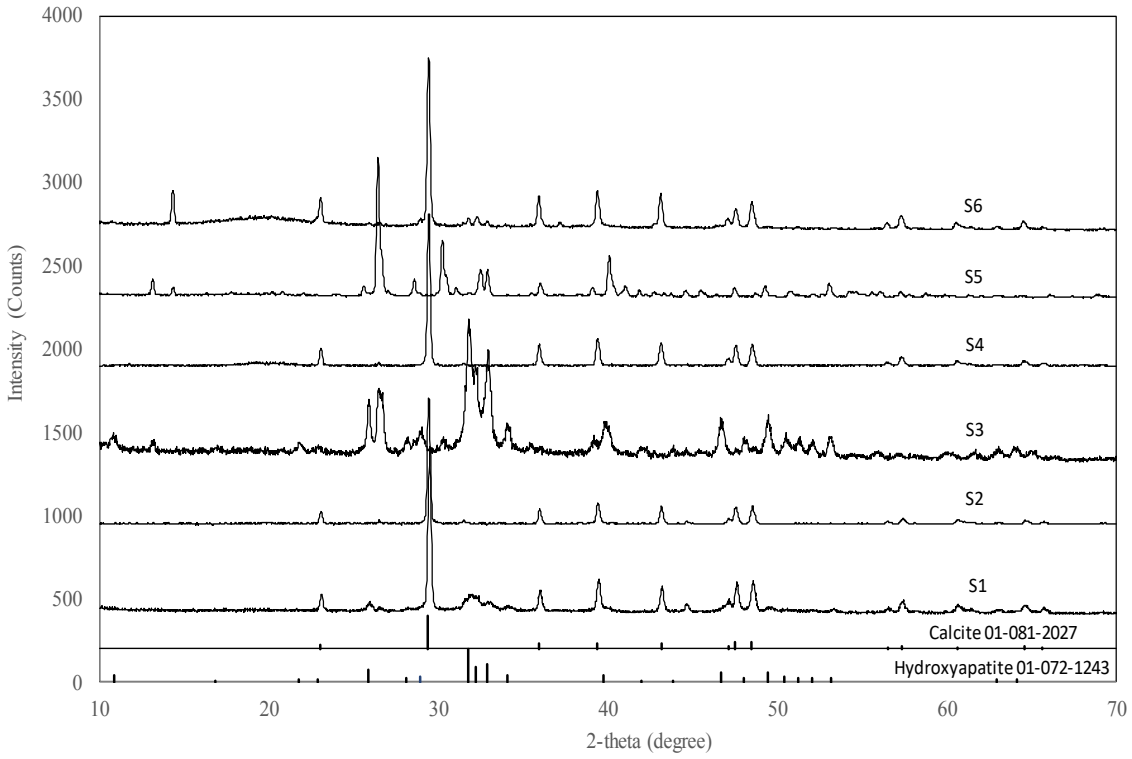

Figure 3.2. X-ray diffraction patterns of dominant mineral content separated from the six infant formula products and reference XRD patterns for calcite and hydroxyapatite.

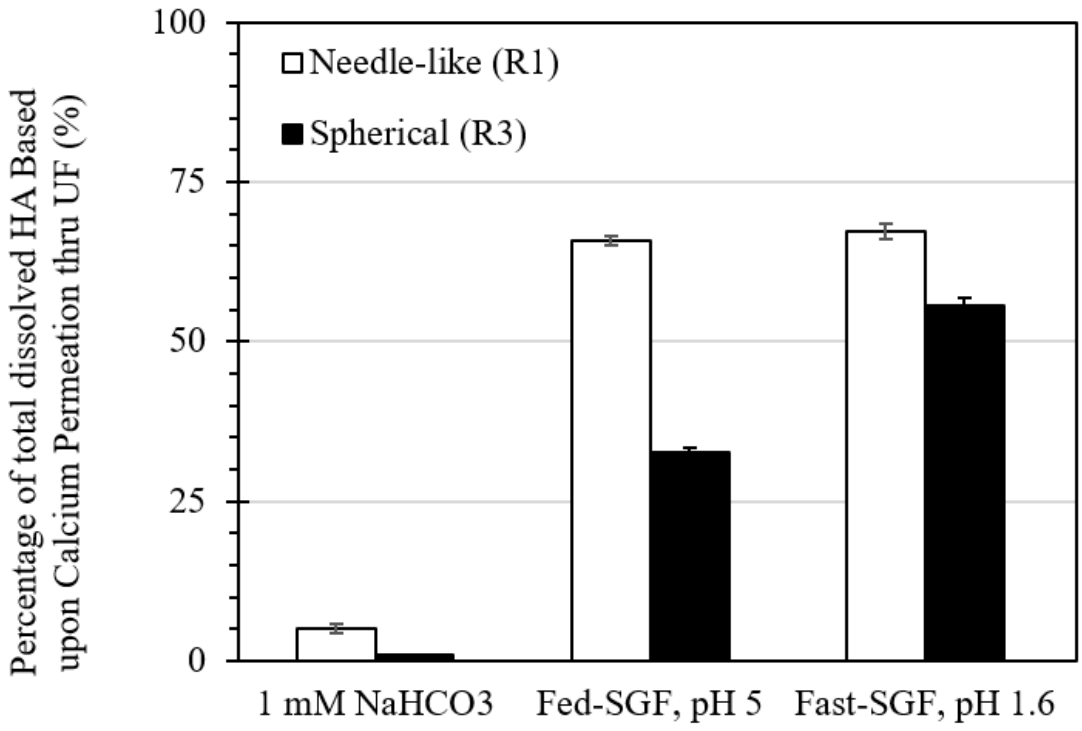

Figure 3.3. Percentage of total dissolved hydroxyapatite in the three simulated biological fluids. Calculations are based upon dissolve calcium (upper plot) and phosphorous (lower plot) measured by ICP-MS in ultrafiltered permeates.

3.6 SUPPLEMENTAL INFORMATION

Background Information on Calcium Phosphate in Foods and Infant Formula Composition

The European Union codes food additives with E-numbers. For example, color additives are all in the E100 series, preservatives are in the E200 series, and anti-oxidants in the E300 series. Because of their versatile use, calcium based additives occur across multiple series, including calcium carbonate for color (E170), preservatives (e.g., calcium sorbate, sulfite), anti-oxidants (calcium ascorbate), emulsifiers (E404 calcium alginate), and other uses (E333 calcium citrate; E327 calcium lactate; E538 calcium oxide; E341 calcium phosphate). Other uses include acid, acidity regulators, anti-caking agents, anti-foaming agents, bulking agents, carriers and carrier solvents, emulsifying salts, firming agents, flavor enhancers, flour treatment agents, foaming agents, glazing agents, humectants, modified starches, packaging gases, propellants, raising agents, and sequestrates.

Calcium phosphate (E341), also known as tricalcium phosphate (TCP), in foods is used as a leavening agent, a polishing material in toothpaste, antioxidant activity promoter and texture stabilizer in canned vegetables, a firming agent or to avoid formation of clumps in foods. Calcium phosphate can be produced through crushing bones or engineered into specific mineral shapes and crystallinity, yet little information is available from manufacturers or suppliers. Unlike other food grade metal-based or metal oxide materials that do not dissolve in water, calcium phosphate is generally referred to as hardly soluble in water but easily dissolved in dilute acids. A large fraction of these other food-grade additives are crystalline and have primary particles below 100 nm in at

least one dimension [26-28, 40, 57, 121]. Hydroxyapatite (HA) can be purchased in various forms, including nano-needle-like crystals that are aggregated together. However, little information exists on the forms of calcium phosphate (i.e., hydroxyapatite) in foods, how to detect it, and whether it undergoes transformations during use or consumption. The scientific community learned many lessons on the significance of nanomaterial transformations with nano-metals (silver, copper, zinc), fullerenes (C_{60} versus hydroxylated C_{60}), and others. Environmental conditions in natural systems (groundwater, lakes, rivers, air, sediments), engineered systems (sewers and wastewater treatment plants), biota (bacteria, fish), and within humans (e.g., protein corona) are critical in understanding the true exposure and toxicity of nanomaterials.

Infant formula is intended to be the sole source of nutrition for infants for the first 12 months leading to heavy regulations requiring sufficient nutrition testing before being marketed. According to Code of Federal Regulations (CFR) Title 21, Volume 2 (21 CFR 107.100), infant formula must have calcium, phosphorus, magnesium, iron, zinc, manganese, copper, iodine, sodium, potassium, and chloride. Although regulation exists on the elements required in the infant formula, guidance lacks on the type or size of the compounds used to provide the nutrients.

Infants receive most of their diet from milk, including the elements calcium and iron [172, 173]. Most infant formulas contain higher concentrations of nutritional elements than those of breast milk because knowledge of how infants utilize these elements is limited [174, 175]. The composition of infant formula is complex [162] and varies by brands [160], including the ratios of calcium to phosphate. Iron fortified infant formulas are also common and recommended at 4 to 12 mg/L [161]. Despite the essential

need of Ca, P, and Fe, little information exists on the mineral forms and sizes for materials in foods generally, and infant formulas specifically. Calcium phosphate is identified on powder infant formulas in the USA, yet little information exists on the mineral form.

Environmental pollutants can occur in infant formula. Lead is carefully measured because of its strong binding capacity with calcium phosphate. Extreme contamination was reported from melamine in infant formula in 2008 which led to rapid development of analytical techniques using conventional strategies and nano-sensing platforms [176-182]. However, there currently is little information or analytical detection strategies for nanomaterials in general, calcium phosphate mineral forms more specifically, for foods (including infant formula).

Additional Method Details

Composition fluids used to evaluate HA dissolution

Four primary solutions were used to conduct HA dissolution tests. First, ultrapure (Millipore) water (DI) without pH adjustment pH ~ 5.8 prior to any HA addition. Chemistries for the other three solutions are summarized in Table SI.3.1. Figure SI.3.1 outlines the step-by-step procedure for conducting the experiments.

Table SI.3.11. Composition of simulated fluid (pH adjusted with HCl/NaOH)

Bicarbonate Buffer Matrix Fluid, pH 8.0	
Composition	**Concentration**
Sodium bicarbonate	1 mM

Simulated Gastric Fluid (SGF), Fasted-State, pH 1.6 [147]	
Composition	**Concentration**
Sodium taurocholate	80 μM
Lecithin	20 μM
Sodium chloride	34.2 mM
Pepsin	0.1 g/L

Simulated Gastric Fluid (SGF), Fed-State, pH 5.0 [147]	
Composition	**Concentration**
Sodium chloride	237 mM
Acetic acid	17.12 mM
Sodium acetate	29.75 mM

1) Media Preparation:
The 1mM NaHCO3 buffer solution and the two gastric fluids were prepared using the recipes found in Table SI.4.1 in clean 1L glass bottles

2) Addition of Materials:
The media solutions were added to clean 50mL plastic centrifuge vials up to 40mL. HAp was weighed out and added in to the media at a 200mg/L concentration

3) Simulated Mixing of Samples:
The media vials were closed and placed in an end-over-end rotational shaker at 45RPM for 2 hours

4) Centrifugation of Samples:
After shaking, 15mL of solution was added immediately to 30kDa ultracentrifugal filters and centrifuged at F=4,000G for 12 minutes.

5) Analysis Preparation of Samples:
The solution that passed through the filters was collected and acidified with 2% HNO_3 for 24 hours. The samples were analyzed using ICP-MS

Figure SI.3.1. Summary of sample preparation for dissolution potential

Ultrafiltration Efficiency Control Experiments

Calcium ion filtering efficiency of 30kDa centrifugal ultrafilters was evaluated by spiking 2 mM of Ca (as $CaCl_2$) to the three media solutions and mixing for 2 hours as in the original dissolution experiments. The concentration of Ca^{2+} spike was selected to be equivalent with the Ca concentration in 200 mg/L HA added in the original experiments. No phosphorous was added, so we could explicitly determine Ca filter efficiency without concern about calcium phosphate solid precipitation. After the 2 hour mixing time, samples were placed in the ultrafilters and centrifuged at F=4,000G for 12 minutes (same conditions as original experiments). Both filtrate and retentate were collected and analyzed by ICP-MS for total dissolved Ca concentration after acidification in 2% nitric acid. Results shown in Table SI.3.2 indicate there were no matrix effects in DI water, 1 mM $NaHCO_3$, or gastric fluids (pH 1.6 or 5.0), and >90% of the spiked Ca^{2+} was recovered. The slightly lower calcium concentrations in 1 mM $NaHCO_3$ may be due to precipitation of calcium carbonate, which was slightly oversaturated under the solution conditions examined (Log SI = 0.4). As expected in ultrafiltration tests, the concentration of calcium in permeate and retentate were equivalent. Parallel experiments with simulated saliva (Table SI.3.3) indicated loss of spiked calcium ion, which we attribute to oversaturation of calcium hydroxyapatite (Log SI ~12). This would precipitate and be trapped on the filter. For this reason, although we conducted experiments with simulated saliva in addition to the fluids listed in Table SI.3.1, we do not report dissolution potential of reference HA in saliva based upon ultrafiltration data.

Table SI.3.2. Ultrafiltration efficiency control tests based upon 2 mM $CaCl_2$ spike. Sample treatment was identical to methodology where 200 mg/L of HA was added (2 hour mixing then centrifuged with F=4000G for 12 minutes)

Matrix description	Ultrafiltration sample	Dissolved Calcium concentration (mM)
DI water	Permeate	1.80
	Retentate	1.86
1 mM $NaHCO_3$	Permeate	1.79
	Retentate	1.81
Gastric Fluid (pH 5)	Permeate	1.96
	Retentate	1.98
Gastric Fluid (pH 1.6)	Permeate	1.77
	Retentate	1.95
Saliva fluid*	Permeate	0.173
	Retentate	0.106

Table SI.3.3. Composition of Simulated Saliva Fluid (SSF) pH 7.4 [147]

Composition	Concentration (g/L)
Unadjusted pH = 7.4	--
Potassium chloride	0.720
Calcium chloride dihydrate	0.220
Sodium chloride	0.600
Potassium phosphate monobasic	0.680
Sodium phosphate dibasic	0.866
Potassium bicarbonate	1.500
Potassium thiocyanate	0.060
Citric acid	0.030

Sample preparation for material characterization

Step-by-step description of sample preparation of electron microscopy samples are summarized in Figures SI.3.2 through SI.3.5. Figure SI.3.6 summarizes the approach to estimate the mass of HA in each infant formula sample. XRD sample preparation is summarized in Figure SI.3.7.

1) Addition of Materials:
First 0.15 grams of sample was added to 40mL of nanopure water in a 50mL plastic centrifuge tube at room temperature (296K). The pH of the solution was 6.68. The samples remained within the centrifuge tube through the entire sample preparation process.

2) Dispersion:
The sample was inverted by hand for 2 minutes to disperse the infant formula.

3) Sonication:
The sample was added to a sonication bath (Branson Ultrasonic Bath, Emerson) with a power output of 80 watts/L for 30 minutes. The temperature of the solution was 300K after 30 minutes of sonication and had a pH of 6.91.

4) Centrifugation:
The solution was then centrifuged at 14,000 G for 12 minutes, and had a temperature of 305K and a pH of 6.94 after centrifugation

5) Decantation:
The top organic phase was decanted off the top by pouring out the solution by hand and discarded, leaving a solid pellet at the bottom of the centrifuge tube.

6) Resuspension:
The pellet was re-suspended in 20mL of water at room temperature (297K) and the solution had a pH of 7.51.

7) Dispersion:
The sample was inverted by hand for 2 minutes to disperse the infant formula.

8) TEM grid:
A TEM grid was placed on a weigh boat, 50 μL of the solution was pipetted onto the TEM grid, a Kimwipe was placed to cover the weigh boat containing the sample to prevent contamination from the air, and was allowed to dry overnight.

Figure SI.3.2. Summary of TEM sample preparation

1) SEM Stub:
A 1 cm by 1 cm piece of double sided carbon tape was placed on to an aluminum SEM stub.

2) Sample:
Infant formula was placed on a weigh boat.

3) Attachment of Sample:
The aluminum stub with carbon tape was pushed into the infant formula, allowing the infant formula stick to the carbon tape.

4) SEM Analysis:
The aluminum stub with infant formula attached to the carbon tape was placed inside the SEM (XL30 ESEM with EDX) for analysis.

Figure SI.3.3 Summary of sample preparation for SEM of infant formula

1) Addition of Materials:
First, 0.15 grams of sample 3 was added to 40mL of nanopure water in a 50mL plastic centrifuge tube at room temperature (296K). The pH of the solution is 6.88.

2) Dispersion:
The solution was inverted by hand for 2 minutes until the powder sample was dispersed into the nanopure water.

3) Sonication:
The solution was added to a sonication bath with a power output of 80 watts/L for 30 minutes. The temperature of the solution was 300K after 30 minutes of sonication and had a pH of 6.84.

4) Centrifugation 1:
The solution was then centrifuged at 14,000 G for 12 minutes, and had a temperature of 305K and a pH of 6.91 after centrifugation

5) Decantation 1:
The top organic phase was decanted off the top by pouring the solution into a new 50mL centrifuge vial. The solid pellet at the bottom of the other centrifuge tube was discarded.

6) Centrifugation 2:
The solution was then centrifuged at 14,000 G for 12 minutes, and had a temperature of 305K and a pH of 6.91 after centrifugation

7) Decantation 2:
The top organic phase was decanted off the top by pouring the solution into a new 50mL centrifuge vial. The solid pellet at the bottom of the other centrifuge tube was discarded.

8) Centrifugation 3:
The solution was then centrifuged at 14,000 G for 12 minutes, and had a temperature of 305K and a pH of 6.91 after centrifugation

9) Decantation 3:
The top organic phase was decanted off the top by pouring the solution into a new 50mL centrifuge vial. The solid pellet at the bottom of the other centrifuge tube was discarded.

10) Addition of Material:
Next, 0.004 grams of calcium chloride, and 0.001 grams of sodium monophosphate was added to the organic phase (mole ratio of 1.67, optimum ration of Ca to P for HA synthesis [1]

11) Sonication:
The solution was added to a sonication bath with a power output of 80 watts/L for 30 minutes. The temperature of the solution was 300K after 30 minutes of sonication and had a pH of 6.84.

12) Centrifugation:
The solution was then centrifuged at 14,000 G for 12 minutes, and had a temperature of 305K and a pH of 6.91 after centrifugation

13) Decantation:
The top organic phase was decanted off the top by pouring out the solution by hand, leaving a solid pellet at the bottom of the centrifuge tube.

14) Resuspension:
The pellet was re-suspended in 20mL of water at room temperature (297K). The solution was inverted by hand for 2 minutes.

15) TEM Grid Preparation
A TEM grid was placed on to a weigh boat, 50 µL of the solution was pipetted onto the TEM grid, a Kim wipe was placed to cover the weigh boat containing the sample to prevent contamination from the air, and allowed to dry overnight.

Figure SI.3.4. Summary of TEM sample preparation for extracting organic phase and adding $CaCl_2$ and Na_2HPO_4 salts

1) Addition of Materials:
First, 0.15 grams of sample 4 was added to 40mL of nanopure water in a 50mL plastic centrifuge tube at room temperature (296K). The pH of the solution is 6.88.

2) Addition of Material:
Next, 0.004 grams of calcium chloride, and 0.001 grams of sodium monophosphate was added to the organic phase (mole ratio of 1.67, optimum ration of Ca to P for HA synthesis [1]

3) Sonication:
The solution was added to a sonication bath with a power output of 80 watts/L for 30 minutes. The temperature of the solution was 300K after 30 minutes of sonication and had a pH of 6.84.

4) Centrifugation:
The solution was then centrifuged at 14,000 G for 12 minutes, and had a temperature of 305K and a pH of 6.91 after centrifugation

5) Decantation:
The top organic phase was decanted off the top by pouring out the solution by hand, leaving a solid pellet at the bottom of the centrifuge tube.

6) Resuspension:
The pellet was re-suspended in 20mL of water at room temperature (297K). The solution was inverted by hand for 2 minutes.

7) TEM Grid Preparation
A TEM grid was placed on to a weigh boat, 50 µL of the solution was pipetted onto the TEM grid, a Kimwipe was placed to cover the weigh boat containing the sample to prevent contamination from the air, and allowed to dry overnight.

Figure SI.3.5. Summary of TEM sample preparation adding $CaCl_2$ and Na_2HPO_4 salts to infant formula for TEM analysis

1) Addition of Materials:
First, the recommended dosing of infant formula, 6.02 grams, was added to the corresponding 40mL of nanopure water in a 50mL plastic centrifuge tube at room temperature (296K). The pH of the solution was 6.82. The samples remained within the centrifuge tube through the entire sample preparation process.

2) Dispersion:
The solution was inverted by hand for 2 minutes until the powder sample was dispersed into the nanopure water.

3) Sonication:
The solution was added to a sonication bath with a power output of 80 watts/L for 30 minutes. The temperature of the solution was 300K after 30 minutes of sonication and had a pH of 6.84.

4) Centrifugation:
The solution was then centrifuged at 14,000 G for 12 minutes, and had a temperature of 305K and a pH of 6.91 after centrifugation

5) Decantation:
The top organic phase was decanted off the top by pouring out the solution by hand and discarded, leaving a solid pellet at the bottom of the centrifuge tube.

6) Resuspension:
The pellet was re-suspended in 40mL of water at room temperature (297K) and inverted by hand for 2 minutes to disperse the infant formula.

7) Centrifugation:
The solution was then centrifuged at 14,000 G for 12 minutes, and had a temperature of 305K and a pH of 6.91 after centrifugation

8) Decantation:
The top organic phase was decanted off the top by pouring out the solution by hand and discarded, leaving a solid pellet at the bottom of the centrifuge tube.

9) Resuspension:
The pellet was re-suspended in 40mL of water at room temperature (297K) and inverted by hand for 2 minutes to disperse the infant formula.

10) Centrifugation:
The solution was then centrifuged at 14,000 G for 12 minutes, and had a temperature of 305K and a pH of 6.91 after centrifugation

11) Decantation:
The top organic phase was decanted off the top by pouring out the solution by hand and discarded, leaving a solid pellet at the bottom of the centrifuge tube.

12) Weighing dried pellet:
The resulting pellet was removed and vacuum freeze dried (FreeZone Freeze Dry System, Labconco). The resulting powder was weighed.

Figure SI.3.6. Summary of sample preparation to calculate HA quantity

1) Addition of Materials:
First, the recommended dosing of infant formula, 6.02 grams, was added to the corresponding 40mL of nanopure water in a 50mL plastic centrifuge tube at room temperature (296K). The pH of the solution was 6.82. The samples remained within the centrifuge tube through the entire sample preparation process.

2) Dispersion:
The solution was inverted by hand for 2 minutes until the powder sample was dispersed into the nanopure water.

3) Sonication:
The solution was added to a sonication bath with a power output of 80 watts/L for 30 minutes. The temperature of the solution was 300K after 30 minutes of sonication and had a pH of 6.84.

4) Centrifugation:
The solution was then centrifuged at 14,000 G for 12 minutes, and had a temperature of 305K and a pH of 6.91 after centrifugation

5) Decantation:
The top organic phase was decanted off the top by pouring out the solution by hand and discarded, leaving a solid pellet at the bottom of the centrifuge tube.

6) Resuspension:
The pellet was re-suspended in 40mL of water at room temperature (297K) and inverted by hand for 2 minutes to disperse the infant formula.

7) Centrifugation:
The solution was then centrifuged at 14,000 G for 12 minutes, and had a temperature of 305K and a pH of 6.91 after centrifugation

8) Decantation:
The top organic phase was decanted off the top by pouring out the solution by hand and discarded, leaving a solid pellet at the bottom of the centrifuge tube.

9) Resuspension:
The pellet was re-suspended in 40mL of water at room temperature (297K) and inverted by hand for 2 minutes to disperse the infant formula.

10) Centrifugation:
The solution was then centrifuged at 14,000 G for 12 minutes, and had a temperature of 305K and a pH of 6.91 after centrifugation

11) Decantation:
The top organic phase was decanted off the top by pouring out the solution by hand and discarded, leaving a solid pellet at the bottom of the centrifuge tube.

12) Sample mounting:
The resulting wet paste was mounted onto zero-background XRD holder for XRD analysis with Siemens D5000

Figure SI.3.7. Summary of sample preparation for XRD analysis

Results and Discussion Points

Electron microscopy results and demonstration that needle-like HA observed in samples were not artifacts of sample preparation

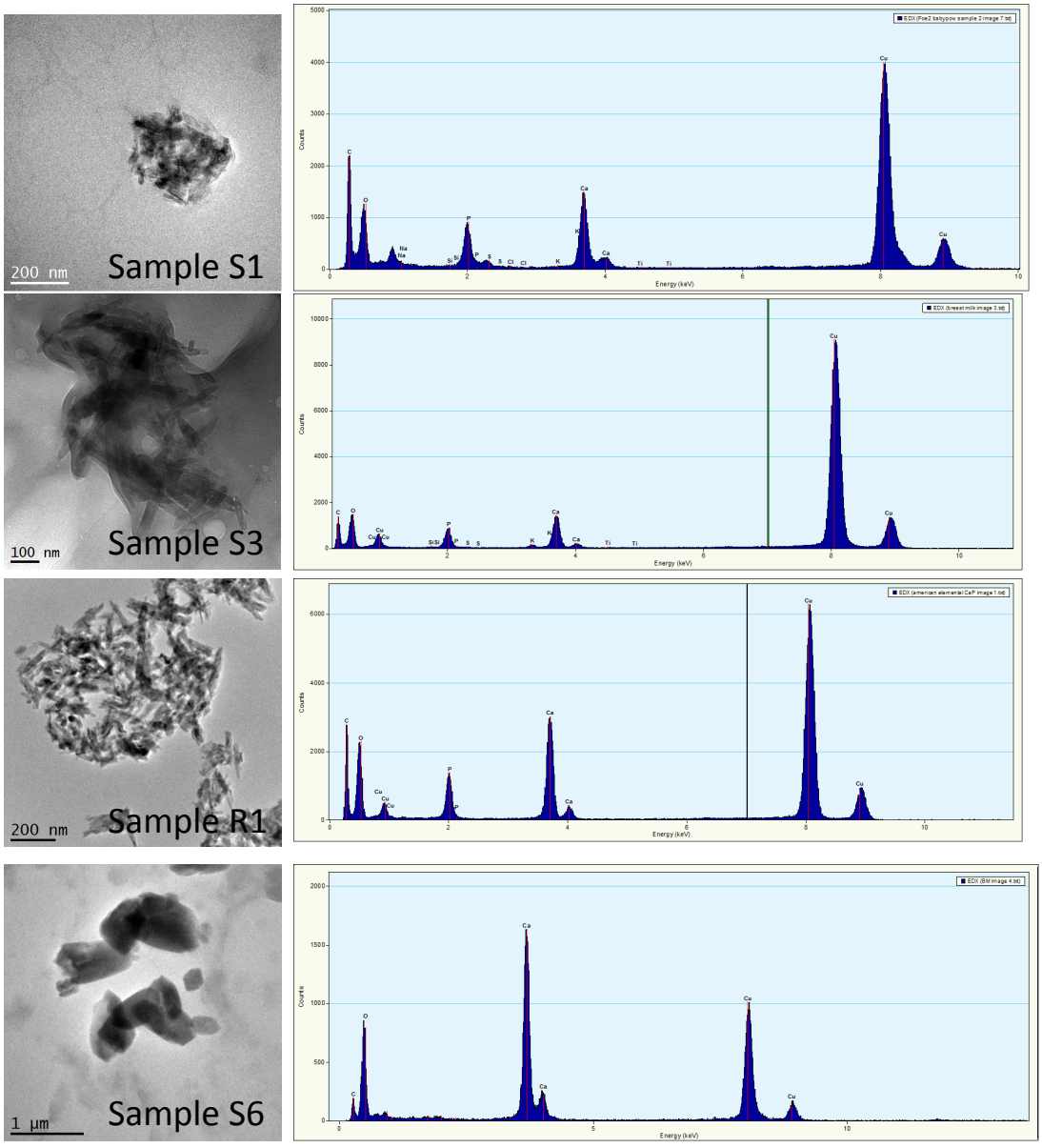

Figure SI.3.8.A TEM and EDX on Calcium Containing Colloidal Material

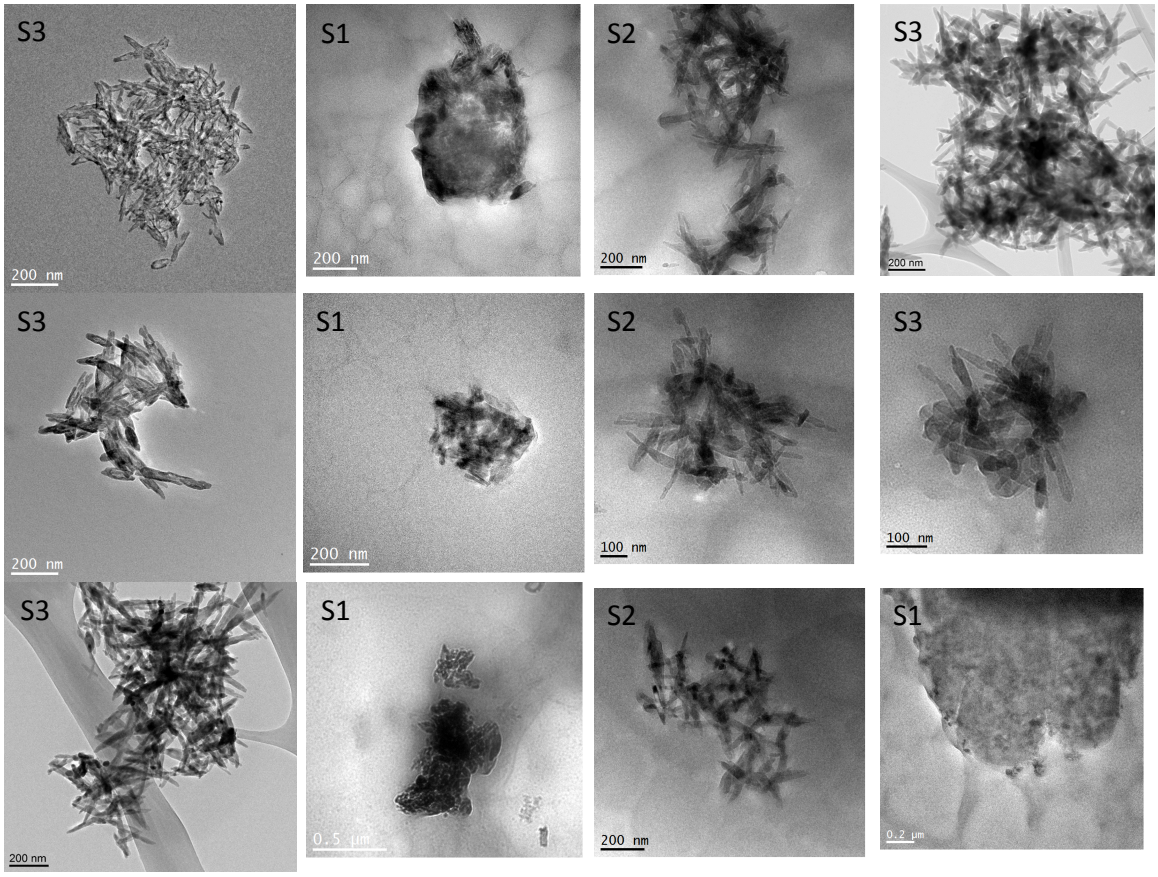

Figure SI.8.B. Additional TEM images from infant formula

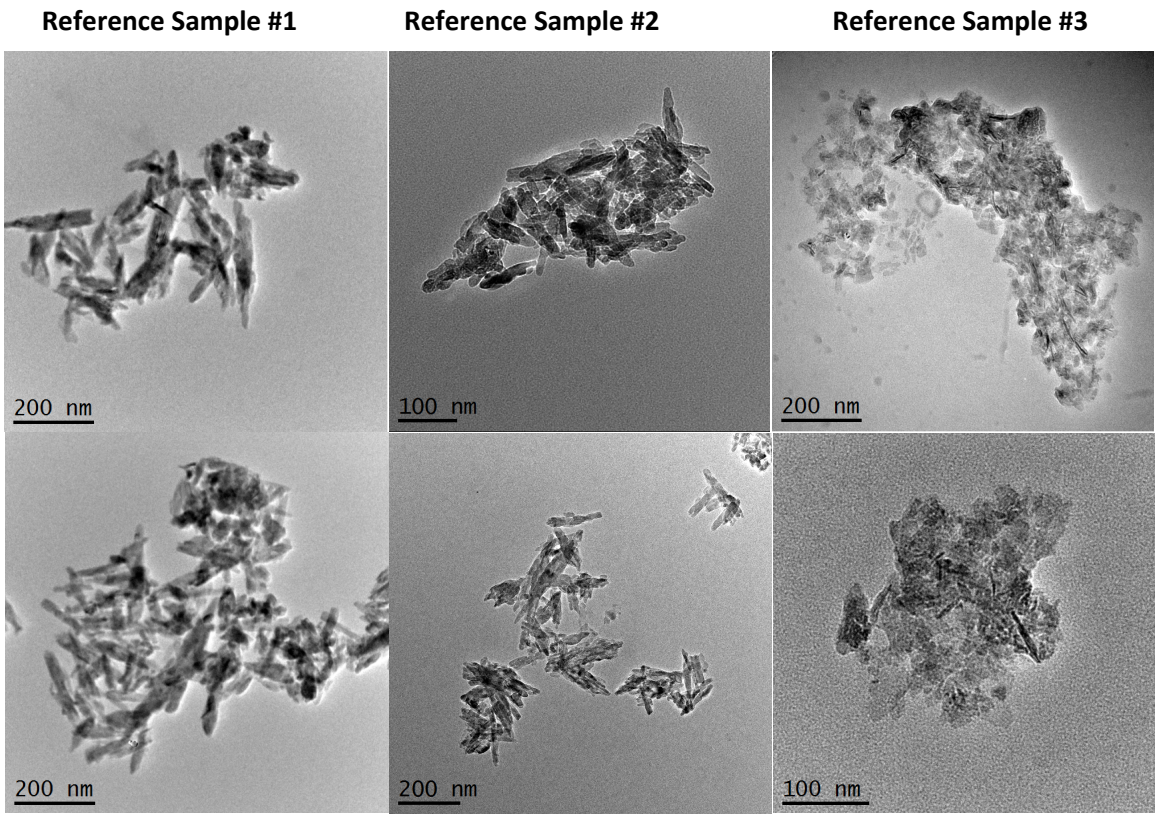

Figure SI.3.9. TEM of two reference samples containing nearly all needle-like HA (#1 and #2) and a third reference material containing mostly non-needle-like and spherical HA (#3).

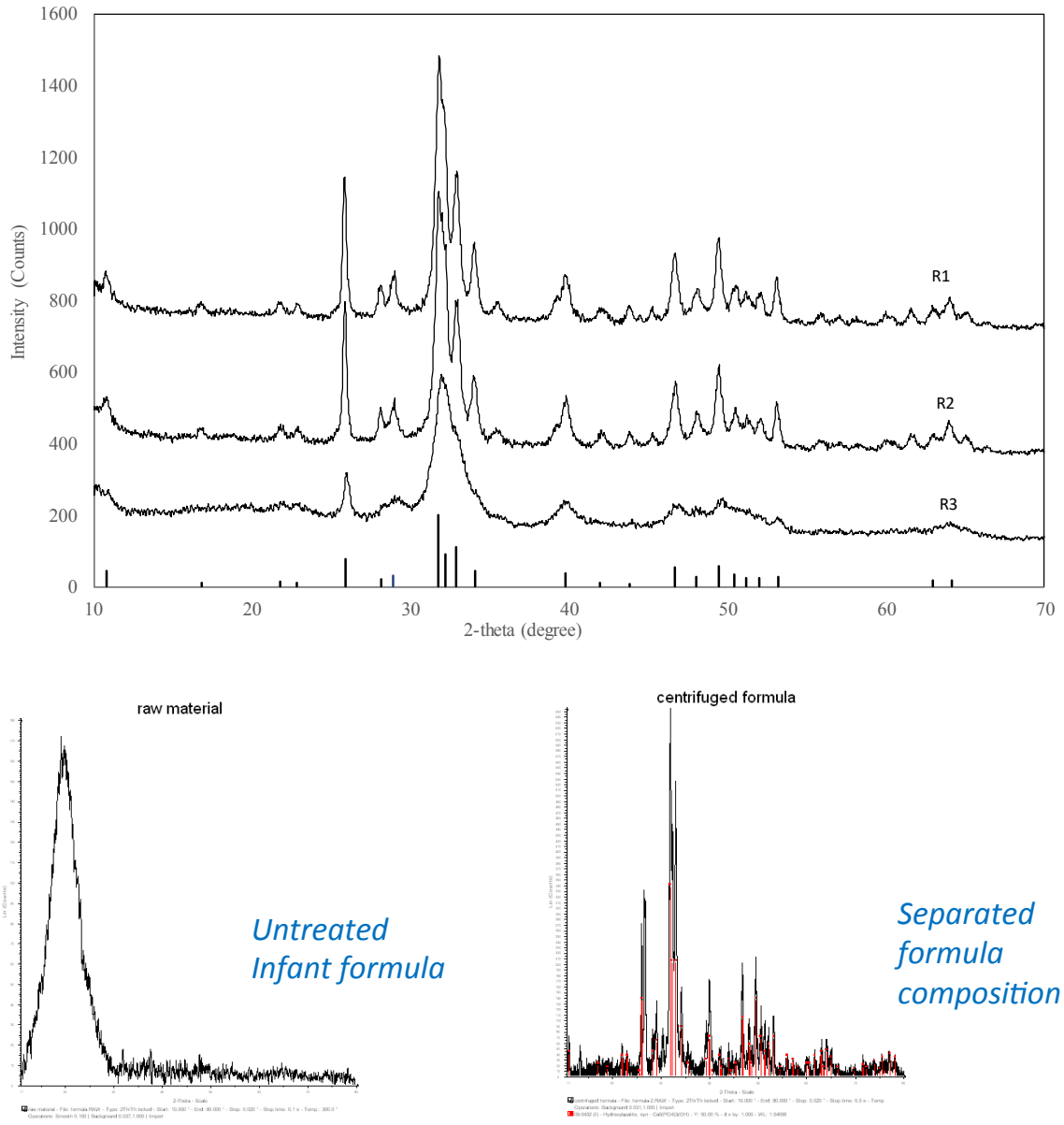

Figure SI.3.10. X-ray diffraction patterns of (A) three hydroxyapatite standard reference materials used to simulate hydroxyapatite nanoparticles in infant formula and reference XRD pattern for hydroxyapatite, and (B) powder infant formula (S3) versus centrifuged pellet from S3.

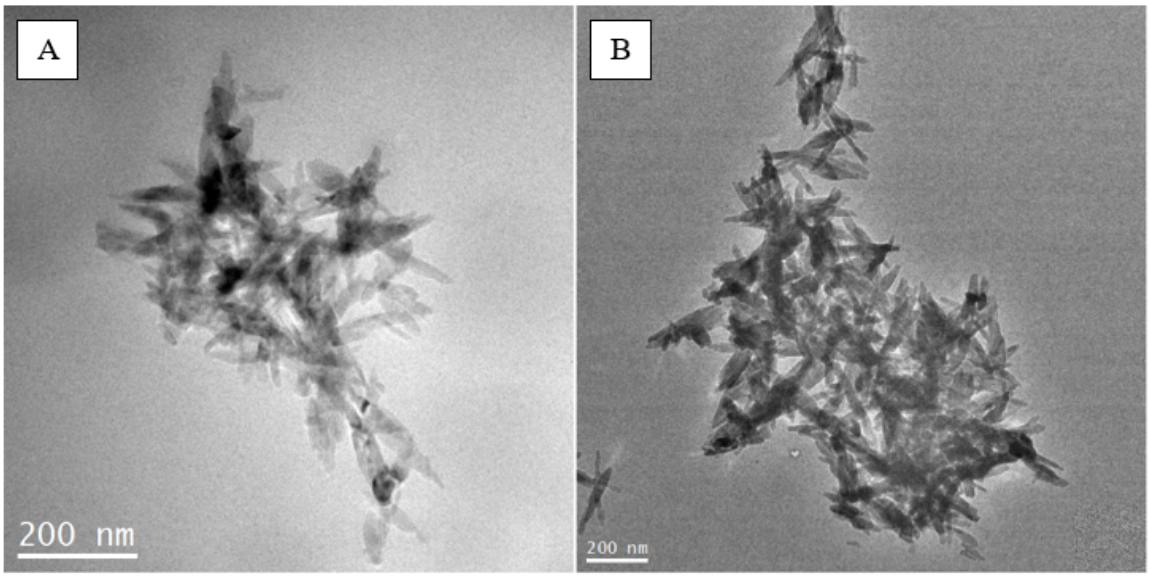

Figure SI.3.11. TEM of sample S3 following sample preparation outlined in Figure SI.3.2 but (A) without sonication versus (B) with sonication. Needle-like HA is present in both images and demonstrates sonication did not induce formation of this structure. Seven additional results are presented (see table below). The overall conclusions of this work support the additional finding that needle-like HA are present in some of the infant formula, and are not artifacts of TEM sample preparation. Step-by-step methods are described in Figures SI.3.1 through SI.3.5. A summary of the results are now included in the supplemental results section (and Table SI.3.4). Primary conclusions from the seven experiments include the following:

1. 0.15 gram of sample S3 was placed in 40 mL and sonicated and prepared for TEM following the original method in the paper. TEM found needle-like HA.
2. Same as #1 but without sonication. TEM found needle-like HA, and we can conclude that sonication did not form need-like HA.
3. Same as #2 but we excluded centrifugation and just added 20 uL of sample onto the TEM grid. TEM found needle-like HA. Therefore, neither sonication nor centrifugation lead to any artifacts.
4. Here the infant formula was prepared by adding the volume/mass to water ratio specified on the infant formula packaging as the "recipe" to prepare the liquid infant formula. Then we applied a completely different centrifugation method presented on-line by EAWAG (https://www.youtube.com/watch?v=PplBlJ7zCCA) after a 100x dilution of the sample. TEM found needle-like HA. Using demonstrates the solid to liquid ratio does not lead to needle-like HA artifacts.
5. 0.15 gram of sample S3 was placed in 40 mL and sonicated/centrifuged as outlined in the original manuscript. The solid pellet was removed. Then we added dissolved calcium chloride and sodium phosphate salts into the supernatant, where any organic polymers would still be present. The concentrations of these added salts were based upon the mass of solids removed as the pellet. The sample was re-sonicated and centrifuged. The small pellet was then analyzed by TEM.

Needle-like HA was *not* detected. This demonstrates that needle-like HA was not generated as an artifact from dissolve Ca/P in the infant formula.

6. Same as #5 above but instead of spiking calcium chloride and sodium phosphate salts into sample S3 (which contained needle-like HA), the test was performed using sample S6 (did not contain needle-like HA, but contained complex organics, etc. in the infant formula). Sample S6 was placed in 40 mL and sonicated/centrifuged as outlined in the original manuscript. The solid pellet was removed. Then we added dissolved calcium chloride and sodium phosphate salts into the supernatant, where any organic polymers would still be present. The concentrations of these added salts were based upon the mass of solids removed as the pellet. The sample was re-sonicated and centrifuged. The small pellet was then analyzed by TEM. Needle-like HA was *not* detected. This demonstrates that needle-like HA was not generated as an artifact from dissolve Ca/P in the infant formula.
7. A 1cm by 1cm piece of double sided carbon tape was placed on to an aluminum SEM stub. Infant formula (sample S3 which contained needle-like HA) was placed in a plastic weighing boat. The aluminum stub with carbon tape was pushed into the infant formula, allowing the dry powder to stick to the carbon tape. The aluminum stub with infant formula powder tape was placed inside the SEM (XL30 ESEM with EDAX) for analysis. No need-like HA was observed. This is attributed to presence of large amounts of other salts and organic materials which dominate by weight over needle-like HA. This was the original motivation for conducting TEM analysis on suspended liquid sample which has the ability, during sample preparation, to separate salts and dissolved organics from nano- and larger scale particles.

Table SI.3.4. Summary of experiments to validate that needle-like HA is not an artifact from electron microscopy sample preparation

Sample	Sonic-ation	Centrifugation	TEM Sample Preparation	Other	Conclusion	TEM Image
1) Original Method	30 min at 80 watts	15,000 G for 15 minutes	-Resuspend pellet into 20 mL of water -20 µL pipetted on to TEM grid	-0.15 grams in 40 ml of water	Presence of Nano needle-like HA	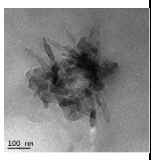
2) Original without sonication	No sonic-ation	15,000 G for 15 minutes	-Resuspend pellet into 20 mL of water -20 µL pipetted on to TEM grid	-0.15 grams in 40 ml of water	Presence of Nano needle-like HA	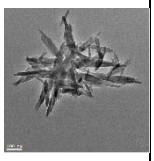
3) Original without sonication or centrifugation	No sonic-ation	No centrifugation	-20 µL pipetted directly on to TEM grid	-0.15 grams in 40 ml of water	Presence of Nano needle-like HA	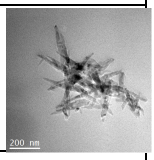
4) EAWAG Method	No sonic-ation	4050 G for 4 hours	-TEM at bottom of vial - liquid is pipetted out of vial and TEM grid is removed for analysis	-6 grams in 40 mL of water (instructions on box) -100X dilution	Presence of Nano needle-like HA	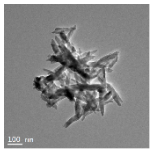
5) Ca/P additive to HA extracted sample 3	30 min at 80 watts	15,000 G for 15 minutes	-Resuspend pellet into 20 mL of water -20 µL pipetted on to TEM grid	-0.15 grams of infant formula into 40 mL of water -Supernatant from centrifugation step was removed and spiked with $CaCl_2H_2O$ and Na_2HPO_4	No Nano needle-like HA	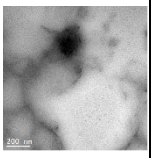
6) Ca/P additive to sample 6 (sample absent of nano needle-like HA)	30 min at 80 watts	15,000 G for 15 minutes	-Resuspend pellet into 20 mL of water -20 µL pipetted on to TEM grid	-0.15 grams in 40 mL of water and spiked with $CaCl_2H_2O$ and Na_2HPO_4	No Nano needle-like HA	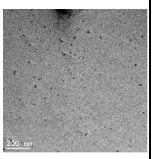

7) SEM analysis of dry powder	No addition to liquid. No sonication. No centrifugation. Sample S3 applied as dry powder to carbon tape on SEM stub	No nano needle-like HA observed	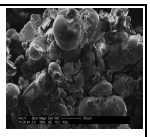

Scanning Electron Microscopy Imaging of Infant Formula and Hydroxyapatite Reference Material

Two samples, Infant formula (sample 3) and HA reference material 1, were analyzed by scanning electron microscopy paired with energy dispersive X-ray spectroscopy (EDX) as dry powders with minimal sample preparation. To prepare the samples, the infant formula and HA reference material were poured into weigh boats. Double sided tape was placed onto an aluminum SEM stub and lightly pushed by hand into the powder samples to adhere the samples to the carbon tape. The samples were sputter coated with Au for 120 seconds (~10nm thick coating) to prevent charging by the electron SEM beam and placed within the SEM (FEI/Philips XL-30 Field Emission ESEM). Needle-like HA materials were characterized in the HA reference material 1 by SEM as shown in Figure SI.3.12-3.14 (average length: 156 ± 43, width: 35 ± 7nm). Sample 3 was analyzed for the presence of needle-like HA as shown in Figure SI.3.15-3.17 (average diameter: 33 ± 28 μm). The abundance of carbon substances in sample 3 prevented meaningful analysis of the sample by SEM. Carbon particulate (figure SI.3.16) was observed in the dry infant formula (diameter: 187 – 499 nm); however, needle-like HA particles were not observed. The needle-like HA is suspected to be within the micron sized carbon compounds. We conclude that the salt and organic matrix that comprises the infant formula prevents detection of the needle-like HA in the powder, and that

separation of the salts and organic matrix is required to detect the needle-like HA which other parts of this paper suggest represents < 1% of the total mass of the powder formula on a mass basis.

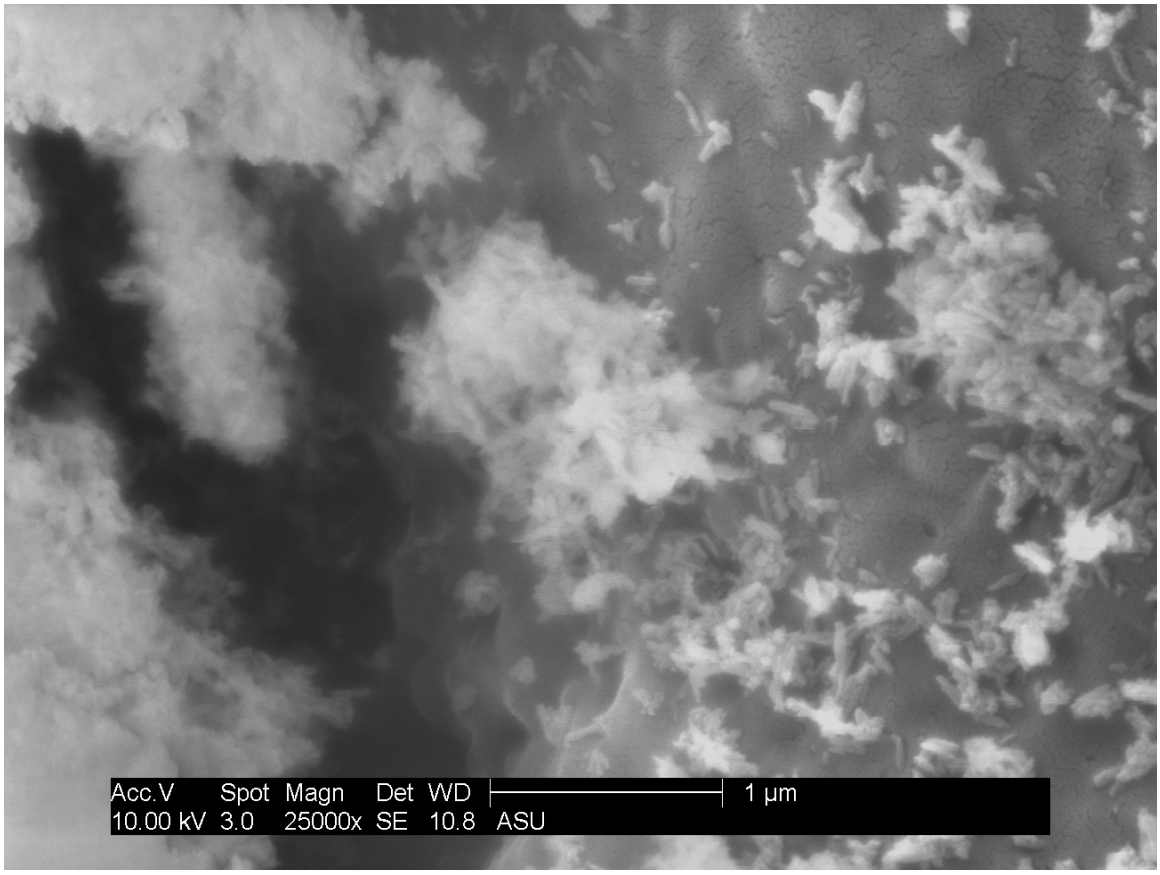

Figure SI.3.12. SEM image of HA reference material 1. Light substances are needle-like HA. The dark background is the carbon tape

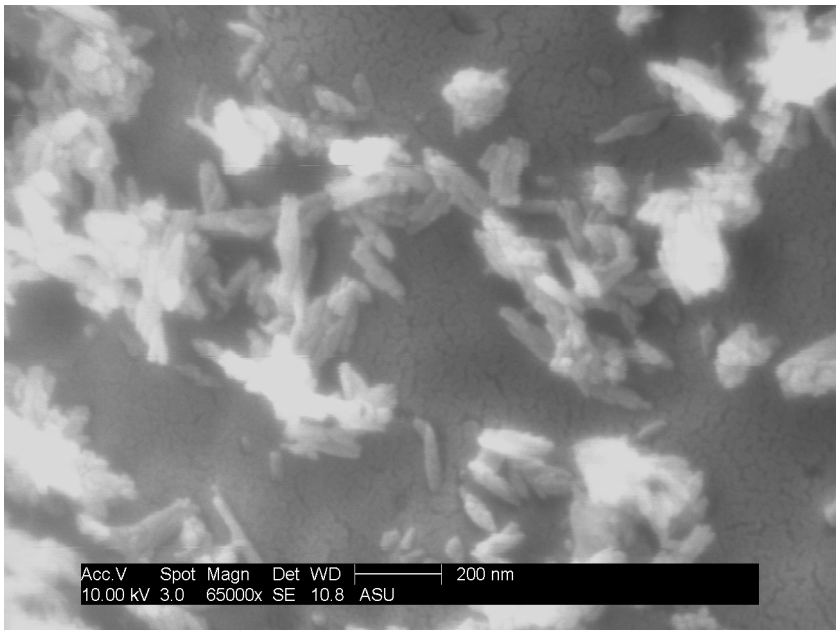

Figure SI.3.13. SEM of needle-like HA reference 1. Background is the carbon tape

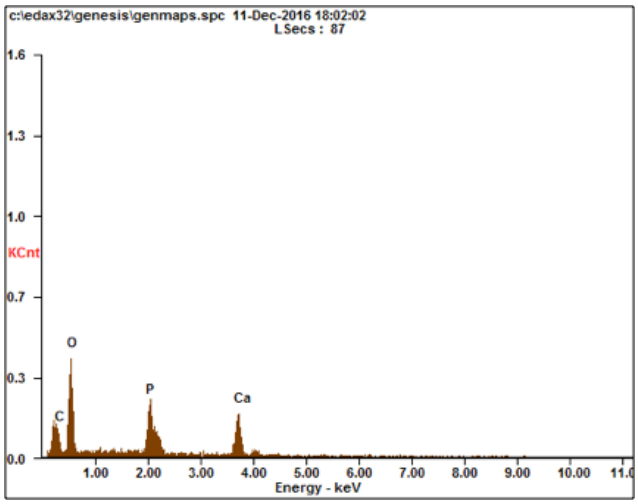

Element	*Wt%*	*At%*
CK	15.32	25.79
OK	38.49	48.63
PK	15.39	10.04
CaK	30.80	15.54
Matrix	Correction	ZAF

Figure SI.3.14. EDX of needle-like HA (confirmed presence of calcium, oxygen, and phosphorous) found in image SI.13.

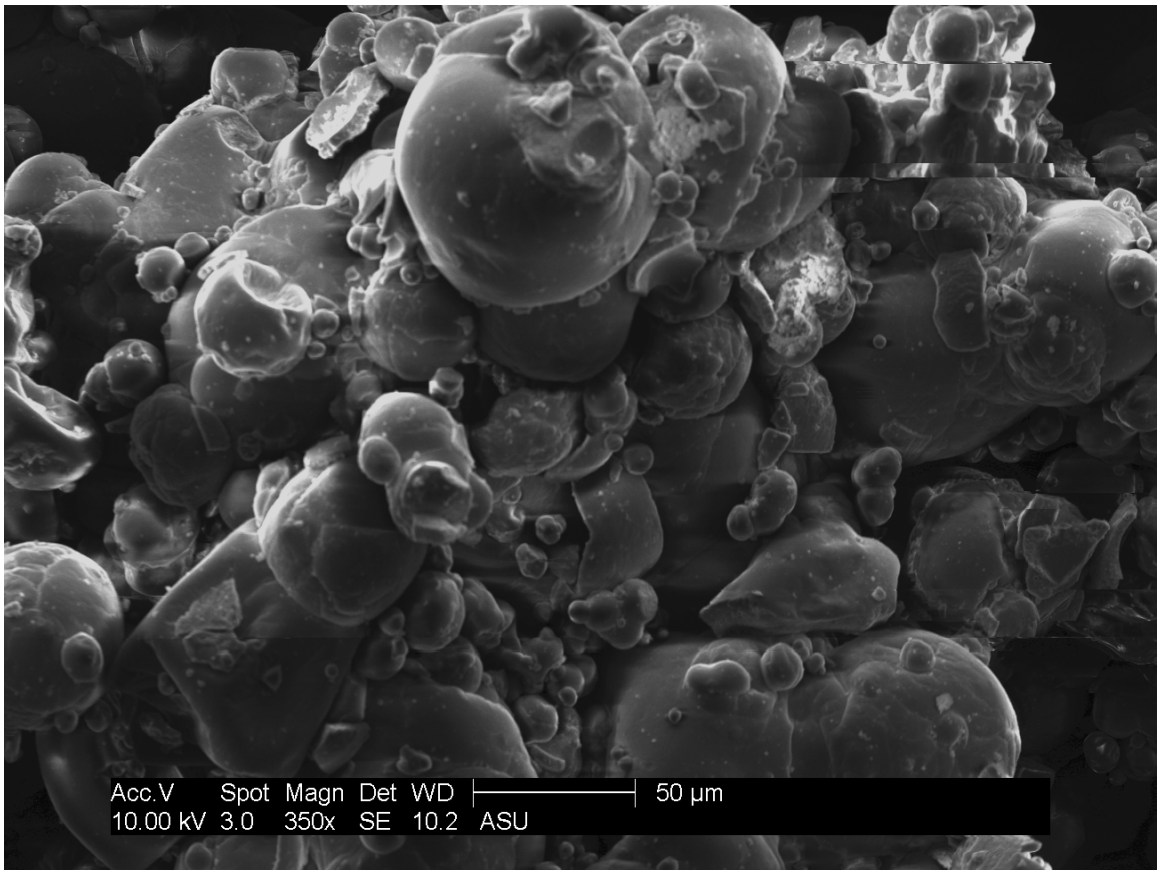

Figure SI.3.15. SEM of dry infant formula sample 3

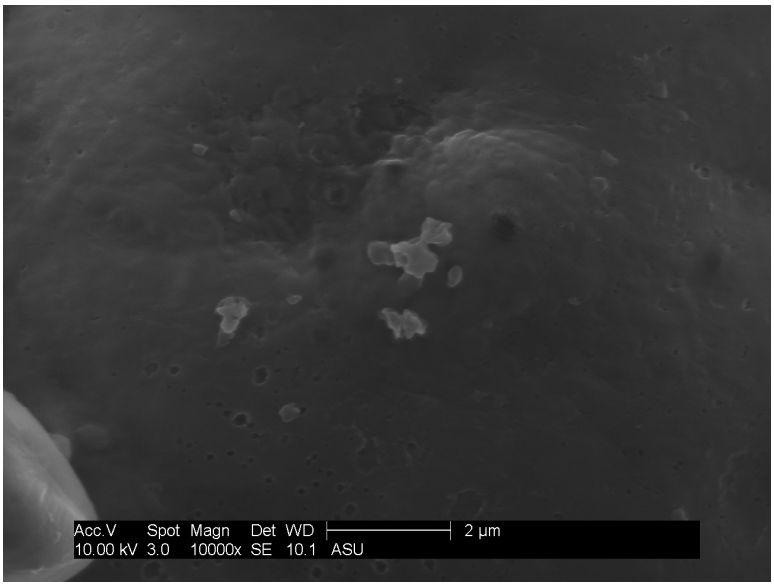

Figure SI.3.16. SEM of dry infant formula 3

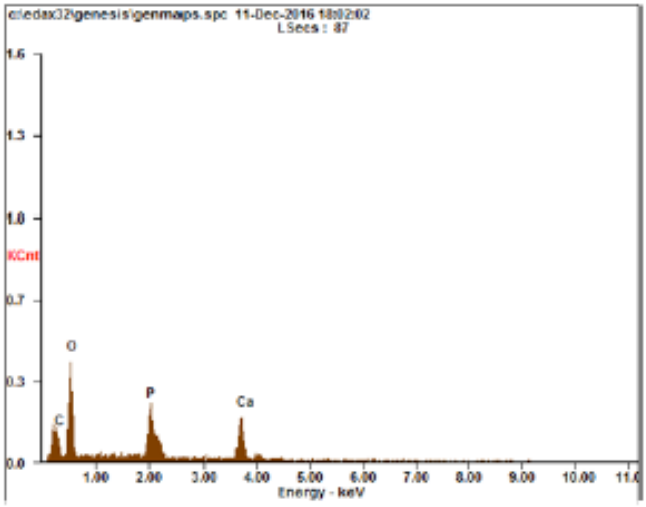

Element	Wt%	At%
CK	15.32	25.79
OK	38.49	48.63
PK	15.39	10.04
CaK	30.80	15.54
Matrix	Correction	ZAF

Figure SI.3.17. EDX characterizing the presence of carbon, oxygen and gold in Figure SI.3.16. Gold peaks are from the goal sputtering.

Reference HA Dissolution Experiments: Phosphate Permeation through UF Plus Visual and Turbidity Changes

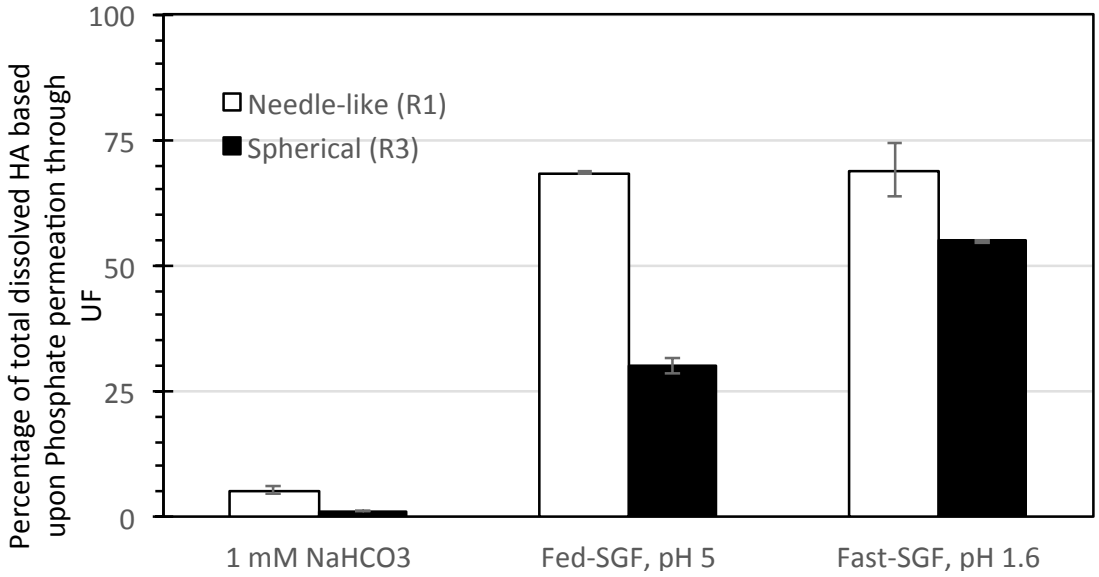

Figure SI.3.18. Percentage of total dissolved hydroxyapatite in the three simulated fluids based upon percentage of phosphate in the ultrafilter permeate relative to the added mass (100 mg HA/L and measured by ICP-MS) present as phosphate.

In addition to measuring calcium and phosphate during ultrafiltration experiments, other measurements with ultrafiltration were also conducted. Within 30 minutes of the end of mixing, the remaining unfiltered samples were analyzed for turbidity (DRT-15CE Turbidimeter), mean size, and polydispersity. A Primetime Turbidity Standard of 0.02NTU (Lot 21202) was used and triplicate turbidity measurements were performed in 4 second intervals. Hydrodynamic diameter was determined by Phase Analysis Light Scattering [PALS] (ZetaPALS, Brookhaven Instruments Corp., NY, USA).

Turbidity did not differ after four hours in the 1 mM bicarbonate solution (pH=8.3) with R1 or R3 suggesting the reference materials did not dissolve. Figure SI.3.19 shows the turbidity in this solution and is the baseline for comparison against HA exposure in other liquids. These results are consistent with the calcium and phosphate UF permeation results.

Turbidity with the spherical HA (R3) did not differ among the simulated biological fluids from the baseline sodium bicarbonate solution. This suggests that only a portion of the HA may readily dissolve, and TEM images suggest the presence of both crystalline and non-crystalline materials. In contrast to these results, turbidity decreased by >90% for the needle-like HA reference materials (R1 and R2) in the two gastric fluids and increased slightly in the shorter exposure period to simulated saliva. These turbidity measurements were consistent with visual assessment of relative "cloudiness", which only decreased for R1 and R2 in the gastric fluids (see photos in Figure SI.3.21). There was no visual precipitation of sediment in any of the vials suggesting the materials dissolved rather than destabilized resulting in the decreased turbidity. Although the turbidity change were not quantified over reaction time, qualitative visual observations indicated near complete dissolution of R1 and R2 within minutes, whereas the spherical HA reference (R3) remained cloudy throughout the experiment.

Mean particle size and polydispersity were also measured by phase-analysis light scattering (PALS) on the same samples as turbidity (Figure SI.3.19). Although PALS assumes spherical particles, they allow for the development of trends of particle hydrodynamic size and polydispersity. The results are consistent with turbidity: mean

diameters decrease by >90% and polydispersities are lower for needle-like HA (R1 and R2) in the two gastric fluids whereas little change occurs for spherical HA (R3) material.

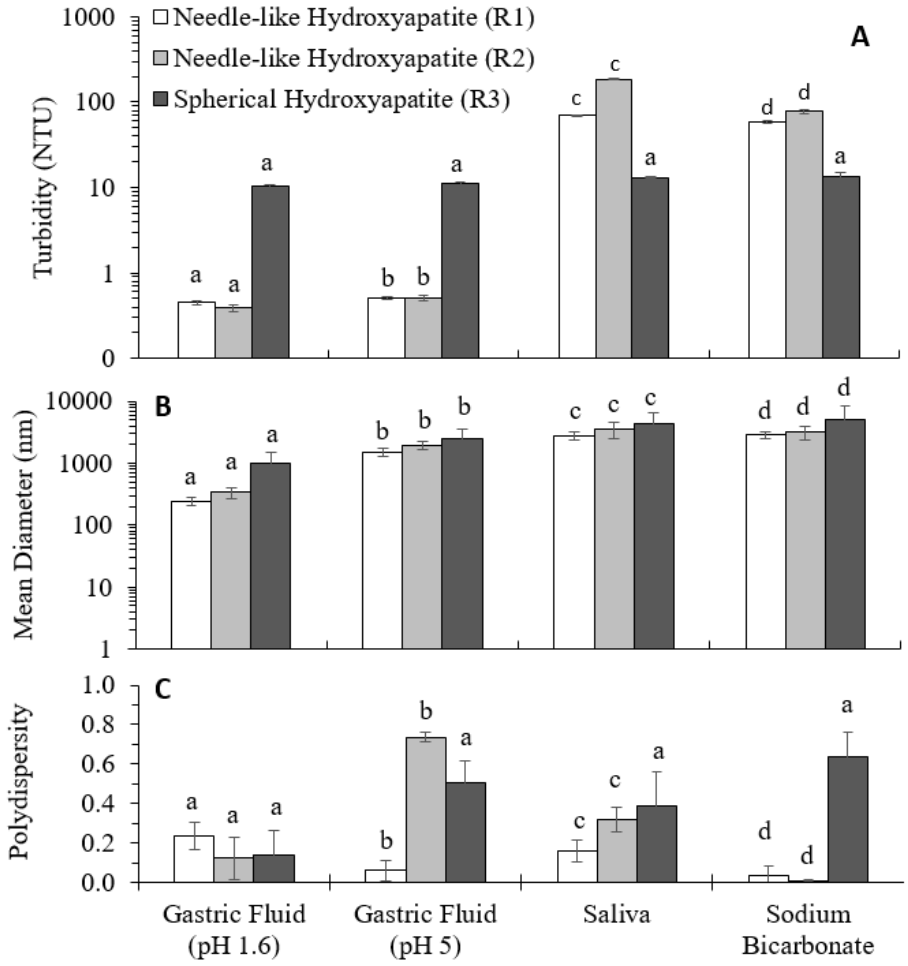

Figure SI.3.19. (A) Turbidity, (B) Mean Diameter, and (C) Polydispersity of the three different reference materials after mixing for two minutes (Saliva) and two hours (Gastric Fluids and Sodium Bicarbonate). One-way analysis of variance (ANOVA) tests were conducted at 95% confidence intervals to determine statistical significance (see Figure SI.3.20). The analysis was conducted to compare each individual reference material across the four simulated biological fluids for each nanomaterial physical property parameter. We did not compare each reference material to each other. We did not compare across the different nanomaterial properties. Turbidity controls containing no reference material were as follows: 1mM sodium bicarbonate (0.29NTU), simulated saliva (2.20NTU), fed-state gastric fluid (0.23NTU), and fasted-state gastric fluid (0.20NTU).

Turbidity ANOVA Analysis														
NP	**R1**				**NP**	**R2**				**NP**	**R3**			
Assay	**Gastric 1.6**	**Gastric 5**	**Saliva**	**SoBi**	**Assay**	**Gastric 1.6**	**Gastric 5**	**Saliva**	**SoBi**	**Assay**	**Gastric 1.6**	**Gastric 5**	**Saliva**	**SoBi**
T1	0.29	0.28	66.80	56.72	**T1**	0.24	0.32	184.80	74.72	**T1**	10.81	11.28	11.20	11.72
T2	0.25	0.25	68.01	59.71	**T2**	0.18	0.24	178.81	82.71	**T2**	9.80	10.56	10.71	12.71
T3	0.22	0.31	67.70	58.70	**T3**	0.15	0.28	189.80	74.70	**T3**	9.60	10.97	10.90	14.70
Mean	0.25	0.28	67.50	58.38	**Mean**	0.19	0.28	184.47	77.38	**Mean**	10.07	10.94	10.94	13.04
95% Conf Interv	-2.35 to 2.86	-2.32 to 2.88	64.90 to 70.11	55.77 to 60.98	**95% Conf Interv**	-2.413 to 2.793	-2.32 to 2.88	181.9 to 187.1	74.77 to 79.98	**95% Conf Interv**	7.47 to 12.67	8.33 to 13.54	8.334 to 13.54	10.44 to 15.65
StDev	0.04	0.03	0.63	1.52	**StDev**	0.05	0.04	5.51	4.61	**StDev**	0.65	0.36	0.25	1.52
Hi	0.29	0.31	68.00	59.70	**Hi**	0.24	0.32	190.00	82.70	**Hi**	10.80	11.30	11.20	14.70
Low	0.22	0.25	66.80	56.70	**Low**	0.15	0.24	179.00	74.70	**Low**	9.60	10.60	10.70	11.70
Median	0.25	0.28	67.70	58.70	**Median**	0.18	0.28	185.00	74.70	**Median**	9.80	11.00	10.90	12.70
Dev From Med	0.02	0.02	0.40	1.00	**Dev From Med**	0.03	0.03	3.67	2.67	**Dev From Med**	0.40	0.24	0.16	0.99

Source of Variation	Sum of Squares	D.F.	Mean Squares	F-value	Source of Variation	Sum of Squares	D.F.	Mean Squares	F-value	Source of Variation	Sum of Squares	D.F.	Mean Squares	F-value
Between	1.19E+04	3	3970	5858	Between	6.84E+04	3	2.28E+04	1766	Between	1.44E+01	3	4.805	6.592
Error	5.421	8	0.677	-	Error	103.3	8	12.92	-	Error	5.831	8	0.7289	-
Total	1.19E+04	11	-	-	Total	6.85E+04	11	-	-	Total	2.03E+01	11	-	-
Result	P-Value = 0.000. Because P value is less than alpha (0.05), these results are significantly different				Result	P-Value = 0.000. Because P value is less than alpha (0.05), these results are significantly different				Result	P-Value = 0.015. Because P value is greater than alpha (0.05), these results are not significantly different			

Mean Diameter ANOVA Analysis														
NP	**R1**				**NP**	**R2**				**NP**	**R3**			
Assay	**Gastric 1.6**	**Gastric 5**	**Saliva**	**SoBi**	**Assay**	**Gastric 1.6**	**Gastric 5**	**Saliva**	**SoBi**	**Assay**	**Gastric 1.6**	**Gastric 5**	**Saliva**	**SoBi**
T1	1741.70	1702.30	8287.59	3262.20	**T1**	1803.20	2281.60	10289.43	3981.00	**T1**	1987.50	1702.30	7593.90	8300.70
T2	1793.10	1284.40	9011.80	2562.00	**T2**	1807.00	1635.80	8289.80	3205.90	**T2**	3011.80	2384.40	11563.60	2041.70
T3	1726.40	1518.10	8878.60	2629.80	**T3**	1920.20	1979.20	9683.45	2354.20	**T3**	2578.60	3518.10	11423.13	5194.40
Mean	1753.73	1501.60	8726.00	2818.00	**Mean**	1843.47	1965.53	9420.89	3180.37	**Mean**	2525.97	2534.93	10193.54	5178.93
95% Conf Interv	1364 to 2143	1112 to 1891	8336 to 9115	2428 to 3207	**95% Conf Interv**	944.6 to 2742	1066 to 2864	8522 to 10319	2281 to 4079	**95% Conf Interv**	-135.3 to 5186	-126 to 5195	7532 to 12854	2518 to 7839
StDev	35.20	209.00	385.47	386.18	**StDev**	66.40	324.00	1026.00	814.00	**StDev**	514.00	917.00	2250.00	3130.00
Hi	1790.00	1700.00	9010.00	3260.00	**Hi**	1920.00	2280.00	10290.00	3980.00	**Hi**	3000.00	3520.00	11560.00	8300.00
Low	1.73E+03	1280.00	8290.00	2560.00	**Low**	1800.00	1640.00	8289.00	2350.00	**Low**	1990.00	1700.00	7590.00	2040.00
Median	1.74E+03	1520.00	8880.00	2630.00	**Median**	1810.00	1980.00	9683.00	3205.00	**Median**	2..58E3	2380.00	11400.00	5190.00
Dev From Med	22.30	139.00	241.00	233.00	**Dev From Med**	38.90	216.00	667.00	542.00	**Dev From Med**	341.00	605.00	1323.00	2086.00

Source of Variation	Sum of Squares	D. F.	Mean Squares	F-value	Source of Variation	Sum of Squares	D. F.	Mean Squares	F-value	Source of Variation	Sum of Squares	D. F.	Mean Squares	F-value
Between	1.04E+08	3	3.46E+07	404.3	Between	1.16E+08	3	3.88E+07	85.14	Between	1.17E+08	3	3.90E+07	9.804
Error	6.85E+05	8	8.57E+04	-	Error	3.64E+06	8	4.56E+05	-	Error	3.19E+07	8	3.99E+06	-
Total	1.05E+08	11	-	-	Total	1.20E+08	11	-	-	Total	1.49E+08	11	-	-
Result	P-Value = 0.000. Because P value is less than alpha (0.05), these results are significantly different				Result	P-Value = 0.000. Because P value is less than alpha (0.05), these results are significantly different				Result	P-Value = 0.005. Because P value is less than alpha (0.05), these results are significantly different			

Polydispersity Statistics													
NP	**R1**				**NP**	**R2**				**NP**	**R3**			
Assay	**Gastric 1.6**	**Gastric 5**	**Saliva**	**SoBi**	**Assay**	**Gastric 1.6**	**Gastric 5**	**Saliva**	**SoBi**	**Assay**	**Gastric 1.6**	**Gastric 5**	**Saliva**	**SoBi**
T1	0.87	0.12	0.35	0.01	**T1**	0.74	0.74	0.50	0.01	**T1**	0.79	0.50	0.34	0.50
T2	0.66	0.04	0.26	0.01	**T2**	0.61	0.76	0.37	0.01	**T2**	0.53	0.62	0.50	0.64
T3	0.70	0.02	0.29	0.09	**T3**	0.40	0.71	0.50	0.01	**T3**	0.46	0.40	0.74	0.76
Mean	0.74	0.06	0.30	0.03	**Mean**	0.58	0.74	0.46	0.01	**Mean**	0.59	0.51	0.53	0.63
95% Conf Interv	0.65 to 0.84	-0.03 to 0.15	0.21 to 0.39	-0.06 to 0.13	**95% Conf Interv**	0.46 to 0.71	0.61 to 0.86	0.33 to 0.58	-0.12 to 0.14	**95% Conf Interv**	0.38 to 0.80	0.29 to 0.72	0.32 to 0.74	0.42 to 0.84
StDev	0.11	0.05	0.05	0.05	**StDev**	0.17	0.03	0.08	0.00	**StDev**	0.17	0.11	0.20	0.13
Hi	0.87	0.12	0.35	0.09	**Hi**	0.74	0.76	0.50	0.01	**Hi**	0.79	0.62	0.74	0.76
Low	0.66	0.02	0.26	0.01	**Low**	0.40	0.71	0.37	0.01	**Low**	0.46	0.40	0.34	0.50
Median	0.70	0.04	0.29	0.01	**Median**	0.61	0.74	0.50	0.01	**Median**	0.53	0.50	0.50	0.64
Dev From Med	0.07	0.03	0.03	0.03	**Dev From Med**	0.11	0.02	0.04	0.00	**Dev From Med**	0.11	0.07	0.13	0.09

Source of Variation	Sum of Squares	D.F.	Mean Squares	F-value	Source of Variation	Sum of Squares	D.F.	Mean Squares	F-value	Source of Variation	Sum of Squares	D.F.	Mean Squares	F-value
Between	9.60E-01	3	3.20E-01	66.29	Between	8.80E-01	3	2.90E-01	32.89	Between	3.00E-02	3	1.00E-02	0.41
Error	3.89E-02	8	4.86E-03	-	Error	7.14E-02	8	8.93E-03	-	Error	2.00E-01	8	2.00E-02	-
Total	1.01E+00	11	-	-	Total	9.50E-01	11	-	-	Total	2.30E-01	11	-	-
Result	P-Value = 0.000. Because P value is less than alpha (0.05), these results are significantly different				Result	P-Value = 0.000. Because P value is less than alpha (0.05), these results are significantly different				Result	P-Value = 0.747. Because P value is greater than alpha (0.05), these results are not significantly different			

Figure SI.3.20. ANOVA statistical analysis of (A) Turbidity, (B) Mean Diameter, and (C) Polydispersity

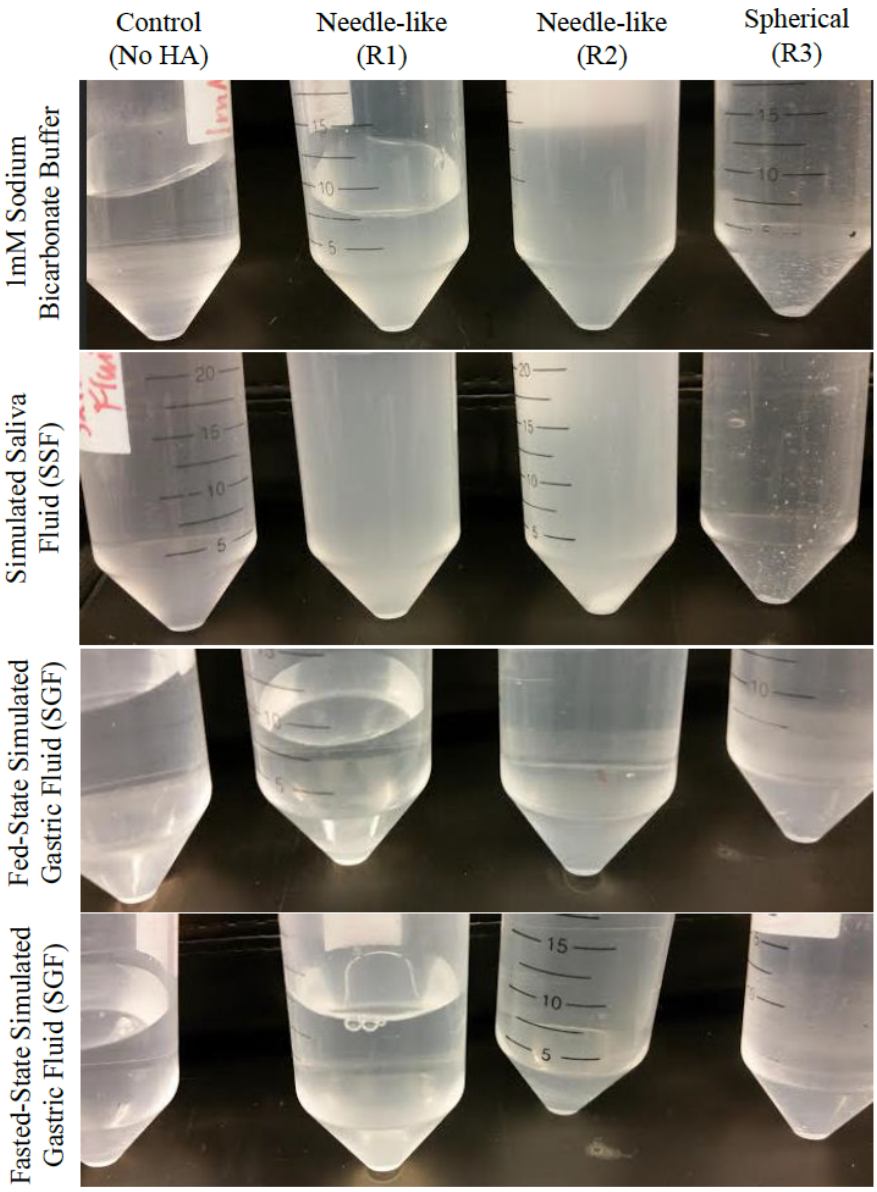

Figure SI.3.21. Photographs show vials containing hydroxyapatite (HA) reference materials (R1, R2, R3) or control (no HA added) in different fluids after the prescribed mixing times. The relative cloudiness of the samples differs among the vials.

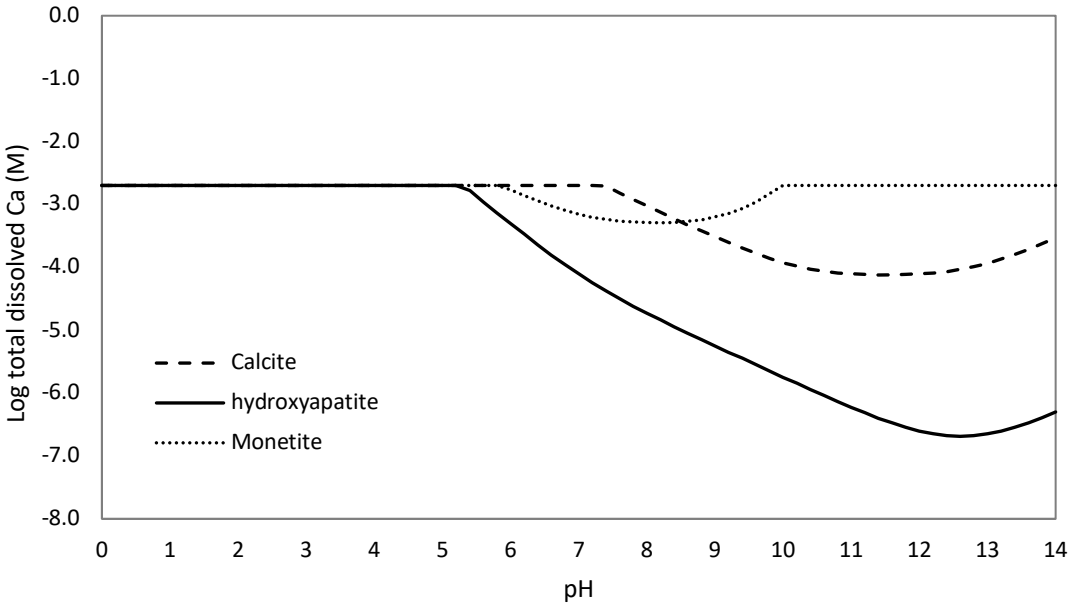

Figure SI.3.22. Calculated total dissolved Ca concentration (Log$[Ca]_T$) as a function of pH in simulated gastric fluid for the three calcium minerals found in infant formula, i.e., hydroxyapatite, calcite, and monetite. Calculations were performed using Visual MINTEQ software (ver. 3.1). Simulation conditions: sodium = 0.267 M, acetate = 0.0469 M, and chloride = 0.237 M. Calcium mineral concentrations: hydroxyapatite = 0.4 mM, calcite = 2 mM, and monetite = 2 mM, to achieve a total Ca concentration of 2 mM for all three minerals.

Estimated Usage of Needle-like Hydroxyapatite

The 2013 global market for infant formula was approximately $41 Billion (US dollar), and growing rapidly in Asia and other markets [165]. The cost of powder formula is on the order of $1 (US) per ounce (based upon market costs in US and web-based reports (e.g., http://www.popsugar.com/moms/How-Much-Infant-Formula-Costs-8104334). Most of the infant formula is powder, as opposed to liquids [165]. We conservatively assume 75% of the market is infant formula. Based upon our estimate of 0.4 wt% HA in the formula from S3 sample, this results in a cost of $8 per gram HA delivered in infant formula. Assuming $41B (US) market at this cost results in

production of up to 5125 metric tons of HA for infant formula alone. Nano-structured needle-like HA was not present in all samples. Assuming only 50% of infant formula uses needle-like HA, the global annual production may be on the order of 2500 metric tons. These estimates (2500-5000 metric ton/year) for needle-like HA in just this one product class (infant formula) is the same order of magnitude for the 2010 global production estimate for carbon nanotubes of 2916-3200 metric ton/year) (Table S4 in [163]). There are uses of needle-like HA in cosmetics [63] and probably many other applications, although data is not readily available.

CHAPTER 4

TOWARDS RAPID ASSESSMENT OF NANOMATERIAL ADDITIVES IN CONSUMER PRODUCTS USING X-RAY FLUORESCENCE

Jared J. Schoepf[1], Pierre Herckes[2], Kiril Hristovski[3], Paul Westerhoff[4]*

* Corresponding Author: p.westerhoff@asu.edu; 480-965-2885; Arizona State University, School of Sustainable Engineering and the Built Environment, Box 3005, Tempe, AZ 85287

1 - Arizona State University, School for Engineering of Matter, Transport, and Energy, Tempe, AZ 85287

2 - Arizona State University, School of Molecular Sciences, Box 1604, Tempe, AZ 85287

3 - Arizona State University, The Polytechnic School, Box 2180, Mesa, AZ 85212-2180

4 - Arizona State University, School of Sustainable Engineering and the Built Environment, Box 3005, Tempe, AZ 85287

4.1 INTRODUCTION

As discussed in detail in Chapters 2 and 3, in recent years, hydroxyapatite, silicon dioxide, and titanium dioxide nanomaterials have found extensive application in food products. Current techniques employed to detect nanomaterials are severely limited by high costs and lengthy sample preparation times. These limitations impose barriers to scaling detection methods to industrially- and medically-relevant conditions [26-34]. X-ray Fluorescence (XRF) has the potential to be utilized before employing more sophisticated pretreatment or analytical instrumentation in a multi-tiered analytical approach.

Portable and lab-based XRF has been used to detect elements in a wide range of fields and samples including in soil [183, 184], rocks [185, 186], sources of lead in homes, paint and toys [187-190], analysis of artwork and artifacts [191-194], and analysis of plastics [195, 196]. However, to the extent of the author's knowledge, there are no reports on applying XRF for nanomaterial detection in food products. X-ray fluorescence identifies a sample's elemental composition by measuring characteristic photons emitted from atoms exposed to X-rays. XRF uses an X-ray tube to ionize atoms in the sample, expelling an inner shell electron from an atom. The energy from the X-ray overcomes the bonding energy of one of the inner orbital electrons of the atom, exciting and expelling the electron. The atom, now unstable, seeks to become stable by an electron in a higher orbital relaxing to a lower energy state, filling an electron vacancy and emitting a photon. The photon, with an energy characteristic of the difference in the two bonding energies of the orbitals, is emitted and measured by the XRF detector. [197]

I hypothesize that a portable XRF system can be used to screen Si- Ti-, Ca-, P-based nanomaterials in food, vitamin supplements, and infant formula with comparable accuracy to inductively coupled plasma – mass spectrometry (ICP-MS). The portability, rapid analysis time, and lower cost of the XRF instrumentation differentiates it from laboratory-based analytical tools (ICP-MS and TEM), thereby facilitating rapid analysis regardless of location.

Because SiO_2, TiO_2, and hydroxyapatite (HA) were found to be the most common nanomaterial additives in food and infant formulas (Chapter 2 and 3), they were selected for evaluating XRF as a pre-screening tool in developing a multi-tiered analytical method. My objective is to detect the presence or absence of nanomaterials at a threshold of 0.01% in powder and solid food, which is the threshold where nanomaterials have been found to cause 50% median lethal concentration to terrestrial and aquatic organisms [120]. To develop the multi-tiered approach, XRF, ICP-MS, and electron microscopy methodologies were first developed by adding pristine, reference SiO_2, TiO_2, and HA food-grade materials to common food ingredients (e.g., flour, sugar, baking soda, and salt) at different loading ratios. The methods were developed before analyzing foods and infant formula procured from the United States of America and Australia that contained labeling information related to the presence of silica or titania or calcium phosphate.

A three-step, multiple lines of evidence approach was employed to screen and verify nanomaterial presence in complex food matrices: 1) screen for Si, Ti, Ca, and P elemental presence in the sample by XRF 3) confirm presence of nano-scale objects by TEM, and 4) confirm quantity of target elements (Si, Ti, Ca, and P) by ICP-MS. To test the validity of the three tier process, the most accepted nanomaterial detection method

(TEM) was performed first, followed by the new XRF methods. Viability of XRF is demonstrated by a high degree of positive nanomaterial detection and low level of false negatives and false positives.

4.2 MATERIALS AND METHODS

Model Solid Food Matrix

Three food ingredients, flour, sugar, and baking soda (labeled as sample ID numbers S1-S3), were purchased in the USA and labelled as a nanomaterial blank. Food ingredients were mixed to create a nanomaterial "blank" combined food matrix (S4) containing flour (38 wt/wt %), sugar (61 wt/wt %), and baking soda (1 wt/wt %), a representative ratio of ingredients in common food products. Table 4.1 contains the complete sample list.

Pristine Food-Grade SiO_2, TiO_2, HA Materials

One powder sample (S5) of pristine food-grade (99% pure) SiO_2, sample identified as food-grade (European Union food code E551), was procured from Chinese vendors and characterized extensively in a previous study [121]. One pristine food-grade (European Union food code E171) TiO_2 powder samples (S6) was procured from a Chinese vendor and characterized in a previous study [59]. One powder (S7), pristine hydroxyapatite (HA), a calcium phosphate compound, was procured from a Chinese vendor and characterized in a previous study [70]. Table 4.2 contains the complete sample list.

Consumer Products

Food products labeled as containing silicon dioxide or titanium dioxide were purchased in 2014 and 2015 and characterized in a previous study (Chapter 2). Food

products purchased in Australia (S8-S21) included candy, powdered sauce/gravy mixes, powdered flavor mixes, frosting, non-dairy creamer powder, cappuccino powder, and salad dressing. Food products purchased in the USA (S21-S35) included hot chocolate powder mix, corn muffin mix, powder flavor mixes, cappuccino powder, vitamin and probiotic supplement capsules, artificial sweetener, gelatin powder, toothpaste, cake mix, and cereal. Vitamin supplements labeled as containing silicon dioxide or titanium dioxide were purchased in 2016 in the United State of America (S36-47). Infant formula was purchased in 2016 from Australia (S48-54). Table 4.2 and 4.3 contains the complete sample list.

Complex Matrices Solutions for Calibration Curve

Calibration curves to calculate the limit of detection of our XRF instrument were developed for each nanomaterial (e.g. SiO_2, TiO_2, and HA) in the nanomaterial "blank" combined food matrix (S4). The nanomaterial "blank" combined food matrix (S4) was spiked with each nanomaterial (10 wt/wt%) in a 50 mL centrifuge tube to create a stock mixture (10g total mass) identified as Stock A. The mixture was inverted by hand for 2 minutes and allowed to roll on a shake table for 24 hours to improve uniformity. The Stock A solution was used to make a new (1 wt/wt% of nanomaterial) Stock B solution, which was inverted by hand for 2 minutes and allowed to roll on a shake table for 24 hours. The new Stock B solution (1 wt/wt%) was diluted to create a new Stock C solution (0.1 wt/wt%). The (0.1 wt/wt%) Stock C solution was inverted by hand for 2 minutes and allowed to roll on a shake table for 24 hours. The stock B solution (1 wt/wt%) was used to create 1,000 ppm, 2,500ppm, and 5,000 ppm of NM in the combined food matrix samples. The stock C solution (0.1 wt/wt%) was used to create 25, 50, 100, and 500 ppm

of NM in combined food matrix samples. All samples were allowed to roll on a shake table for 24 hours to improve uniformity. A calibration curve as described above was developed for each NM separately and analyzed by XRF. Table 4.4 contains the complete sample list.

ICP-MS Sample Preparation & Instrumentation

Solid samples (~0.25 g) were added to 8 mL concentrated nitric acid (70%) and 2 mL hydrofluoric acid (47-51%) (Ultra-Trace Metal Grade, JT Baker) and microwave digested. During microwave digestion, the temperature was initially increased to 150 °C over 15 minutes, and then increased to 180 °C over another 15 minute period. Once 180 °C was reached, the temperature was kept constant for 20 minutes before cooling the samples to room temperature. To remove hydrofluoric acid from solution after digestion, the digested sample was reacted with 10 mL boric acid (4.5% w/v). The remaining liquid was analyzed for elemental composition by ICP-MS (Thermo Fisher X-Series II). The detection limits of ^{28}Si, ^{31}P, ^{44}Ca, ^{47}Ti in food products were ~50 ppb, ~50 ppb, ~50 ppb, ~0.75 ppb (ng/g of food), respectively.

TEM and Energy-Dispersive X-ray (EDX) Spectroscopy

Solid samples (~0.15 g) were suspended in 40 mL Ultrapure water (18.2 MΩ cm, Nanopure Infinity, Barnstead), sonicated (Branson ultrasonic bath - 80 Watts/L) for 30 minutes, and then centrifuged at F = 14,000 G for 15 minutes to dissolve and separate organics from particulate matter. The organics-rich supernatant was poured off, leaving a particulate composed pellet at the bottom of the centrifuge tube. The pellet was re-suspended in 20 mL ultrapure water and sonicated for 5 minutes to re-disperse the particles. A 20 µL aliquot of the mixture was pipetted onto a Ted Pella carbon type B,

200 mesh copper TEM grid and allowed to dry overnight prior to TEM/EDX analysis (Philips CM200 and JEOL 2010F). Mean particle diameter was measured manually with ImageJ software on 250 particles.

XRF Sample Preparation & Instrumentation

X-ray fluorescence (XRF, Niton XL3t GOLDD+, Thermo Fisher Scientific, Waltham, MA, USA) requires minimal sample preparation for solid samples. The configuration is shown in Figure SI.4.1. Samples were placed within an XRF sampling cup (Premier Lab) which was composed of a cup with a thin (8μm) carbon film to support the sample. The Niton XL3t GOLDD+ uses four X-ray energy levels and filters, main, light, heavy, and low to detect elements between Mg and U. The XRF analyzer was used in mining mode with the software algorithm and calibration completed by Thermo Scientific. The built-in algorithm calculates the concentration (ppm) of each element and the corresponding error (two standard deviation). The instrument manufacturer reports the limit of detection for each element (Mg – U) for each measurement as three standard deviation (99.7% confidence level) or multiplying the XRF output error (two standard deviation as calculated by the Niton XL3t GOLDD+ software) by 1.5 to obtain three standard deviation. A timeframe of 120 seconds was used for each energy level (e.g. main, light, heavy, and low) for powder samples unless otherwise noted.

The limit of detection was also calculated statically to confirm the application of the manufacture's "mining mode" for complex food matrices by the addition of reference nanomaterials to a nanomaterial "blank" combined food matrix (S5) as outlined in Table 4.4. The XRF produces a digital reading with energy spectrum from 1 keV to 20 keV on the x-axis and signal (counts) on the y-axis. The persistent peaks at 1.74, 2.02, 3.69, and

4.51 keV (K-α emission, the transition of an L orbital electron to the K orbital) indicate the presence of Si, P, Ca, and Ti, respectively. Elemental analysis was statistically evaluated using the signal to noise ratio (S/N). Assuming Gaussian distribution, a S/N of 3.29 represents 3.29 standard deviations from the background noise, which corresponds to a 99.95% confidence interval that a peak is present. A value of 3.29 was chosen as recommended by IUPAC [198] for XRF.

Calculation of the Limit of Detection

The XRF software algorithm and elemental calibration was validated by developing a calibration curve and calculating the limit of detection. Analyzing the complex matrix calibration curve solutions (25 - 100,000 ppm of each NM in the combined food matrix S4) for the signal at the corresponding energy for each element (Si, Ti, Ca, and P), the signal height (counts) was measured. The background signal of the blank (S4) was subtracted from the signal height to obtain the peak height (counts) [199], graphed in Figure 4.1.

The instrument limit of detection (LOD) was calculated using the below equation [199]:

$$LOD = \frac{3.29 \times \sqrt{2} \times C_A}{I_P - I_b} \times \sqrt{\frac{I_b}{t/2}}$$

In the above equation, 3.29 is the recommended 99.95% confidence interval, $\sqrt{2}$ is due to the two required measurements (sample of interest and blank sample), C_A is the concentration (ppm) of the analyte (nanomaterial) added to the sample, I_p is the intensity under the analyte peak of the sample, I_b is the blank sample (S4) peak under the analyte

peak, t is the total time of analysis (time of analyte analysis plus the time of the blank sample analysis).

4.3 RESULTS

TEM Characterization of Reference NM Food Additives and Extracted NMs from Consumer Products

Procured nanomaterials were characterized by TEM for particle size, aggregation state, elemental composition, and morphology. Detailed discussion of the reference food-grade SiO_2, TiO_2, and HA additives are provided in our previous work [54, 57, 70]. A key observation is that the reference TiO_2 food-grade materials and the TiO_2 extracted from food products contained similar TiO_2 size distributions with 20% to 30% of the primary particles exhibiting sizes < 100 nm (nanomaterials) based upon particle number counting. The reference food-grade SiO_2 material contained similar particle size distributions as material extracted from food products and vitamin supplements with primary SiO_2 particles 10 to 20 nm in diameter and agglomerates ranging between 1,000 and 1,800 nm. The reference food-grade HA material contained similar particle size distributions as material extracted from infant formula with primary HA particles 30 ± 5 nm (width) by 131 ± 25 nm (length). TEM images presented in Figure 4.2 are illustrative of the size and morphology detected in all of the vitamin samples; TEM images of additional vitamin supplement samples and infant formulas are shown in Figure SI.4.2 and SI.4.3. Table 4.1 summarizes the size and composition of colloids detected by TEM/EDX in the reference nanomaterials (S5-S7). The blank food ingredients (S1-S3) and combined complex food matrix (S4) did not contain SiO_2 or TiO_2.

Tables 4.2 and 4.3 summarize the size and composition of nanomaterials detected by TEM/EDX in the food products (S8-35), vitamin supplements (S36-47), and infant formulas (S48-54).The average primary SiO_2 particle size was between 10 and 33 nm, with all particulate matter present as larger SiO_2 agglomerates. In contrast, the average TiO_2 particle size was > 100 nm (Table 4.2)—except for S32 (toothpaste) at 32 nm—with all particulate matter present as larger TiO_2 agglomerates. The size distribution of TiO_2 particles in the consumer samples was consistent with our previously published data [57], showing ~20% to 40% of the primary TiO_2 particles were < 100 nm in at least one dimension. The infant formulas contained two morphologies, need-like and spherical nanoparticles. The typical primary needle-like Ca, P, and O containing particle size was between 65 and 211 nm in length, and 7 and 21 nm in width, with all particulate matter present as larger agglomerates. The average spherical Ca, P, and O containing particle was between 123 and 5,404 nm in diameter, with all particulate matter present as larger agglomerates. TEM/EDX analysis of the food products and vitamin supplements (n=40) showed they contained SiO_2 (n=26), TiO_2 (n=8), neither (n=7), or both (n=1), with no samples containing Ca, or P particulate. One sample (S10; hard candy) contained both SiO_2 and TiO_2. Neither SiO_2 nor TiO_2 was detected in three food samples (S30, S33, and S34; gelatin powder, cake mix, and cereal, respectively), vitamin supplements (S38, S41, S42), and infant formulas (S48-54). TEM/EDX analysis of the infant formula (n=7) showed all samples (S48-54) contained Ca, P, and O containing particles with (n=3) containing needle-like Ca, P, and O (S48-54) and (n=4) containing spherical Ca, P, and O containing particulate (S47-50).

The ingredient labels contained information on material content which is also summarized in Tables 4.2 and 4.3. Of the 25 samples labeled as containing Si-based ingredients, TEM/EDX confirmed the presence of SiO_2 in 22 products (3 samples were found absent of SiO_2 by TEM). Overall 3 samples were identified as containing SiO_2 by TEM/EDX that were not labeled as containing SiO_2. All 9 samples identified as containing TiO_2 by TEM/EDX were also labeled as containing Ti-based solids, while all 7 vitamin supplements labeled as containing TiO_2 were found absent of TiO_2 by TEM. The 7 infant formula lacked labeling information.

Quantification by ICP-MS of SiO_2, TiO_2, HA in Consumer Products

ICP-MS does not differentiate between ionic, nano, or larger particle forms initially present in the consumer product. ICP-MS measured the elemental Si, Ti, Ca, and P concentrations in each product after digestion. Tables 1, 2, and 3 summarize Si, Ti, Ca, and P concentrations as determined via ICP-MS for blank food ingredients, combined complex food matrix, reference food-grade materials, and digested consumer products. Silicon concentrations range from non-detect (<50 ppb) to 189,000 ppm (18.9 wt%), and titanium concentrations range from non-detect (<0.75ppb) to 3,000 ppm (0.3 wt%) for food products and vitamin supplements. Calcium concentrations range from 3,657 to 4,662 ppm and phosphorus concentrations range from 1,404 to 2,821 ppm in the infant formulas.

Limit of Detection of XRF on Complex Food Matrices

Figure 4.3 shows XRF spectra of representative samples of reference nanomaterials. The highest intensity peak (K-α emission peaks for Ti at 4.51 keV, Si at 1.75 keV, Ca at 3.69 keV, P at 2.01 keV), corresponding to the largest S/N ratios, were

chosen for the remainder of the analysis. There was no signal interference from any of the elements at these peaks from other elements. Each element has multiple emission peaks. The absence or presence of each element was determined based on the S/N ratio for each peak.

As summarized in Table 4.1, all reference food-grade nanomaterials (S5-S7) resulted in S/N>3 by XRF for either Ti, Si, Ca, or P. None of the blank food ingredients (S1-S4) had detectable Si or Ti; while the baking powder (S3), and combined food matrix had detectable Ca, and P (Table 4.1). Table 4.3 lists the peak height (counts), and the instrument provided concentration (ppm). The peak height (counts) vs. energy (keV) was plotted for each element (Ti, Si, Ca, or P) in the combined food matrix (S4) in Figure 4.1. The background signal of Ca, and P in the blank were subtracted from the combined food matrix spiked with HA readings. The slope of each element in the cookie mix was 0.11, 0.04, 0.04, and 0.02 for Ti, P, Ca, and Si respectively. The R^2 values were 0.99, 0.96, 0.99, and 0.99 for Ti, P, Ca, and Si respectively. Table 4.5 lists the calculated instrument limit of detection (LOD) and the manufacture instrument LOD. The calculated LOD was 42, 69, 22, and 3 ppm for Si, P, Ca, and Ti respectively and the instrument provided LOD was 45, 24, 23, and 7 ppm for Si, P, Ca and Ti respectively.

XRF Analysis on Food Products, Vitamin Supplements, and Infant Formulas

Table 4.2 summarizes the tested consumer products and the respective concentration of Si, Ti, Ca, and P. The concentration of Si in the food products and vitamin supplements ranged from <LOD (<45ppm) to 59,918 ppm (6.0 wt%) and the concentration of Ti in the food products and vitamin supplements ranged from <LOD (<7ppm) to 23,320 ppm (2.3 wt%). The concentration of Ca in the infant formula ranged

from 3,657 to 4,662 ppm (0.47 wt%) and the concentration of P ranged from 2,198 to 4,257 ppm (0.43 wt%).

4.4 COMPARISON OF DETECTION METHODS

Data on 28 food products and 12 vitamin supplements indicate the presence of SiO_2 and TiO_2 based upon the food product package label or analysis using TEM, ICP-MS, and XRF. Package label information was not available for the 7 infant formulas. TEM detected nano Si in 25 samples and nano Ti in 9 samples. Figure 4.4 compares the TEM results to each of the methods listed above: ICP-MS and XRF. TEM is considered the gold standard for detecting the presence/absence of nanoparticles in samples albeit being the most costly. Comparing the food product label information to TEM, three samples (toothpaste product S30, Vitamins S8 and S41) were labeled as containing SiO_2 but TEM did not detect SiO_2, representing a "false positive" for food labeling information. TEM detected SiO_2 in three samples (S9, S18, and S31) not labeled as containing Si-materials, and these would be considered "false negative" for reliance upon food labeling alone. In food products, all products labeled as containing TiO_2 also had detectable TiO_2 by TEM/EDX analysis. Thus there were no "false positives" or "false negatives" between TEM/EDX and product labels for Ti-containing solids. For vitamin supplements, seven samples were labeled as containing TiO_2 but no samples had detectable TiO_2 in the powder. The TiO_2 is suspected to be present in the outer vitamin capsule. Figure 4.4 was developed to compare the agreement and false positive or false negative detection of SiO_2, TiO_2, and calcium phosphate for the experimental methods. False positive is defined where TEM did not detect Si, Ti, Ca, or P while the other

analytical method did detect the presence of Si, Ti, Ca, or P, and false negative being the absence of Si, Ti, Ca, or P by TEM but presence by the other method.

For all food samples labeled on the package as containing Si-materials, ICP-MS detected Si. Silicon was also detected by ICP-MS in three samples where TEM confirmed presence of SiO_2 even though not labeled as containing Si on the food packaging (false negative for the food package label). Only one sample (S9) had confirmed SiO_2 by TEM and XRF but was not detected by ICP-MS, which was the only false negative by ICP-MS. The S9 sample is a two-layer candy. SiO_2 was detected in the thin, hard, outer candy layer by TEM but not in the inner chewy candy. We believe that silica represents only a small mass of the overall candy product and was likely below the ICP-MS detection limit of 50 ppb (ng/g) for Si. Twelve samples had detectable Si by ICP-MS, eight of which were not labeled as containing Si-materials and all twelve of which did not have TEM-confirmed SiO_2. Therefore, these samples were false nanomaterial positives by ICP-MS. These samples likely had Si-containing chemicals such as calcium silicate rather than SiO_2. Relying upon ICP-MS alone for the presence or absence of nanoparticles would have resulted in 12 out of 36 samples (33%) as “false-positives” results for the presence of nanoparticles, confirming the use of TEM as the gold standard for nanomaterial detection.

For all food and vitamin supplement samples labeled as containing Ti-materials, Ti was detected by ICP-MS (Table 4.2). Most of these samples contained more than 100 ppm of Ti. Food samples without Ti-materials on the label had detectable, but lower Ti concentrations (Table 4.2). Sample S9 contained a low Ti concentration but contained detectable TiO_2 particles by TEM/EDX. This sample was composed of a hard outer-layer

and softer inner-layer. It is likely that TiO_2 was only present in the outer layer, which resulted in a low Ti concentration of 38 ppm upon acid digestion and ICP-MS analysis. All TiO_2 containing samples fit into two groups as samples with less than 50 ppm Ti (suspected a trace or incidental concentration not requiring food product labelling – FDA Code of Regulations 21 CFR 101.100(a)(3)) or samples with 50 to 100 ppm Ti. Overall, relying upon ICP-MS for the presence or absence of nanoparticles (based upon confirmed TEM detection of TiO_2) led to only 3 false-positives (S9, S50, S51) if a 100 ppm Ti threshold was applied, but a higher number of false-positives if a lower threshold (i.e., any detectable Ti) was used to define a substance as containing nanomaterials.

Comparing XRF to the package label, XRF identified silicon in 24 of 25 samples. XRF found 10 samples with silicon that were not listed on the label. US food manufactures are not required to label trace or incidental concentration of ingredients according to the FDA, and Australia Food Standard 1.2.4 does not require labelling of ingredients below 5% that do "not perform a technological function in the final food." The 10 food products were deemed below this limit by the food manufactures and confirmed by ICP-MS. Comparing XRF to the package label for titanium, XRF correctly identified titanium in 12 of the 16 samples according to their package label. XRF was unable to detect titanium in the vitamin supplements, TiO_2 is suspected to be in the outer pill capsule. Additional XRF analysis of the pill capsule found TIO_2 in 2 out of 4 vitamin supplements originally missed by XRF. XRF found 11 samples with titanium that were not labeled to contain titanium by the food manufacturer. These samples were deemed below the concentration limit by the food manufactures and confirmed by ICP-MS.

Comparing XRF to ICP-MS data, XRF identified 31 of 36 samples with silicon. There were 5 samples that XRF did not find silicon present. The 5 samples had concentration between 515 and 5,421 ppm, within the calculated and instrument LOD. Of the five, four were not labeled as containing SiO_2, potential false positives by ICP-MS due to sample preparation and contamination. XRF analyzes samples with minimal sample preparation, minimizing contamination. ICP-MS found all 40 food samples to contain titanium. XRF detected Ti in 23 of the 40 samples. Of the 17 missed samples that XRF did not find to contain titanium all had between 3 and 52 ppm, near the limit of detection of XRF. All seven infant formula samples contained Ca, and P by ICP-MS and XRF.

Analyzing the food products, XRF found 9 out of 9 TEM-confirmed samples to contain Ti. For Si, XRF found 17 out of 17 TEM confirmed samples to contain Si. XRF had no false positives in food products compared to TEM. Analyzing the vitamin supplements, XRF found 7 out of 8 TEM-confirmed samples to contain Si. No vitamin samples had TEM-confirmed Ti. XRF and TEM confirmed Ca and P in all infant formulas.

XRF is an accurate method to detect Si, Ti, Ca, and P in food matrices with strong agreement with the product label, detecting Si and Ti in 96% and 75% (100% Ti in food products) of the food, and vitamin supplements labeled as containing each material, respectively. XRF also detected Si and Ti in samples that were not marked on the label but confirmed to have Si and Ti present by ICP-MS. Due to the limited sample preparation and minimal time requirements, XRF allows for high throughput of samples compared to ICP-MS meeting the requirements as a pre-screening tool.

The development of XRF to detect nanomaterials in complex matrices allows for a tiered analytical approach (Figure 4.5) using XRF as pre-screening techniques followed by standard techniques (TEM and ICP-MS) to fully characterize the sample. Tier one answers the question "What elements are present?" by implementing XRF to identify the presence or absence of elements (e.g., Si, Ti, Ca, and P) suspected to be present as nanomaterials (e.g., SiO_2 or TiO_2 or HA). Samples absent of elements suspected to be present as nanomaterials are not further analyzed while samples present continue to tier two. Tier two (TEM) is completed for particle sizing, morphology, and composition, and tier three (ICP-MS) is completed for elemental composition of the bulk sample. Through the use of a tiered analytical approach, samples are pre-screened for elemental composition, reducing the number of samples requiring analysis by expensive and time intensive TEM and ICP-MS analysis. Using XRF as a pre-screening approach, 6 out of 40 samples for Si would have been eliminated, with 1 false negative, and 17 samples out of 40 samples for Ti would have been eliminated with no false negatives. XRF, as a rapid technique (~5 minutes per sample) has been proven a robust strategy to rapid screen for the presence of elements suspected to be present as nanomaterials in food matrices.

4.5 CONCLUSIONS

XRF was demonstrated to be a feasible technique to determine the presence or absence of silicon, titanium, calcium, and phosphorus in solid and powder food samples. Advantages of XRF are: (a) rapid detection of Si, Ti, Ca, and P; (b) reduced pre-treatment and analysis costs per sample. The XRF technique lends itself to analysis of additional food matrices to screen for nanomaterials in food products.

Using a tiered approach (Figure 4.5), XRF can be used to reduce the number of samples that require TEM resulting in higher throughput of samples and a reduced cost. This would be a tier 1 analysis, or first line of evidence that nanomaterials may exist. If additional evidence is needed, then TEM could be applied. If element-specific concentrations are needed, then ICP-MS could be applied.

Although ICP-MS had the best detection of Si, Ti, Ca, and P in the sample, ICP-MS does not provide presence or absence of nanomaterials, rather purely the concentration of Si, Ti, Ca, and P in the sample. The Si, Ti, Ca, and P may be present as agglomerates or micrometer-sized particles, and it is difficult to say if nanomaterials are present rather than larger, micrometer-sized particles. While detection limits of ICP-MS are much lower than XRF, it is difficult to compare "detection limits" of mass concentration from ICP-MS versus TEM. TEM only provides "presence or absence" and perhaps relative abundance. TEM analysis on food samples with very low nanomaterials content can be time-consuming and difficult to prove absence as nanoparticles could be present but below detection capabilities of TEM. Single particle ICP-MS currently has minimum size detection limits for Si > 200 nm [38], which is much larger than the primary particles and agglomerates would have. This size limit confounds detection issues across multiple dwell times, making them difficult to detect and quantify. Likewise, Ti minimum size limit for spICP-MS is > 100 nm [38].

With the projected increased use of nanomaterials, a rapid analysis technique is essential to monitoring nanomaterials across various matrices to determine the exposure to humans in consumer products, manufacturing facilities, and the environment. The rapid results when monitoring for presence of nanomaterials allows researchers to

develop a strategic analysis plan for further, in-depth analysis and characterization of nanomaterials. A promising application is for real-time health exposure analysis for industrial workers where saliva and mucus can be dispersed in water and analyzed for a real-time exposure extent.

4.6 ACKNOWLEDGMENTS

Partial funding was provided from the US Environmental Protection Agency through the STAR program (RD83558001) and the National Science Foundation (CBET 1336542). We gratefully acknowledge the use of the facilities within the LeRoy Eyring Center for Solid State Science at Arizona State University.

Table 4.1. Summary of Measurements for Food Ingredient and Pure Food-grade Additives (*designate samples from different vendors; ND = not detected; "+" indicates Si, Ti, Ca, or P was detected by XRF or TEM)

Sample Type and ID	Silicon-Based Measurements		Titanium-Based Measurements		Calcium-Based Measurements		Phosphorus-Based Measurements	
	XRF	TEM/ EDX	XRF	TEM/ EDX	XRF	TEM/EDX	XRF	TEM/ EDX
Food Ingredients								
Flour (S1)	ND	ND	ND	ND		ND		ND
Sugar (S2)	ND	ND	ND	ND		ND		ND
Baking powder (S3)	ND	ND	ND	ND		ND		ND
Combined matrix (S4)	ND	ND	ND	ND		ND		ND
Food-grade Additives*								
E551-E (S5)	+	+	-	-	-	-	-	-
E171-A (S6)	-	-	+	+	-	-	-	-
HA (S7)	-	-	+	+	+	+	+	+

Table 4.2. Summary of Measurements for Manufactured Food and Vitamin Supplements; ND = not detected; "+" indicates Si and Ti detected by XRF)

	Silicon-Based Measurements				Titanium-Based Measurements			
	Package Label	XRF (ppm)	TEM (Avg. Diam., nm)	ICP-MS (μg/g)	Package Label	XRF (ppm)	TEM (Avg. Diam., nm)	ICP-MS (μg/g)
Australian Foods								
S8) Soft Candy	-	97	-	-	+	460	102	548
S9) Hard Candy	-	227	32	-	+	2,303	176	38
S10) Mint Candy	-	77	-	-	+	2,948	150	211
S11) Gum	-	94	-	150	+	3,337	130	262
S12) Hard Candy	-	55	-	78	+	4,262	123	1,044
S13) White Sauce	+	561	10	234	-	-	-	9
S14) Meat Gravy	+	643	15	305	-	-	-	5
S15) Taco Seasoning	+	8,827	21	2,697	-	19	-	12
S16) Frosting	-	-	-	-	+	2,827	148	2,435
S17) Non-dairy Creamer powder	+	4,333	24	944	-	-	-	8
S18) Cappuccino powder	-	3,033	15	648	-	23	-	9
S19) Chicken Salt	+	10,194	21	2,694	-	-	-	14
S20) Caesar Dressing	-	-	-	1,584	+	985	115	993
S21) Gum	-	1,743	-	4,076	+	4,443	105	3,061
USA Foods								
S22) Hot Chocolate Mix	+	2,249	22	4,535	-	12	-	29
S23) Corn Muffin Mix	+	120	19	4,833	-	-	-	40
S24) Taco Seasoning	+	27,135	25	1,328	-	21	-	3
S25) Hazelnut Cappuccino	+	5,542	18	5,759	-	-	-	28
S26) Vitamin B12 Supplement	+	13,533	20	16,195	-	170	-	33
S27) Artificial Sweetener	+	1,470	33	6,429	-	-	-	39
S28) Cappuccino	+	16,704	18	8,304	-	36	-	31
S29) Vitamin D3	+	8,062	18	1,576	-	175	-	3

supplement								
S30) Gelatin powder	-	-	-	5,421	-	1,009	-	81
S31) Milk Chocolate Cocoa Mix	-	1,746	26	5,154	-	27	-	36
S32) Toothpaste	+	59,918	-	189,038	+	242	37	146
S33) Cake Mix	-	95	-	5301	-	-	-	42
S34) Cereal	-	450	-	1881	-	-	-	17
S35) Probiotic	+	1,767	19	16,337	-	-	-	50
Vitamin Supplements	Package Label	XRF (ppm)	TEM (Avg ± 1 STD, nm)	ICP-MS (μg/g)	Package Label	XRF (ppm)	TEM (Avg ± 1 STD, nm)	ICP-MS (μg/g)
S36) Vitamin 1	+	8,683	12 ± 3	320	-	-	-	6
S37) Vitamin 2	+	5,647	10 ± 2	586	+	-	-	11
S38) Vitamin 3	+	301	-	181	+	23,320	-	165
S39) Vitamin 4	+	232	15 ± 4	460	+	18	-	342
S40) Vitamin 5	+	-	12 ± 4	515	+	-	-	5
S41) Vitamin 6	+	61	-	557	+	-	-	2
S42) Vitamin 7	-	-	-	548	-	-	-	2
S43) Vitamin 8	+	20,263	18 ± 7	382	+	97	-	179
S44) Vitamin 9	+	5,558	18 ± 4	453	-	65	-	166
S45) Vitamin 10	+	1,791	16 ± 6	165	-	36	-	240
S46) Vitamin 11	-	-	-	574	+	-	-	3
S47) Vitamin 12	+	2,111	20 ± 10	449	-	-	-	52

Table 4.3. Summary of Measurements for Manufactured Infant Formula Products; ND = not detected; "+" indicates Ca, or P was detected by XRF)

	Calcium-Based Measurements		Phosphorus-Based Measurements		TEM/EDX	XRD
	XRF	ICP-MS	XRF	ICP-MS		
	(ppm)	(μg/g)	(ppm)	(μg/g)	(Avg ± 1 STD, nm)	
Australian Infant Formula						
S48) Formula 1	7,962	4,662	4,257	2,821	Ca, P, O 65 ± 20 (length) by 18 ± 7 (width)	HA
S49) Formula 2	7,582	3,967	4,094	2,434	Ca, P, O 144 ± 153 (length) by 43 ± 21 (width)	HA
S50) Formula 3	6,307	3,657	2,733	1,661	Ca, P, O 211 ± 95 (length) by 23 ± 7 (width)	HA
S51) Formula 4	6,603	3,777	2,198	1,404	Ca, P, O 134 ± 44 (diameter)	Calcite
S52) Formula 5	6,620	3,939	3,198	2,097	Ca, P, O 752 ± 127 (diameter)	Calcite
S53) Formula 6	6,786	3,740	2,989	1,674	Ca, P, O 445 – 5,404	Calcite
S54) Formula 7	8,278	4,426	3,740	2,063	Ca, P, O 154 ± 136 (diameter)	Calcite

Table 4.4. Summary of complex food matrix calibration curve. Limit of detection was calcualted for each element (Si, P, Ca, Ti) in a combined food matrix. Each XRF signal (ppm) was divided by the molar ratio of the element in the compound to convert the elemental signal (ppm) to the compound signal (ppm) as recommended by the manufacturer, Thermo Scientific.

$$\text{XRF Resonse (NM ppm)} = \frac{\text{XRF Elemental Output Signal (ppm)}}{\text{Element molar mass/ Compound molar mass}}$$

	XRF Response (ppm)			
Concentration added to Blank Complex Food Matrix	**TiO_2**	**SiO_2**	**HA (Ca)**	**HA (P)**
Blank	<LOD	<LOD	419	3,125
25 ppm	58	<LOD	<LOD	<LOD
50 ppm	112	<LOD	128	649
100 ppm	200	355	153	351
500 ppm	868	1,102	837	930
1,000 ppm	2,016	1,835	1,857	2,454
2,500 ppm	3,098	5,008	4,585	3,125
5,000 ppm	8,656	10,747	8,884	9,687
10,000 ppm	15,607	19,278	15,070	14,747
100,000 ppm	148,333	193,855	135,887	141,577

Table 4.5. Comparison of the calculated LOD and LOD reported by manufacturer. The LOD is calculated using the 500 ppm sample [199].

Complex Food Matrix	**Si**	**P**	**Ca**	**Ti**
Calculated LOD (ppm) (Calibration Curve)	42	69	22	3
Instrument LOD (ppm) (1.5*Error of Blank)	45	24	23	7

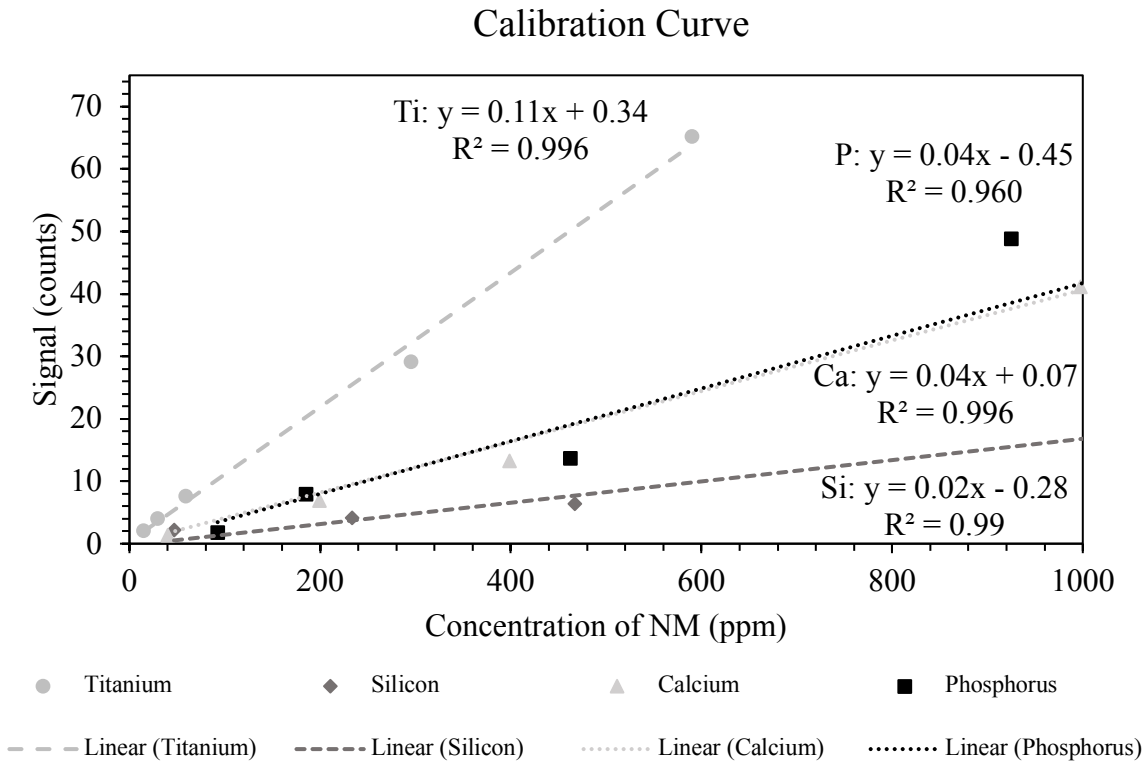

Figure 4.1. Graph of Concentraiton of NM (Table 4.4) for x-axis and signal (counts) for y-axis.

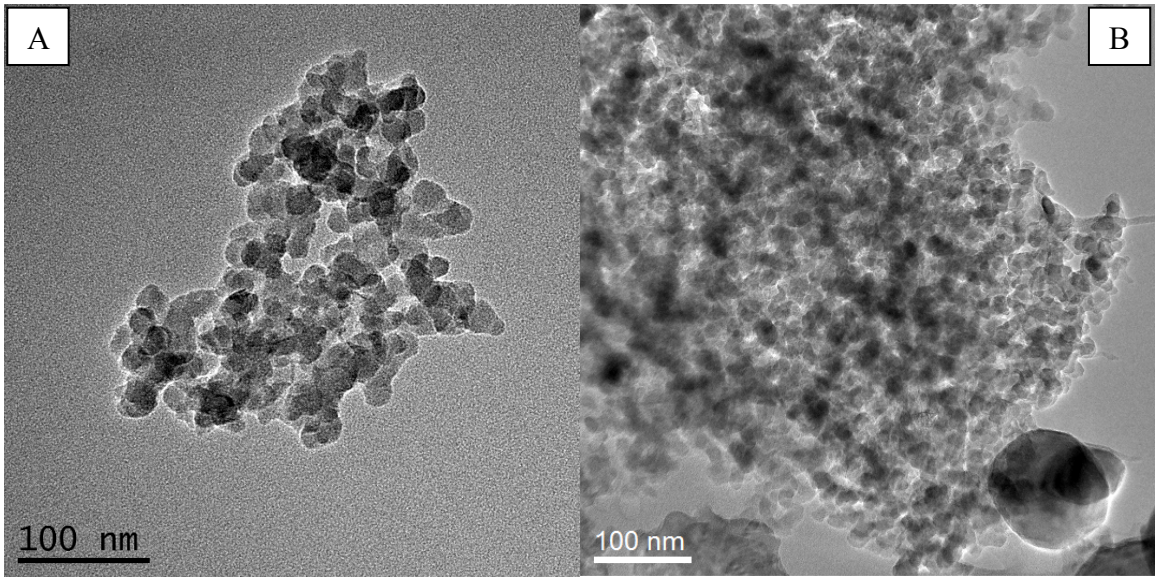

Figure 4.2. TEM of (A) reference food-grade SiO_2 powder, (B) SiO_2 in vitamin supplement 9 (S44)

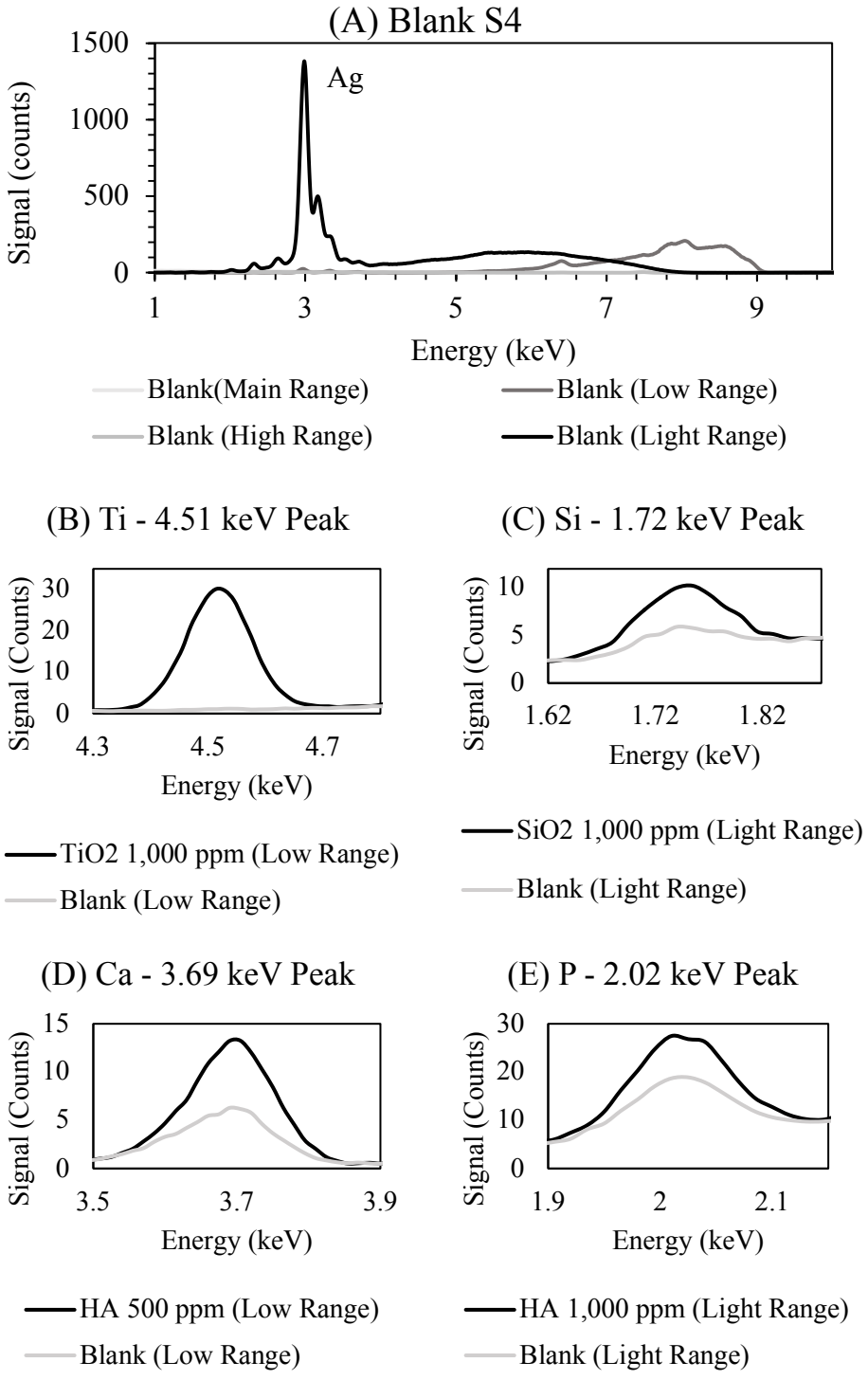

Figure 4.3. XRF graph (Energy (keV) vs. Signal (Counts)) of the spectra of the following: A) Blank Sample (S4) Ag peak is from XRF Ag anode for X-ray creation,

B)1,000 ppm TiO_2 in the blank matrix (S4) and the blank (S4), C) 1,000 ppm SiO_2 in the blank food matrix (S4) and the blank (S4), D) 1,000 ppm HA in the blank food matrix (S4) and the blank (S4), E) 1,000 ppm HA in the blank food matrix (S4) and the blank (S4).

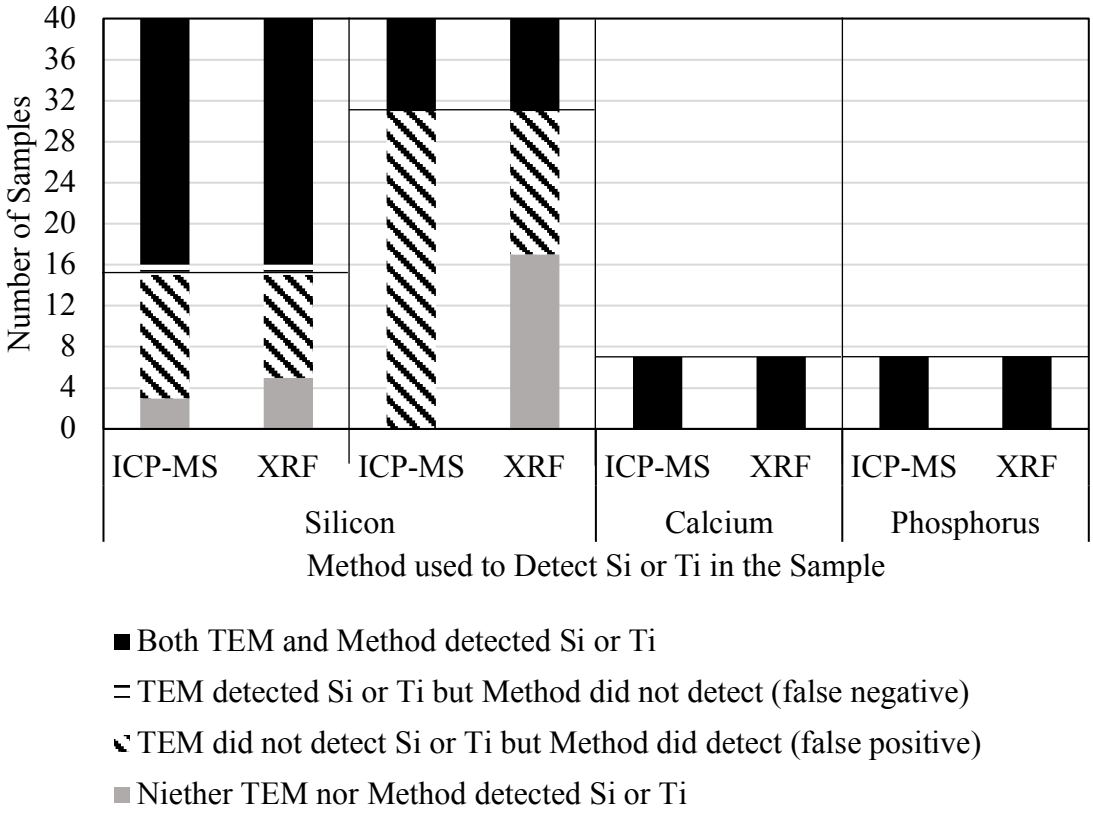

Figure 4.4. Comparison of a method (ICPS and XRF) to TEM for Si and Ti in the 40 consumer products (28 food products and 12 vitamin supplements) and the comparison of Ca and P in the 7 infant formulas. Grey denotes neither method detected Si nor Ti or Ca nor P, black denotes both methods detected Si or Ti for consumer products or Ca or P for infant formulas. The horizontal line section denotes false negatives where TEM detected Si or Ti, or Ca or P but the method (ICP-MS or XRF) did not. The slashed line denotes

false positive where the method (ICP-MS or XRF) detected Si or Ti, or Ca or P, while TEM did not.

4.7 SUPPLEMENTAL INFORMATION

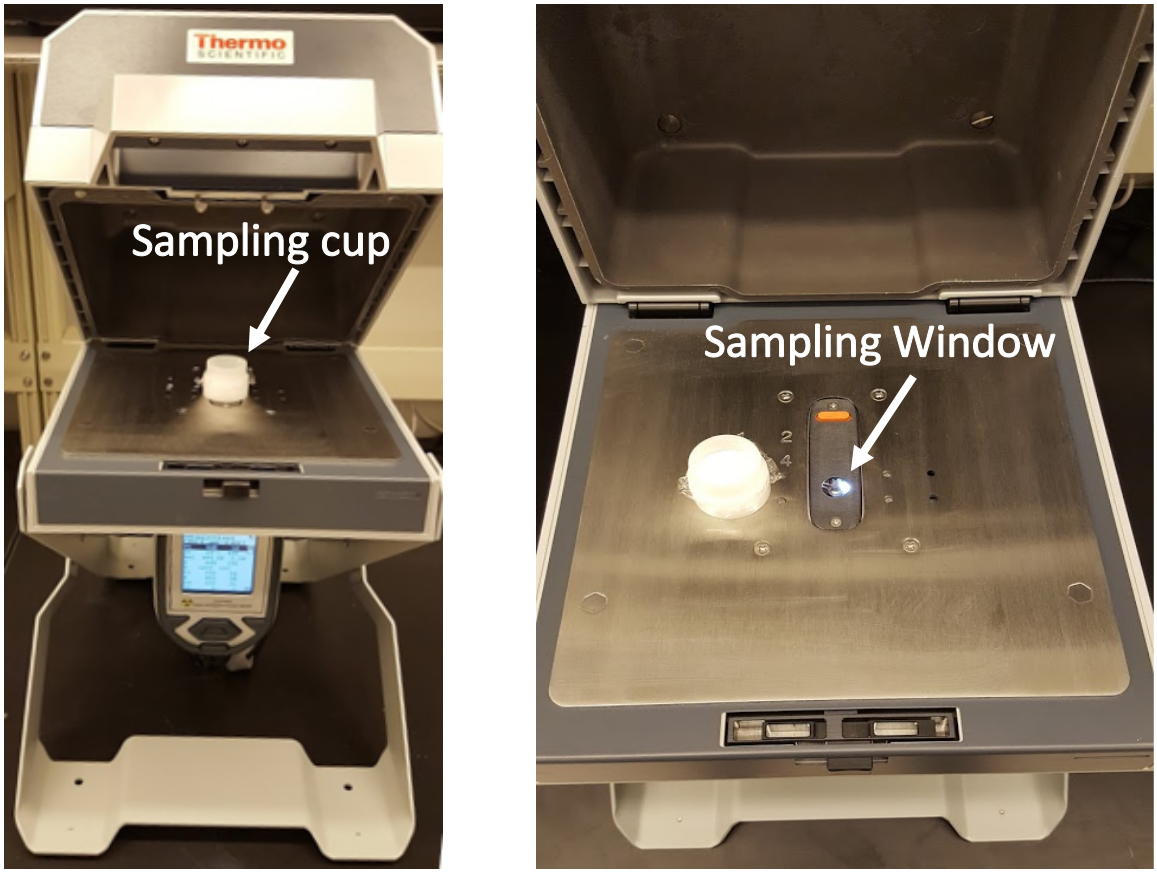

Figure SI.4.1. Set up of Niton XL3t GOLDD+, Thermo Fisher Scientific

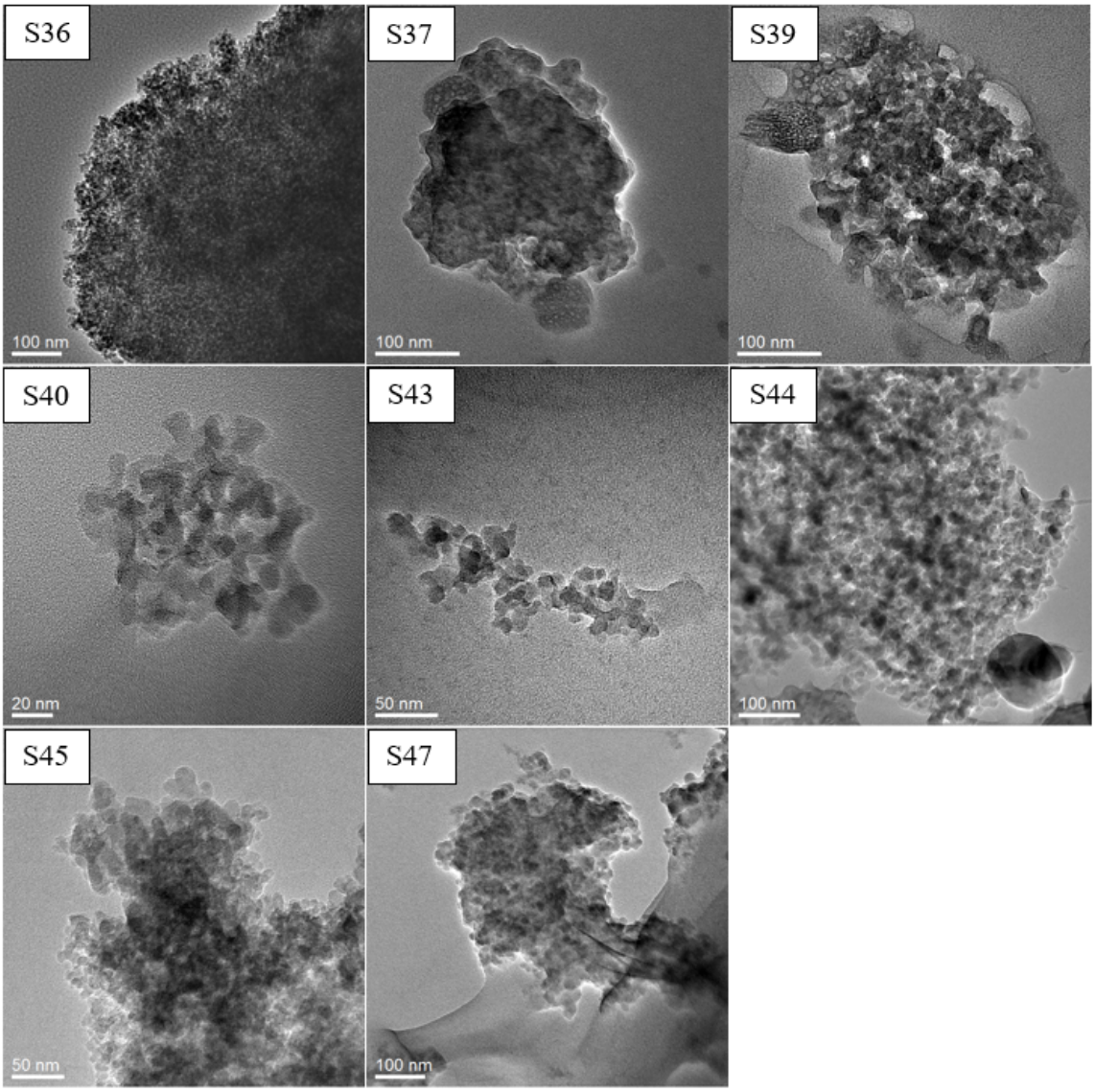

Figure SI.4.2. Tranmission electron microscopy of vitamin supplements containing silicon dioxide

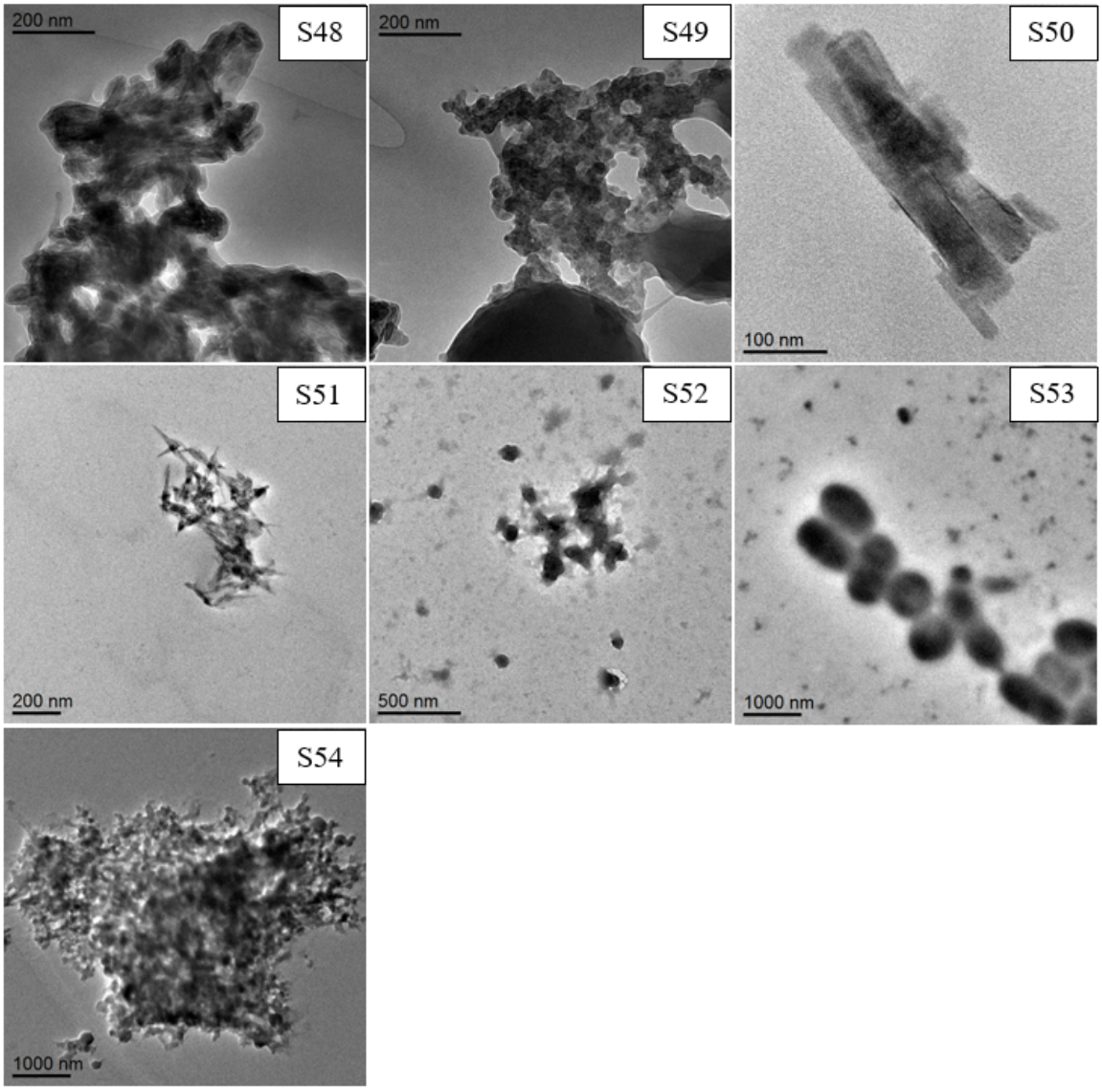

Figure SI.4.3. Transmission electron microscopy of calciun phosphate identified in the infant formulas

CHAPTER 5

APPLICATION OF PORTABLE X-RAY FLUORESCENCE ON BIOLOGICAL AND ENVIRONMENTAL MATRICES

5.1 INTRODUCTION

Nanomaterials' (NMs) beneficial characteristics are improving consumer products and industrial processes; however, NMs have been identified as a new class of pollutants due to release during product use and disposal [14, 15]. The unknown environmental interaction of NMs and subsequent characteristic changes (morphology, size, and surface coating) due to their interaction with plants and animals, exposure to UV sunlight, and heat from burning, has raised regulatory and health concerns [15-23]. The National Institute of Environmental Health and Sciences (NIEHS) recognizes the benefit of NMs; however, highlights the problem "little is known about the human and environmental risks". The National Nanotechnology Initiative (NNI) Environmental, Health, and Safety Research Strategy is to "Develop measurement tools to detect and identify engineered nanoscale materials in products and relevant matrices" [24]. Analytical techniques to detect nanomaterials in environmental and biological samples often require extensive sample preparation and/or specialized equipment [32, 200] limiting large scale nanomaterial monitoring and real-time human exposure assessment. A need exists for a rapid technique to prescreen samples for absence or presence for evaluating nanomaterial exposure for health assessment, and to eliminate environmental samples deemed free of nanomaterials.

The goal of this chapter is to explore the suitability of a rapid analytical technique, X-ray Fluorescence (XRF), as a pre-screening method that requires minimal

sample preparation for elements commonly used in nanomaterials (e.g., Si, Ti). XRF has the potential to be utilized before employing more sophisticated pretreatment or analytical instrumentation (e.g., ICP-MS, and TEM) in a multi-tiered analytical approach. The objective of this chapter is to 1) detect Ti, Si, Ca, and P in water, water with natural organic matter, and biological (simulated saliva and sweat) samples (tier one of tiered framework) and 2) investigate if cloud point extraction and filtration can extract sufficient quantities of nanomaterials for detection by XRF (tier two of tiered framework).

The application of XRF (tier one approach) on ultrapure water was first investigated to validate the instrument's capabilities of detecting elements (Ti, Si, Ca, and P) present as nanomaterials (TiO_2, SiO_2, and HA) in liquids followed by water with natural organic matter (NOM) as an environmentally relevant matrix. XRF additionally was applied to biological matrices (simulated saliva and sweat) and cotton swabs dipped in biological matrices to investigate XRF as a pre-screening tool to detect exposure to titanium dioxide. Titanium dioxide, silicon dioxide, and hydroxyapatite nanomaterials from our previous studies (Chapter 2, 3, and 4) were chosen based on their direct human contact in food (TiO_2, SiO_2, and HA characterized in Chapter 2, 3, and 4) and sunscreen (Chapter 6) with suspected release into the environment after product use [201].

Extraction of nanomaterials by physical filtration and cloud point extraction combined with XRF was investigated as a tier two approach to detect elements present as nanomaterials in the small sample mass (<1g) of the cloud point extraction surfactant, and on the surface of a filter (~20 mg). Cloud point extraction (CPE), an extraction technique, employs the use of a surfactant solution to separate a sample into an

immiscible surfactant-rich and surfactant free phase [55]. At particular temperatures, the surfactant assembles into micelles, which interact and concentrates analytes into a surfactant-rich phase. Centrifugation is used to separate the phases, concentrating the analytes [56, 202]. Cloud point extraction has been proven a robust technique to concentrate nanomaterials in environmental samples in our previous study [203].

I hypothesize physical filtration and/or cloud point extraction extracts nanomaterials from the bulk sample reducing XRF detection limits of elements suspected to be present as nanomaterials by 50X in solid and liquid samples (goal of 1 μg/g limit of detection). The goal is based on the threshold where less than 1% of terrestrial and aquatic species exhibit sensitivity (e.g. lethal concentration, half maximum effect concentration, median lethal dose, lowest observed effect concentration, no observed effect concentration, and half maximum inhibitory concentration) to the nanomaterials [53]. The goal is used as a metric of success to validate the tier two approach as a framework for a global nanomaterial monitoring.

With the projected increased use of nanomaterials, a rapid analysis technique is essential to monitoring nanomaterials across various matrices to determine the exposure to humans in consumer products, manufacturing facilities, and the environment. Combining XRF with cloud point extraction and the filtration method, the nanomaterial presence in liquid samples can be determined in near real-time and at lower cost than other elemental analysis techniques. The rapid results when monitoring for presence of nanomaterials allows researchers to develop a strategic analysis plan for further, in-depth analysis and characterization of nanomaterials. A promising application is for real-time

health exposure analysis for industrial workers where saliva and mucus can be dispersed in water and analyzed for a real-time exposure extent.

5.2 MATERIALS AND METHODS

Pristine Food-Grade SiO_2, TiO_2, HA Materials

One powder sample of pristine food-grade (99% pure) SiO_2, sample identified as food-grade (European Union food code E551), was procured from Chinese vendors and characterized extensively in a previous study [121]. One pristine food-grade (European Union food code E171) TiO_2 powder sample was procured from a Chinese vendor and characterized in a previous study [59]. One powder, pristine hydroxyapatite (HA), a calcium phosphate compound, was procured from a Chinese vendor and characterized in a previous study [70].

Nanomaterials in Water

Each nanomaterial (SiO_2, TiO_2, HA) was added to Ultrapure water (18.2 MΩ cm, Nanopure Infinity, Barnstead) to create a stock solution of 0.1 wt%. Dilutions from stock solution were used to create solutions between 15ppm and 750ppm for XRF calibration curves. Table 5.1 contains the complete sample list.

Organic Matter in Water Matrix

Natural organic matter (Suwannee River – (SRHA) standards) was purchased from the International Humic Substances Society (IHSS, Atlanta, GA, USA). The NOM was added to Ultrapure water (18.2 MΩ cm, Nanopure Infinity, Barnstead) to create a stock NOM water solution. A 200 μg/L solution was made and sonicated for 30 minutes (Branson ultrasonic bath - 80 W/L). Aliquots of the NOM solution were added to water

with NMs for a final solution concentration of 5 μg/mL NOM for the calibration curve. Table SI5.1 contains the complete sample list.

Simulated Body Fluids and Cotton Swabs

Simulated saliva body fluid, and simulated sweat body fluid were mixed to create a complex biological matrix, respectively, following a previously published recipe [148]. The simulated saliva ingredients, potassium chloride (0.72 g/L), calcium chloride dehydrate (0.22 g/L), sodium chloride (0.6 g/L), potassium phosphate monobasic (0.68 g/L), sodium phosphate dibasic (0.866 g/L), and citric acid (0.03 g/L) were mixed with a stir bar on a stir plate for 24 hours to dissolve ingredients. The simulated sweat fluid ingredients, sodium chloride (2.92 g/L), calcium chloride (0.166 g/L), magnesium sulfate (0.12 g/L), and potassium phosphate monobasic (1.02 g/L), were mixed with a stir bar on a stir plate for 24 hours to dissolve ingredients. A calibration curve of titanium dioxide (15 – 750 ppm of TiO_2) in the simulated fluids was created for detection by XRF. Additionally cotton swabs, procured from USA manufacturers, were dipped into simulated biological fluids. Table SI.5.3 contains the complete sample list.

A candy and sunscreen, labeled as containing TiO_2 were procured from US manufactures. Human saliva, and human sweat were captured on to a cotton swab and immediately analyzed by XRF as a nanomaterial blank. Sunscreen was applied to human skin, and after exercise, sweat of the region was sampled by a cotton swab. The candy was eaten, and a cotton swab of the inside mouth was immediately obtained and analyzed by XRF.

Cloud Point Extraction Procedure

All chemicals were obtained from Sigma-Aldrich (MO, USA). Triton X-114 (TX-114) was used for surfactant. A modified CPE procedure that has demonstrated high efficiency was used for all tests [203]. Nanomaterial (e.g. TiO_2, SiO_2, and HA) suspensions (40mL) were prepared in ultrapure water, and organic rich water (Suwannee River NOMs) in concentrations of 0.1 ppm, 0.5ppm, 1ppm, 5ppm, 10 ppm, and 20ppm. Suspensions were inverted by hand for 2 minutes. Next the 40 mL solutions were combined with 400 µL of 1.25 M sodium acetate solution, 100 µL of 1 M acetic acid, 1.0 mL of saturated EDTA solution, and 1.0 mL of a 10% TX-114 solution (w/w in water). The suspension was mixed on a vortex in a polypropylene centrifuge tube (VWR). The suspension was incubated at 45 °C in a water bath for 30 min, inverted by hand for 2 minutes, incubated at 45 °C in a water bath for an additional 30 min, centrifuged at 3,000 G for 12 minutes, and cooled to ~4 °C. Once cooled, the supernatant was pipetted off leaving a ~0.5 mL surfactant rich phase used for analysis.

Filtration of Nanomaterials in Water

Nanomaterials (TiO_2, SiO_2, and HA) samples were added to Ultrapure water for a concentration of 0.1ppm (µg/mL) and shaken for 2 minutes or until well dispersed and then further sonicated (Branson ultrasonic bath - 80 Watts/L) for 30 minutes. Samples (~25 mL) were first filtered using an 8 µm pore sized cellulose paper filter (Whatman 2 - Cellulose Paper Filter) to remove large particulate matter and then filtered using a 0.1 µm polyethersulfone membrane filter (Sterlitech filter) to capture nanoparticles or nanoparticle aggregates for analysis [122]. Analysis was completed at 5, 10, 15, 20, and 25 mL of 0.1 ppm (µg/mL) nanomaterial solution with theoretical loading masses of 0.5,

1, 1.5, 2, and 2.5 μg to develop a calibration curve. The 0.1 μm filter was air dried at room temperature for 15 minutes before analyzing its surface by XRF. I hypothesized that passing water samples through 0.1 μm filters could retain enough colloids on the filter surface to reach detectable levels. Concentration of solids in water and the volume of sample filtered were designed to avoid cake filtration on the membrane surfaces.

XRF Sample Preparation & Instrumentation

X-ray fluorescence (XRF, Niton XL3t GOLDD+, Thermo Fisher Scientific, (Waltham, MA, USA) required minimal sample preparation for filter and liquid samples. The configuration is shown in Figure SI.4.1. Samples were placed within an XRF sampling cup (Premier Lab) which was composed of a cup with a thin (8μm) carbon film to support the sample. The Niton XL3t GOLDD+ uses four x-ray energy levels and filters, main, light, heavy, and low to detect elements between Mg and U. The XRF analyzer was used in mining mode with the software algorithm and calibration completed by Thermo Scientific. The built-in algorithm calculates the concentration (ppm) of each element and the corresponding error (two standard deviation). A timeframe of 120 seconds was used for each energy level (e.g. main, light, heavy, and low) for samples unless otherwise noted. The persistent peaks at 1.74, 2.02, 3.69, and 4.51 keV indicate the presence Si, P, Ca, and Ti respectively. The signal of each element was calculated by the peak height at 1.74, 2.02, 3.69, and 4.51 keV for Si, P, Ca, and Ti respectively, minus the height of the signal of the blank sample (signal at 1.74, 2.02, 3.69, and 4.51 keV for Si, P, Ca, and Ti respectively). Elemental analysis was statistically evaluated using the signal to noise ratio (S/N). Assuming Gaussian distribution, an S/N of 3.29 represents 3.29 standard deviations from the background noise, which corresponds to a 99.95%

confidence interval that a peak is present. A value of 3.29 was chosen as recommended by IUPAC [198] for XRF.

Calculation of the Limit of Detection

The XRF software algorithm and elemental calibration was validated by developing a calibration curve and calculating the limit of detection. Analyzing the matrix calibration curve solutions (NMs spiked into water, water with NOM, NMs filtered from water) for the signal at the corresponding energy for each element (Si, Ti, Ca, and P), the signal height (counts) was measured. The background signal of the blank (water, water with NOM, simulated sweat, simulated saliva, blank filter) was subtracted from the signal height to obtain the peak height (counts) [199], graphed in Figures 5.1, 5.2, 5.4.

The instrument limit of detection (LOD) was calculated using the below equation [199]:

$$LOD = \frac{3.29 \times \sqrt{2} \times C_A}{I_P - I_b} \times \sqrt{\frac{I_b}{t/2}}$$

In the above equation, 3.29 is the recommended 99.95% confidence interval, $\sqrt{2}$ is due to the two required measurements (sample of interest and blank sample), C_A is the concentration (ppm) of the analyte (nanomaterial) added to the sample, I_p is the intensity under the analyte peak of the sample, I_b is the blank sample peak under the analyte peak, t is the total time of analysis (time of analyte analysis plus the time of the blank sample analysis).

5.3 RESULTS

Nanomaterials in Water and Water with Natural Organic Matter

Figure 5.1 graphs the XRF signal (counts) vs. the spiked concentration of the nanomaterial (TiO_2, SiO_2, and HA) in nanopure water. XRF detected the presence of Ti, Si, Ca, and P in all water samples with spiked concentrations between 15 and 750 ppm. A linear best fit line was calculated with the corresponding R^2 values of 0.96, 0.96, 0.97, and 0.92 for Ti, Si, Ca, and P, respectively. The LOD of Ti, Si, and Ca in water were calculated to be 5, 24, 20 ppm, respectively.

Figure 5.2 graphs the XRF signal (counts) vs. the spiked concentration of the nanomaterial (TiO_2, SiO_2, and HA) in water with NOMs. XRF detected the presence of Ti, Si, Ca, and P in all water with NOM samples with spiked concentrations between 15 and 750ppm. A linear best fit line was calculated with the corresponding R^2 values of 0.98, 0.96, 0.96, and 0.91 for Ti, Si, Ca, and P, respectively. The LOD of Ti, Si, and Ca in water with NOM were calculated to be 6, 25, 21 ppm, respectively.

Cloud Point Extraction of Water and Water with Natural Organic Matter

Table 5.1 lists the presence or absence (<LOD) of Ti, Si, Ca, and P in the surfactant phase of cloud point extraction in water and water with organics. The resulting surfactant phase of water samples spiked with TiO_2 followed by CPE had presence of Ti in initial spiked concentrations of 0.1, 1, 5, 10, 20 ppm and absence of Ti at an initial spiked concentration of 0.5 ppm. The resulting surfactant phase of water samples spiked with HA followed by CPE had presence of Ca in initial spiked concentrations of 0.1, 1, 5, 10, 20 ppm and absence of Ca at an initial spiked concentration of 0.5 ppm. Silicon and phosphorous were absent in all water samples spiked with SiO_2, and HA respectively.

The resulting surfactant phase of water with NOM samples spiked with TiO_2 followed by CPE had presence of Ti in initial spiked concentrations of 0.5, 1, 5, 10, 20 ppm and absence of Ti at an initial spiked concentration of 0.1 ppm. The resulting surfactant phase of water with NOM samples spiked with SiO_2 followed by CPE had presence of Si in initial spiked concentrations of 1, 5, 10, 20 ppm and absence of Si at initial spiked concentrations of 0.1 and 0.5 ppm. Calcium and phosphorous were absent in all water with NOM samples spiked with HA.

Simulated Body Fluids

Figure 5.3 graphs the XRF signal (ppm) on the y-axis and the spiked TiO_2 concentration (ppm) on the x-axis of TiO_2 spiked into simulated saliva, simulated sweat, cotton swabs with simulated saliva, and cotton swabs with simulated sweat. Titanium was detected in all matrices, saliva, sweat, cotton swab with saliva, and cotton swab with sweat, with R^2 values of 0.97, 0.96 0.98, and 0.94 respectfully. Cotton swabs of human saliva and sweat were found absent of titanium and identified as TiO_2 blanks (Table 5.2). Analysis of unaltered solid food candy and sunscreen samples identified the presence of titanium (Table 5.2). XRF analysis of human saliva after consumption of the solid food candy identified the presence of titanium on the cotton swab. XRF analysis of a cotton swab containing human sweat of a sunscreen containing region on the human skin identified the presence of titanium (Table 5.2). The LOD of Ti in simulated sweat, simulated saliva, simulated sweat on a cotton swab, simulated saliva on a cotton swab were calculated to be 2, 2, 5, and 10 ppm, respectively.

Filtration of Nanomaterials in Water

Figure 5.4 depicts the XRF Signal (counts) vs. the calculated mass of a nanomaterial (TiO_2, SiO_2, and HA) filtered from water. XRF detected titanium, calcium, and silicon at all volumes of 0.1 μg/g of NM solution filtered. A linear best fit line was calculated with R^2 values of 0.94, 0.99, and 0.82 for Ca, Ti, and Si respectively.

5.4 DISCUSSION

Comparing XRF analysis of NMs in water and water with natural organic matter, XRF had high (>0.91) correlation R^2 values for all NMs in both matrices. The slope of the calibration curve was found to be similar between the two matrices for Ti and Si showing minimal effect of the organic background matrix. The calibration slope of 0.7 and 2.8 for calcium and phosphorous, respectively, in water and 0.3 and 1.2 for calcium and phosphorus in water with NOM shows the organic background matrix has an effect on the detection of Ca and P by XRF. The LOD of Ti, Si, and Ca in water and water with NOM were similar with less than 5% variance.

Comparing XRF detection of elements in the surfactant phase of CPE of water to the surfactant phase of water with NOM, XRF had high detection of Ti, detecting Ti in 5 out of 6 tested concentrations in water and 5 out of 6 tested concentrations in water with NOM. XRF did not detect Si in water; however, detected Si in the surfactant phase of the CPE of water with NOM for concentrations 1 to 20 ppm. XRF detected Ca in the surfactant phase of HA spiked in water for 5 out of 6 samples and did not detect Ca in the HA spiked in water with NOM. XRF did not detect P in either the surfactant phase from CPE of water or water with NOM. The change in detection of Ca, and Si can be a result of a few possibilities, including: 1) the inherent properties of the instrument to detect

elements in a low sample mass, a challenge for XRF [197] , or 2) the addition of NOM, known to change the surface characteristics of nanomaterials [204], reduced the extraction efficiency of Ca while improving the extraction of Si. Additional research is necessary.

Comparing filtration to CPE (Figure 5.4 and Table 5.1), XRF detected Ti, Si, Ca, and P on the surface of all filters used to filter water spiked with NMs. XRF had improved detection of Ti, Si, Ca, and P on the surface of the filter compared to the surfactant phase of CPE. Albeit the low sample mass of the filter (20 mg), the nanomaterials are concentrated on the surface of the filter closest to the XRF detector compared to CPE where the nanomaterials are within the ~1 g of surfactant. Additionally, the concentration of the nanomaterials in relation to background matrix (filter or surfactant) is higher for the filter than for the surfactant (5mL filtered of 0.1 ppm solution (0.5 microgram of NM) on a 20mg filter (500 ppm of NM in filter), compared to 40 mL solution of 0.1 ppm (4 microgram of NM) in 1,000 mg of surfactant phase (40 ppm of NM in surfactant)).

Comparing the biological fluids, XRF detected Ti in both simulated sweat and simulated saliva, and in simulated sweat and saliva on a cotton swab. XRF additionally detected the absence of Ti in human saliva and sweat, and detected the presence of Ti in the human saliva after eating candy, and in human sweat on a region with sunscreen application.

5.5 CONCLUSION

XRF was demonstrated as a feasible technique to determine the presence or absence of silicon, titanium calcium, phosphorous, nano silicon, nano titanium, nano

calcium, and nano phosphorous in both water and water with natural organic matter samples. XRF meet the goal of detecting Ti, Si, and Ca with a LOD below 50 ppm for liquid samples and below 1 ppm for extracted samples. Additionally XRF was demonstrated as a feasible technique to detect titanium in biological matrices for application as a rapid exposure test for risk assessment. Advantages of XRF are: (a) rapid detection (<10 min) of Ti, Si, Ca, and P, (b) rapid detection of Ti, Si, Ca, and P containing nanomaterials; and (c) reduced pre-treatment and analysis costs per sample. The present techniques, XRF and XRF combined with filtration, lends itself to analysis of additional environmental and biological matrices as a screening technique.

XRF as a tier one and tier two approach (Figure 1.1) can be used to rapidly detect the presence of Ti, Si, Ca, and P in water and water with NOM (environmental samples). The application of filtration with XRF can be used as an additional screening process to determine if elements suspected to be present as nanomaterials are present. XRF as a tier one and tier two process will reduce the number of samples that require TEM resulting in higher throughput of samples and a reduced cost.

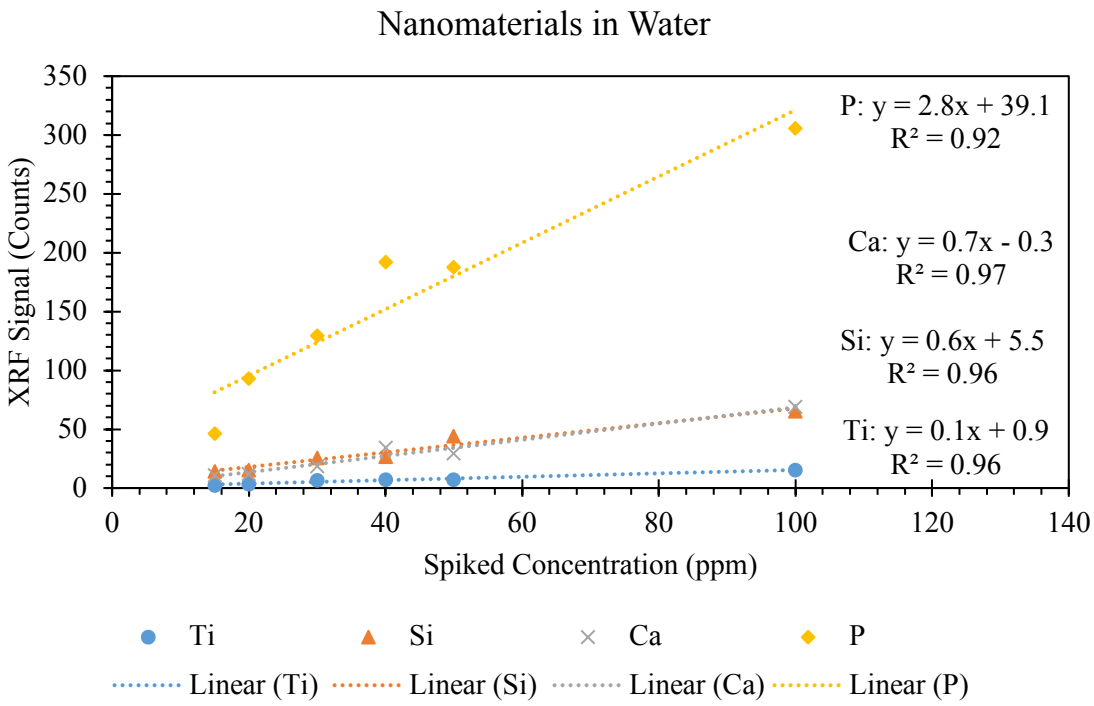

Figure 5.1. Graph of the XRF Signal (counts) on the y-axis the spiked nanomaterial concentration (ppm) in water on the x-axis

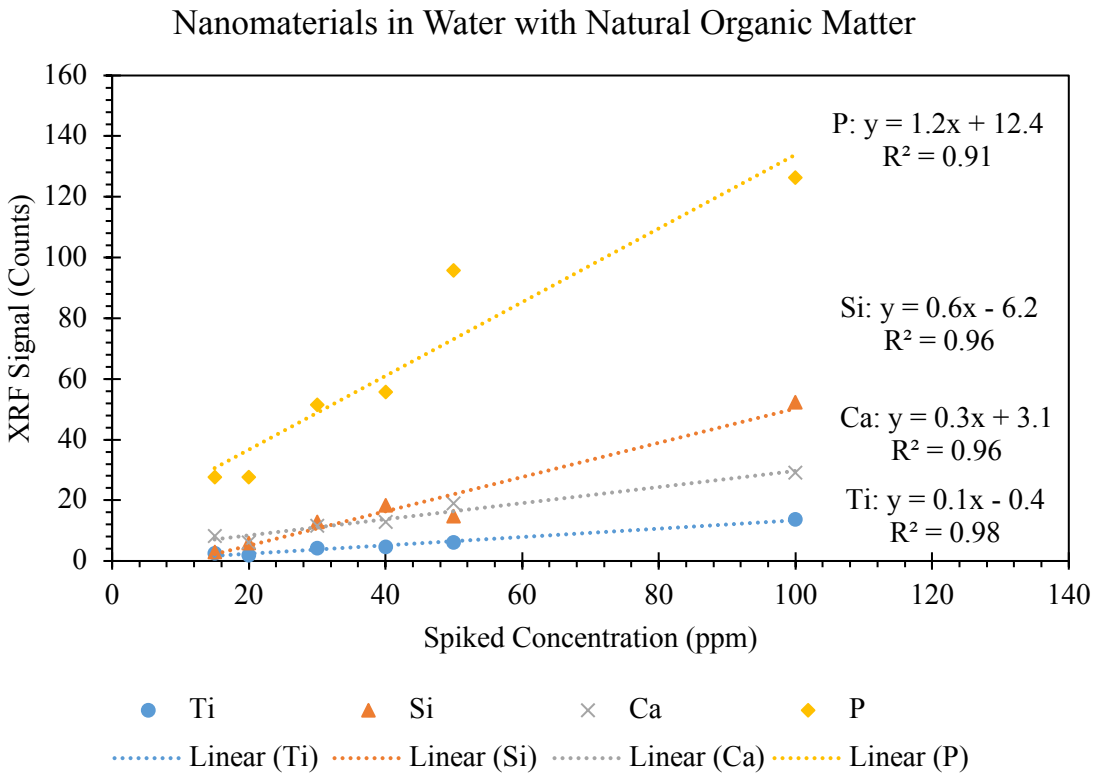

Figure 5.2. Graph of the XRF Signal (counts) on the y-axis and the spiked nanomaterial concentration (ppm) in water with natural organic matter on the x-axis

Table 5.1. Summary of XRF measurements for cloud point extraction; <LOD = not detected (below limit of detection); "+" indicates Ti, Si, Ca, or P was detected by XRF)

CPE of Water (ppm)	Ti	Si	Ca	P
20	+	<LOD	+	<LOD
10	+	<LOD	+	<LOD
5	+	<LOD	+	<LOD
1	+	<LOD	+	<LOD
0.5	<LOD	<LOD	<LOD	<LOD
0.1	+	<LOD	+	<LOD

CPE of Water with Organics (ppm)	Ti	Si	Ca	P
20	+	+	<LOD	<LOD
10	+	+	<LOD	<LOD
5	+	+	<LOD	<LOD
1	+	+	<LOD	<LOD
0.5	+	<LOD	<LOD	<LOD
0.1	<LOD	<LOD	<LOD	<LOD

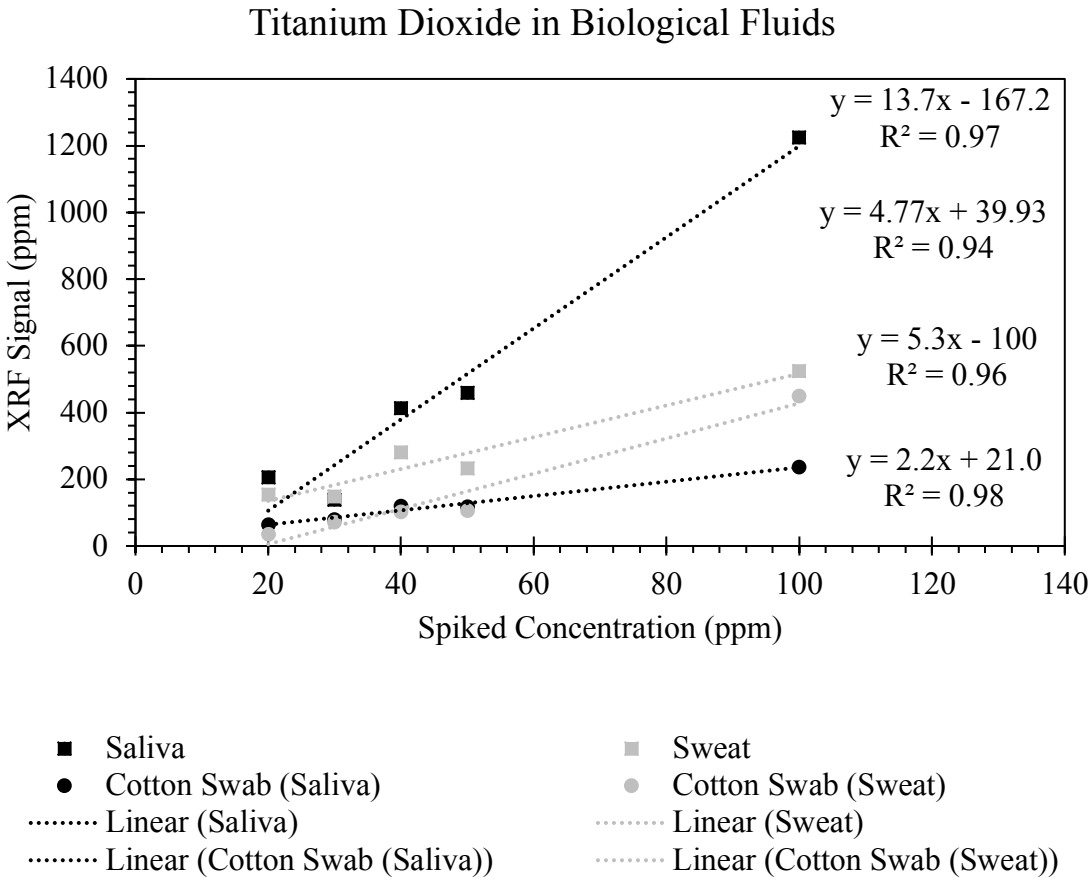

Figure 5.3. Graph of XRF signal (ppm) on the y-axis and the spiked nanomaterial concentration (ppm) in saliva, sweat, saliva on a cotton swab, and sweat on a cotton swab on the x-axis

Table 5.2. Summary of XRF measurements on biological fluids and titanium dioxide; <LOD = not detected (below limit of detection); "+" indicates Ti, detected by XRF)

Matrix	**Ti**
Human Saliva (Blank)	<LOD
Candy	+
Human Saliva After Eating Candy	+
Human Sweat (Blank)	<LOD
Sunscreen	+
Sunscreen in Human Sweat	+

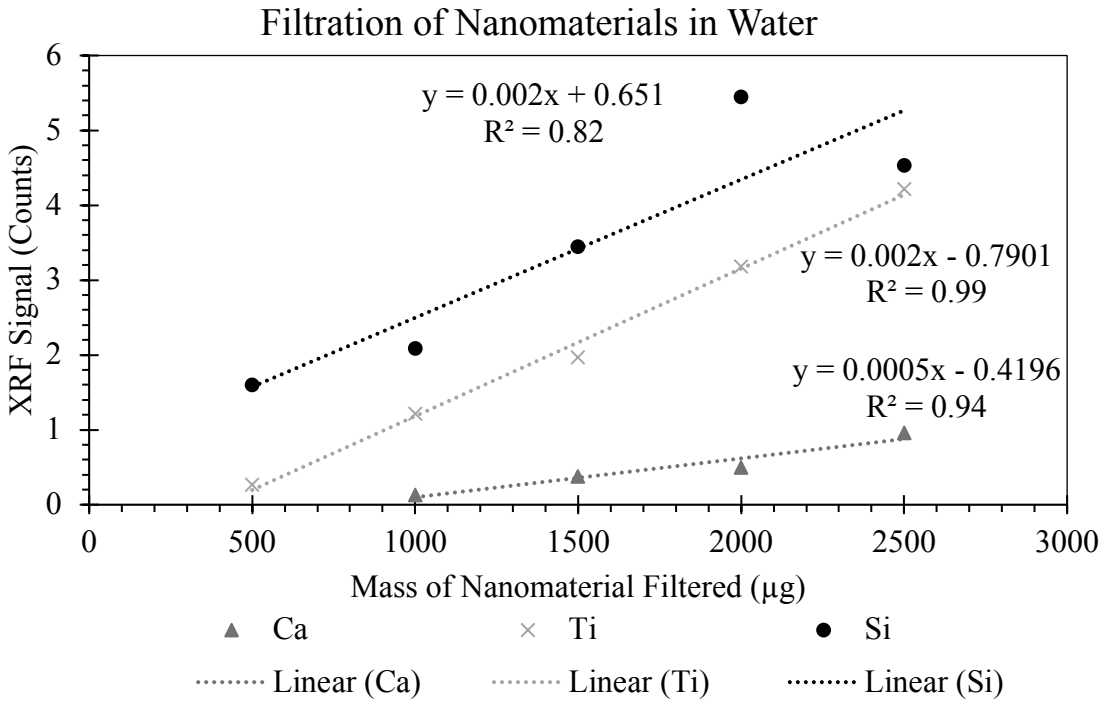

Figure 5.4. Graph of XRF signal (counts) on the y-axis and mass of nanomaterial filtered (microgram) on the x-axis

5.6 SUPPLEMENTAL INFORMATION

Table SI.5.1. Comparison of the XRF signal (ppm) of Ti, Si, Ca, and P to the spiked concentration of the nanomaterial (ppm) in water, and water with organics

Water with Nanomaterials Spiked NM Concentration (ppm)	Ti	Si	Ca	P
15	2	14	11	46
20	3	15	12	93
30	7	26	19	129
40	7	27	34	192
50	7	44	29	188
100	15	66	69	306
500	98	372	406	1,258
750	112	660	500	1,602

Table SI.5.2. Comparison of the XRF signal (ppm) of Ti, Si, Ca, and P to the spiked concentration of the nanomaterial (ppm) in water with organics

Water with Organics (5 µg/g) Spiked NM Concentration (ppm)	Ti	Si	Ca	P
15	2	3	8	28
20	2	6	6	28
30	4	13	12	51
40	5	18	13	56
50	6	15	19	96
100	14	52	29	126
500	62	239	200	786
750	137	426	254	1,055

Table SI.5.3 Recipe for simulated sweat and saliva

Simulated Sweat	(g/L)
Potassium Chloride	0.72
Calcium Chloride Dehydrate	0.22
Sodium Chloride	0.6
Potassium Phosphate Monobasic	0.68
Sodium Phosphate Dibasic	0.866
Citric Acid	0.03

Simulated Saliva	(g/L)
Sodium Chloride	2.92
Calcium Chloride	0.166
Magnesium Sulfate	0.12
Potassium Phosphate Monobasic	1.02

Table SI.5.4. Comparison of the XRF signal (ppm) of Ti, Si, Ca, and P to the spiked concentration of the nanomaterial (ppm) in saliva, sweat, saliva on a cotton swab, and sweat on a cotton swab

TiO_2 Spiked Concentration in Fluid (ppm)	Saliva (XRF ppm Signal)	Sweat (XRF ppm Signal)	Cotton Swab with Simulated Saliva (XRF ppm Signal)	Cotton Swab with Simulated Sweat (XRF ppm Signal)
750	7,238	8,884	3,809	3,498
500	5,267	4,624	2,105	2,180
100	1,225	525	237	450
50	459	234	119	106
40	414	280	120	103
30	139	149	79	73
20	206	155	65	35

CHAPTER 6

ELECTRON MICROSCOPY OF COMPLEX MATRICES

Initial research to quantify the concentration of Si and Ti in wastewater effluent (Nogales, AZ) fueled the development for a tiered analytical approach due to the complicated sample preparation and nanomaterial detection techniques. The development of expertise in transmission electron microscopy (TEM) and scanning electron microscopy (SEM) facilitated understanding of nanomaterial morphology, surface coatings, aggregation, elemental and composition of nanomaterials in consumer products. The TEM and sample preparation expertise was developed through collaboration with colleagues resulting in co-authored manuscripts. Below are the manuscripts, authors, sample preparation, representative TEM images and role involved in each collaboration. Complete TEM and SEM analysis with EDX elemental data can be found in the Appendix.

Survey of food-grade silica dioxide nanomaterial occurrence, characterization, human gut impacts and fate across its lifecycle (Published)

Authors: Y. Yang, JJ Faust, **J. Schoepf**, K. Hristovski, D. Capco, P. Herckes, P. Westerhoff

Role: I characterized SiO_2 nanomaterials using dynamic light scattering (DLS), Zetapotential, and TEM with EDX. Investigated the application of DLS for characterization of NMs compared to TEM analysis, aiding in the development tier three in tiered framework.

Sample Preparation: Six food-grade silicon dioxide nanomaterials were obtained from commercial venders in the USA and China. Powder samples (~0.125 g)

were suspended in 40 mL ultrapure water, sonicated for 30 minutes (Branson ultrasonic bath - 80 W/L) to disperse particles, and then centrifuged at F = 14,000 G for 15 minutes to separate dissolved ions from particulate. The supernatant was poured off, leaving a particulate composed pellet at the bottom of the centrifuge tube. The pellet was re-suspended in 20 mL ultrapure water and sonicated for 5 minutes to re-disperse the particles. A 20 μL aliquot of the solution was pipetted onto a Ted Pella carbon type B, 200 mesh copper TEM grid and allowed to dry overnight prior to TEM/EDX analysis (Philips CM200). Mean particle diameter was measured manually with ImageJ software on 250 particles.

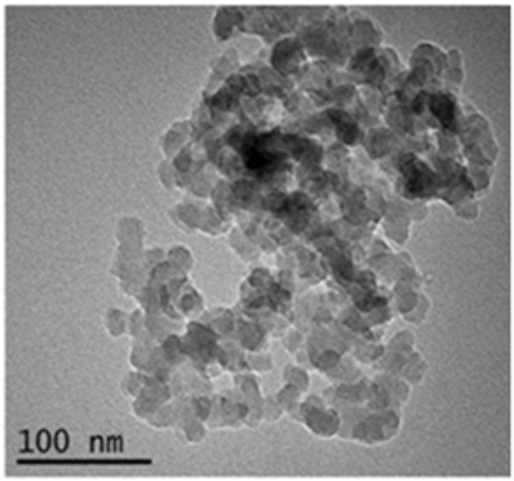

Figure 6.1. TEM image of food grade silicon dioxide

Initial application of TEM solidified the importance of electron microscopy and the scientific community's notation of TEM as the "gold standard" of nanomaterial characterization.

Prospecting nanomaterials in aqueous environments by cloud-point extraction coupled with transmission electron microscopy (Published)

Authors: Y. Yang, R. Reed, **J. Schoepf**, K. Hristovski, P. Herckes, P. Westerhoff

Role: Analyzed environmental samples by TEM with EDX searching for presence of nanomaterials. Investigated CPE to concentrate samples followed by TEM to detect nanomaterials as a sample preparation technique for application in tiered analytical process.

Sample Preparation: All chemicals were obtained from Sigma-Aldrich (MO, USA) unless specifically states. We used the surfactant Triton X-114 (TX-114) for CPE. A modified CPE procedure that has a demonstrated high extraction efficiency was used for all tests [205, 206]. Firstly, nanomaterial suspension with an initial concentration of 1 mg/L was prepared in ultrapure water (details in SI information). After that, 40 mL of 1 mg/L was combined with 400 μL of 1.25 M sodium acetate solution, 100 μL of 1 M acetic acid, 1.0 mL of saturated EDTA solution, and 1.0 mL of a 10% TX-114 solution (w/w in water) [205, 206]. The suspension was mixed on a vortex in a polypropylene centrifuge tube (VWR, USA), incubated at 40 °C in a water bath for 30 min, centrifuged at 2650g for 12 min, and eventually cooled at 4 °C. The aqueous supernatant solution was pipetted out, and 0.5 mL of the surfactant phase remaining at the bottom of the tube was used for further study.

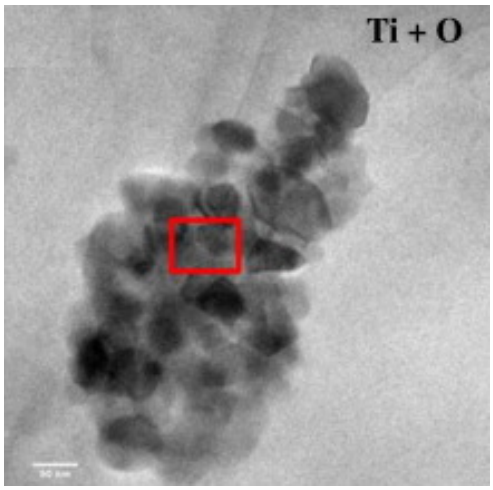

Figure 6.2. TEM image of Titanium Dioxide

Superfine powdered activated carbon incorporated into electrospun polystyrene fibers preserve adsorption capacity (Published)

Authors: O. Apul, N. von Hoogesteijn, **J. Schoepf**, D. Ladner, K. Hristovski, P. Westerhoff (Published)

Role: Developed analysis technique to characterize superfine powder activated carbon (SPAC) and electrospun nanofibers using TEM with EDX. Applied tiered analytical approach using XRF to characterize elements present in activated carbon and continued to tier three to characterize NMs by TEM. Additionally, XRF was used to compare elemental composition of activated carbon compared to activated carbon incorporated into electrospun polystyrene fibers, confirming the presence of activated carbon in the fibers through analyzing elemental ratio of contaminates from SPAC manufacturing process.

Sample Preparation: Visual characterization of the media was conducted via high resolution transmission electron microscopy (HR-TEM) and scanning electron microscopy (SEM). TEM was used to locate the graphitic allotropes of SPAC particles

within the polymeric matrix. For TEM imaging: the powdered SPACs (~0.125 grams each) were suspended in 40 mL of ultrapure water and sonicated for 30 minutes to disperse particles. The solution (~20 μL) was pipetted onto a Ted Pella carbon type B, 200 mesh copper TEM grid and allowed to dry overnight. The PS and SPAC-PS composite fibers were brushed lightly against a Ted Pella carbon type B, 200 mesh copper TEM grid allowing the fibers to electrostatically adhere to the TEM grid. Microscopy was performed on a Philips CM200 TEM equipped with energy-dispersive X-ray spectroscopy (EDX) for elemental analysis. Particle and fiber sizing was performed using ImageJ. The scale bar was used to set the scale for calculating the width of each particle and fiber using ImageJ software.

SEM was used to characterize the fibrous structure of electrospun fiber and the distribution of SPAC particles. Samples were mounted on stainless steel stubs on carbon tape and sputter coated (Pt-Au) for SEM imaging. SEM micrographs were obtained using a JEOL 2010F. The SEM images were processed using ImageJ software to determine the average particle diameter.

The XRF measurements were performed to characterize the elemental composition of PS pellets, neat PS fibers and PS-SPAC composite fibers. A handheld X-Ray Fluorescence device (Niton XL3t GOLDD+, Thermo Fisher Scientific) equipped with an Ag anode (6 - 50 kV, 0 - 200 124 μA, 10mm spot size) and Silicon Drift Detector was used to analyze samples. Four proprietary primary filters, with a measurement time of 60 seconds each, allow for analysis of Mg – U elements. The filters optimize excitation energies in four ranges, reducing spectral background under analyte lines, to

selectively filter primary X-Rays from the tube. The portable XRF directly reports concentration of elements and error (i.e., two standard deviation).

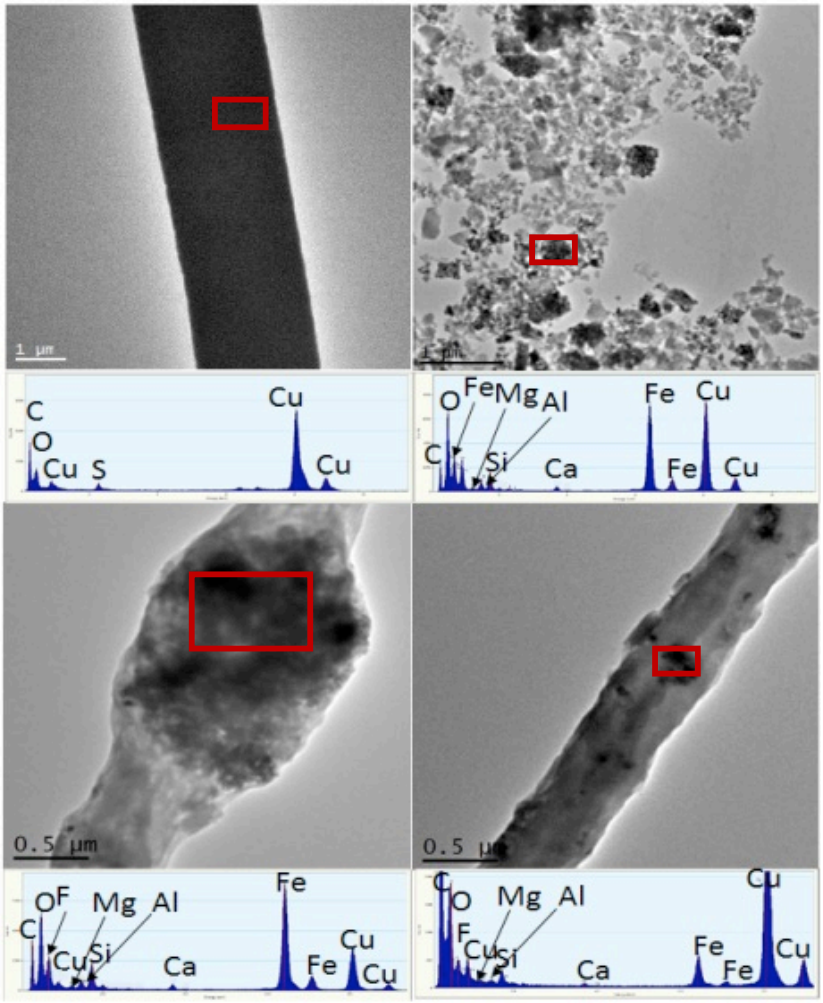

Figure 6.3. TEM images and corresponding EDX analysis of (A) pristine electrospun polystyrene, (B) SPAC powder and (C)-(D) SPAC-PS composite.

Trade-offs in ecosystem impacts from nanomaterial versus organic chemical ultraviolet filters in sunscreens (Published)

Authors: D. Hanigan, L. Truong, R. Tanguay, **J. Schoepf**, T. Nosaka, A. Mulchandani, P. Westerhoff

Role: Applied tier analytical technique to characterize nanomaterials in sunscreens. Applied XRF analysis to screen for Zn and Ti presence in sunscreen samples. All samples contained Zn or Ti and continued to tier three for TEM with EDX analysis. Aided in the development of a nanomaterial extraction technique to remove NMs from sunscreen for TEM analysis to characterize size, morphology, and crystallinity of NMs.

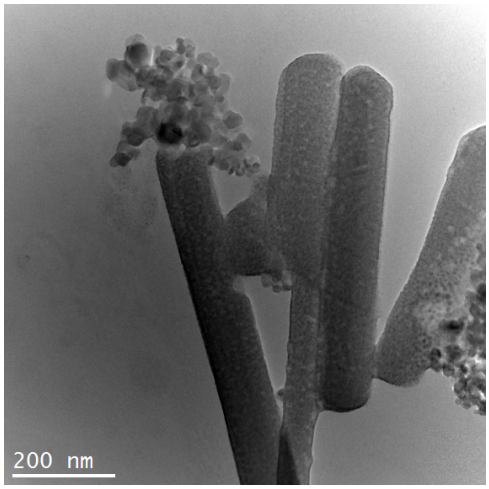

Figure 6.4. Transmission electron microscopy image of Sunscreen containing nano titanium dioxide and nano zinc oxide

Coupling light emitting diodes with photocatalyst-coated optical fibers improves quantum efficiency of pollutant oxidation (Published)

Authors: L. Ling, H. Tugaoen, J. Brame, S. Sinha, C. Li**, J. Schoepf**, K. Hristovski, J. Kim, C. Shang, P. Westerhoff

Role: Developed analytical technique to measure thickness of TiO_2 coating on glass fiber and percent coverage using XRF, LIBS, and SEM with EDX. Validated LIBS tiered analytical technique through detection of Ti with LIBS, continuing to tier three to characterize TiO_2 nanomaterials by SEM with EDX. Investigated the application of the

Focus Ion Beam (FIB) paired with SEM as a tier in the NM detection framework for nanomaterial coatings.

Sample preparation: Quartz fibers were cut using a ceramic blade. Samples were adhered to an aluminum SEM stub with double sided carbon tape. Samples were sputter coated for 120 seconds with Au/Pd and analyzed by a FEI XL30 scanning electron microscope (SEM) coupled with EDX.

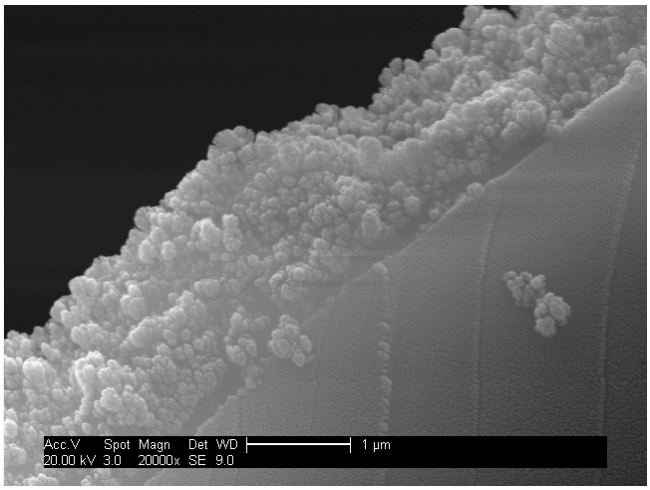

Figure 6.5. SEM image of a titanium dioxide coated fiber

The efficacy of engineered TiO_2 nanoparticles in a commercial floor coating and environmental implications (Published)

Authors: Y. Bi, T. Zaikova, **J. Schoepf**, P. Herckes, J. Hutchison, P. Westerhoff

Role: Analyzed titanium dioxide nanomaterials extracted from commercial floor coatings by TEM and SEM. Investigated separation techniques to extract titanium dioxide from floor coatings.

Sample Preparation: The extracted solids were characterized for particle morphology, mean particle size, and elemental composition by a JEOL 2010F TEM coupled with energy dispersive X-ray spectroscopy (EDX). Approximately 50 mg of sample was

resuspended in 50 mL Nanopure water after 30 min sonication. A small aliquot (10 µL) was pipetted onto a Ted Pella 200 mesh carbon type B TEM grid and allowed to dry overnight under ambient conditions. The obtained TEM images were then examined by ImageJ software with statistical analysis.

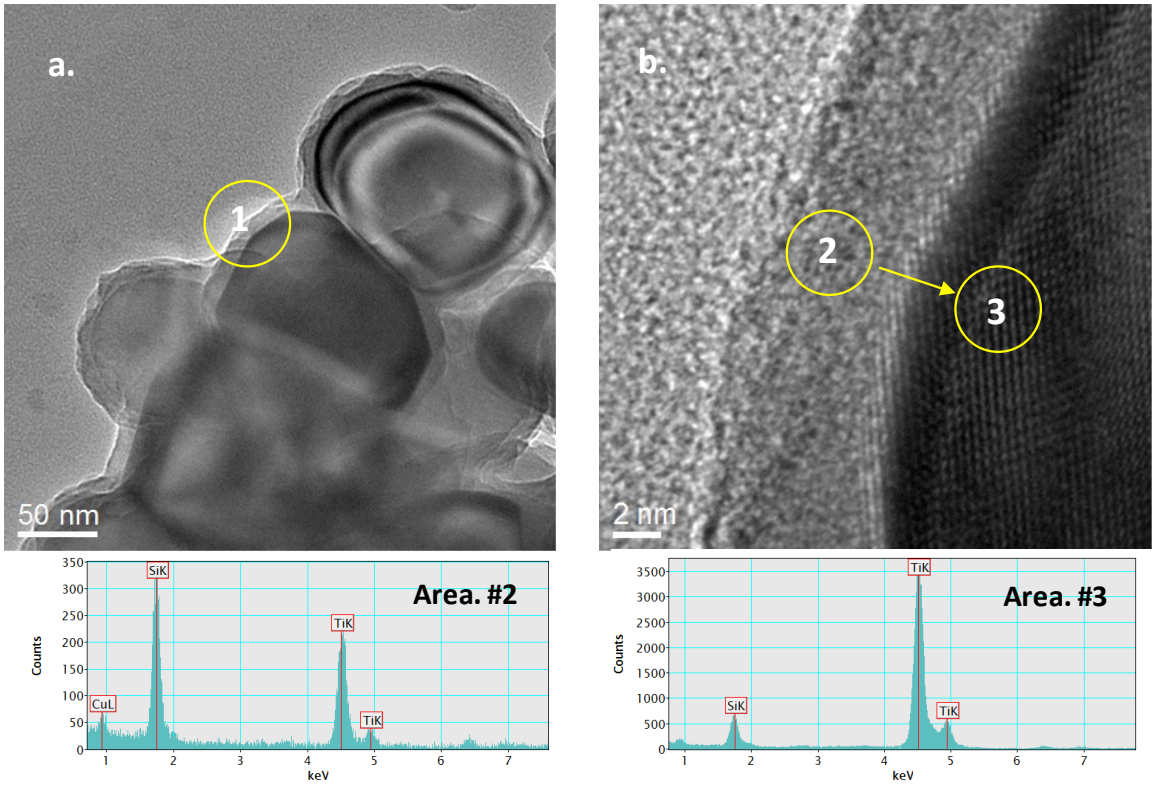

Figure 6.6. (a) Representative TEM image of TiO_2 nanoparticles isolated from the commercial coating product. (b) HRTEM image of the edge of a TiO_2 particle (area #1). EDX spectra were collected across the layer at the particle surface. Significantly higher Si/Ti peak intensity ratio was observed in area #2 (1.48) than area #3 (0.08). The presence of a ~6 nm thick silicon-rich layer was found on TiO_2 surface.

Feasibility of using single particle ICP-MS for monitoring metal-containing particles in tap waters (In Draft)

Authors: A. Venkatesan, B. Rodríguez, A. Marcotte, X. Bi, **J. Schoepf**, J. Ranville, P. Herckes, P. Westerhoff

Role: Analyzed titanium dioxide nanomaterials extracted from commercial floor coatings by TEM and SEM. Investigated separation techniques to extract titanium dioxide from floor coatings.

Sample Preparation: About 50 mL tap water sample was sonicated for five minutes to suspend particles. A Ted Pella 200 mesh carbon type B TEM grid was placed at the bottom of the tap water sample in a centrifuge tube. The sample was centrifuged at 4,600 G for 4 hours to settle any metal-containing particles present on to the surface of the TEM grid. Microscopy was performed on a JEOL 2010F TEM (Peabody, MA, USA) with energy dispersive X-ray spectroscopy (EDX). EDX data is reported in a counts vs. energy (KeV) graph. Copper peaks are a result of the copper TEM grids used for analysis. Mean particle diameter was measured manually with ImageJ™ software.

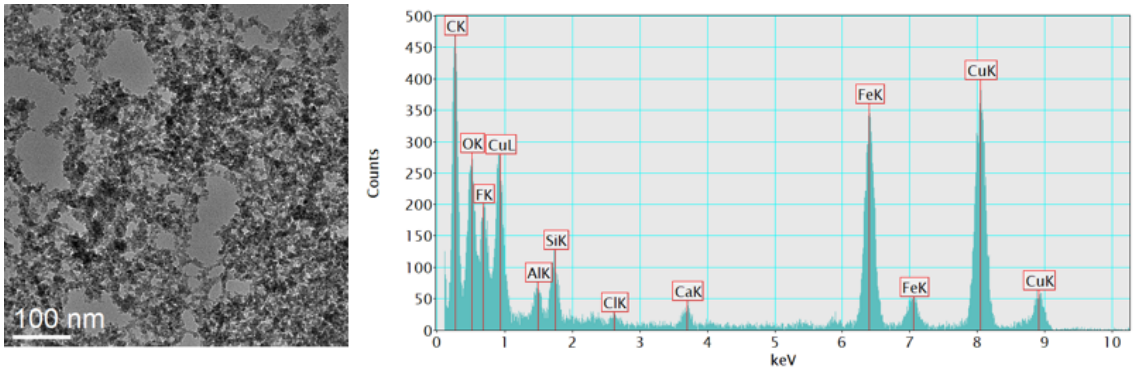

Figure 6.7. Identification by TEM and elemental analysis (EDX) of Fe-containing nanoparticles in tap water. Note: Cu detected is from TEM grid.

CHAPTER 7

SYNTHESIS

7.1 INTRODUCTION

The overarching goal of this dissertation is the development of a tiered nanoparticle detection framework that first rapidly (<10 minutes) detects nanoparticle presence in complex matrices, followed by the characterization of occurrence, morphology, aggregation, and elemental composition of the nanomaterials. This chapter combines each chapter and reviews the hypotheses to build the overall story of the dissertation.

Hypotheses:

1. Portable LIBS and XRF instruments can detect at concentrations above 50 ppm specific elements (Ti, Si, and Ca) present in nanomaterials (TiO_2, SiO_2, and hydroxyapatite ($Ca_5(PO_4)_3(OH)$) contained in solid food and water matrices.
2. Physical filtration and cloud point extraction processes separate and concentrate nanomaterials (TiO_2, SiO_2, and hydroxyapatite ($Ca_5(PO_4)_3(OH)$) from the food and water samples and improves by 50X the LIBS and XRF detection limits of Ti, Si, and Ca elements.
3. Artifact-free detection of size, morphology and composition of nanomaterials (TiO_2, SiO_2, and hydroxyapatite ($Ca_5(PO_4)_3(OH)$) in food and water samples can be achieved through reproducible suspension and centrifugation preparation techniques.

4. A five step tiered analysis scheme can reduce the time and need from presence/absence screening through mineral characterization of TiO2, SiO2 or $Ca_5(PO_4)_3(OH)$ in solid food and liquid water matrices.

Hypothesis 1: Detection of Nanomaterials with LIBS and XRF Instruments

Hypothesis: Portable LIBS and XRF instruments can detect, at concentrations above 50 ppm, specific elements (Ti, Si, and Ca) present in nanomaterials (TiO_2, SiO_2, and hydroxyapatite ($Ca_5(PO_4)_3(OH)$) contained in solid food and water matrices. LIBS and XRF were used to investigate spiked NMs (TiO_2, SiO_2, and HA) in a model food and model liquid matrix to calculate the limit of detection of each technique. For solid samples, LIBS limit of detection (LOD) for Ti (LOD ~380 µg/g), Si (~LOD 3,900 µg/g), and Ca (~LOD 550 µg/g) did not meet the proposed goal (50 µg/g), rejecting the hypothesis. Inherent energy requirement problems to excite particulates in liquid samples prevents LIBS analysis of liquid samples [207], rejecting the hypothesis for LIBS of liquid samples. To meet the goal, XRF was investigated as an analytical technique to detect elements in solid and liquid samples. XRF successfully met the goal (50 µg/g or ppm) of detecting elements in the bulk sample for Ti, Si, and Ca in both solid and liquid samples with LOD of 3, 43, and 22 ppm of Ti, Si, and Ca in a complex food matrix, and 5, 24, and 20 ppm in a liquid matrix. Comparing the techniques, LIBS outperforms XRF when analyzing nanomaterials present on the surface of samples and low mass samples (<1 g) due to the 200 µm diameter laser compared to XRF requiring an infinitely thick sample (>1 cm thick) and large excitation beam (10 mm diameter) while XRF outperforms LIBS in LOD. Albeit the higher LOD of LIBS, both techniques lend themselves to rapid analysis of nanomaterials in food matrices. Overall,

LIBS and XRF analysis was performed on a variety of nanomaterial additives and food products (>60 samples) to test the detection capabilities of nanomaterials. LIBS is an accurate method to detect Si and Ti in food matrices with strong agreement with the product label, detecting Si and Ti in 93% and 89% of the samples labeled as containing each material, respectively. XRF is an accurate method to detect Si, Ti, and Ca in food matrices with strong agreement with the product label, detecting Si and Ti in 96% and 75% (100% Ti in food products) of the food, and vitamin supplements labeled as containing each material, respectively.

Hypothesis 2: Detection of Extracted Materials with LIBS and XRF Instruments

Hypothesis: Physical filtration and cloud point extraction processes separate and concentrate nanomaterials (TiO_2, SiO_2, and hydroxyapatite ($Ca_5(PO_4)_3(OH)$) from the food and water samples and improves by 50X the LIBS and XRF detection limits of Ti, Si, and Ca elements (goal of 1 μg/g limit of detection).

Filtration and cloud point extraction were applied to a model liquid matrix to investigate the detection of NMs on to the surface of a filter and in the surfactant phase of CPE, respectively. Filtration was applied to extract nanomaterials from the bulk sample to both concentrate the sample to lower the limit of detection of LIBS as well as extract nanomaterials from the bulk. Physical filtration concentrated silicon dioxide and titanium dioxide in food products on to the surface of the filter, allowing dissolved organics and inorganics to pass through the filter. LIBS found the presence (99.7% confidence level) of Si and Ti on the surface of a filter. LIBS analysis of the 0.2 μm filter identified nano silicon in 7 out of 17 food products confirmed by TEM to contain nano Si and 6 out of 9 TEM-confirmed samples to contain Ti confirming the hypothesis. Based on the

concentration of Si and Ti in food products by ICP-MS, LIBS analysis of the filter did not meet the 1 μg /g goal, XRF was investigated as an alternate detection technique.

Filtration and CPE of NMs spiked into a model liquid matrix and analyzed by XRF found the presence of Si, Ti, and Ca on the surface of a filter and in the surfactant phase of CPE of water. Physical filtration combined with XRF to detect Ti, Si, and Ca was completed to compare detection techniques of LIBS and XRF on low mass samples. XRF identified Ti, Si, and Ca on the surface of the filter confirming the hypothesis and meeting the 1 μg/g goal. Albeit the low mass of the filter (20 mg), the loaded NM is present at a high surface concentration allowing for XRF to identify the elements. An additional technique, cloud point extraction, was investigate as a suspected superior technique to filtration as CPE allows for the concentration of 40 mL of volume compared to physical filtration's 5 mL of volume. CPE was performed on samples (water and water with natural organic matter) spiked with TiO_2, SiO_2, and HA, to test the feasibility of XRF to detect the elements in the surfactant rich phase of CPE. XRF identified Ti, and Ca in the surfactant rich phase in water matrices, and Ti and Si in water with NOM. XRF was unable to detect Si, and P in water matrices, and Ca and P in water with organic matrices. XRF requires sufficient mass or volume of CPE phase for detection, the low mass sample (<1g) of the surfactant rich phase and the NMs dispersed throughout the surfactant compared to directly on the surface of the filter limits detection by XRF. CPE for Ti confirmed the hypothesis and met the 0.5 ng/g goal. Improvements to XRF of CPE surfactant for the detection of Si, Zn, Ca, and P are needed.

Physical filtration and CPE confirmed the hypothesis and met the 1 μg/g goal. Both techniques have applications in food and environmental matrices to lower the limit

of detection and extract colloid-size materials. Filtration combined with XRF provided the lowest limit of detection and simplest sample preparation procedure compared to LIBS and CPE. Rapid sample preparation and analysis allows filtration with XRF to be a crucial technique for global monitoring of nanomaterials in food and environmental matrices.

Hypothesis 3: Characterization of Nanomaterials with TEM

Hypothesis: Artifact-free detection of size, morphology and composition of nanomaterials (TiO_2, SiO_2, and hydroxyapatite ($Ca_5(PO_4)_3(OH)$) in food and water samples can be achieved through reproducible suspension and centrifugation preparation techniques.

Nanomaterials were characterized by size, morphology, aggregation state, surface coating, and crystallinity by TEM. Main challenges of complex matrices include carbon contamination and low nanomaterial concentration (outlined in Chapter 3) as a result of high organic carbon content in the sample. Chapter 3 supplemental information outlines numerous sample preparation techniques which were applied to analyze needle-like hydroxyapatite identified in infant formula. In summary all tested sample preparation techniques provided TEM images of HA; however, image clarity varied immensely. Although removal of organic carbon is a necessity, sample preparation resulting in nanomaterial artifacts poses a more challenging problem. A simple centrifugation step to separate the dissolved natural organic matter from particulate proved a key step to improve image quality, while minimizing formation of artifacts, confirming the hypothesis.

Comparing the TEM sample preparation techniques outlined in this dissertation (Chapters 2, 3, 4 and 6), the best technique for analyzing nanomaterials at low weight percent with high organic content was the EAWAG method [208]. The EAWAG method employs a similar centrifugation step; however, differs by placing the TEM grid at the bottom of the centrifuge vial allowing centrifugation to concentrate and capture the particulate directly onto the grid, limiting artifact formation due to drying the particles on the TEM as outlined in Chapters 2, 3, and 4, and 6. The lower dilution factor (10X) additionally provided superior organic compound dissolution and removal which resulted in the highest quality images. TEM reports and images can be found in Appendix A.

Hypothesis 4: Rapid Assessment of Nanomaterials Using a Tiered Approach

Hypothesis: A five step tiered analysis scheme can reduce the time and need from presence/absence screening through mineral characterization of TiO2, SiO2 or $Ca_5(PO_4)_3(OH)$ in solid food and liquid water matrices.

A tiered approach involving LIBS, XRF, TEM, ICP-MS and XRD was applied to a variety of matrices (food, infant formula, vitamin supplements, water, water with organics, and simulated biological fluids) to validate the application of a tiered approach to pre-screen samples. Figure 1.1 outlines the tiered approach decision flowchart. LIBS and XRF identified Si and Ti in food products validating the instruments pre-screening capabilities. Filtration and CPE were investigated as tier two to extract colloidal sized particulate and using LIBS and XRF instruments to detect (presence/absence) of the elemental composition of the particulate. TEM characterized the sample, informing occurrence, morphology, and crystallinity of the sample. ICP-MS quantified the bulk elemental composition of the sample, inferring the maximum concentration of nano-sized

components. XRD identified the mineral phase (hydroxyapatite compared to calcite etc.). No one technique characterizes nanomaterials in a complex sample, each technique is necessary to characterize nanomaterials in a complex matrix for use in toxicology studies [52, 209]. This dissertation develops a tiered approach to systematically characterize nanomaterials, while using a pass/fail tiered process to eliminate samples, reducing sample preparation time and cost per sample for analysis.

LIBS determined the absence of Si in 8 out of 28 samples and absence of Ti in 14 out of 28 samples confirming the analytical techniques ability to reduce sample size requiring TEM and ICP-MS. XRF identified absence of Si in 6 out of 40 samples, with 1 false negative, and absence of Ti in 17 samples out of 40 samples with no false negatives. LIBS and XRF were validated as a tier one approach to prescreen samples for presence or absence of elements of interest (Ti and Si in food products and vitamin supplements, Ca and P in infant formulas, as well as Ti, Si, Ca, and P in biological fluids and environmental matrices).

Tier two further pre-screened samples for colloidal sized particulate by elemental analysis with LIBS or XRF. Using filtration and CPE to extract nanomaterials from the bulk sample, tier two provided another level of pre-screening. Albeit challenges detecting silicon on filters by LIBS, tier two provides an additional pre-screening tier for elemental detection of colloidal sized components.

Samples passing tier two are characterized by TEM, ICP-MS, and XRD. The standard techniques characterize the particulate size, morphology, bulk concentration of elements, and mineral phase of the particulate. In total, the first two tiers screen samples, eliminating samples absent of nanomaterials before expensive and time intensive

characterize. The combination of LIBS, XRF, TEM, ICP-MS, and XRD are confirmed as a robust method to rapidly pre-screen samples followed by extensive nanomaterial characterization.

CHAPTER 8

CONCLUSIONS AND RECOMMENDATIONS FOR FUTURE RESEARCH

The overarching goal of this dissertation is the development of a tiered nanoparticle detection framework that first rapidly detects nanoparticle presence in complex matrices, followed by the characterization of occurrence, morphology, surface coating, aggregation, and elemental composition.

8.1 CONCLUSIONS

Chapter 2: Towards Rapid Assessment of Nanomaterial Additives in Foods with Laser Induced Breakdown Spectroscopy

LIBS is an accurate method to detect Si and Ti in food matrices (tier one approach) with strong agreement with the product label, detecting Si and Ti in 93% and 89% of the samples labeled as containing each material, respectively. As a tier two approach, LIBS on the 0.2 μm filter identified nano silicon in 42% of samples confirmed by TEM to contain nano Si and 67% of TEM-confirmed samples to contain Ti. LIBS is confirmed as a pre-screening (tier one) approach to detect Si and Ti in complex food matrices and filtration combined with LIBS is confirmed as a proven technique (tier two) to detect colloidal-sized Si and Ti on the surface of a filter.

Chapter 3: Detection and Dissolution of Needle-Like Hydroxyapatite Nanomaterials in Infant Formula

TEM identified the presence of needle-like hydroxyapatite in 50% of USA infant formula. Neither TEM sample preparations methods used formed artifacts. Comparison of the TEM sample preparation techniques proved the EAWAG method provided superior TEM image quality without the formation of sample preparation artifacts. In

conclusion, the dissolution of HA in simulated gastric fluid found needle-like HA to dissolve more completely than spherical HA.

Chapter 4: Towards Rapid Assessment of Nanomaterial Additives in Consumer Products by X-Ray Fluorescence

XRF is and accurate method to detect Ti, Si, and Ca in food and liquid matrices. XRF identified Ti, Si, and Ca in 100% of samples TEM-confirmed to contain Ti, Si, and Ca respectively. Applying XRF as a pre-screening approach, 6 out of 40 samples for Si would have been eliminated with 1 false negative and 17 samples out of 40 samples for Ti would have been eliminated with no false negatives. In conclusion, XRF is validated as a superior technique to LIBS for detecting NMs in food matrices with an improved LOD and accuracy in food and liquid matrices.

Chapter 5: Application of Portable XRF on Biological and Environmental Matrices

XRF identified Si, Ti, and Ca loaded on to a 0.1 μm filter and Ti in the surfactant rich phase of CPE of water and water with NOM. Improvements are necessary for CPE and XRF detection of Si, and Ca. XRF combined with filtration is a robust tier two approach and superior to LIBS combined with filtration (Colloidal-LIBS).

Chapter 6: Electron Microscopy of Complex Matrices

Sample preparation techniques were developed for TEM of nanomaterials (SiO_2, TiO_2, HA, and ZnO) in complex matrices (polystyrene, quartz fiber, activated carbon, sunscreen and consumer floor coating). Below are the co-authored manuscripts.

Co-authored Publications:

1) *Survey of food-grade silica dioxide nanomaterial occurrence, characterization, human gut impacts and fate across its lifecycle* (Published)
2) *Prospecting nanomaterials in aqueous environments by cloud-point extraction coupled with transmission electron microscopy* (Published)
3) *Superfine powdered activated carbon incorporated into electrospun polystyrene fibers preserve adsorption capacity* (Published)
4) *Trade-offs in ecosystem impacts from nanomaterial versus organic chemical ultraviolet filters in sunscreens* (Published)
5) *Coupling light emitting diodes with photocatalyst-coated optical fibers improves quantum efficiency of pollutant oxidation* (Published)
6) *The efficacy of engineered TiO_2 nanoparticles in a commercial floor coating and environmental implications* (Published)
7) *Feasibility of using single particle ICP-MS for monitoring metal-containing particles in tap waters* (In Draft)

Sample preparation techniques were developed to facilitate characterization of nanomaterials in complex matrices by TEM. I developed extraction methods to remove and concentrate nanomaterials from complex matrices on to the surface of the TEM and SEM grids while limiting artifact formation. The development of expertise in TEM and SEM facilitated understanding of nanomaterial morphology, surface coatings, aggregation, elemental and composition of nanomaterials in consumer products allowing for the development of the tiered approach.

8.2 RECOMMENDATIONS FOR FUTURE RESEARCH

Widespread application of nanomaterials in industrial processes and consumer products has resulted in the release of nanomaterials into the environment. To understand the effect of nanomaterials on the environment, the exposure must be quantified for exposure monitoring as well as aiding in concentration relevant toxicity testing. Current ecotoxicity data explores pristine nanomaterials with limited data exploring toxicity of nanomaterials released from consumer products in relevant environmental conditions. Characterization of nanomaterials in the environment is required to test nanomaterial toxicity under relevant conditions. Current nanomaterial detection techniques are prohibitively expensive and time intensive for the application of global nanomaterial monitoring. LIBS and XRF have been proven as first tier rapid screening techniques to reduce sample size for Ti, Si, Ca, and P. To increase the impact of the tiered approach, additional research is necessary to test LIBS and XRF instruments for detection of additional nanomaterials and complex matrices.

The top ten nanomaterials in production are silicon dioxide, cerium oxide, carbon nanotubes, nanoclays, aluminum oxide, copper, iron, zinc oxide, titanium dioxide and silver used in industries and complex matrices such as: automotive, catalysts, electronics and optics, energy and environment, coatings, paints, pigments, personal care products, and medical [201]. The tiered approach in this dissertation is proven as a robust strategy for detection of Si, Ti, Ca, and P, future research should be focused on applying the tiered approach to the remaining top nanomaterials in the additional matrices for application as a global monitoring technique. The impact regions of high interest are silicon dioxide in biological fluids (e.g. saliva) to detect workplace exposure to SiO_2. Additionally research

focused on the application of physical filtration and cloud point extraction on the above nanomaterials and matrices are also needed to optimize the tiered approach.

Future research on optimizing filtration and cloud point extraction is necessary and will result in lower detection limits and improved accuracy with less false positives and negatives. Optimizing surfactant and salt ratios as well as operating conditions (temperature, stir time, centrifugation speed and time) for a variety of nanomaterials has potential to increase efficiency and therefore detection capabilities. The continued use of nanomaterials will result in their continued release, and the tiered approach is a robust method to detect nanomaterials for use as a global monitoring program.

REFERENCES

1. Sadat-Shojai, M., et al., *Synthesis methods for nanosized hydroxyapatite with diverse structures.* Acta Biomaterialia, 2013. **9**(8): p. 7591-7621.

2. Charitidis, C.A., et al., *Manufacturing nanomaterials: from research to industry.* Manufacturing Rev., 2014. **1**: p. 11.

3. Cao, G., *Synthesis, properties and applications*. World Scientific.

4. Khot, L.R., et al., *Applications of nanomaterials in agricultural production and crop protection: A review.* Crop Protection, 2012. **35**: p. 64-70.

5. Salata, O.V., *Applications of nanoparticles in biology and medicine.* Journal of Nanobiotechnology, 2004. **2**: p. 3-3.

6. Daer, S., et al., *Recent applications of nanomaterials in water desalination: A critical review and future opportunities.* Desalination, 2015. **367**: p. 37-48.

7. Gaya, U.I. and A.H. Abdullah, *Heterogeneous photocatalytic degradation of organic contaminants over titanium dioxide: a review of fundamentals, progress and problems.* Journal of Photochemistry and Photobiology C: Photochemistry Reviews, 2008. **9**(1): p. 1-12.

8. Weir, A., et al., *Titanium dioxide nanoparticles in food and personal care products.* Environmental science & technology, 2012. **46**(4): p. 2242-2250.

9. Peleg, M. and A.M. Hollenbach, *Flow conditioners and anticaking agents.* Food Technology (USA), 1984.

10. Marambio-Jones, C. and E.M. Hoek, *A review of the antibacterial effects of silver nanomaterials and potential implications for human health and the environment.* Journal of Nanoparticle Research, 2010. **12**(5): p. 1531-1551.

11. Ren, G., et al., *Characterisation of copper oxide nanoparticles for antimicrobial applications.* International journal of antimicrobial agents, 2009. **33**(6): p. 587-590.

12. Becheri, A., et al., *Synthesis and characterization of zinc oxide nanoparticles: application to textiles as UV-absorbers.* Journal of Nanoparticle Research, 2008. **10**(4): p. 679-689.

13. Tschoppe, P., et al., *Enamel and dentine remineralization by nano-hydroxyapatite toothpastes.* journal of dentistry, 2011. **39**(6): p. 430-437.

14. Benn, T.M. and P. Westerhoff, *Nanoparticle Silver Released into Water from Commercially Available Sock Fabrics.* Environmental Science & Technology, 2008. **42**(11): p. 4133-4139.
15. Gottschalk, F. and B. Nowack, *The release of engineered nanomaterials to the environment.* J Environ Monit, 2011. **13**(5): p. 1145-55.

16. Klaine, S.J., et al., *Nanomaterials in the environment: behavior, fate, bioavailability, and effects.* Environmental Toxicology and Chemistry, 2008. **27**(9): p. 1825-1851.

17. Canady, R.A., *The uncertainty of nanotoxicology: report of a society for risk analysis workshop.* Risk Analysis, 2010. **30**(11): p. 1663-1670.

18. García, A., et al., *Effect of cerium dioxide, titanium dioxide, silver, and gold nanoparticles on the activity of microbial communities intended in wastewater treatment.* Journal of hazardous materials, 2012. **199**: p. 64-72.

19. Silva, R.M., et al., *Biological response to nano-scale titanium dioxide (TiO2): role of particle dose, shape, and retention.* Journal of Toxicology and Environmental Health, Part A, 2013. **76**(16): p. 953-972.

20. Wang, Y., et al., *Susceptibility of young and adult rats to the oral toxicity of titanium dioxide nanoparticles.* Small, 2013. **9**(9-10): p. 1742-1752.

21. Koivisto, A., et al., *Industrial worker exposure to airborne particles during the packing of pigment and nanoscale titanium dioxide.* Inhalation toxicology, 2012. **24**(12): p. 839-849.
22. McCracken, C., et al., *Minimal intestinal epithelial cell toxicity in response to short-and long-term food-relevant inorganic nanoparticle exposure.* Chemical research in toxicology, 2013. **26**(10): p. 1514-1525.

23. Shi, H., et al., *Titanium dioxide nanoparticles: a review of current toxicological data.* Particle and fibre toxicology, 2013. **10**(1): p. 1.

24. NSET/NEHI, *Environmental Health and Safety.* 2011.

25. Committee, E.S., *Guidance on the risk assessment of the application of nanoscience and nanotechnologies in the food and feed chain.* EFSA Journal, 2011. **9**(5).

26. Singh, G., et al., *Measurement Methods to Detect, Characterize, and Quantify Engineered Nanomaterials in Foods.* Comprehensive Reviews in Food Science and Food Safety, 2014. **13**(4): p. 693-704.

27. Szakal, C., et al., *Measurement of Nanomaterials in Foods: Integrative Consideration of Challenges and Future Prospects.* Acs Nano, 2014. **8**(4): p. 3128-3135.

28. Canady, R. and L. Tsytsikova, *NanoRelease Food Additive: Supporting methods to measure food nanomaterials.* Abstracts of Papers of the American Chemical Society, 2013. **245**.

29. Dudkiewicz, A., et al., *Characterization of nanomaterials in food by electron microscopy.* Trac-Trends in Analytical Chemistry, 2011. **30**(1): p. 28-43.

30. Linsinger, T.P.J., et al., *Validation of methods for the detection and quantification of engineered nanoparticles in food.* Food Chemistry, 2013. **138**(2-3): p. 1959-1966.

31. Luo, P., et al., *Visualization and characterization of engineered nanoparticles in complex environmental and food matrices using atmospheric scanning electron microscopy.* Journal of Microscopy, 2013. **250**(1): p. 32-41.

32. Gallego-Urrea, J.A., J. Tuoriniemi, and M. Hassellov, *Applications of particle-tracking analysis to the determination of size distributions and concentrations of nanoparticles in environmental, biological and food samples.* Trac-Trends in Analytical Chemistry, 2011. **30**(3): p. 473-483.

33. Fanali, C., et al., *Capillary-liquid chromatography (CLC) and nano-LC in food analysis.* Trac-Trends in Analytical Chemistry, 2013. **52**: p. 226-238.

34. Li, Y.S. and J.S. Church, *Raman spectroscopy in the analysis of food and pharmaceutical nanomaterials.* Journal of Food and Drug Analysis, 2014. **22**(1): p. 29-48.

35. Farre, M., J. Sanchis, and D. Barcelo, *Analysis and assessment of the occurrence, the fate and the behavior of nanomaterials in the environment.* Trac-Trends in Analytical Chemistry, 2011. **30**(3): p. 517-527.

36. Lapresta-Fernandez, A., et al., *A General Perspective of the Characterization and Quantification of Nanoparticles: Imaging, Spectroscopic, and Separation Techniques.* Critical Reviews in Solid State and Materials Sciences, 2014. **39**(6): p. 423-458.

37. Galbacs, G., *A critical review of recent progress in analytical laser-induced breakdown spectroscopy.* Analytical and Bioanalytical Chemistry, 2015. **407**(25): p. 7537-7562.

38. Lee, S., et al., *Nanoparticle Size Detection Limits by Single Particle ICP-MS for 40 Elements.* Environmental Science & Technology, 2014. **48**(17): p. 10291-10300.

39. Dudkiewicz, A., et al., *Characterization of nanomaterials in food by electron microscopy.* TrAC Trends in Analytical Chemistry, 2011. **30**(1): p. 28-43.

40. Yada, R.Y., et al., *Engineered Nanoscale Food Ingredients: Evaluation of Current Knowledge on Material Characteristics Relevant to Uptake from the Gastrointestinal Tract.* Comprehensive Reviews in Food Science and Food Safety, 2014. **13**(4): p. 730-744.

41. Talmon, Y., *Transmission electron microscopy of complex fluids: the state of the art.* Berichte der Bunsengesellschaft für physikalische Chemie, 1996. **100**(3): p. 364-372.

42. IUTA, B., B. RCI, and T. IFA, *Tiered Approach to an Exposure Measurement and Assessment of Nanoscale Aerosols Released from Engineered Nanomaterials in Workplace Operations, 2011, Air Quality and Sustainable Nanotechnology, Institute of Energy and Environmental Technology eV (IUTA).* Federal Institute for Occupational Safety and Health (BAuA): p. 16.

43. Aschberger, K., et al., *Analysis of currently available data for characterising the risk of engineered nanomaterials to the environment and human health — Lessons learned from four case studies.* Environment International, 2011. **37**(6): p. 1143-1156.

44. Fabrega, J., et al., *Silver nanoparticles: behaviour and effects in the aquatic environment.* Environment international, 2011. **37**(2): p. 517-531.

45. Handy, R.D., et al., *Ecotoxicity test methods for engineered nanomaterials: practical experiences and recommendations from the bench.* Environmental Toxicology and Chemistry, 2012. **31**(1): p. 15-31.

46. Ma, H., P.L. Williams, and S.A. Diamond, *Ecotoxicity of manufactured ZnO nanoparticles–a review.* Environmental pollution, 2013. **172**: p. 76-85.

47. Menard, A., D. Drobne, and A. Jemec, *Ecotoxicity of nanosized TiO 2. Review of in vivo data.* Environmental Pollution, 2011. **159**(3): p. 677-684.

48. Miralles, P., T.L. Church, and A.T. Harris, *Toxicity, uptake, and translocation of engineered nanomaterials in vascular plants.* Environmental science & technology, 2012. **46**(17): p. 9224-9239.

49. Holden, P.A., et al., *Considerations of Environmentally Relevant Test Conditions for Improved Evaluation of Ecological Hazards of Engineered Nanomaterials.* Environmental Science & Technology, 2016. **50**(12): p. 6124-6145.

50. Radad, K., et al., *Recent advances in benefits and hazards of engineered nanoparticles.* Environmental toxicology and pharmacology, 2012. **34**(3): p. 661-672.

51. Tourinho, P.S., et al., *Metal-based nanoparticles in soil: Fate, behavior, and effects on soil invertebrates.* Environmental Toxicology and Chemistry, 2012. **31**(8): p. 1679-1692.

52. Sharifi, S., et al., *Toxicity of nanomaterials.* Chemical Society Reviews, 2012. **41**(6): p. 2323-2343.

53. Garner, K.L., et al., *Species Sensitivity Distributions for Engineered Nanomaterials.* Environmental Science & Technology, 2015. **49**(9): p. 5753-5759.

54. Yang, Y., et al., *Survey of food-grade silica dioxide nanomaterial occurrence, characterization, human gut impacts and fate across its lifecycle.* Science of The Total Environment, 2016. **565**: p. 902-912.

55. Paleologos, E.K., D.L. Giokas, and M.I. Karayannis, *Micelle-mediated separation and cloud-point extraction.* TrAC Trends in Analytical Chemistry, 2005. **24**(5): p. 426-436.

56. Bezerra, M.d.A., M.A.Z. Arruda, and S.L.C. Ferreira, *Cloud point extraction as a procedure of separation and pre-concentration for metal determination using spectroanalytical techniques: a review.* Applied Spectroscopy Reviews, 2005. **40**(4): p. 269-299.

57. Yang, Y., et al., *Characterization of food-grade titanium dioxide: the presence of nanosized particles.* Environmental science & technology, 2014. **48**(11): p. 6391-6400.

58. Yang, Y.-X., et al., *Evaluation of the toxicity of food additive silica nanoparticles on gastrointestinal cells.* Journal of Applied Toxicology, 2014. **34**(4): p. 424-435.

59. Yang, Y., et al., *Characterization of Food-Grade Titanium Dioxide: The Presence of Nanosized Particles.* Environmental Science & Technology, 2014. **48**(11): p. 6391-6400.

60. Weir, A., et al., *Titanium Dioxide Nanoparticles in Food and Personal Care Products.* Environ. Sci. Tech., 2012. **46**(4): p. 2242-2250.

61. Oberdörster, G., et al., *Principles for characterizing the potential human health effects from exposure to nanomaterials: elements of a screening strategy.* Particle and fibre toxicology, 2005. **2**(1): p. 1.

62. Colvin, V.L., *The potential environmental impact of engineered nanomaterials.* Nature biotechnology, 2003. **21**(10): p. 1166-1170.

63. SCCS, *Opinion on Hydroxyapatite (nano)*. 2015, European Union Scientific Committee on Consumer Safety: Luxembourg. p. 55.

64. Greenwood, N.N., A. Earnshaw, and Knovel, *Chemistry of the elements*. Vol. 2nd;2;. 1998, Oxford;Boston;: Butterworth-Heinemann.

65. Chaudhry, Q. and L. Castle, *Food applications of nanotechnologies: An overview of opportunities and challenges for developing countries.* Trends in Food Science & Technology, 2011. **22**(11): p. 595-603.

66. Weiss, J., P. Takhistov, and D.J. McClements, *Functional materials in food nanotechnology.* Journal of Food Science, 2006. **71**(9): p. R107-R116.

67. Dan, N., *Transport and release in nano-carriers for food applications.* Journal of Food Engineering, 2016. **175**: p. 136-144.

68. Farhoodi, M., *Nanocomposite Materials for Food Packaging Applications: Characterization and Safety Evaluation.* Food Engineering Reviews, 2016. **8**(1): p. 35-51.

69. Tiede, K., et al., *Detection and characterization of engineered nanoparticles in food and the environment.* Food Additives and Contaminants, 2008. **25**(7): p. 795-821.

70. Schoepf, J.J., et al., *Detection and dissolution of needle-like hydroxyapatite nanomaterials in infant formula.* NanoImpact, 2017. **5**: p. 22-28.

71. Garcia, A., et al., *Effect of cerium dioxide, titanium dioxide, silver, and gold nanoparticles on the activity of microbial communities intended in wastewater treatment.* Journal of Hazardous Materials, 2012. **199**: p. 64-72.

72. Silva, R.M., et al., *Biological Response to nano-scale Titanium Dioxide (TiO2): Role of particle dose, shape, and retention.* Journal Of Toxicology And Environmental Health-Part A-Current Issues, 2013. **76**(16): p. 953-972.

73. Wang, Y., et al., *Susceptibility of Young and Adult Rats to the Oral Toxicity of Titanium Dioxide Nanoparticles.* Small, 2013. **9**(9-10): p. 1742-1752.

74. Koivisto, A.J., et al., *Industrial worker exposure to airborne particles during the packing of pigment and nanoscale titanium dioxide.* Inhalation Toxicology, 2012. **24**(12): p. 839-849.

75. McCracken, C., et al., *Minimal Intestinal Epithelial Cell Toxicity in Response to Short- and Long-Term Food-Relevant Inorganic Nanoparticle Exposure.* Chemical Research in Toxicology, 2013. **26**(10): p. 1514-1525.

76. Shi, H.B., et al., *Titanium dioxide nanoparticles: a review of current toxicological data.* Particle and Fibre Toxicology, 2013. **10**.

77. Cushen, M., et al., *Evaluation and Simulation of Silver and Copper Nanoparticle Migration from Polyethylene Nanocomposites to Food and an Associated Exposure Assessment.* Journal of Agricultural and Food Chemistry, 2014. **62**(6): p. 1403-1411.

78. Fage, S.W., et al., *Titanium: a review on exposure, release, penetration, allergy, epidemiology, and clinical reactivity.* Contact Dermatitis, 2016. **74**(6): p. 323-345.

79. Shakeel, M., et al., *Toxicity of Nano-Titanium Dioxide (TiO2-NP) Through Various Routes of Exposure: a Review.* Biological Trace Element Research, 2016. **172**(1): p. 1-36.

80. Cremers, D.A., et al., *Laser-Induced Breakdown Spectroscopy, Elemental Analysis*, in *Encyclopedia of Analytical Chemistry*. 2006, John Wiley & Sons, Ltd.

81. Martin, M.Z., S. Wullschleger, and C. Garten. *Laser-induced breakdown spectroscopy for environmental monitoring of soil carbon and nitrogen*.

82. Martin, M.Z., et al., *Elemental Analysis of Environmental and Biological Samples Using Laser-Induced Breakdown Spectroscopy and Pulsed Raman Spectroscopy.* Journal of Dispersion Science and Technology, 2005. **25**(5): p. 687-694.

83. Bublitz, J., et al., *Laser-induced breakdown spectroscopy for soil diagnostics.* European Journal of Soil Science, 2001. **52**(2): p. 305-312.

84. Mirov, S.B., et al. *Novel laser breakdown spectrometer for environmental monitoring*.

85. Hahn, D.W., *Laser-induced breakdown spectroscopy for sizing and elemental analysis of discrete aerosol particles.* Applied Physics Letters, 1998. **72**(23): p. 2960.

86. Hahn, D.W., W.L. Flower, and K.R. Hencken, *Discrete particle detection and metal emissions monitoring using laser-induced breakdown spectroscopy*. 1997: United States.

87. Pandhija, S. and A.K. Rai, *Screening of brick-kiln area soil for determination of heavy metal Pb using LIBS.* Environmental Monitoring and Assessment, 2009. **148**(1): p. 437-447.

88. Pandhija, S., et al., *Contaminant concentration in environmental samples using LIBS and CF-LIBS.* Applied Physics B, 2010. **98**(1): p. 231-241.

89. Rodriguez-Celis, E.M., et al., *Laser induced breakdown spectroscopy as a tool for discrimination of glass for forensic applications.* Analytical and Bioanalytical Chemistry, 2008. **391**(5): p. 1961-1968.

90. Dockery, C.R. and S.R. Goode, *Laser-induced breakdown spectroscopy for the detection of gunshot residues on the hands of a shooter.* Applied optics, 2003. **42**(30): p. 6153.

91. Arp, Z.A., et al., *Feasibility of generating a useful laser-induced breakdown spectroscopy plasma on rocks at high pressure: preliminary study for a Venus mission.* Spectrochimica Acta Part B: Atomic Spectroscopy, 2004. **59**(7): p. 987-999.

92. Arp, Z.A., D.A. Cremers, and R.C. Wiens. *Application of laser induced breakdown spectroscopy (LIBS) to Mars polar exploration : LIBS analysis of water ice and water ice/soil mixtures*. DOE.

93. Sallé, B., et al., *Laser-induced breakdown spectroscopy for space exploration applications: Influence of the ambient pressure on the calibration curves prepared from soil and clay samples.* Spectrochimica Acta Part B: Atomic Spectroscopy, 2005. **60**(4): p. 479-490.

94. Sallé, B., et al., *Evaluation of a compact spectrograph for in-situ and stand-off Laser-Induced Breakdown Spectroscopy analyses of geological samples on Mars missions.* Spectrochimica Acta Part B: Atomic Spectroscopy, 2005. **60**(6): p. 805-815.

95. Sallé, B., et al., *Laser-Induced Breakdown Spectroscopy for Mars surface analysis: capabilities at stand-off distances and detection of chlorine and sulfur elements.* Spectrochimica Acta Part B: Atomic Spectroscopy, 2004. **59**(9): p. 1413-1422.

96. Wiens, R.C. and S. Maurice, *ChemCam's Cost a Drop in the Mars Bucket.* Science, 2008. **322**(5907): p. 1464-1464.

97. Brennetot, R., et al., *Mars analysis by laser-induced breakdown spectroscopy (MALIS): influence of mars atmosphere on plasma emission and study of factors influencing plasma emission with the use of doehlert designs.* Appl Spectrosc, 2003. **57**(7): p. 744-52.

98. Knight, A.K., et al., *Characterization of laser-induced breakdown spectroscopy (LIBS) for application to space exploration*. 2000: United States.

99. Fabre, C., et al., *Palaeofluid chemistry of a single fluid event: a bulk and in-situ multi-technique analysis (LIBS, Raman Spectroscopy) of an Alpine fluid (Mont-Blanc).* Chemical Geology, 2002. **182**(2): p. 249-264.

100. Marquardt, B.J., et al., *Novel probe for laser-induced breakdown spectroscopy and Raman measurements using an imaging optical fiber*. 1998: United States.

101. Sharma, S.K., et al., *Combined remote LIBS and Raman spectroscopy at 8.6 m of sulfur-containing minerals, and minerals coated with hematite or covered with basaltic dust.* Spectrochimica Acta Part A: Molecular and Biomolecular Spectroscopy, 2007. **68**(4): p. 1036-1045.

102. Wiens, R.C., et al., *Joint analyses by laser-induced breakdown spectroscopy (LIBS) and Raman spectroscopy at stand-off distances.* Spectrochimica Acta Part A: Molecular and Biomolecular Spectroscopy, 2005. **61**(10): p. 2324-2334.

103. Castillejo, M., et al., *Analysis of pigments in polychromes by use of laser induced breakdown spectroscopy and Raman microscopy.* Journal of Molecular Structure, 2000. **550**(1-3): p. 191-198.

104. Effenberger, A.J. and J.R. Scott, *Effect of Atmospheric Conditions on LIBS Spectra*. 2010, USDOE: United States.

105. Shu, R., et al., *Laser-induced breakdown spectroscopy based detection of lunar soil simulants for moon exploration.* Chinese Optics Letters, 2007. **5**(1): p. 58-59.

106. Gallou, G., et al., *Aerosols Analysis by LIBS for Monitoring of Air Pollution by Industrial Sources.* Aerosol Science and Technology, 2011. **45**(8): p. 918-926.

107. Mukherjee, D., A. Rai, and M. Zachariah, *Quantitative laser-induced breakdown spectroscopy for aerosols via internal calibration: Application to the oxidative coating of aluminum nanoparticles.* Journal of aerosol science, 2006. **37**(6): p. 677-695.

108. Jurado-L pez, A. and M.D. Luque de Castro, *Laser-induced breakdown spectrometry in the jewellery industry. Part I. Determination of the layer*

thickness and composition of gold-plated pieces. Journal of Analytical Atomic Spectrometry, 2002. **17**(5): p. 544-547.

109. Jurado-Lopez, A. and M.D. Luque de Castro, *Chemometric approach to laser-induced breakdown analysis of gold alloys.* Appl Spectrosc, 2003. **57**(3): p. 349-52.

110. Kraushaar, M., R. Noll, and H.U. Schmitz, *Slag analysis with laser-induced breakdown spectrometry.* Applied spectroscopy, 2003. **57**(10): p. 1282-1287.

111. Mateo, M.P., L.M. Cabalin, and J.J. Laserna, *Automated line-focused laser ablation for mapping of inclusions in stainless steel.* Appl Spectrosc, 2003. **57**(12): p. 1461-7.

112. Palanco, S. and J.J. Laserna, *Full automation of a laser-induced breakdown spectrometer for quality assessment in the steel industry with sample handling, surface preparation and quantitative analysis capabilities.* Journal of Analytical Atomic Spectrometry, 2000. **15**(10): p. 1321-1327.

113. Sattmann, R., V. Sturm, and R. Noll, *Laser-induced breakdown spectroscopy of steel samples using multiple Q-switch Nd:YAG laser pulses.* Journal of Physics D: Applied Physics, 1995. **28**: p. 2181.

114. Sturm, V., L. Peter, and R. Noll, *Steel Analysis with Laser-Induced Breakdown Spectrometry in the Vacuum Ultraviolet.* Applied Spectroscopy, 2000. **54**(9): p. 1275-1278.

115. Sturm, V., et al., *Bulk analysis of steel samples with surface scale layers by enhanced laser ablation and LIBS analysis of C, P, S, Al, Cr, Cu, Mn and Mo.* Journal of Analytical Atomic Spectrometry, 2004. **19**(4): p. 451-456.

116. Thiem, T.L., et al., *Quantitative Simultaneous Elemental Determinations in Alloys Using Laser-Induced Breakdown Spectroscopy (LIBS) in an Ultra-High Vacuum.* Applied Spectroscopy, 1994. **48**(1): p. 58-64.

117. Sabsabi, M. and P. Cielo, *Quantitative Analysis of Aluminum Alloys by Laser-Induced Breakdown Spectroscopy and Plasma Characterization.* Applied Spectroscopy, 1995. **49**(4): p. 499-507.

118. Cáceres, J.O., et al., *Quantitative analysis of trace metal ions in ice using laser-induced breakdown spectroscopy.* Spectrochimica Acta Part B: Atomic Spectroscopy, 2001. **56**(6): p. 831-838.

119. Stipe, C.B., et al., *Evaluation of laser-induced breakdown spectroscopy (LIBS) for measurement of silica on filter samples of coal dust.* Appl Spectrosc, 2012. **66**(11): p. 1286-93.

120. Garner, K.L. and A.A. Keller, *Emerging patterns for engineered nanomaterials in the environment: a review of fate and toxicity studies.* Journal of Nanoparticle Research, 2014. **16**(8): p. 1-28.

121. Yang, Y., et al., *Survey of food-grade silica dioxide nanomaterial occurrence, characterization, human gut impacts and fate across its lifecycle.* Science of the Total Environment, in-press (2016).

122. Ladner, D.A., et al., *Functionalized nanoparticle interactions with polymeric membranes.* Journal of Hazardous Materials, 2012. **211**: p. 288-295.

123. Babushok, V.I., et al., *Double pulse laser ablation and plasma: Laser induced breakdown spectroscopy signal enhancement.* Spectrochimica Acta Part B: Atomic Spectroscopy, 2006. **61**(9): p. 999-1014.

124. Kiser, M.A., et al., *Biosorption of nanoparticles to heterotrophic wastewater biomass.* Water Research, 2010. **44**(14): p. 4105-4114.

125. Kiser, M.A., et al., *Titanium Nanomaterial Removal and Release from Wastewater Treatment Plants.* Environmental Science & Technology, 2009. **43**(17): p. 6757-6763.

126. Keller, A.A. and A. Lazareva, *Predicted releases of engineered nanomaterials:From global to regional to local.* Environ. Sci. Tech. Letters, 2014. **1**(1): p. 65-70.

127. Mueller, N.C. and B. Nowack, *Exposure modeling of engineered nanoparticles in the environment.* Environmental Science & Technology, 2008. **42**(12): p. 4447-4453.

128. Piccinno, F., et al., *Industrial production quantities and uses of ten engineered nanomaterials in Europe and the world.* Journal of Nanoparticle Research, 2012. **14**(9).

129. Gottschalk, F., T. Sun, and B. Nowack, *Environmental concentrations of engineered nanomaterials: Review of modeling and analytical studies.* Environmental Pollution, 2013. **181**: p. 287-300.

130. Reed, R.B., et al., *Solubility of nano-zinc oxide in environmentally and biologically important matrices.* Environmental Toxicology and Chemistry, 2012. **31**(1): p. 93-99.

131. Robichaud, C.O., et al., *Estimates of Upper Bounds and Trends in Nano-TiO2 Production As a Basis for Exposure Assessment* Environ. Sci. Technol., 2009. **43**(12): p. 4227-4233.

132. Kaegi, R., et al., *Fate and transformation of silver nanoparticles in urban wastewater systems.* Water Research, 2013. **47**(12): p. 3866-3877.

133. Thalmann, B., et al., *Sulfidation Kinetics of Silver Nanoparticles Reacted with Metal Sulfides.* Environmental Science & Technology, 2014. **48**(9): p. 4885-4892.

134. Conway, J.R., et al., *Aggregation, Dissolution, and Transformation of Copper Nanoparticles in Natural Waters.* Environmental Science & Technology, 2015. **49**(5): p. 2749-2756.

135. Hong, J., et al., *Toxic effects of copper-based nanoparticles or compounds to lettuce (Lactuca sativa) and alfalfa (Medicago sativa).* Environmental Science-Processes & Impacts, 2015. **17**(1): p. 177-185.

136. Lenton, S., et al., *A review of the biology of calcium phosphate sequestration with special reference to milk.* Dairy Science & Technology, 2015. **95**(1): p. 3-14.

137. Miretzky, P. and A. Fernandez-Cirelli, *Phosphates for Pb immobilization in soils: a review.* Environmental Chemistry Letters, 2008. **6**(3): p. 121-133.

138. Piccoli, P. and P. Candela, *Apatite in Felsic Rocks - A Model for the estimation of initial halogen concentrations in the Bishop Tuff (Long Valley) and Tuolumine Intrusive Suite (Sierra-Nevada Baltholith) magmas* American Journal of Science, 1994. **294**(1): p. 92-135.

139. Vance, M.E., et al., *Nanotechnology in the real world: Redeveloping the nanomaterial consumer products inventory.* Beilstein Journal of Nanotechnology, 2015. **6**: p. 1769-1780.

140. de-Bashan, L.E. and Y. Bashan, *Recent advances in removing phosphorus from wastewater and its future use as fertilizer (1997-2003).* Water Research, 2004. **38**(19): p. 4222-4246.

141. Wiesner, M.R., et al., *Meditations on the Ubiquity and Mutability of Nano-Sized Materials in the Environment.* Acs Nano, 2011. **5**(11): p. 8466-8470.

142. Boisson, J., et al., *Evaluation of hydroxyapatite as a metal immobilizing soil additive for the remediation of polluted soils. Part 1. Influence of hydroxyapatite on metal exchangeability in soil, plant growth and plant metal accumulation.* Environmental Pollution, 1999. **104**(2): p. 225-233.

143. Fuller, C.C., et al., *Mechanisms of uranium interactions with hydroxyapatite: Implications for groundwater remediation.* 2002. **36**(2): p. 158-165.

144. Fan, X., D.J. Parker, and M.D. Smith, *Adsorption kinetics of fluoride on low cost materials.* Water Research, 2003. **37**(20): p. 4929-4937.

145. Straub, D.A., *Calcium supplementation in clinical practice: a review of forms, doses, and indications.* Nutrition in Clinical Practice, 2007. **22**(3): p. 286-296.

146. Ruegsegger, P., A. Keller, and M.A. Dambacher, *Comparison of the treatment effects of Ossein-Hydroxyapatite compound and calcium carbonate in osteoporotic females.* Osteoporosis International, 1995. **5**(1): p. 30-34.

147. Marques, M.R.C., R. Loebenberg, and M. Almukainzi, *Simulated Biological Fluids with Possible Application in Dissolution Testing.* Dissolution Technologies, 2011. **18**(3): p. 15-28.

148. Marques, M.R., R. Loebenberg, and M. Almukainzi, *Simulated biological fluids with possible application in dissolution testing.* Dissolution Technol, 2011. **18**(3): p. 15-28.

149. Ennos, A.E., *The origin of specimen contamination in the electron microscope.* British Journal of Applied Physics, 1953. **4**(4): p. 101-106.

150. Zhang, Y., et al., *Synthesis of nanorod and needle-like hydroxyapatite crystal and role of pH adjustment.* Journal of Crystal Growth, 2009. **311**(23-24): p. 4740-4746.

151. Cornelis, G., et al., *Retention and Dissolution of Engineered Silver Nanoparticles in Natural Soils.* Soil Science Society of America Journal, 2012. **76**(3): p. 891-902.

152. Brasiliense, V., et al., *Correlated Electrochemical and Optical Detection Reveals the Chemical Reactivity of Individual Silver Nanoparticles.* Journal of the American Chemical Society, 2016. **138**(10): p. 3478-3483.

153. Erickson, H.P., *Size and Shape of Protein Molecules at the Nanometer Level Determined by Sedimentation, Gel Filtration, and Electron Microscopy.* Biological Procedures Online, 2009. **11**(1): p. 32-51.

154. Montano, M.D., et al., *Improvements in the detection and characterization of engineered nanoparticles using spICP-MS with microsecond dwell times.* Environmental Science-Nano, 2014. **1**(4): p. 338-346.

155. Bi, X.Y., et al., *Quantitative resolution of nanoparticle sizes using single particle inductively coupled plasma mass spectrometry with the K-means clustering*

algorithm. Journal of Analytical Atomic Spectrometry, 2014. **29**(9): p. 1630-1639.

156. Pace, H.E., et al., *Single particle inductively coupled plasma-mass spectrometry: a performance evaluation and method comparison in the determination of nanoparticle size.* Environmental science & technology, 2012. **46**(22): p. 12272-12280.

157. Hassellov, M., et al., *Nanoparticle analysis and characterization methodologies in environmental risk assessment of engineered nanoparticles.* Ecotoxicology, 2008. **17**(5): p. 344-361.

158. Arvidsson, R., et al., *Challenges in Exposure Modeling of Nanoparticles in Aquatic Environments.* Human and Ecological Risk Assessment, 2011. **17**(1): p. 245-262.

159. Cwiertny, D.M., et al., *Surface chemistry and dissolution of α-FeOOH nanorods and microrods: Environmental implications of size-dependent interactions with oxalate.* Journal of Physical Chemistry C, 2009. **113**(6): p. 2175-2186.

160. Greer, F.R., *Calcium, Phosphorous, and Magnesium - How much is too much for infant formulas.* Journal of Nutrition, 1989. **119**(12): p. 1846-1851.

161. Moy, R.J.D., *Iron fortification of infant formula.* Nutrition Research Reviews, 2000. **13**(2): p. 215-227.

162. Thompkinson, D.K. and S. Kharb, *Aspects of infant food formulation.* Comprehensive Reviews in Food Science and Food Safety, 2007. **6**(4): p. 79-102.

163. Keller, A.A., et al., *Global life cycle releases of engineered nanomaterials.* Journal of Nanoparticle Research, 2013. **15**(6).

164. Keller, A.A., et al., *Release of engineered nanomaterials from personal care products throughout their life cycle.* Journal of Nanoparticle Research, 2014. **16**(7): p. 1-10.

165. Kent, G., *Global infant formula: monitoring and regulating the impacts to protect human health.* International Breastfeeding Journal, 2015. **10**.

166. Bronner, F., *Recent developments in intestinal calcium absorption.* Nutrition Reviews, 2009. **67**(3): p. 109.

167. Pansu, D., et al., *Duodenal and ileal calcium absorption in the rat and effects of vitamin D.* The American journal of physiology, 1983. **244**(6): p. G695-700.

168. Jaeger, P. and W.G. Robertson, *Role of dietary intake and intestinal absorption of oxalate in calcium stone formation.* Nephron - Physiology, 2004. **98**(2): p. p64-p71.

169. Pal, A.K., et al., *Linking Exposures of Particles Released From Nano-Enabled Products to Toxicology: An Integrated Methodology for Particle Sampling, Extraction, Dispersion, and Dosing.* Toxicological Sciences, 2015. **146**(2): p. 321-333.

170. Cohen, J.M., G.M. DeLoid, and P. Demokritou, *A critical review of in vitro dosimetry for engineered nanomaterials.* Nanomedicine, 2015. **10**(19): p. 3015-3032.

171. DeLoid, G., et al., *Estimating the effective density of engineered nanomaterials for in vitro dosimetry.* Nature Communications, 2014. **5**.

172. Bass, J.K. and G.M. Chan, *Calcium nutrition and metabolism during infancy.* Nutrition, 2006. **22**(10): p. 1057-1066.

173. Nguyen, T.T.P., et al., *A comprehensive review on in vitro digestion of infant formula.* Food Research International, 2015. **76**: p. 373-386.

174. Lonnerdal, B., *Effects of milk and milk components on calcium, magnesium, and trace element absorption during infancy.* Physiological Reviews, 1997. **77**(3): p. 643-669.

175. Abrams, S.A., *Building bones in babies: Can and should we exceed the human milk-fed infant's rate of bone calcium accretion?* Nutrition Reviews, 2006. **64**(11): p. 487-494.

176. Ai, K., Y. Liu, and L. Lu, *Hydrogen-Bonding Recognition-Induced Color Change of Gold Nanoparticles for Visual Detection of Melamine in Raw Milk and Infant Formula.* Journal of the American Chemical Society, 2009. **131**(27): p. 9496-+.

177. Ding, N., et al., *Colorimetric Determination of Melamine in Dairy Products by Fe(3)O(4) Magnetic Nanoparticles-H(2)O(2)-ABTS Detection System.* Analytical Chemistry, 2010. **82**(13): p. 5897-5899.

178. Gossner, C.M.-E., et al., *The Melamine Incident: Implications for International Food and Feed Safety.* Environmental Health Perspectives, 2009. **117**(12): p. 1803-1808.

179. Guan, N., et al., *Melamine-Contaminated Powdered Formula and Urolithiasis in Young Children.* New England Journal of Medicine, 2009. **360**(11): p. 1067-1074.

180. Mauer, L.J., et al., *Melamine Detection in Infant Formula Powder Using Near- and Mid-Infrared Spectroscopy.* Journal of Agricultural and Food Chemistry, 2009. **57**(10): p. 3974-3980.

181. Sun, F., et al., *Analytical methods and recent developments in the detection of melamine.* Trac-Trends in Analytical Chemistry, 2010. **29**(11): p. 1239-1249.

182. Venkatasami, G. and J.R. Sowa, Jr., *A rapid, acetonitrile-free, HPLC method for determination of melamine in infant formula.* Analytica Chimica Acta, 2010. **665**(2): p. 227-230.

183. Radu, T. and D. Diamond, *Comparison of soil pollution concentrations determined using AAS and portable XRF techniques.* Journal of Hazardous Materials, 2009. **171**(1): p. 1168-1171.

184. Shefsky, S. *Comparing Field Portable X-Ray Fluorescence (XRF) to laboratory analysis of heavy metals in soil*. in *International Symposium of Field Screening Methods for Hazardous Wastes and Toxic Chemicals, Las Vegas, NV, 29–31 January*. 1997.

185. Ramsey, M.H., et al., *An objective assessment of analytical method precision: comparison of ICP-AES and XRF for the analysis of silicate rocks.* Chemical Geology, 1995. **124**(1): p. 1-19.

186. Brown, G., D.J. Hughes, and J. Esson, *New XRF data retrieval techniques and their application to USGS standard rocks.* Chemical Geology, 1973. **11**(3): p. 223-229.

187. Kuruvilla, A., et al., *Portable lead analyzer to locate source of lead.* Indian journal of pediatrics, 2004. **71**(6): p. 495-499.

188. Reames, G. and L.L. Lance, *Childhood lead poisoning investigations: Evaluating a portable instrument for testing soil lead.* Journal of environmental health, 2002. **64**(8): p. 9.

189. Reames, G. and M. Valerie Charlton MPH, *Lead detection in food, medicinal, and ceremonial items using a portable X-ray fluorescence (XRF) instrument.* Journal of environmental health, 2013. **75**(6): p. 16.

190. Clark, C., et al., *Lead in paint and soil in Karnataka and Gujarat, India.* Journal of Occupational and Environmental Hygiene, 2005. **2**(1): p. 38-44.

191. Moioli, P. and C. Seccaroni, *Analysis of art objects using a portable x-ray fluorescence spectrometer.* X-Ray Spectrometry, 2000. **29**(1): p. 48-52.

192. Bronk, H., et al., *ArtTAX-a new mobile spectrometer for energy-dispersive micro X-ray fluorescence spectrometry on art and archaeological objects.* Fresenius' journal of analytical chemistry, 2001. **371**(3): p. 307-316.

193. Shackley, M.S., *An introduction to X-ray fluorescence (XRF) analysis in archaeology*, in *X-ray fluorescence spectrometry (XRF) in geoarchaeology*. 2011, Springer. p. 7-44.

194. Odegaard, N., et al., *Use of handheld XRF for the study of pesticide residues on museum objects.* Investigation of Solid Phase Microextraction Sampling for Organic Pesticide Residues on Museum Collections. Mark Ormsby, Jessica S. Johnson, Susan Heald, Lauren Chang, and Jenifer Bosworth 1 Testing Cultural Material for Arsenic and Interpreting the Results: A Case Study at Carnegie Museum of Natural History Barbara Hamann 13, 2006. **20**(1-2): p. 42-48.

195. Mans, C., et al., *Development of suitable plastic standards for X-ray fluorescence analysis.* Spectrochimica Acta Part B: Atomic Spectroscopy, 2007. **62**(2): p. 116-122.

196. Kadachi, A.N. and M.A. Al-Eshaikh, *Limits of detection in XRF spectroscopy.* X-Ray Spectrometry, 2012. **41**(5): p. 350-354.

197. Beckhoff, B., et al., *Handbook of practical X-ray fluorescence analysis*. 2007: Springer Science & Business Media.

198. Currie, L.A., *Nomenclature in evaluation of analytical methods including detection and quantification capabilities (IUPAC Recommendations 1995).* Pure and applied chemistry, 1995. **67**(10): p. 1699-1723.

199. Rousseau, R.M., *Detection limit and estimate of uncertainty of analytical XRF results.* The Rigaku Journal, 2001. **18**(2): p. 33-47.

200. Tiede, K., et al., *Detection and characterization of engineered nanoparticles in food and the environment.* Food Additives and Contaminants, 2008. **25**(7): p. 795-821.

201. Keller, A.A. and A. Lazareva, *Predicted Releases of Engineered Nanomaterials: From Global to Regional to Local.* Environmental Science & Technology Letters, 2014. **1**(1): p. 65-70.

202. Carabias-Martınez, R., et al., *Surfactant cloud point extraction and preconcentration of organic compounds prior to chromatography and capillary electrophoresis.* Journal of Chromatography A, 2000. **902**(1): p. 251-265.

203. Yang, Y., et al., *Prospecting nanomaterials in aqueous environments by cloud-point extraction coupled with transmission electron microscopy.* Science of the Total Environment, 2017. **584**: p. 515-522.

204. Brar, S.K., *Nanomaterials in the environment*. 2015, Reston, Virginia: American Society of Civil Engineers.

205. Hartmann, G. and M. Schuster, *Species selective preconcentration and quantification of gold nanoparticles using cloud point extraction and electrothermal atomic absorption spectrometry.* Analytica chimica acta, 2013. **761**: p. 27-33.

206. Hartmann, G., C. Hutterer, and M. Schuster, *Ultra-trace determination of silver nanoparticles in water samples using cloud point extraction and ETAAS.* Journal of Analytical Atomic Spectrometry, 2013. **28**(4): p. 567-572.

207. Cremers, D.A., L.J. Radziemski, and T.R. Loree, *Spectrochemical analysis of liquids using the laser spark.* Applied spectroscopy, 1984. **38**(5): p. 721-729.

208. Hagendorfer, H., et al., *Characterization of Silver Nanoparticle Products Using Asymmetric Flow Field Flow Fractionation with a Multidetector Approach – a Comparison to Transmission Electron Microscopy and Batch Dynamic Light Scattering.* Analytical Chemistry, 2012. **84**(6): p. 2678-2685.

209. Braakhuis, H.M., et al., *Physicochemical characteristics of nanomaterials that affect pulmonary inflammation.* Particle and fibre toxicology, 2014. **11**(1): p. 18.

APPENDIX A

DATA COLLECTED AUGUST 2013-MAY 2017

Vitamin Supplement Consumer Report

- Twelve consumer products were analyzed

Transmission Electron Microscopy (TEM) paired with Energy Dispersive X-ray Spectroscopy (EDX) Sample Preparation

- TEM is the gold standard method for determine the shape, morphology and size distribution of particles, but cannot be used to determine quantity of nanoparticles in samples.
- Sample preparation involved:
    - The dry samples (~0.15 g each) were suspended in 40 mL ultrapure water and sonicated for 30 minutes to suspend particles. These samples were centrifuged at 15,000 G for 15 minutes to settle any particles present. The organics-rich supernatant was poured off, leaving a pellet of particulate matter in the centrifuge tube. This was re-suspended in 20 mL ultrapure water, and then ~10 µL volumes were pipetted onto a Ted Pella carbon type-B transmission electron microscopy grid and allowed to dry.
    - Microscopy was performed on a JEOL 2010F transmission electron microscope with energy dispersive X-ray spectroscopy. EDX data is reported in a counts vs. energy (keV) graph. Peaks report elemental presence at a respective K or L line for each element (CaK or CK refers to calcium or carbon respectively at a K emission line). Copper peaks are a result of the copper TEM grids used for analysis.
- Mean particle diameter was measured manually with ImageJ software. Particle number size distributions were developed and the percentage of particles less than 100 nm in width determined.

Scanning Electron Microscopy (TEM) paired with Energy Dispersive X-ray Spectroscopy (EDX) Sample Preparation

- SEM is the gold standard method for determining the shape, morphology and size distribution of particles on the surface of a solid, but cannot be used to determine quantity of nanoparticles in samples.
- Sample preparation involved:
    - Gelatin capsules were opened and inside powder was discarded
    - Gel capsules were adhered to aluminum SEM stubs with carbon tape as well as cut with a stainless steel razor blade for a cross-sectional analysis labeled “Cross-Sectional View”
    - Samples were sputter coated with Au and Pd for 120 seconds
    - Microscopy was performed on a Philips XL30 FEG scanning electron microscope with energy dispersive X-ray spectroscopy. EDX data is reported in a counts vs. energy (keV) graph. Peaks report elemental presence at a respective K or L line for each element (CaK or CK refers to calcium or carbon respectively at a K emission line). Copper peaks are a result of the copper TEM grids used for analysis.
- Mean particle diameter was measured manually with ImageJ software. Particle number size distributions were developed

Sample Orientation

Surface View

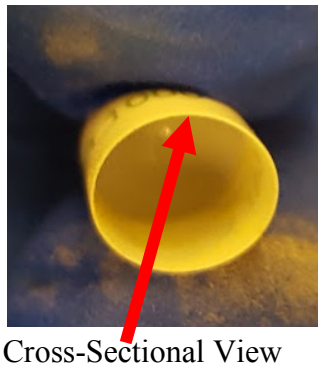

Cross-Sectional View

- Each sample analyzed on the surface and within the capsule
    - Surface View: Outer surface of the capsule
    - Cross-Sectional View: Capsule was cut and the inside (inner wall) was analyzed

Analysis of Particle Size

- Sizing analysis was performed using ImageJ, a free image processing program available from the National Institute of Health. The number of primary particles was noted and were sized. The scale bar was used to set the scale for calculating each particle's diameter. In the case of high aspect ratio structures both a width and length were measured. Error is reported as +/- 1 standard deviation.

X-ray Fluorescence (XRF) Sample Preparation

- XRF is a rapid screening analytical technique capable of detecting higher concentrations of elements (>0.1 wt%). Analysis is conducted on dry samples and requires minimal sample preparation.
- Sample in sampling cup was placed on XRF sampling window
- Samples were analyzed by XRF for bulk elemental composition and reported as absence or presence of silicon, titanium, calcium, and phosphorous

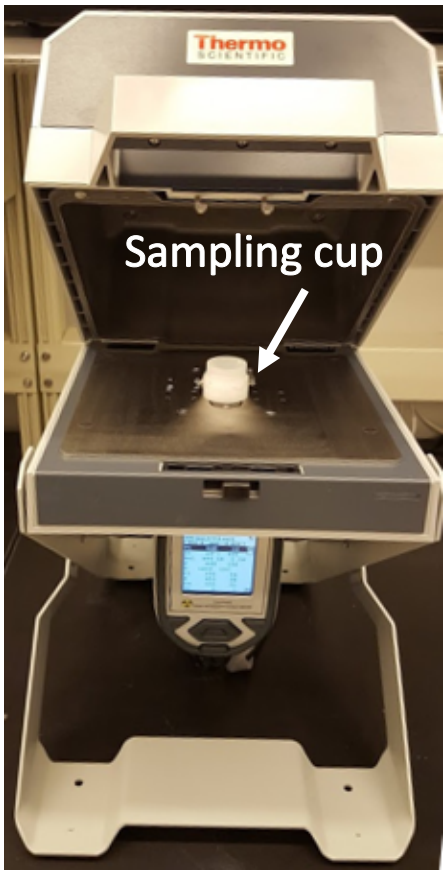

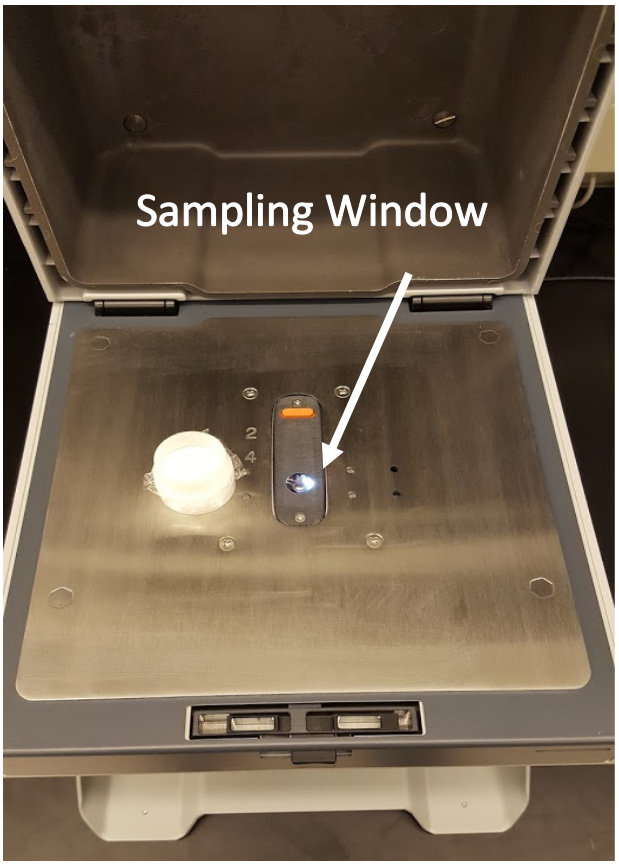

Figure 1. XRF Setup Schematic

XRF Sample Preparation

- Pills were placed directly onto the X-ray fluorescence (XRF) sampling window and analyzed
- Pills with white capsules had their powder contents emptied into an XRF sampling cup and analyzed (results labelled as "powder")
- White pill capsules were analyzed separately without powder contents (results labelled as "capsule")
- Liquid (Silver Biotics, Pharmanex Red Pill, and Usana Coquinone 30) were poured into an XRF sampling cup and analyzed

Inductively Coupled Plasma – Mass Spectrometry (ICP-MS) Sample Preparation

- ICP-MS is a highly sensitive analytical method to detect elements in samples. Samples must be digested and analyzed in liquid form
- Titanium, Silicon, Calcium, Phosphorous, and Silver concentrations were measured
- Solid samples (~0.25 g) were added to 9 mL concentrated nitric acid (70%) and 1 mL hydrofluoric acid (47-51%) (ACS Grade), and microwave digested. During microwave digestion, the temperature was initially increased to 150°C over 15 minutes, and then increased to 180°C over another 15 minute period. Once 180 °C were reached, the temperature was kept constant for a period of 20 minutes before cooling the samples to room temperature. To remove hydrofluoric acid from solution after digestion, the digested sample was reacted with 10 mL boric acid (4.5% w/v).

X-ray Diffraction (XRD) Sample Preparation

- XRD analysis provides information on the crystalline structure of minerals.
- The presence of organics or non-crystalline material in complex samples can interfere with XRD spectral analysis, and therefore were removed prior to XRD analysis.
- Sample preparation involved:
    - ~10 grams of the dry sample was added to 40 mL of Nanopure™ water in a centrifuge vial and vigorously shaken for 2 minutes and then sonicated (Branson Sonicator Bath – 80 watt) for 30 minutes to disperse the powder
    - The vial was centrifuged at 15,000G for 15 minutes to separate the solution into a particulate bottom phase and a top dissolved organic phase
    - The top phase was decanted and disposed followed by the addition of 40 mL of Nanopure ™ water to the vial. The centrifugation, decantation, and water addition was repeated 2 more times.
    - After the third centrifugation, the top phase was decanting, leaving a pellet that was allowed to air dry for several days, and then analyzed by XRD (Siemens D5000)

Vitamin Supplement Sample 1: Ageloc Night

- TEM confirmed the presence of Si, and O containing particles (162 were counted)
  - Primary particles
    - Average diameter: 12 ± 3 nm
    - 100% of particles below 100 nm
  - Spherical morphology
  - Aggregate particles
    - 29 – 762 nm
- XRD identified Si and O particulate as SiO_2
- ICP-MS found the concentration of:
  - Silicon: 320 µg/g
  - Titanium: 6 µg/g
  - Calcium: 534 µg/g
  - Phosphorus: 693 µg/g
- XRF identified:
  - Silicon: Present
  - Titanium: Absent
  - Calcium: Present
  - Phosphorus: Present

Figure A1: Vitamin Supplement 1

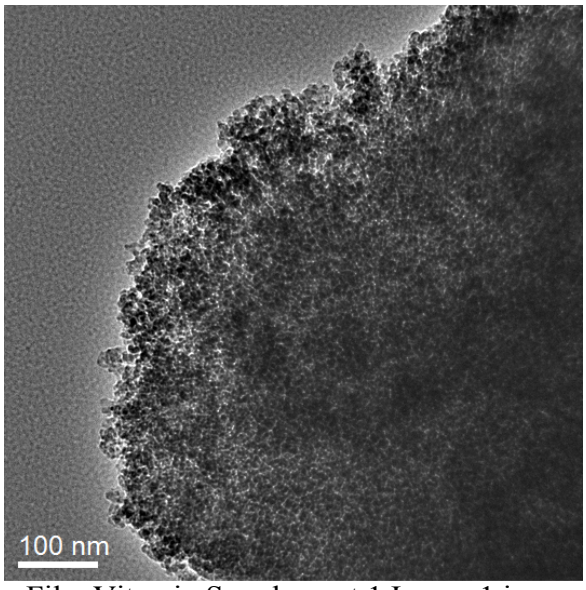

File: Vitamin Supplement 1 Image 1.jpeg

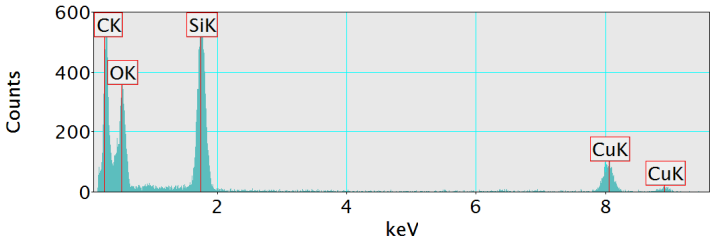

File: Vitamin Supplement 1 TEM EDX of Image 1.jpeg

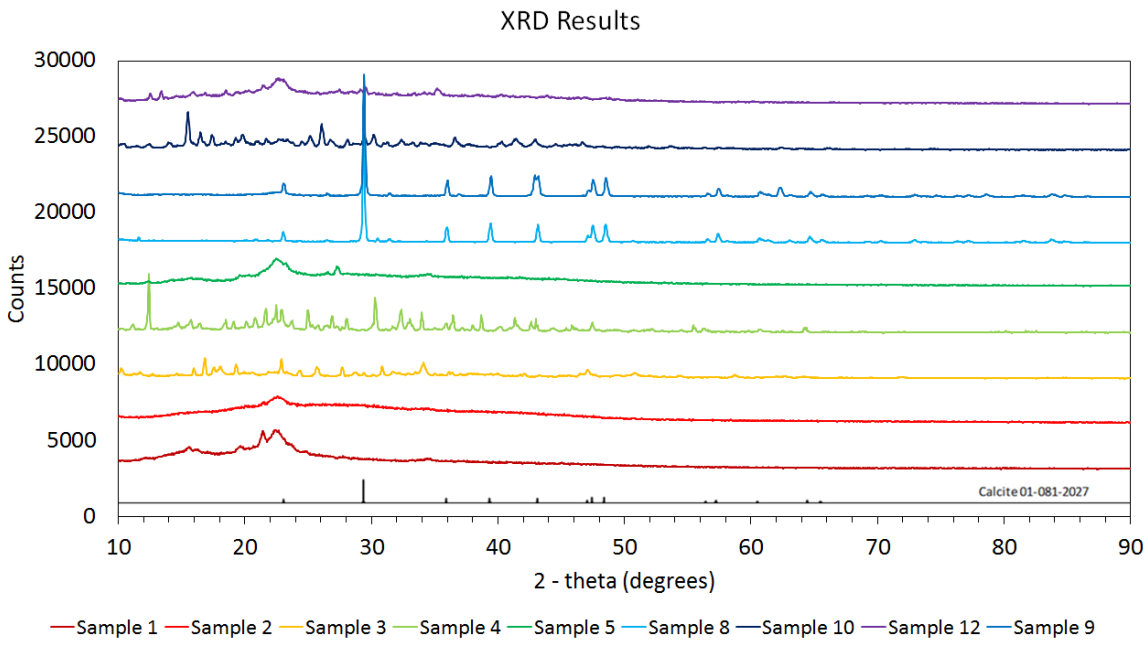

- XRD analysis confirmed the presence of crystalline SiO_2 (samples 1, 2, 3, 4, 5, 9, 10, and 12), calcite (samples 8, 9, and 10), monetite (sample 4)and MgO (sample 10)

Vitamin Supplement Sample 2: Ageloc Day

- TEM confirmed the presence of Si, and O containing particles (66 were counted)
    - Primary particles
        - Average diameter: 10 ± 2 nm
        - 100% of particles below 100 nm
    - Spherical morphology
    - Aggregate particles
        - 29 – 762 nm
- XRD identified Si, and O particulate as SiO_2
- ICP-MS found the concentration of:
    - Silicon: 586 µg/g
    - Titanium: 11 µg/g
    - Calcium: 1,333 µg/g
    - Phosphorus: 4,446 µg/g
- XRF (Capsule of pill) identified:
    - Silicon: Present
    - Titanium: Absent
    - Calcium: Present
    - Phosphorus: Present
- XRF (Powder within pill capsule) identified:
    - Silicon: Absent
    - Titanium: Present
    - Calcium: Absent
    - Phosphorus: Absent

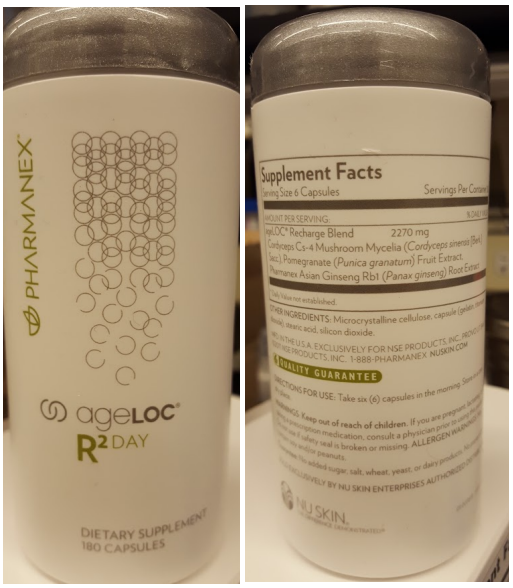

Figure A2: Vitamin Supplement 2

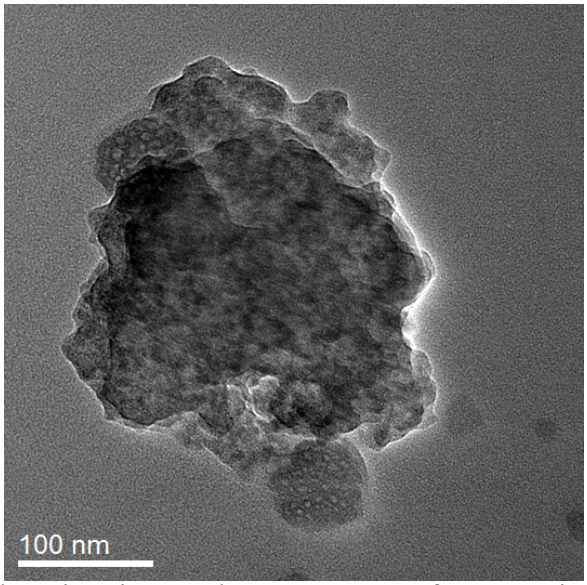

File: Vitamin Supplement 2 TEM of Image 1.jpeg

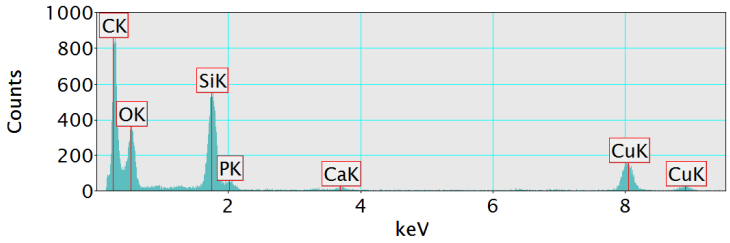

File: Vitamin Supplement 2 TEM EDX of Image #2.jpeg

Vitamin Supplement Sample 2 SEM
Cross-Sectional View

- Presence of Ti, O, and C
- Black box indicates location of EDX elemental measurement
- Au and Pd present from sputtering step

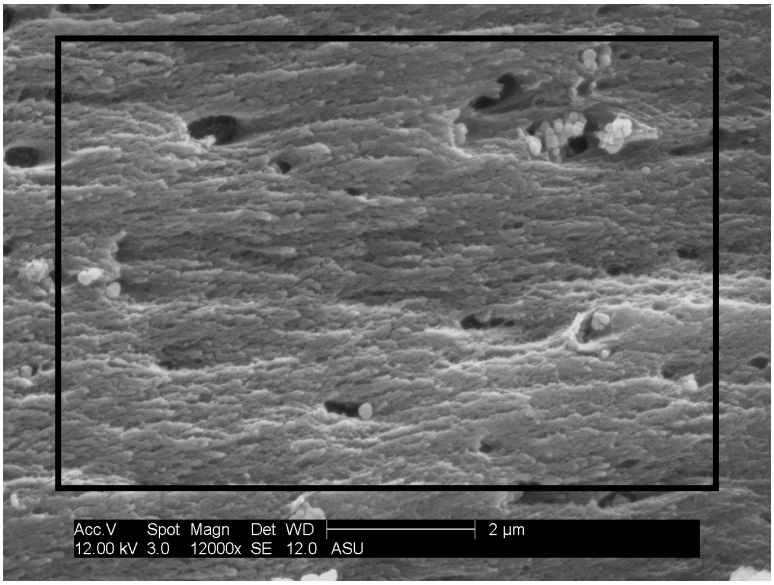

File: Vitamin Supplement 2 SEM Image 1.jpeg

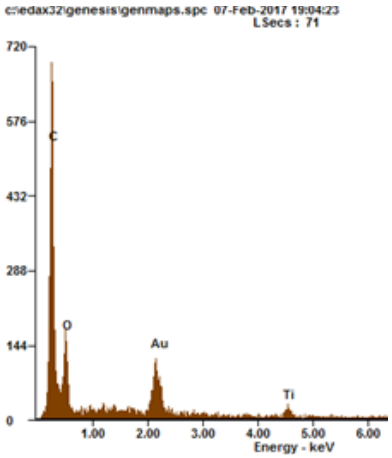

Element	Wt%	At%
CK	58.48	80.79
OK	13.97	14.99
AuM	21.97	01.91
TiK	05.58	02.00
Matrix	Correction	ZAF

Table A1. SEM EDX Results of Vitamin Sample 2 Image 1

File: Vitamin Supplement 2 SEM EDX Image 1.jpeg

Presence of Ti, O, and C

- Ti particulate
  - Diameter: 53 nm
- Black box indicates location of EDX elemental measurement
- Au and Pd present from sputtering step

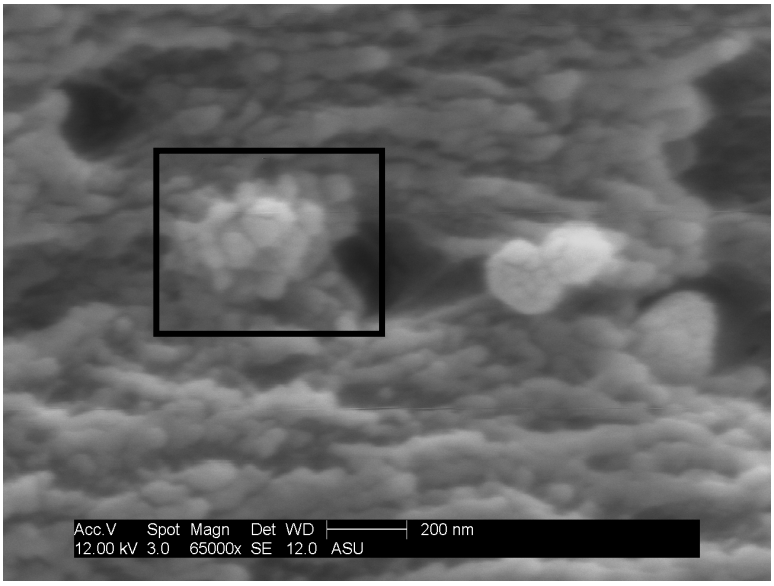

File: Vitamin Supplement 2 SEM Image 2.jpeg

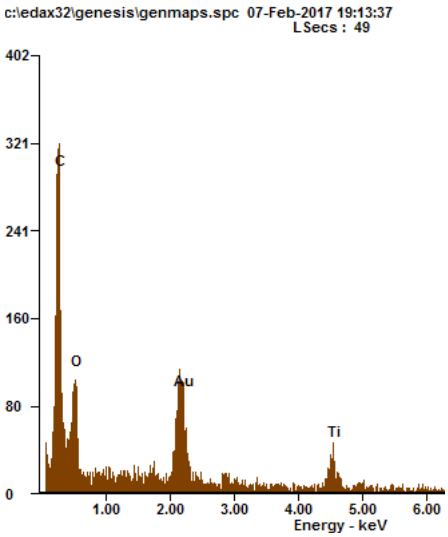

File: Vitamin Supplement 2 SEM EDX of Image 2.jpeg

Element	Wt%	At%
CK	43.23	73.08
OK	13.73	17.42
AuM	27.28	02.81
TiK	15.77	06.68
Matrix	Correction	ZAF

Table A2. SEM EDX Results of Vitamin Supplement 2 Image 2

Presence of Ti, O, and C

- Ti Particulate
- Diameter:
    - 162 – 200 nm
- Black box indicates location of EDX elemental measurement
- Au and Pd present from sputtering step

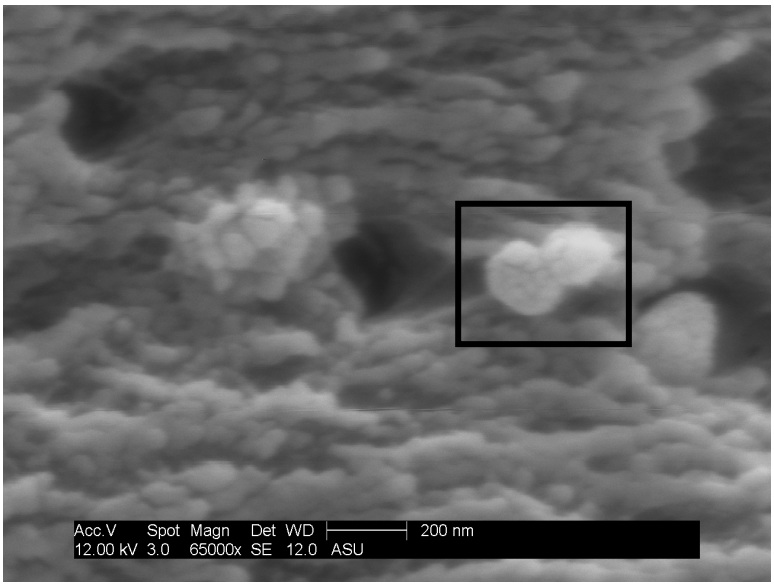

File: Vitamin Supplement 2 SEM Image 3.jpeg

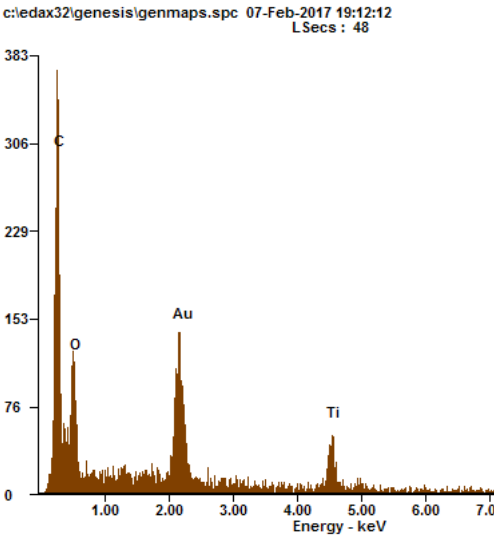

File: Vitamin Supplement 2 SEM EDX of Image 3.jpeg

Element	Wt%	At%
CK	40.39	71.63
OK	13.26	17.66
AuM	29.41	03.18
TiK	16.93	07.53
Matrix	Correction	ZAF

Table A3. SEM EDX of Vitamin Supplement 2 Image 3

- **P**resence of Ti, O, and C
    - Diameter: 170 – 276 nm
    - Aggregate Diameter: 1,080 nm
- Black box indicates location of EDX elemental measurement
- Au and Pd present from sputtering step

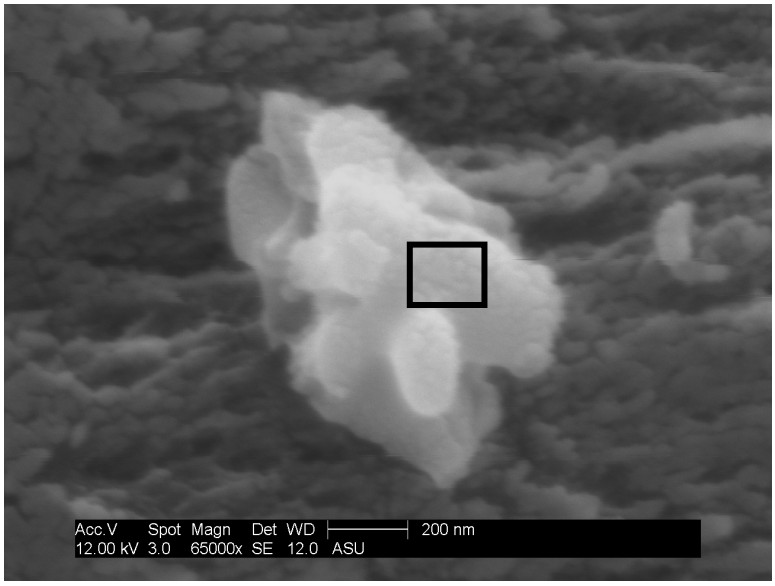

File: Vitamin Supplement 2 SEM Image 4.jpeg

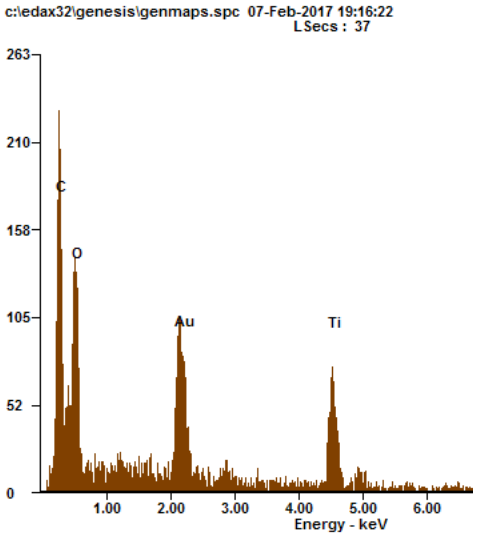

File: Vitamin Supplement 2 SEM EDX of Image 4.jpeg

Element	Wt%	At%
CK	27.08	54.17
OK	18.87	28.34
AuM	25.31	03.09
TiK	28.73	14.41
Matrix	Correction	ZAF

Table A4. SEM EDX of Vitamin Supplement 2 Image 4

Vitamin Supplement Sample 3: Pharmanex Lifepack Nano – White Pill

- TEM confirmed the presence of Mg, Ca, O containing particles (182 were counted)
  - Primary particles
    - Average Length: 56 ± 30 nm
    - Average Width: 22 ± 10 nm
    - 100% of particles below 100 nm
  - Rectangular, rod, and irregular morphology
  - Aggregate particles
    - 161 – 2,581 nm
- XRD identified SiO_2
- ICP-MS found the concentration of:
  - Silicon: 181 µg/g
  - Titanium: 165 µg/g
  - Calcium: 170,821 µg/g
  - Phosphorus: 307 µg/g
- XRF identified:
  - Silicon: Present
  - Titanium: Present
  - Calcium: Present
  - Phosphorus: Present

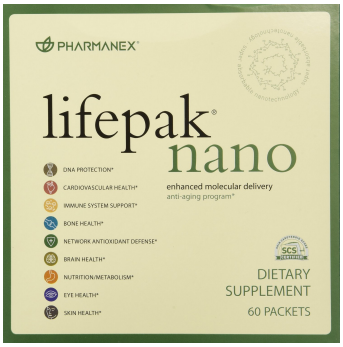

Figure A3.A. Vitamin Supplement 3

Figure A3.B. Vitamin Supplement 3

Figure A3.D: Vitamin Supplement 3, 4, 5, 6

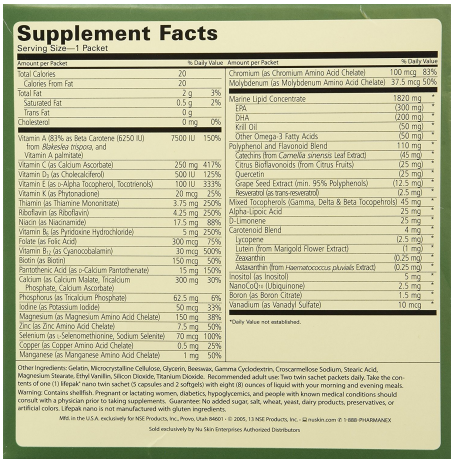

Figure A3.C. Vitamin Supplement 3

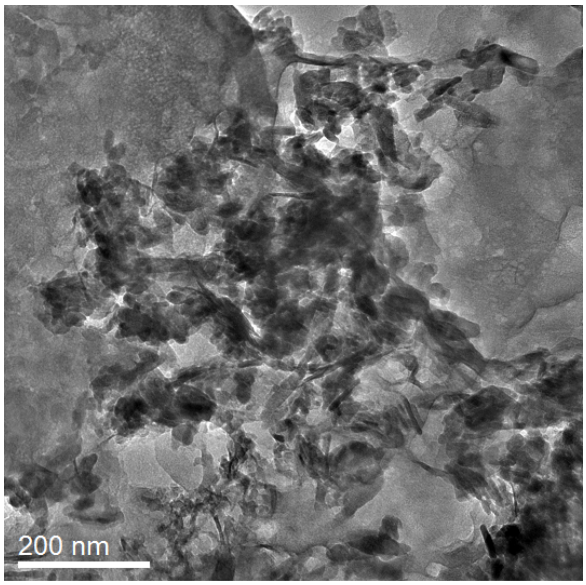

File: Vitamin Supplement 3 TEM of Image 1.jpeg

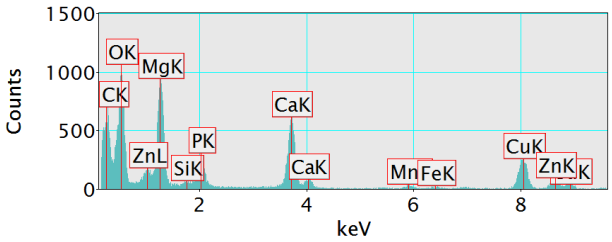

File: Vitamin Supplement 3 EDX of Image 1.jpeg

Vitamin Supplement Sample 3 SEM
Surface View
Ti <LOD
Black box indicates location of EDX elemental measurement
Au and Pd present from sputtering step

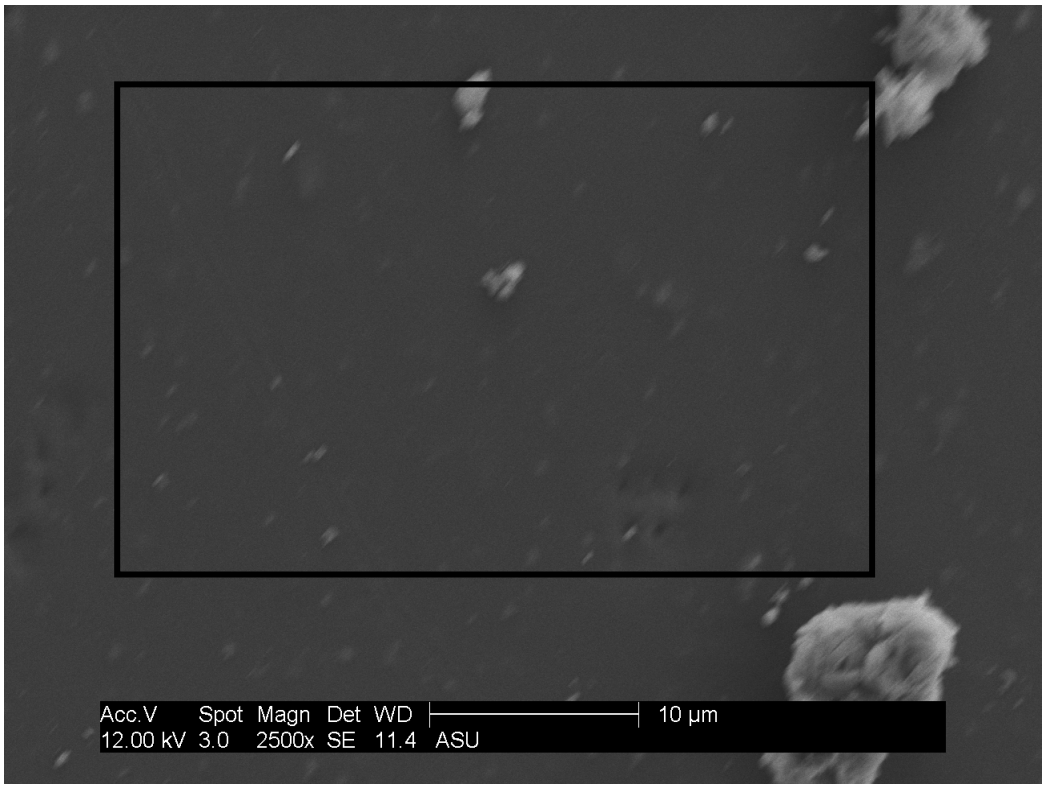

File: Vitamin Supplement 3 SEM Image 1.jpeg

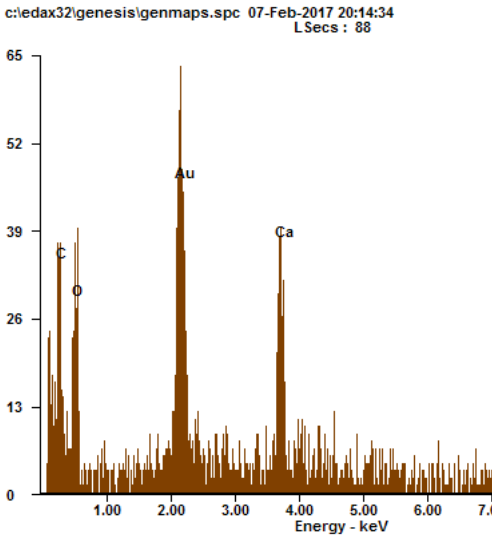

Element	Wt%	At%
CK	21.47	49.62
OK	17.68	30.66
AuM	40.65	05.73
CaK	20.20	13.99
Matrix	Correction	ZAF

Table A.5. EDX Results of Vitamin Supplement 3 Image 1

File: Vitamin Supplement 3 SEM EDX of Image 1.jpeg

- Presence of Ti, O, Ca, and C
- Ti Particulate
    - Diameter: 138 – 564 nm
- Black box indicates location of EDX elemental measurement
- Au and Pd present from sputtering step

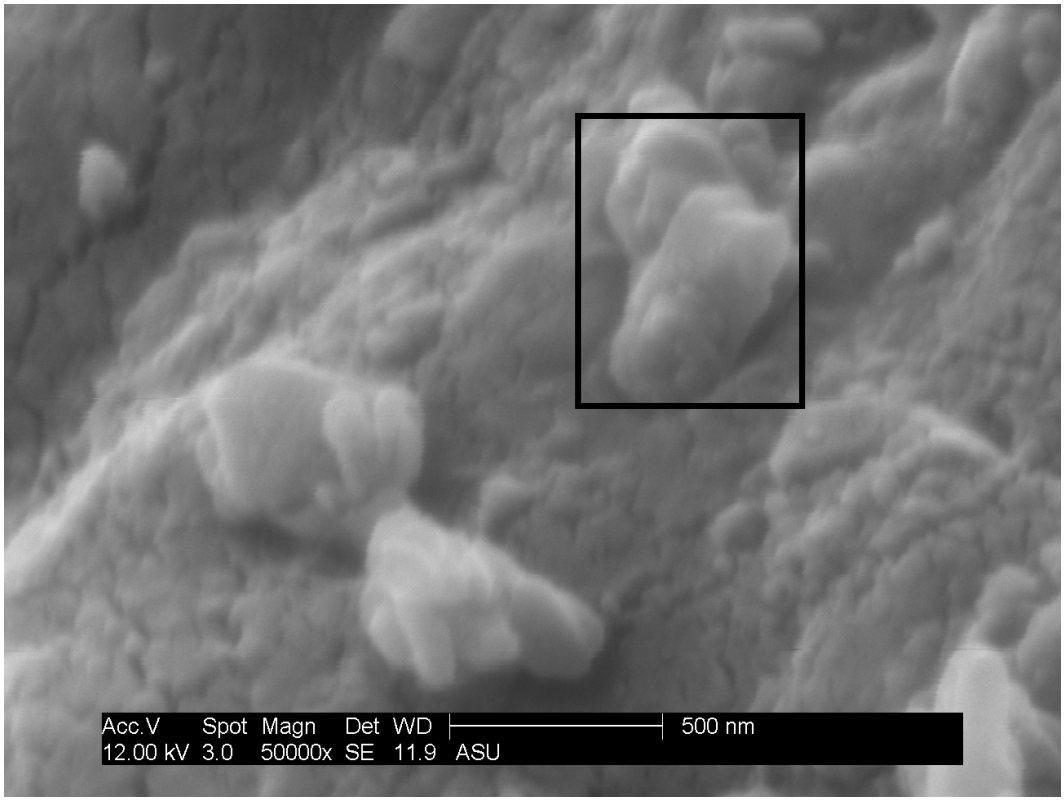

File: Vitamin Supplement 3 SEM Image 2.jpeg

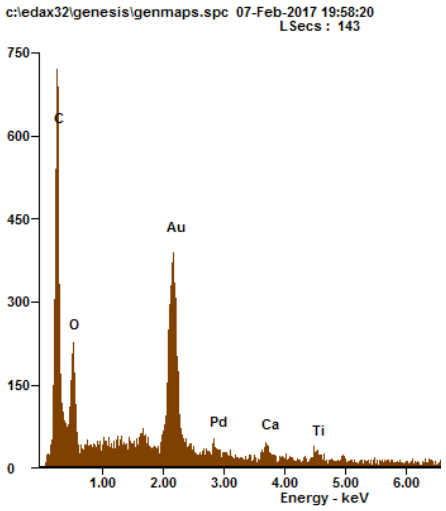

File: Vitamin Supplement 3 SEM EDX of Image 2.jpeg

Element	Wt%	At%
CK	45.82	77.75
OK	12.81	16.33
AuM	35.48	03.67
PdL	01.77	00.34
CaK	01.93	00.98
TiK	02.19	00.93
Matrix	Correction	ZAF

Table A.6 SEM EDX Results of Vitamin Supplement 3 Image 2

Cross-Sectional View

- Ti <LOD
- Ca Particulate
    - Diameter: 204 – 2,682 nm
- Black box indicates location of EDX elemental measurement
- Au and Pd present from sputtering step

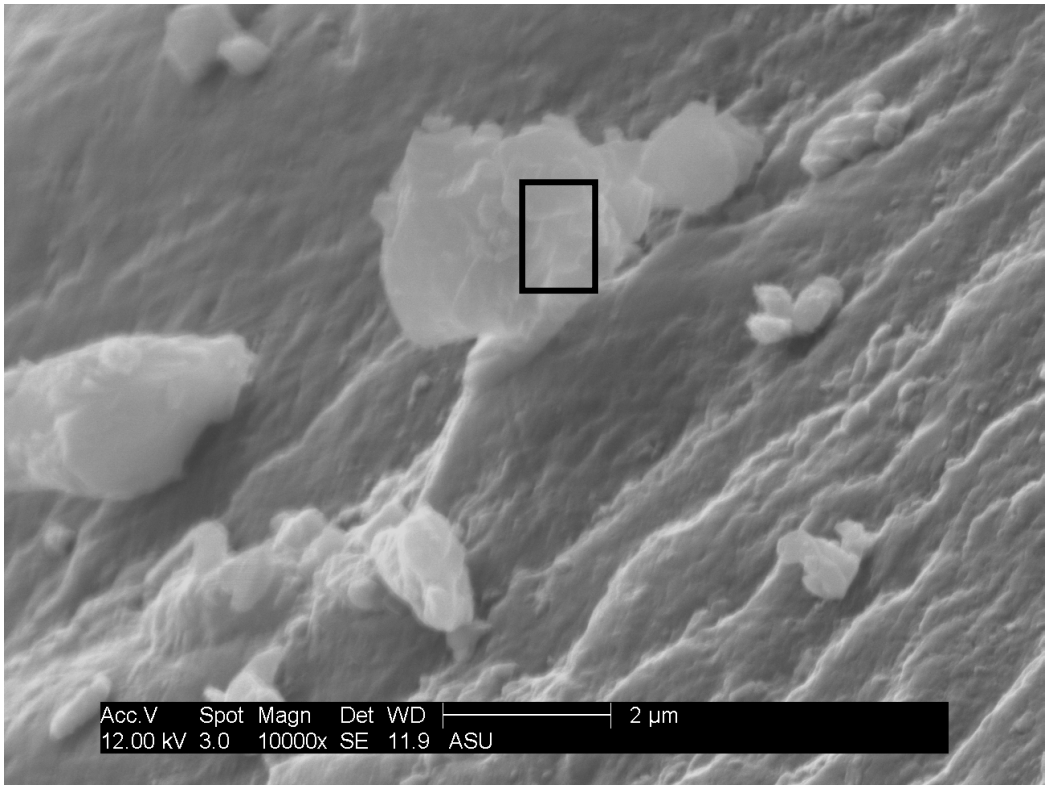

File: Vitamin Supplement 3 SEM Image 3.jpeg

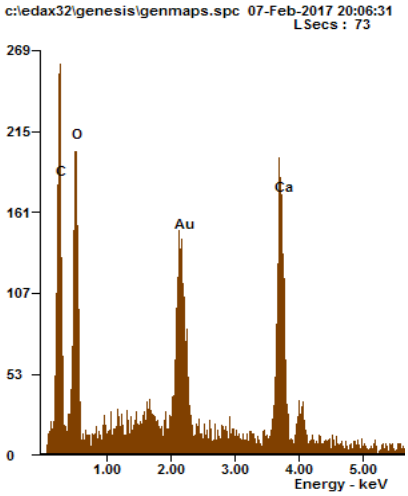

File: Vitamin Supplement 3 SEM EDX of Image 3.jpeg

Element	Wt%	At%
CK	28.11	51.91
OK	23.24	32.22
AuM	25.09	02.83
CaK	23.56	13.04
Matrix	Correction	ZAF

Table A.7. SEM EDX Results of Vitamin Supplement 3 Image 3

Vitamin Supplement Sample 4: Pharmanex Lifepack Nano – Yellow Pill

- TEM confirmed the presence of Si and O containing particles (146 were counted)
  - Primary particles
    - Average Diameter: 15 ± 4 nm
    - 100% of particles below 100 nm
  - Spherical morphology
  - Aggregate particles
    - 77 – 653 nm
- TEM confirmed the presence of Ca and O containing particles (49 were counted)
  - Primary Particles
    - Average Diameter: 128 ± 131 nm
    - 65% of particles found were below 100 nm
  - Irregular morphology
- XRD identified Si and O particulate as SiO_2 and identified Ca, C, and O particulate as monetite
- ICP-MS found the concentration of:
  - Silicon: 460 µg/g
  - Titanium: 342 µg/g
  - Calcium: 85,349 µg/g
  - Phosphorus: 5,032 µg/g
- XRF identified:
  - Silicon: Present
  - Titanium: Absent
  - Calcium: Present
  - Phosphorus: Absent

Figure A3.D: Vitamin Supplement 3, 4, 5, 6

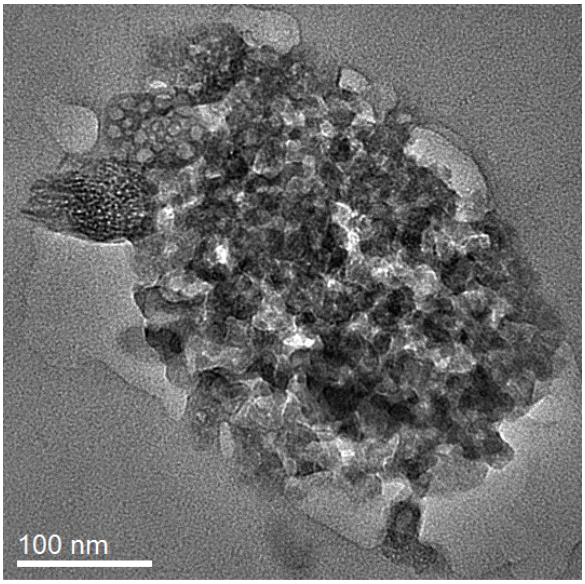

File: Vitamin Supplement 4 TEM Image 1.jpeg

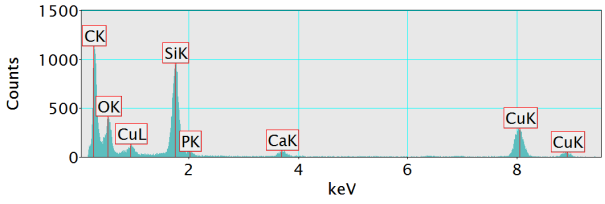

File: Vitamin Supplement 4 TEM EDX of Image 1.jpeg

Vitamin Supplement Sample 4 SEM
Cross-Sectional View

- Ti <LOD
- Black box indicates location of EDX elemental measurement
-

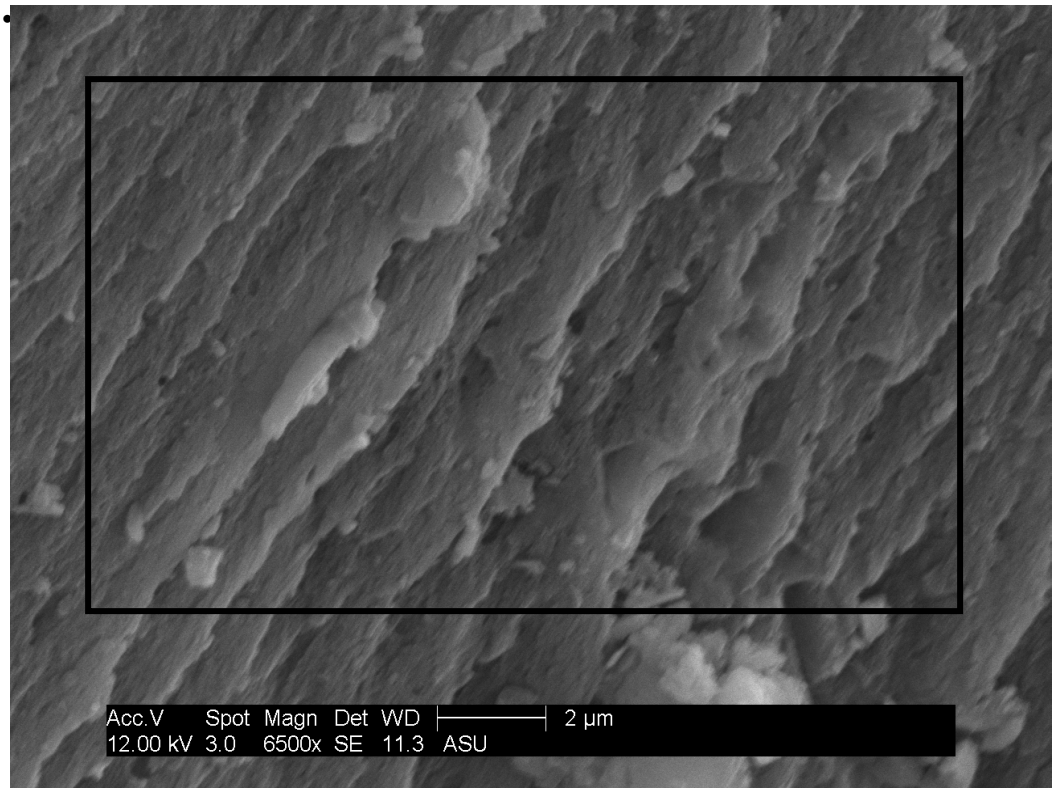

File: Vitamin Supplement 4 SEM Image 1.jpeg

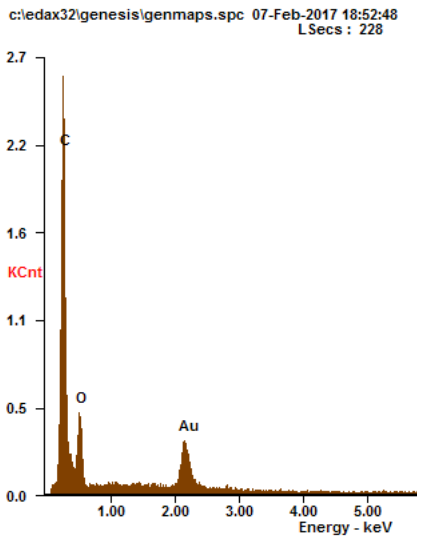

File: Vitamin Supplement 4 SEM EDX of Image 4.jpeg

Element	Wt%	At%
CK	65.75	85.06
OK	13.71	13.31
AuM	20.55	01.62
Matrix	Correction	ZAF

Table A.8. SEM EDX Results of Vitamin Supplement 3 Image 2

Vitamin Supplement Sample 5: Pharmanex Lifepack Nano – Brown Pill

- TEM confirmed the presence of Si and O containing particles (153 were counted)
  - Primary particles
    - Average Diameter: 12 ± 4 nm
    - 100% of particles below 100 nm
  - Spherical morphology
  - Aggregate particles
    - 100 – 556 nm
- TEM confirmed the presence of crystalline carbon containing particles (38 were counted)
  - Primary Particles
    - Average Length: 1,050 ± 921 nm
    - Average Width: 295 ± 252 nm
    - 33% of particles found were below 100 nm
  - Rod morphology
- XRD identified Si and O particulate as SiO_2
- ICP-MS found the concentration of:
  - Silicon: 515 µg/g
  - Titanium: 5 µg/g
  - Calcium: 535 µg/g
  - Phosphorus: 78 µg/g
- XRF identified:
  - Silicon: Absent
  - Titanium: Present
  - Calcium: Present
  - Phosphorus: Absent

Figure A5. Vitamin Supplement 5

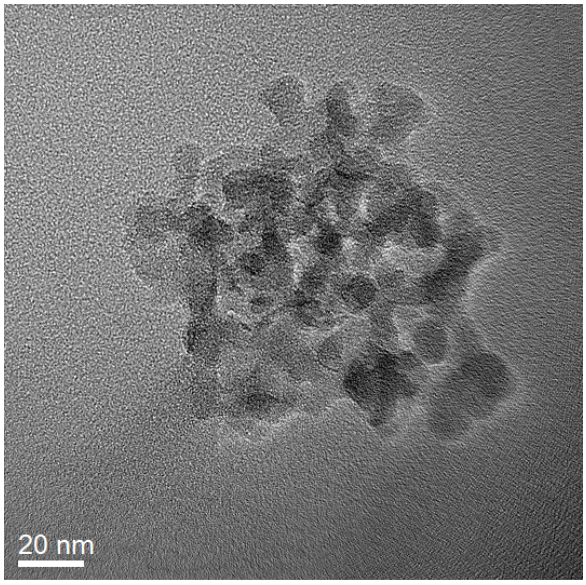

File: Vitamin Supplement 5 TEM Image 1.jpeg

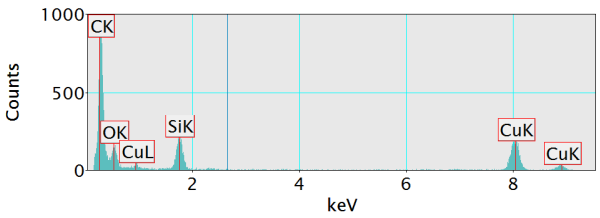

File: Vitamin Supplement 5 TEM EDX of Image 1.jpeg

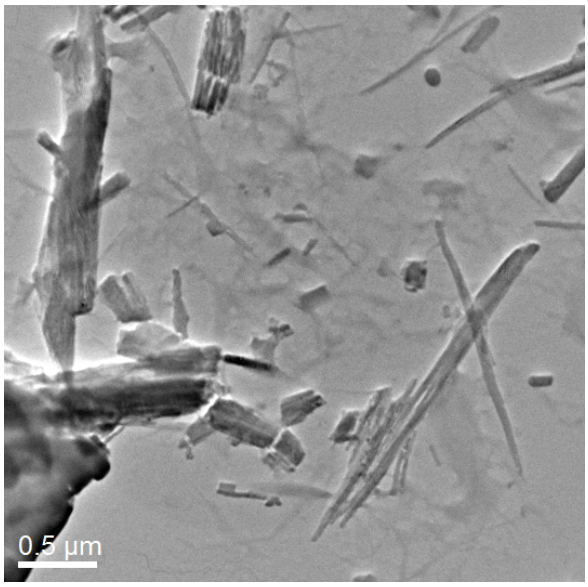

File: Vitamin Supplement 5
TEM Image 2.jpeg

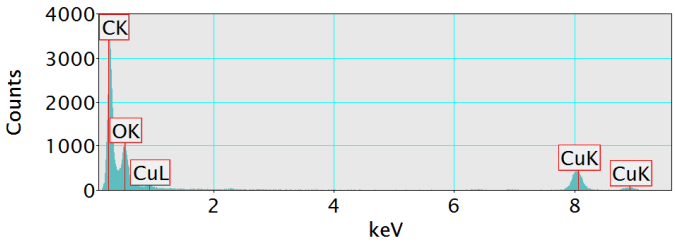

File: Vitamin Supplement 5
TEM EDX of Image 1.jpeg

Vitamin Supplement Sample 6: Pharmanex Lifepack Nano – Red Pill

- TEM confirmed the carbon goo
  - No particulate detected
- XRD not completed due to liquid sample
- ICP-MS found the concentration of:
  - Silicon: 557 µg/g
  - Titanium: 2 µg/g
  - Calcium: <LOD
  - Phosphorus: 285 µg/g
- XRF identified:
  - Silicon: Absent
  - Titanium: Absent
  - Calcium: Absent
  - Phosphorus: Present

Figure A6: Vitamin Supplement 6

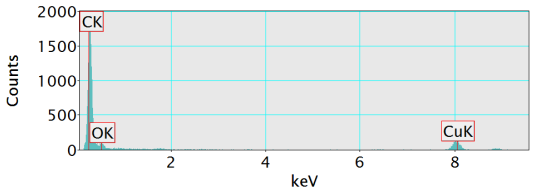

File: Vitamin Supplement 6
TEM EDX of Image 1.jpeg

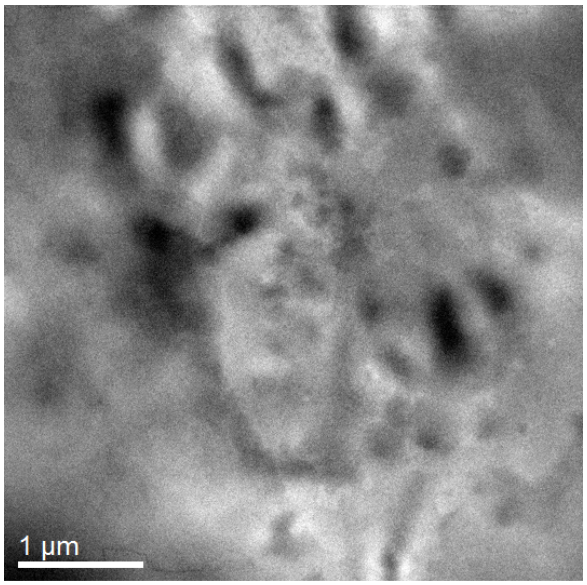

File: Vitamin Supplement 6
TEM Image 1.jpeg

Vitamin Supplement Sample 7: Silver Biotics

- TEM confirmed the presence of Ag particles (357 were counted)
  - Primary particles
    - Average Length: 35 ± 13 nm
  - Spherical morphology
- XRD not completed due to liquid sample
- ICP-MS found the concentration of:
  - Silicon: 548 µg/g
  - Titanium: 3 µg/g
  - Silver: 27 µg/g
- XRF identified:
  - Silicon: Absent
  - Titanium: Absent
  - Silver: Present

Figure A7.A. Vitamin Supplement 7

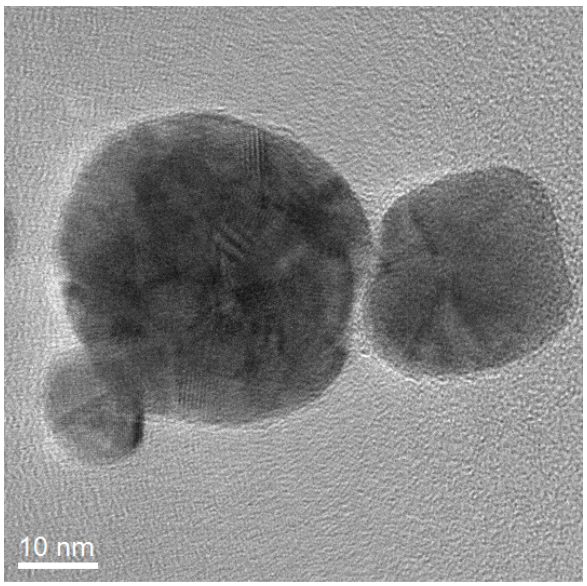

File: Vitamin Supplement 7
TEM Image 1.jpeg

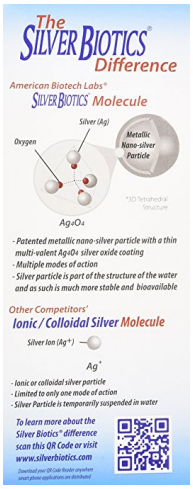

Figure A7.B. Vitamin Supplement 7

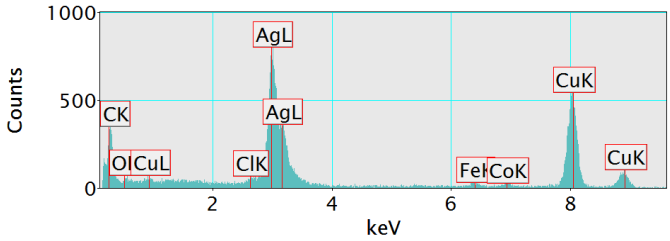

File: Vitamin Supplement 7
TEM EDX of Image 1.jpeg

Vitamin Supplement Sample 8: Herbalife Male Factor 1000

- TEM confirmed the presence of Ca and O containing particles (289 were counted)
  - Primary particles
    - Average Diameter: 18 ± 7 nm
    - 100% of particles below 100 nm
  - Spherical morphology
- XRD identified Ca and O particulate as calcite
- ICP-MS found the concentration of:
  - Silicon: 382 µg/g
  - Titanium: 179 µg/g
  - Calcium: 133,791 µg/g
  - Phosphorus: 2,506 µg/g
- XRF (Capsule of pill) identified:
  - Silicon: Present
  - Titanium: Present
  - Calcium: Present
  - Phosphorus: Absent
- XRF (Powder within pill capsule) identified:
  - Silicon: Present
  - Titanium: Present
  - Calcium: Present
  - Phosphorus: Present

Figure A.8.A. Vitamin Supplement 8

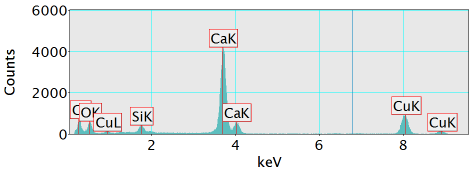

File: Vitamin Supplement 8 TEM EDX of Image 1.jpeg

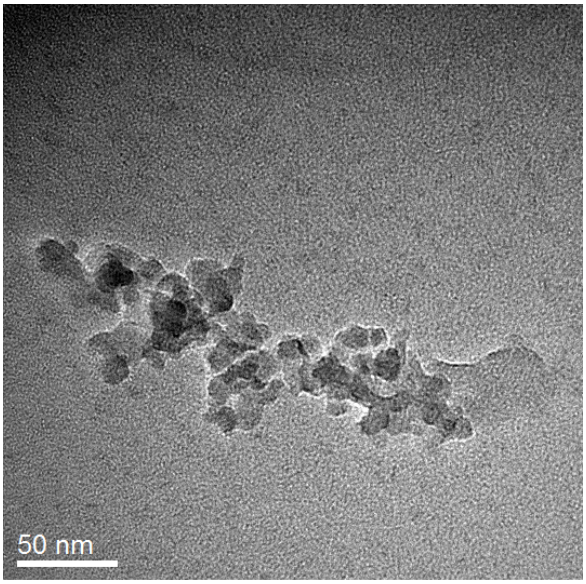

File: Vitamin Supplement 8 TEM Image 1.jpeg

Vitamin Supplement Sample 8 SEM
Surface View

- Ti <LOD
- Black box indicates location of EDX elemental measurement
- Au and Pd present from sputtering step

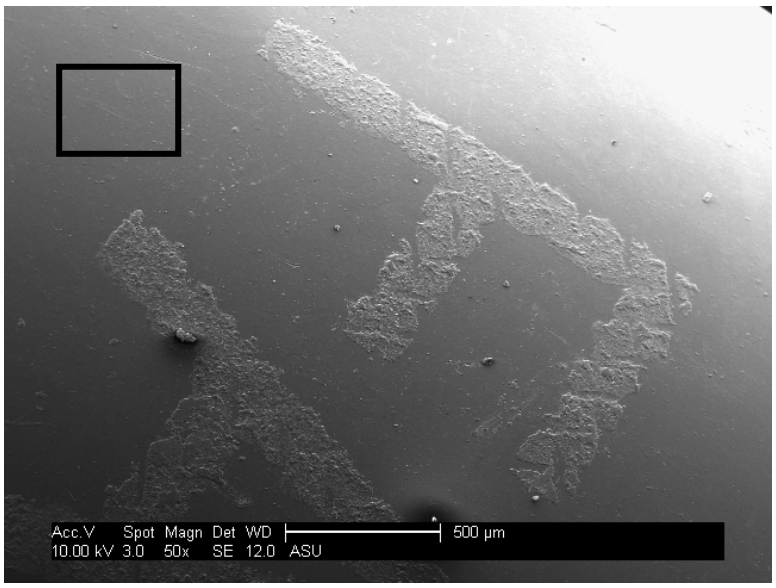

File: Vitamin Supplement 8 SEM of Image 1.jpeg

Figure A.8.B. Vitamin Supplement 8

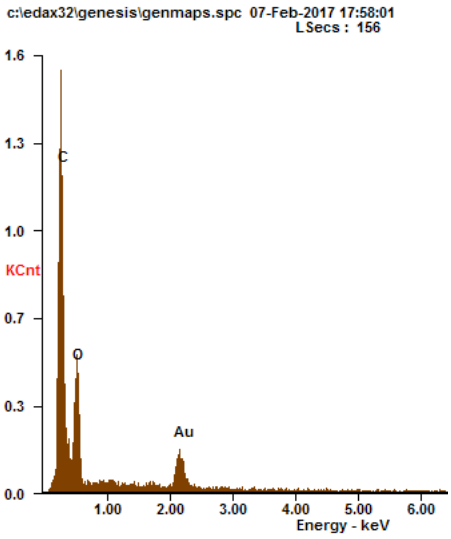

File: Vitamin Supplement 8 SEM EDX of Image 1.jpeg

Element	Wt%	At%
CK	61.72	78.25
OK	21.49	20.45
AuM	16.79	01.30
Matrix	Correction	ZAF

Table A.9. Results of EDX on Vitamin Supplement 8 SEM of Image 1.jpeg

- Presence of Ti, O, C, Fe, Na, Al, Si, and Ca
- Black box indicates location of EDX elemental measurement
- Au and Pd present from sputtering step

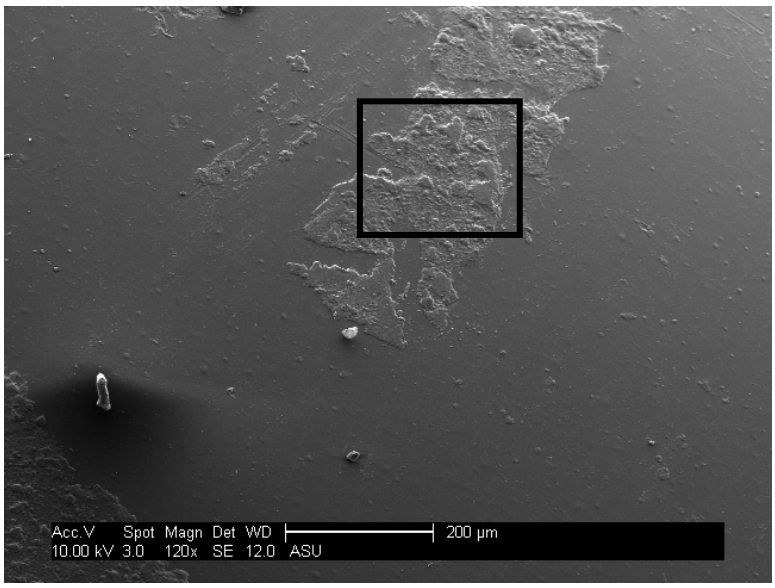

File: Vitamin Supplement 8 SEM of Image 2.jpeg

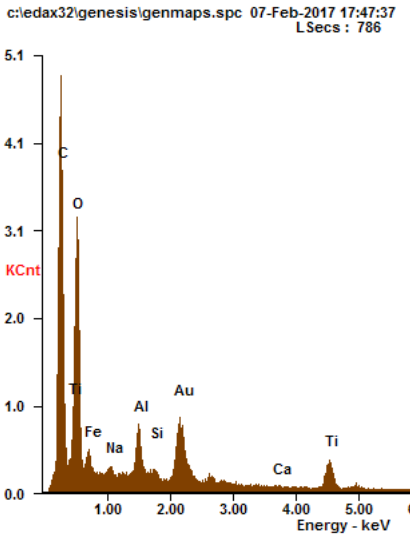

File: Vitamin Supplement 8 SEM EDX of Image 2.jpeg

Element	Wt%	At%
CK	41.30	63.49
OK	22.31	25.75
FeL	09.13	03.02
NaK	00.43	00.34
AlK	03.13	02.14
SiK	00.52	00.34
AuM	13.84	01.30
CaK	00.22	00.10
TiK	09.11	03.51
Matrix	Correction	ZAF

Table A.10. Results of EDX on Vitamin Supplement 8 SEM of Image 2.jpeg

- Presence of Ti, O, C, Fe, Na, Al, Si, And Ca
- Ti particulate
- Diameter: 42 – 2,451 nm
- Black box indicates location of EDX elemental measurement
- Au and Pd present from sputtering

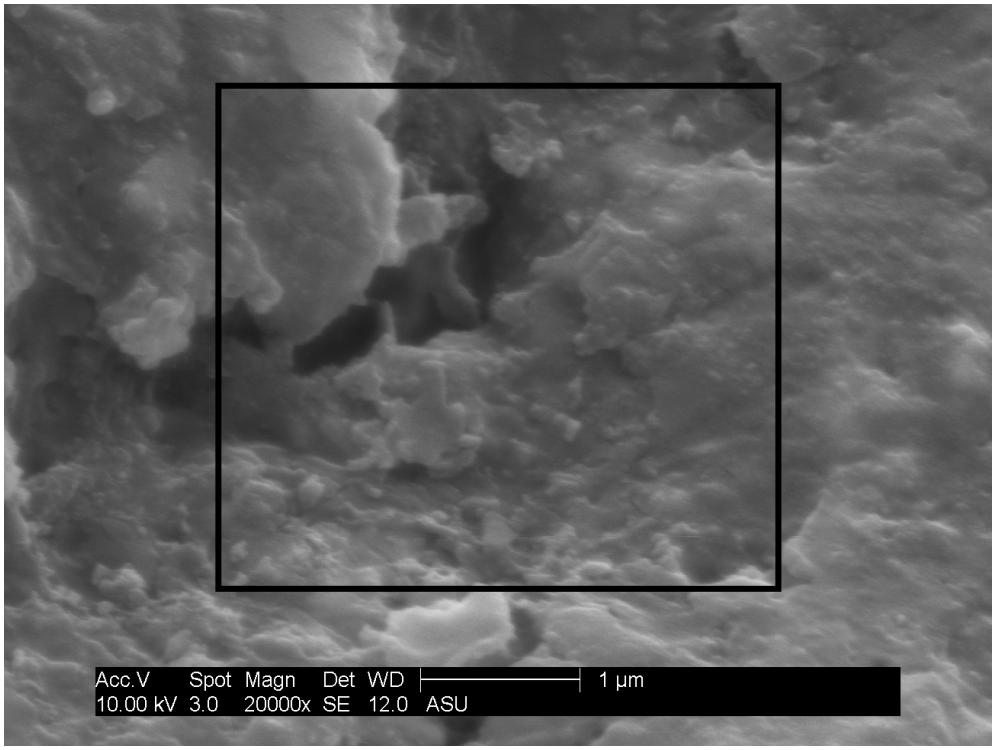

File: Vitamin Supplement 3 SEM of Image 3.jpeg

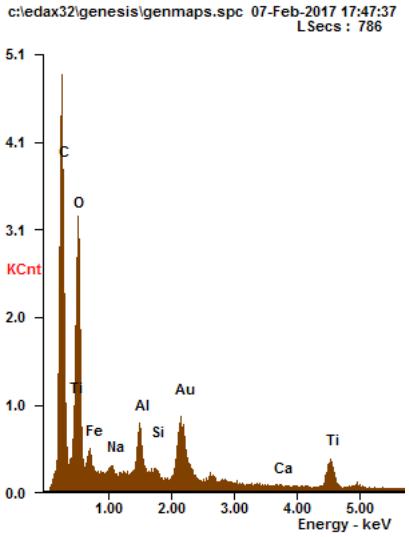

File: Vitamin Supplement 3 SEM EDX of Image 3.jpeg

Element	Wt%	At%
CK	41.30	63.49
OK	22.31	25.75
FeL	09.13	03.02
NaK	00.43	00.34
AlK	03.13	02.14
SiK	00.52	00.34
AuM	13.84	01.30
CaK	00.22	00.10
TiK	09.11	03.51
Matrix	Correction	ZAF

Table A11. Results of EDX on Vitamin Supplement 8 SEM of Image 3.jpeg

Vitamin Supplement Sample 9: Calcium Plus

- TEM confirmed the presence of Si and O containing particles (224 were counted)
    - Primary particles
        - Average Diameter: 18 ± 4 nm
        - 100% of particles below 100 nm
    - Spherical morphology
    - Aggregate particles
        - 225– 518 nm
- TEM confirmed the presence of Mg, Ca, and O containing particles (458 were counted)
    - Primary Particles
        - Average Diameter: 310 ± 372 nm
        - 0.2% of particles found were below 100 nm
    - Spherical morphology
    - Size range
        - 74 – 5,096 nm
- TEM confirmed the presence of Ca, and O containing particles (34 were counted)
    - Primary Particles
        - Average Diameter: 55 ± 40 nm
        - 88% of particles found were below 100 nm
    - Irregular morphology
    - Aggregate particle
        - 609 nm by 687 nm
- XRD identified Ca and O particulate as calcite and identified Si and O particulate as SiO_2
- ICP-MS found the concentration of:
    - Silicon: 453 µg/g
    - Titanium: 166 µg/g
    - Calcium: 287,300 µg/g
    - Phosphorus: 77 µg/g
- XRF Identified:
    - Silicon: Present
    - Titanium: Present
    - Calcium: Present
    - Phosphorus: Absent

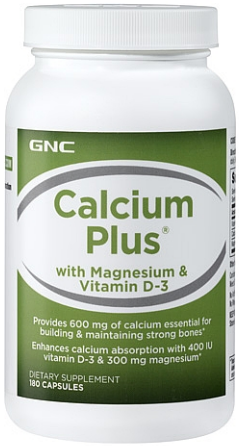

Figure A9.A. Vitamin Supplement 9

Supplement Facts

Serving Size Three Capsules
Servings Per Container 60

Amount Per Serving		% Daily Value
Vitamin D (as Cholecalciferol D-3)	400 IU	100%
Calcium (as Calcium Carbonate)	600 mg	60%
Magnesium (as Magnesium Oxide)	300 mg	75%

Figure A9.B. Vitamin Supplement 9

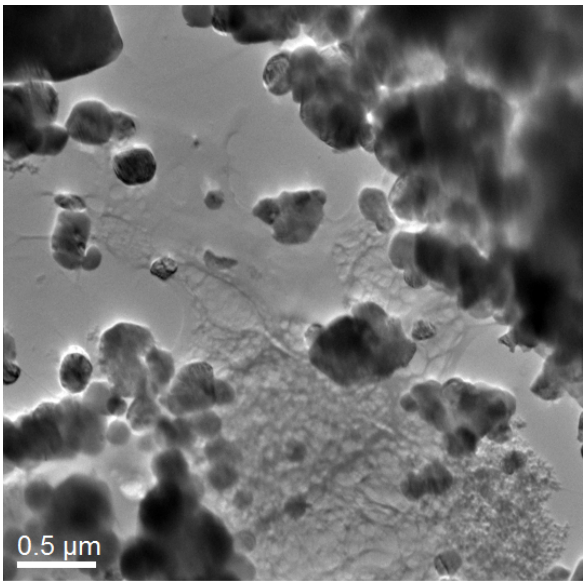

File: Vitamin Supplement 9 TEM Image 1.jpeg

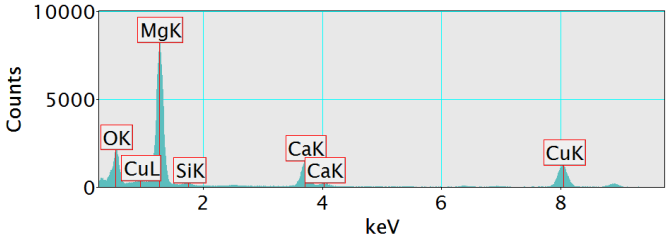

File: Vitamin Supplement 9 TEM EDX of Image 1.jpeg

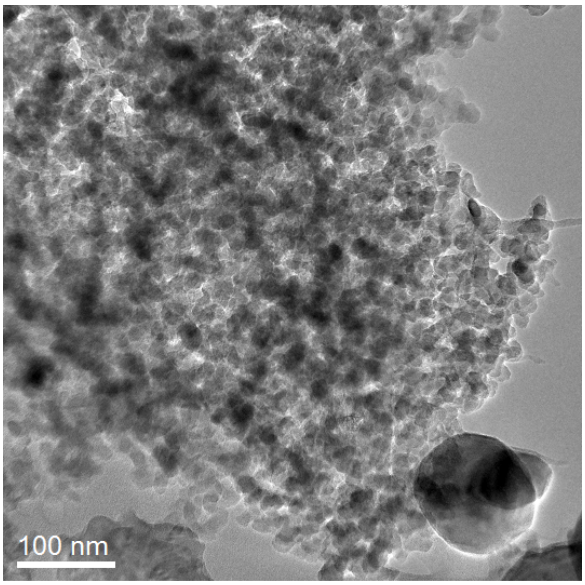

File: Vitamin Supplement 9 TEM Image 2.jpeg

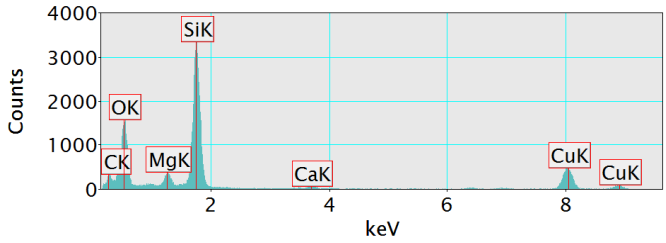

File: Vitamin Supplement 9 TEM
EDX of Image 2.jpeg

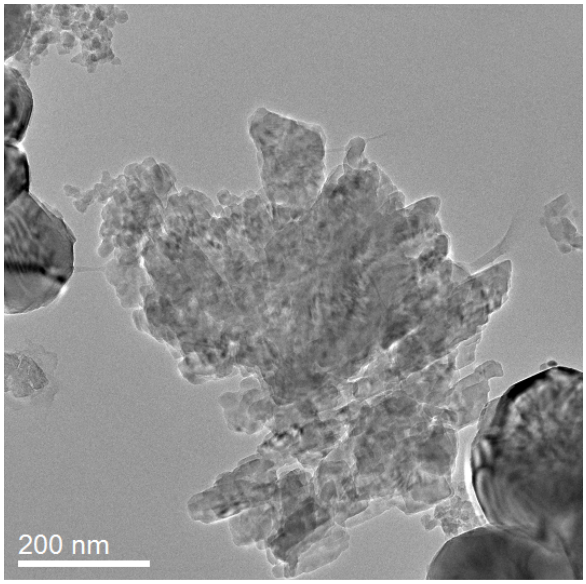

File: Vitamin Supplement 9 TEM
Image 3.jpeg

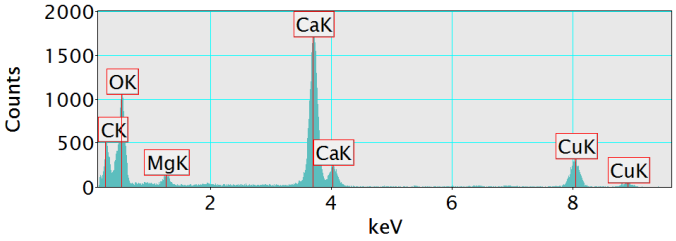

File: Vitamin Supplement 9 TEM
EDX Image 3.jpeg

Vitamin Supplement Sample 10: Usana Core Minerals

- TEM confirmed the presence of Si and O containing particles (391 were counted)
    - Primary particles
        - Average Diameter: 16 ± 6 nm
        - 100 of particles below 100 nm
    - Spherical morphology
    - Aggregate particles
        - 141 – 1,522 nm
- TEM confirmed the presence of Ca and O containing particles (74 were counted)
    - Primary Particles
        - Average Diameter: 346 ± 822 nm
        - 66% of particles below 100 nm
    - Spherical morphology
        - Size range: 9 – 5,537 nm

Figure A10.A. Vitamin Supplement 10

- TEM confirmed the presence of Mg and O containing particles (98 were counted)
    - Primary Particles
        - Average Diameter: 272 ± 412 nm
        - 30% of particles below 100 nm
    - Irregular morphology
    - Size range: 24 – 2,435 nm
- XRD identified Si and O particulate as SiO_2, identified Mg and O particulate as MgO, and identified Ca and O particulate as Calcite
- ICP-MS found the concentration of:
    - Silicon: 165 µg/g
    - Titanium: 240 µg/g
    - Calcium: 57,799 µg/g
    - Phosphorus: 1,116 µg/g
- XRF identified:
    - Silicon: Present
    - Titanium: Absent
    - Calcium: Present
    - Phosphorus: Present

US Core Minerals

DIRECTIONS: TAKE TWO (2) TABLETS TWICE DAILY, PREFERABLY WITH FOOD.

SUPPLEMENT FACTS

SERVING SIZE: 2 TABLETS

AMOUNT PER SERVING		%DV
VITAMIN C (AS MAGNESIUM ASCORBATE AND CALCIUM ASCORBATE)	300 mg	500%
CALCIUM (AS CALCIUM CITRATE AND CALCIUM ASCORBATE)	112.5 mg	10%
IODINE (AS POTASSIUM IODIDE)	250 µg	170%
MAGNESIUM (AS MAGNESIUM CITRATE AND MAGNESIUM ASCORBATE)	112.5 mg	30%
ZINC (AS ZINC CITRATE)	10 mg	70%
SELENIUM (AS L-SELENOMETHIONINE AND SODIUM SELENITE)	100 µg	140%
COPPER (AS COPPER GLUCONATE)	1 mg	50%
MANGANESE (AS MANGANESE GLUCONATE)	1 mg	50%
CHROMIUM (AS CHROMIUM POLYNICOTINATE)	150 µg	130%
MOLYBDENUM (AS MOLYBDENUM CITRATE)	25 µg	35%
BORON (AS BORON CITRATE)	1500 µg	†
SILICON (AS CALCIUM SILICATE)	2 mg	†
VANADIUM (AS VANADIUM CITRATE)	20 µg	†
ULTRA TRACE MINERALS	1500 µg	†
N-ACETYL L-CYSTEINE	80 mg	†

†DAILY VALUE NOT ESTABLISHED.

OTHER INGREDIENTS: MICROCRYSTALLINE CELLULOSE, MODIFIED CELLULOSE, CROSCARMELLOSE SODIUM, ASCORBYL PALMITATE, ORGANIC MALTODEXTRIN, PREGELATINIZED STARCH, SILICON DIOXIDE, VANILLA EXTRACT, ORGANIC SUNFLOWER LECITHIN, ORGANIC PALM OLEIN, ORGANIC GUAR GUM.

KEEP OUT OF REACH OF CHILDREN. CONSULT YOUR PHYSICIAN IF YOU ARE PREGNANT, NURSING, TAKING A PRESCRIPTION DRUG, OR HAVE A MEDICAL CONDITION.

LABORATORY TESTED, QUALITY GUARANTEED. MEETS USP SPECIFICATION FOR UNIFORMITY, POTENCY, AND DISINTEGRATION, WHERE APPLICABLE.

THERE IS A SAFETY SEAL UNDER THE CAP. DO NOT USE IF THE SEAL IS BROKEN OR MISSING.

USANA HEALTH SCIENCES, INC., 3838 W. PARKWAY BLVD., SALT LAKE CITY, UTAH 84120 USA

STORE BELOW 25° C MADE IN USA

102.010104 LB.000702

Figure A10.B. Vitamin Supplement 10

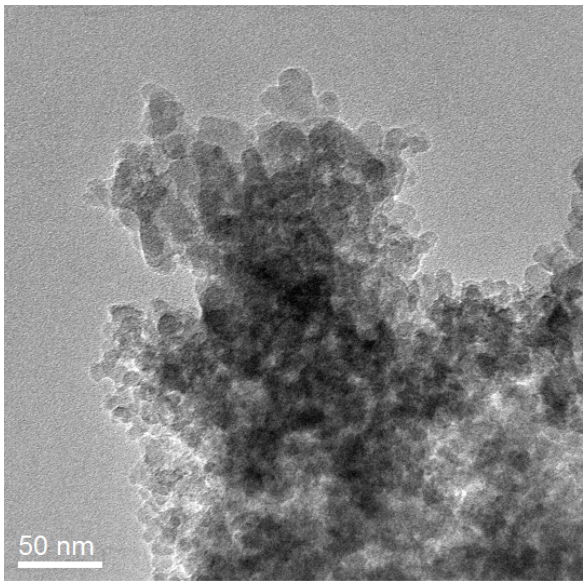

File: Vitamin Supplement 10 TEM Image 1.jpeg

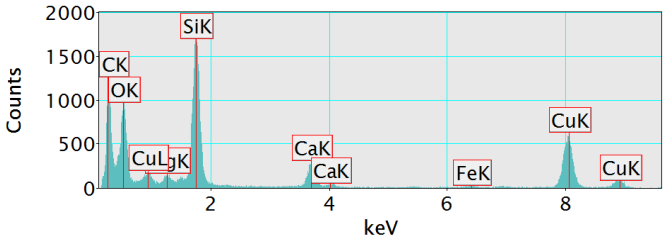

File: Vitamin Supplement 10 TEM EDX of Image 1.jpeg

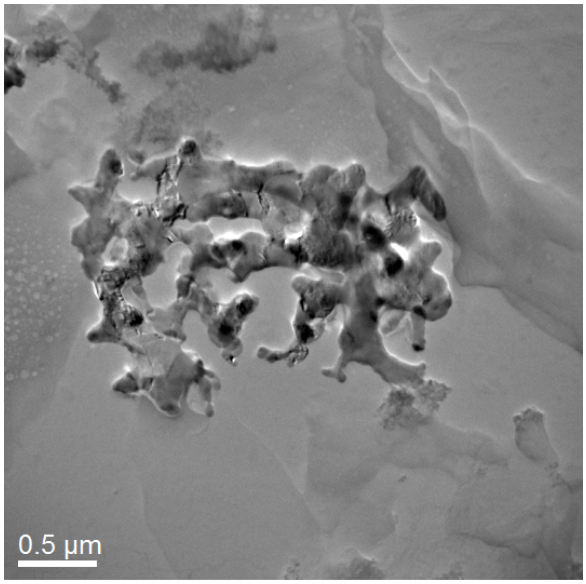

File: Vitamin Supplement 10 TEM Image 2.jpeg

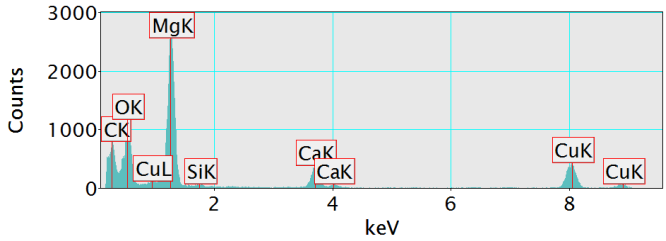

File: Vitamin Supplement 10 TEM EDX of Image 2.jpeg

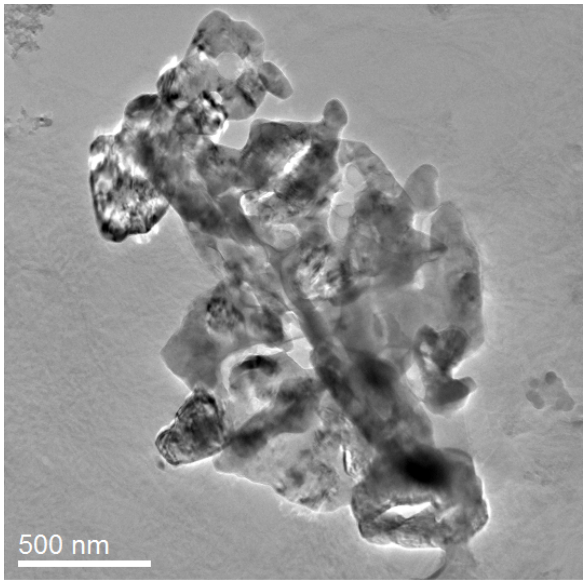

File: Vitamin Supplement 10 TEM EDX of Image 3.jpeg

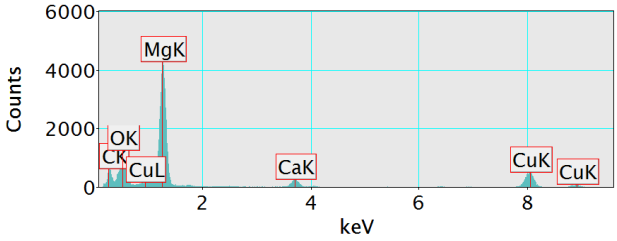

File: Vitamin Supplement 10 TEM EDX of Image 1.jpeg

Vitamin Supplement Sample 11: Usana Coquinone 30

- TEM confirmed the absence of particulate
- XRD not completed due to liquid sample
- ICP-MS found the concentration of:
  - Silicon: 574 µg/g
  - Titanium: 3 µg/g
  - Calcium: 115 µg/g
  - Phosphorus: 2,330 µg/g
- XRF identified:
  - Silicon: Absent
  - Titanium: Absent
  - Calcium: Present
  - Phosphorus: Present

Figure A11.A. Vitamin Supplement 11

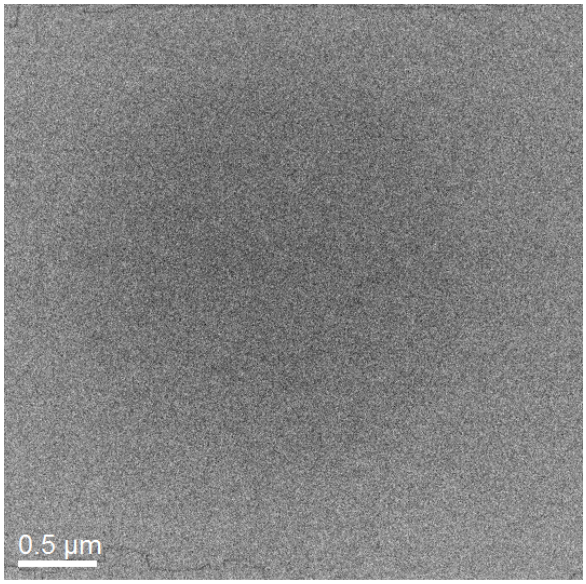

File: Vitamin Supplement 11 TEM EDX of Image 1.jpeg

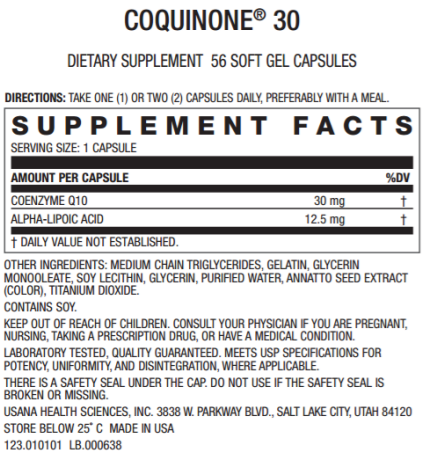

COQUINONE® 30

DIETARY SUPPLEMENT 56 SOFT GEL CAPSULES

DIRECTIONS: TAKE ONE (1) OR TWO (2) CAPSULES DAILY, PREFERABLY WITH A MEAL.

SUPPLEMENT FACTS

SERVING SIZE: 1 CAPSULE

AMOUNT PER CAPSULE		%DV
COENZYME Q10	30 mg	†
ALPHA-LIPOIC ACID	12.5 mg	†

† DAILY VALUE NOT ESTABLISHED.

OTHER INGREDIENTS: MEDIUM CHAIN TRIGLYCERIDES, GELATIN, GLYCERIN MONOOLEATE, SOY LECITHIN, GLYCERIN, PURIFIED WATER, ANNATTO SEED EXTRACT (COLOR), TITANIUM DIOXIDE.

CONTAINS SOY.

KEEP OUT OF REACH OF CHILDREN. CONSULT YOUR PHYSICIAN IF YOU ARE PREGNANT, NURSING, TAKING A PRESCRIPTION DRUG, OR HAVE A MEDICAL CONDITION.

LABORATORY TESTED, QUALITY GUARANTEED. MEETS USP SPECIFICATIONS FOR POTENCY, UNIFORMITY, AND DISINTEGRATION, WHERE APPLICABLE.

THERE IS A SAFETY SEAL UNDER THE CAP. DO NOT USE IF THE SAFETY SEAL IS BROKEN OR MISSING.

USANA HEALTH SCIENCES, INC. 3838 W. PARKWAY BLVD., SALT LAKE CITY, UTAH 84120

STORE BELOW 25° C MADE IN USA

123.010101 LB.000638

Figure A11.B. Vitamin Supplement 11

Vitamin Supplement Sample 12: Usana Vita-Antioxidant

- TEM confirmed the presence of Si and O containing particles (204 were counted)
  - Primary particles
    - Average Diameter: 20 ± 10 nm
    - 100% of particles below 100 nm
  - Spherical morphology
  - Aggregate particles
    - 71 – 704 nm
- XRD identified Si and O particulate as SiO_2
- ICP-MS found the concentration of:
  - Silicon: 449 µg/g
  - Titanium: 52 µg/g
  - Calcium: 11,957 µg/g
  - Phosphorus: 1,968 µg/g
- XRF identified:
  - Silicon: Present
  - Titanium: Absent
  - Calcium: Present
  - Phosphorus: Present

Figure A12.A. Vitamin Supplement 12

US Vita-Antioxidant

DIRECTIONS: ADULTS TAKE TWO (2) TABLETS TWICE DAILY, PREFERABLY WITH FOOD.

SUPPLEMENT FACTS

SERVING SIZE: 2 TABLETS

AMOUNT PER SERVING		%DV	AMOUNT PER SERVING		%DV
VITAMIN A (AS 25% RETINYL ACETATE, AND 75% (4500 IU) AS BETA CAROTENE AND MIXED CAROTENOIDS)	6000 IU	120%	MIXED TOCOPHEROLS (D-GAMMA, D-DELTA, D-BETA TOCOPHEROL)	40 mg	†
VITAMIN C (AS POLY C® BLEND: POTASSIUM, CALCIUM, MAGNESIUM, AND ZINC ASCORBATES)	200 mg	330%	INCELLIGENCE™ COMPLEX		
VITAMIN D3 (AS CHOLECALCIFEROL)	1000 IU	250%	ALPHA LIPOIC ACID	50 mg	
VITAMIN E (AS D-ALPHA TOCOPHERYL SUCCINATE)	100 IU	330%	MERIVA® BIOAVAILABLE CURCUMIN COMPLEX (*CURCUMA LONGA* L., ROOT)*	36 mg	
VITAMIN K (AS K1 [PHYTONADIONE] AND K2 [MK-7 MENAQUINONE])	270 µg	340%	GREEN TEA EXTRACT (*CAMELLIA SINENSIS* HUNT., LEAVES)	35 mg	
VITAMIN B1 (AS THIAMIN HCL)	15 mg	1000%	QUERCETIN DIHYDRATE	30 mg	
VITAMIN B2 (AS RIBOFLAVIN)	15 mg	880%	RUTIN	20 mg	
NIACIN (AS NIACINAMIDE AND NIACIN)	20 mg	100%	HESPERIDIN (*CITRUS SPP.* L., FRUIT)	20 mg	
VITAMIN B6 (AS PYRIDOXINE HCL)	16 mg	800%	RESVERATROL	20 mg	
FOLATE (AS FOLIC ACID)	300 µg	80%	OLIVOL® (OLIVE FRUIT EXTRACT, *OLEA EUROPAEA* L., FRUIT)**	15 mg	
VITAMIN B12 (AS CYANOCOBALAMIN)	100 µg	1670%	INOSITOL	64 mg	†
BIOTIN	150 µg	50%	CHOLINE BITARTRATE	125 mg	†
PANTOTHENIC ACID (AS D-CALCIUM PANTOTHENATE)	45 mg	450%	COENZYME Q10	6 mg	†
			LUTEIN (*TAGETES ERECTA* L., FLOWER)	300 µg	†
			LYCOPENE	500 µg	†

†DAILY VALUE NOT ESTABLISHED

OTHER INGREDIENTS: MICROCRYSTALLINE CELLULOSE, MODIFIED STARCH, CROSCARMELLOSE SODIUM, SILICON DIOXIDE, ASCORBYL PALMITATE, ORGANIC MALTODEXTRIN, VANILLA EXTRACT, ORGANIC SUNFLOWER LECITHIN, ORGANIC PALM OLEIN, ORGANIC GUAR GUM.

LABORATORY TESTED, QUALITY GUARANTEED. MEETS USP SPECIFICATIONS FOR UNIFORMITY, POTENCY, AND DISINTEGRATION, WHERE APPLICABLE.

*MERIVA® IS A REGISTERED TRADEMARK OF INDENA S.p.A.

**PROTECTED UNDER US PATENTS 6,358,542 OR 6,361,803

KEEP OUT OF REACH OF CHILDREN. CONSULT YOUR PHYSICIAN IF YOU ARE PREGNANT, NURSING, TAKING A PRESCRIPTION DRUG, OR HAVE A MEDICAL CONDITION.

THERE IS A SAFETY SEAL UNDER THE CAP. DO NOT USE IF THE SEAL IS BROKEN OR MISSING.

USANA HEALTH SCIENCES, INC., 3838 W. PARKWAY BLVD., SALT LAKE CITY, UTAH 84120 USA

STORE BELOW 25° C. MADE IN USA

103.010104 LB.000703

Figure A12.B. Vitamin Supplement 12

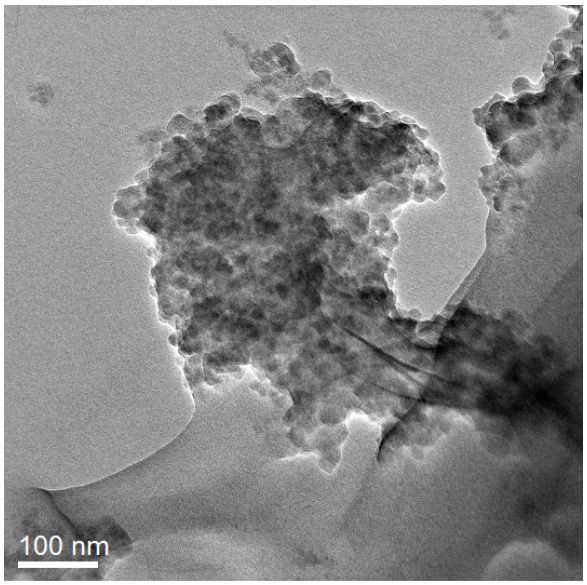

File: Vitamin Supplement 12 TEM of Image 1.jpeg

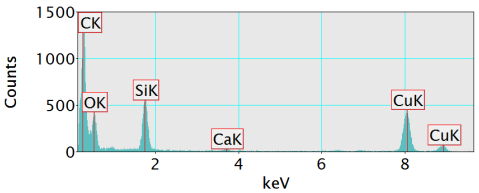

File: Vitamin Supplement 12 TEM EDX of Image 1.jpeg

Needle-like Hydroxyapatite Reference Material

- 99% pure food-grade product purchased from USA manufacturer (American Elemental, CA; https://www.americanelements.com/hydroxyapatite-nanopowder-1306-06-5) – Product code CA-PATOH-02-NP
- Needle-like hydroxyapatite structures dominated the product
- 250 particles counted with 100% of particles with one dimension less than 100nm
- Average particle size: 131 ± 25 nm (width) and 30 ± 5 nm (length)

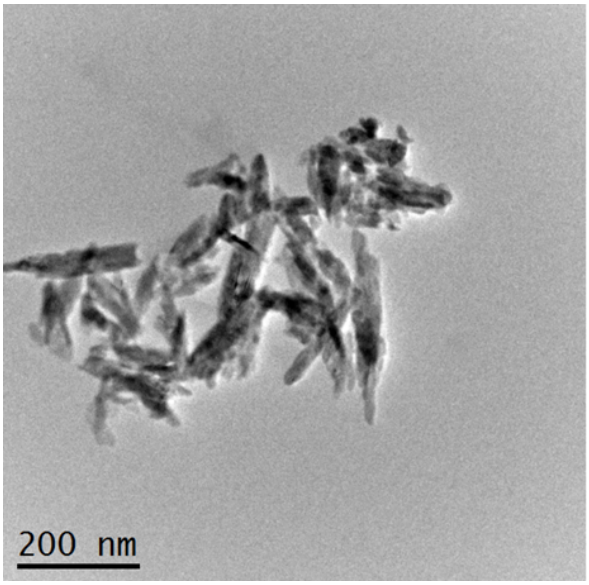

File: HA TEM of Image 1.jpeg

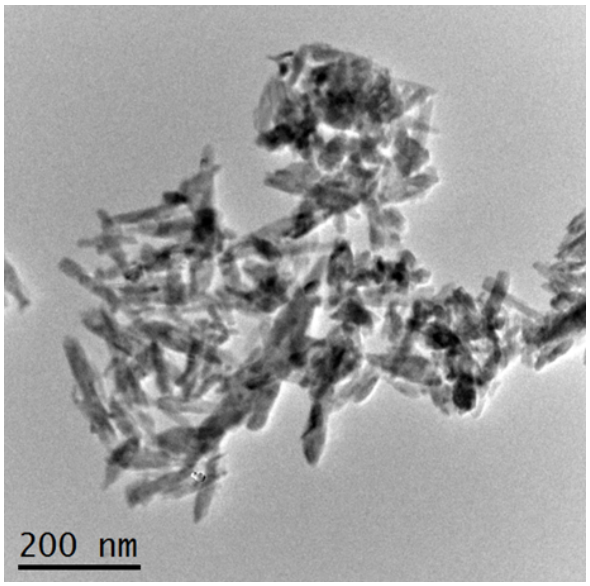

File: HA TEM of Image 2.jpeg

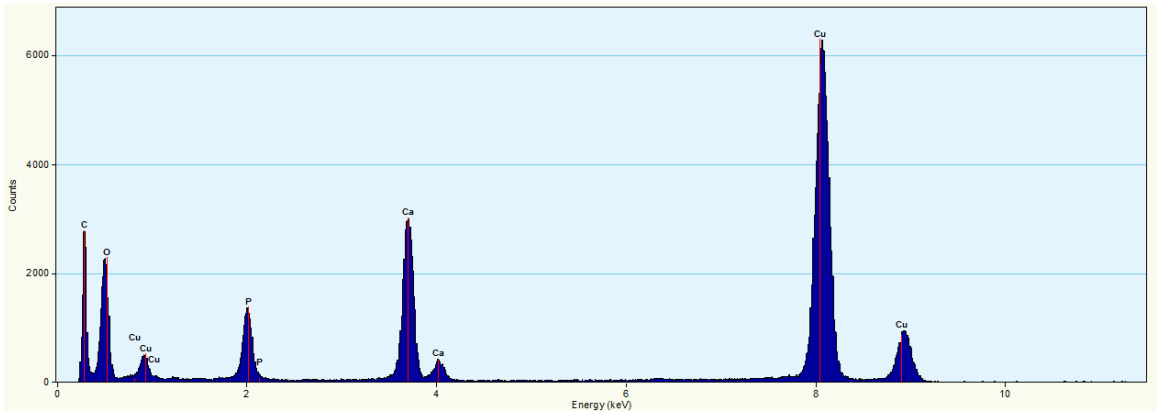

File: HA TEM EDX of Image 1.jpeg

Australian Procured Infant Formula Report

- Seven infant formula products were analyzed

Australian Infant Formula Sample 1: Nature's Way Kids Smart 1

TEM confirmed the presence of Ca, P, and O containing particles (129 were counted)

  - Primary particles
    - Average Length: 65 ±20 nm
    - Average Width: 18 ± 7 nm
    - 100% of particles below 100 nm
  - Needle-like morphology
- TEM confirmed the presence of Si, and O containing particles (43 were counted)
  - Primary Particles
    - Average Diameter: 27 ± 5 nm
    - 100% of particles found were below 100 nm
  - Aggregate particles
    - 561 – 810 nm

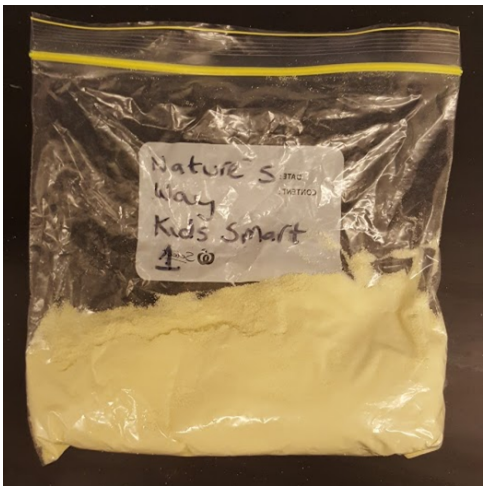

Figure A13. AUS Infant Formula 1

- XRF detected the presence of Ca and P, but Si and Ti were below detection limits.
- ICP-MS found the concentration of:
  - Calcium: 4662 µg/g
  - Phosphorus: 2821 µg/g
- XRD identified Ca, P, and O particulate as hydroxyapatite

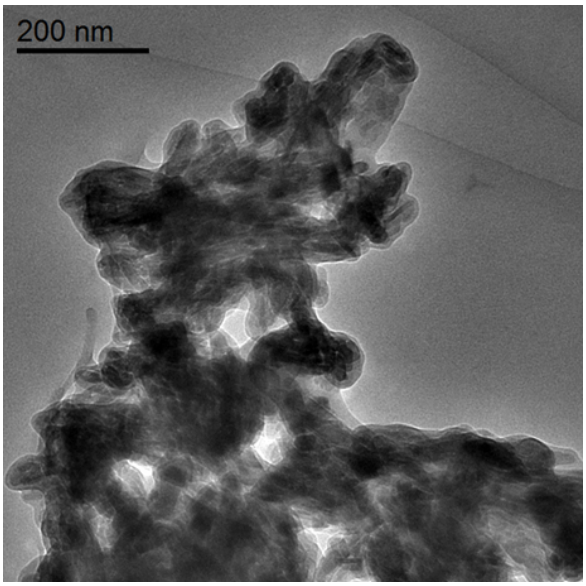

File: AUS Infant Formula 1 TEM of Image 1.jpeg

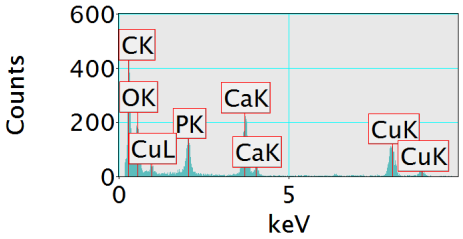

File: AUS Infant Formula 1 TEM EDX of Image 1.jpeg

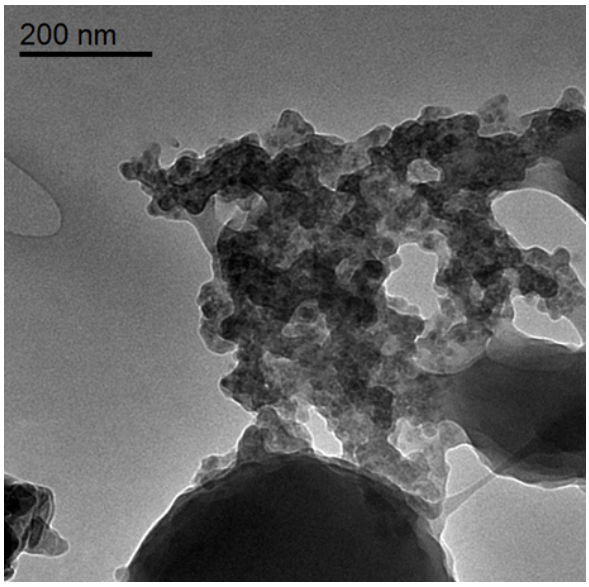

File: AUS Infant Formula 1 TEM
of Image 2.jpeg

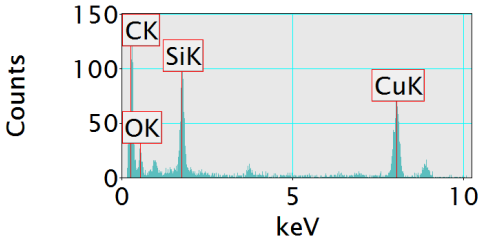

File: AUS Infant Formula 2 TEM
EDX of Image 1.jpeg

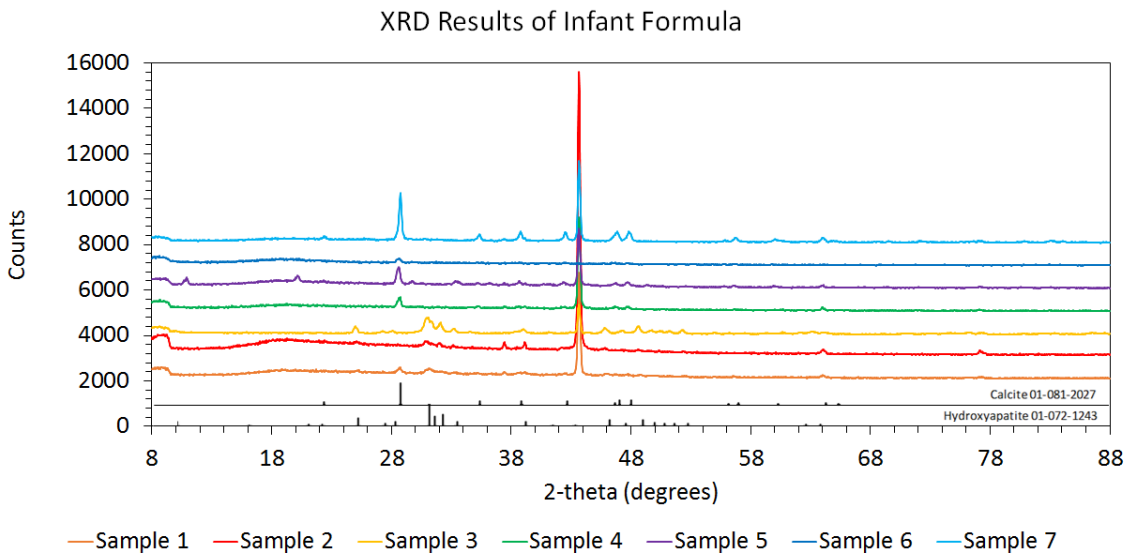

Figure A15. XRD analysis detected the presence of hydroxyapatite in Nature's Way Kids Smart 1, Nestlé NAN H.A. 1 and Heinz Nurture Original 1 and the presence of calcite in the remaining four samples

Australian Infant Formula Sample 2: Heinz Nurture Original 1

- TEM confirmed the presence of Ca, P, and O containing particles (78 were counted)
  - Primary particles
    - Average Length: 144 ± 153 nm
    - Average Width: 43 ± 31 nm
    - 100% of particles below 100 nm
  - Aggregate particles
    - 648 - 1318 nm
  - Rectangular morphology
- XRF detected the presence of Ca and P, but Si and Ti were below detection limits.
- ICP-MS found the concentration of:
  - Calcium: 3967 µg/g
  - Phosphorus: 2434 µg/g
- XRD identified Ca, P, and O particulate as hydroxyapatite

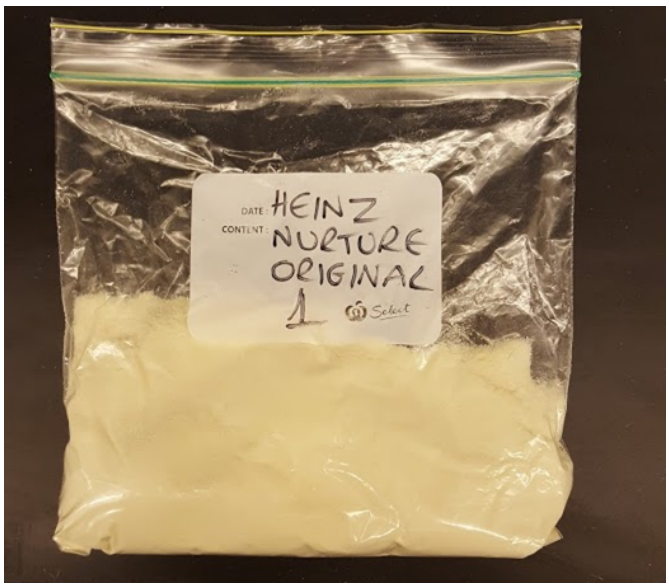

Figure A16. AUS Infant Formula 2

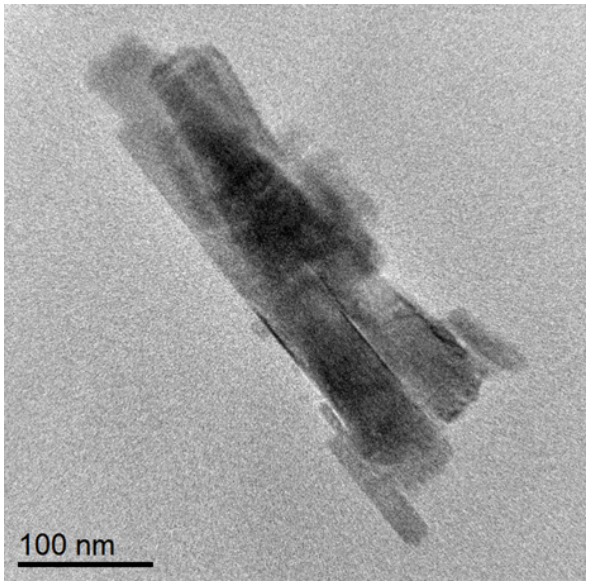

File: AUS Infant Formula 2 TEM of Image 1.jpeg

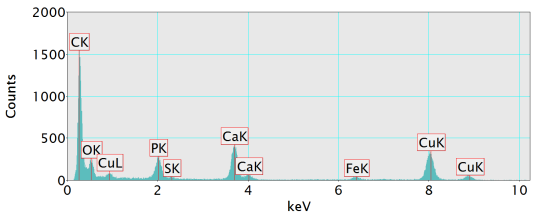

File: AUS Infant Formula 2 TEM EDX of Image 1.jpeg

Australian Infant Formula Sample 3: Nestlé NAN H.A. Gold 1

- TEM confirmed the presence of Ca, P, and O containing particles (287 were counted)
  - Primary particles
    - Average Length: 211 ± 95 nm
    - Average Width: 23 ± 7 nm
    - 100% of particles below 100 nm in one dimension
  - Needle-like morphology
  - Aggregate particles
    - 296 – 2982 nm
- XRF detected the presence of Ca and P, but Si and Ti were below detection limits.
- ICP-MS found the concentration of:
  - Calcium: 3657 µg/g
  - Phosphorus: 1661 µg/g
- XRD identified Ca, P, and O particulate as hydroxyapatite

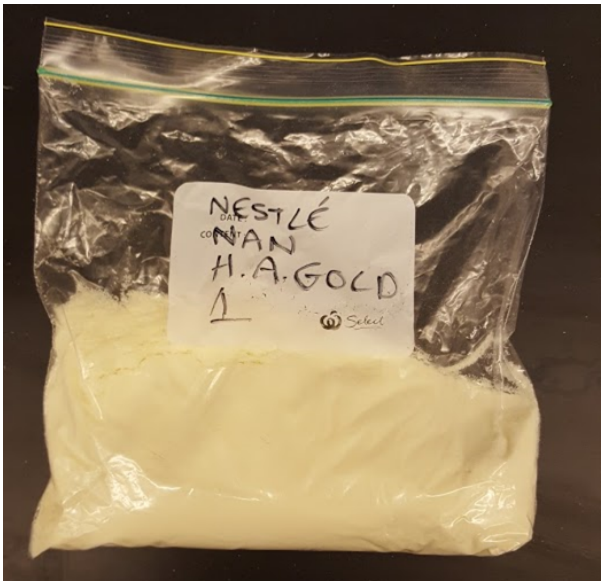

Figure A17. AUS Infant Formula 3

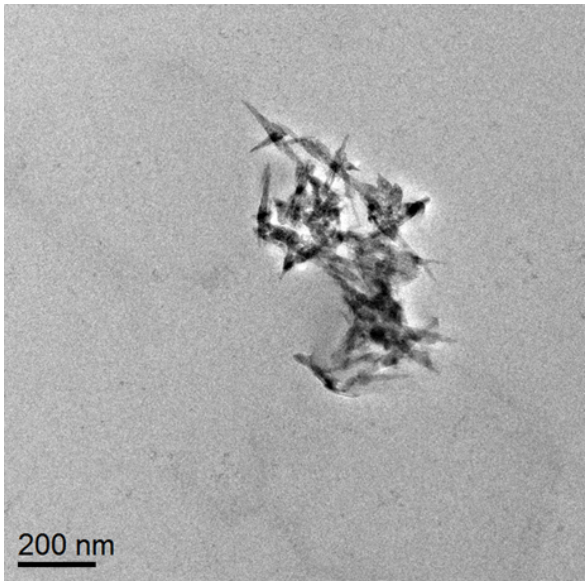

File: AUS Infant Formula 3 TEM of Image 1.jpeg

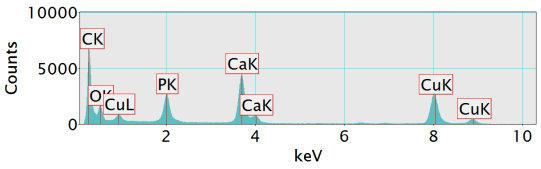

File: AUS Infant Formula 3 TEM EDX of Image 1.jpeg

Australian Infant Formula Sample 4: Aptamil Profutura 1

- Primarily carbon complex organic matrix with Ca, P, and O
- TEM confirmed the presence of Ca, P, and O containing particles (49 were counted)
    - Primary particles
        - Average diameter: 134 ± 44 nm
        - 20% of particles below 100 nm
    - Spherical morphology
    - Aggregate particles
        - 408 – 1789 nm
- XRF detected the presence of Ca and P, but Si and Ti were below detection limits.
- ICP-MS found the concentration of:
    - Calcium: 3777 µg/g
    - Phosphorus: 1404 µg/g
- XRD identified Ca, P, and O particulate as calcite

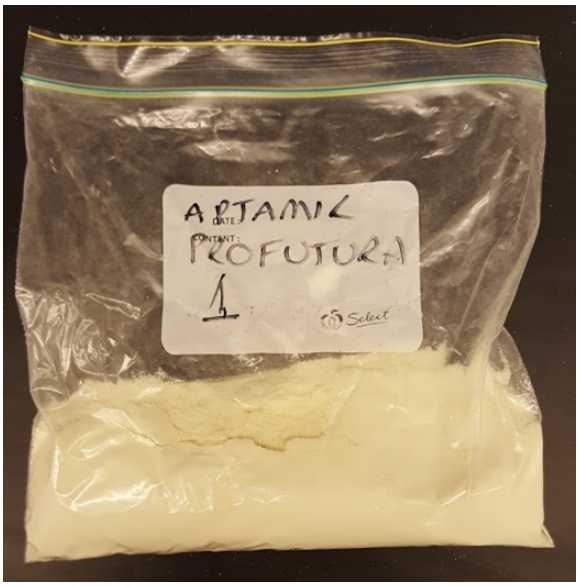

Figure A18. AUS Infant Formula 4

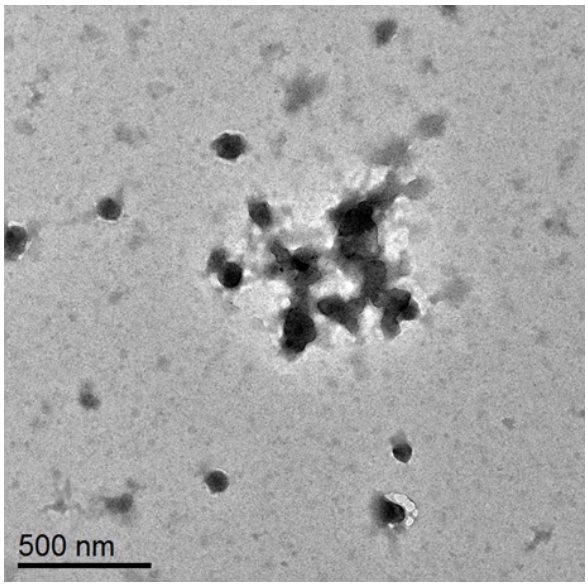

File: AUS Infant Formula 4 TEM of Image 1.jpeg

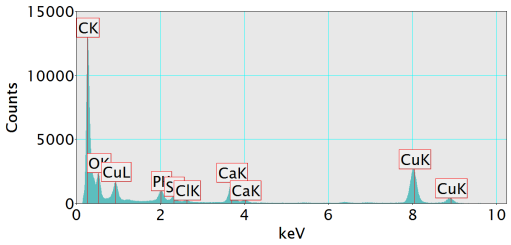

File: AUS Infant Formula 4 TEM EDX of Image 1.jpeg

Australian Infant Formula Sample 5: A2 Platinum 1

- TEM confirmed the presence of Ca, P, and O containing particles (71 were counted)
    - Primary particles
        - Average diameter: 752 ± 127nm
        - None of the particles were below 100 nm
    - Spherical morphology
    - Aggregate particles
        - 1315 – 6272 nm
- XRF detected the presence of Ca and P, but Si and Ti were below detection limits.
- ICP-MS found the concentration of:
    - Calcium: 3939 µg/g
    - Phosphorus: 2098 µg/g
- XRD identified Ca, P, and O particulate as calcite

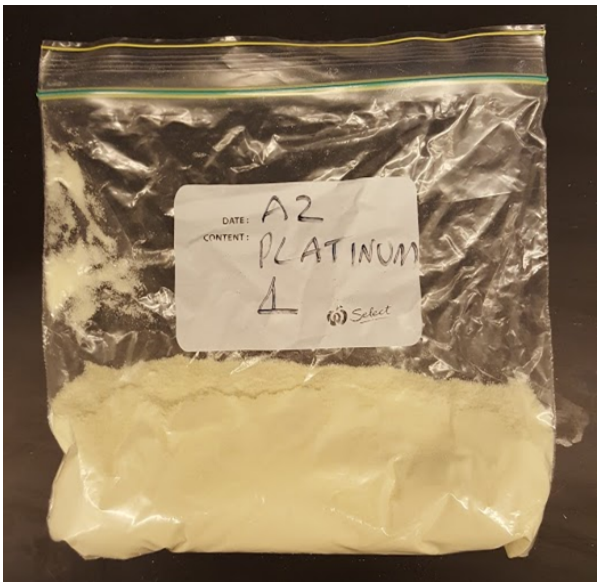

Figure A19. AUS Infant Formula 5

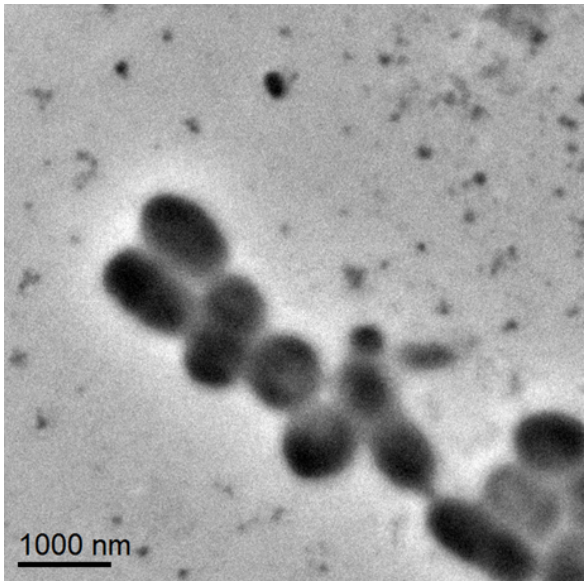

File: AUS Infant Formula 5 TEM of Image 1.jpeg

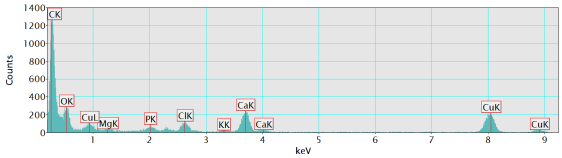

File: AUS Infant Formula 4 TEM EDX of Image 1.jpeg

Australian Infant Formula Sample 6: Karicare Plus 1

- TEM confirmed the presence of carbon complex organic matrix with Ca, P, and O
  - Aggregates
    - 445 – 5404 nm
  - No nanoparticles (< 100nm present)
- XRF detected the presence of Ca and P, but Si and Ti were below detection limits.
- ICP-MS found the concentration of:
  - Calcium: 3740 µg/g
  - Phosphorus: 1674 µg/g
- XRD identified C, Ca, P, and O particulate as calcite

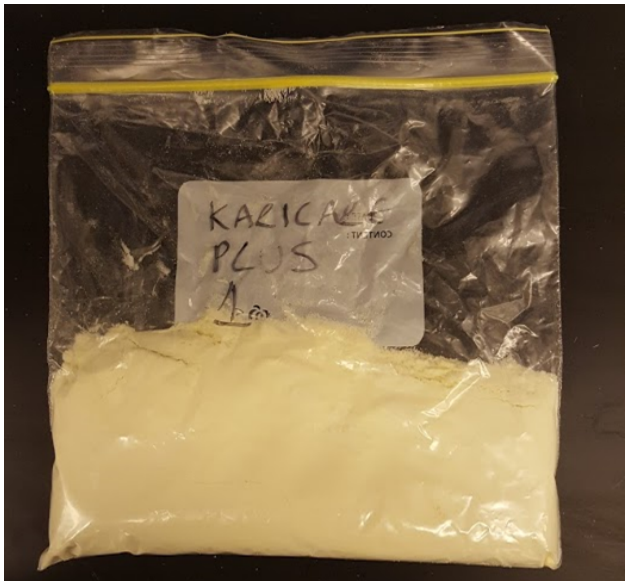

Figure A20. AUS Infant Formula 6

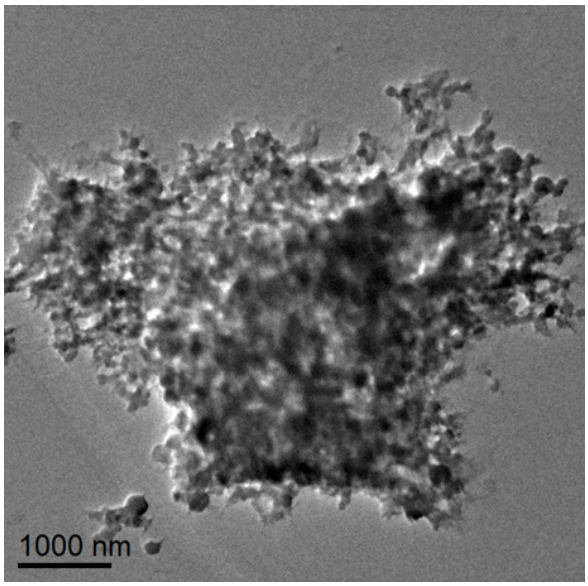

File: AUS Infant Formula 6 TEM of Image 1.jpeg

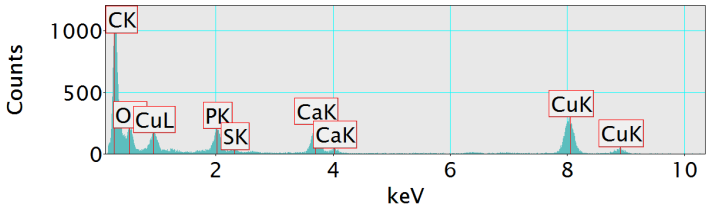

File: AUS Infant Formula 6 TEM EDX of Image 1.jpeg

Australian Infant Formula Sample 7: Blackmores Newborn Formula 1

- TEM confirmed the presence of Ca, and O containing particles (64 were counted)
  - Primary particles
    - Average diameter: 154 ± 136 nm
    - 38% of particles below 100 nm
  - Aggregate particles
    - 492 – 4592 nm
- XRF detected the presence of Ca and P, but Si and Ti were below detection limits.
- ICP-MS found the concentration of:
  - Calcium: 4426 µg/g
  - Phosphorus: 2063 µg/g
- XRD identified Ca, C, and O particulate as calcite

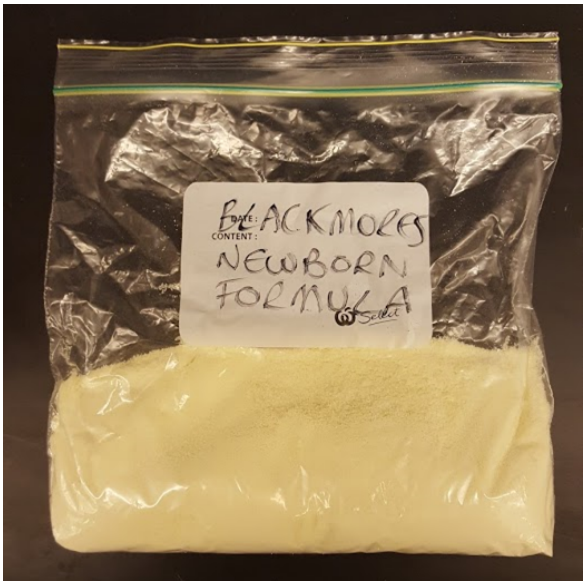

Figure A21. AUS Infant Formula 7

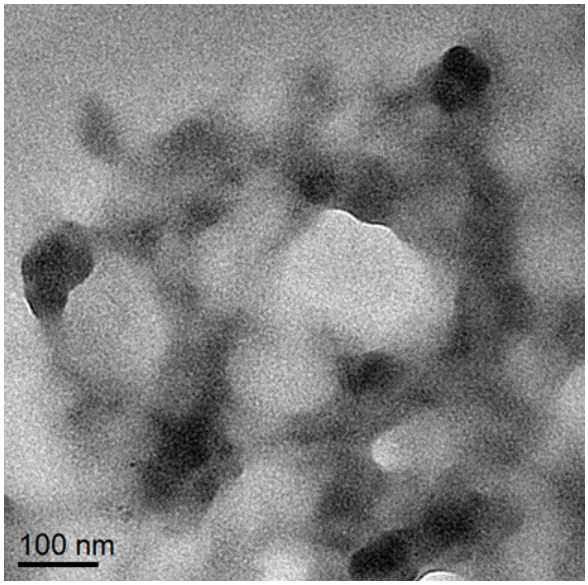

File: AUS Infant Formula 7 TEM of Image 1.jpeg

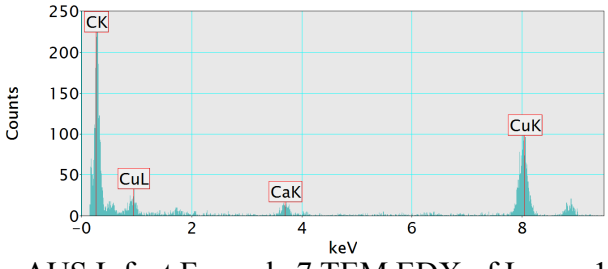

File: AUS Infant Formula 7 TEM EDX of Image 1.jpeg

European Procured Infant Formula Report

- Four infant formula products were analyzed

European Infant Formula Sample 1: SMA Pro

- TEM confirmed the presence of a carbon matrix
- No nanoparticles detected by TEM
- XRD did not identify a mineral phase
- ICP-MS found the concentration of:
  - Silicon: 554 µg/g
  - Titanium: 15 µg/g
  - Calcium: 2,998 µg/g
  - Phosphorus: 1,206 µg/g

Figure A22. EU Infant Formula 1

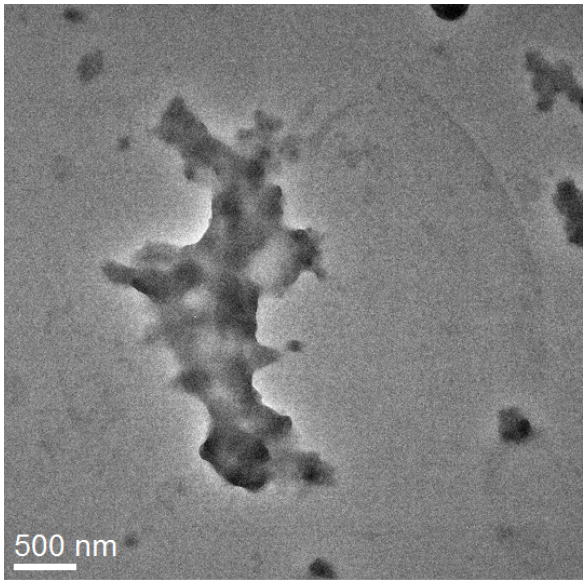

File: EU Infant Formula 1 TEM of Image 1.jpeg

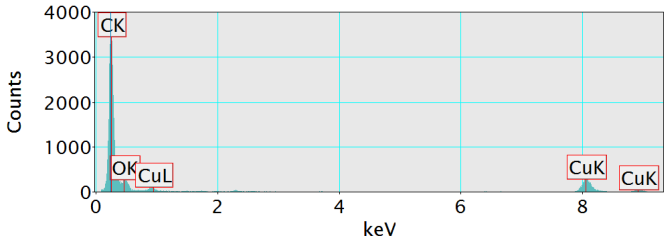

File: EU Infant Formula 1 TEM EDX of Image 1.jpeg

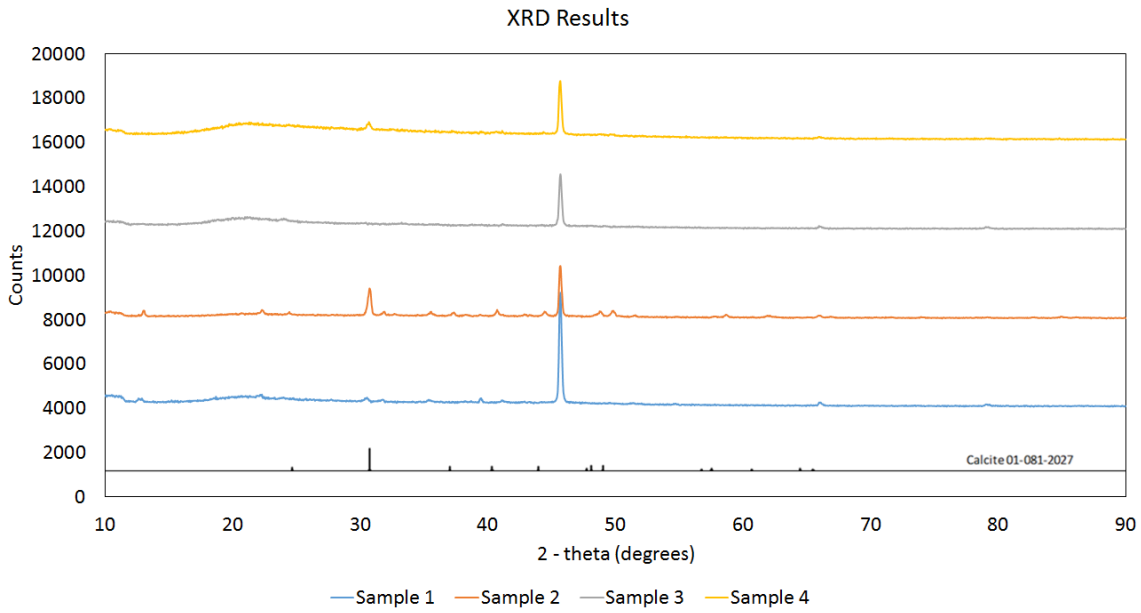

Figure A22. XRD analysis confirmed the presence of calcite in sample 2 and suspected presence of silicon dioxide in sample 3

European Infant Formula Sample 2: Humana

- TEM confirmed the presence of carbon matrix
- TEM did not find particulate matter
- XRD identified calcite
- ICP-MS found the concentration of:
    - Silicon: 554 µg/g
    - Titanium: 23 µg/g
    - Calcium: 4,920 µg/g
    - Phosphorus: 2,155 µg/g

Figure A23. EU Infant Formula 2

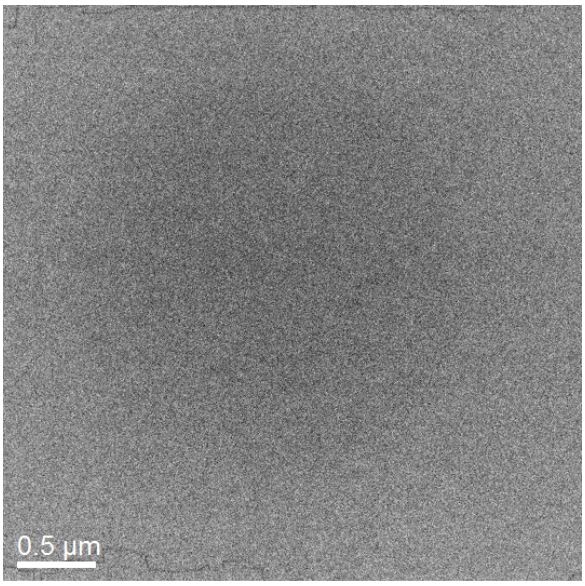

File: EU Infant Formula 2 TEM of Image 1.jpeg

- TEM confirmed the presence of complex carbon matrix

European Infant Formula Sample 3: Nestle Junior

- TEM confirmed the presence of Ca, P, and O containing particles (85 were counted)
  - Primary particles
    - Average diameter: 39 ± 18 nm
  - Irregular morphology
  - Aggregate particles
    - 1,116 – 2,867 nm
- XRD suspected presence of SiO_2
- ICP-MS found the concentration of:
  - Silicon: 578 µg/g
  - Titanium: 31 µg/g
  - Calcium: 6,752 µg/g
  - Phosphorus: 2,451 µg/g

Figure A24. EU Infant Formula 3

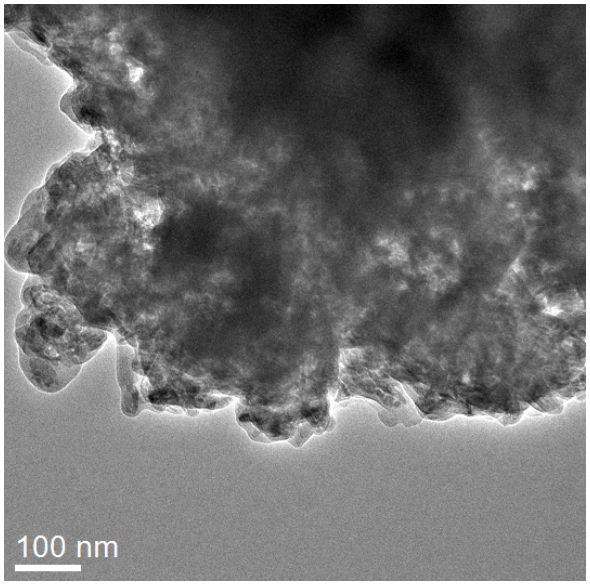

File: EU Infant Formula 3 TEM of Image 1.jpeg

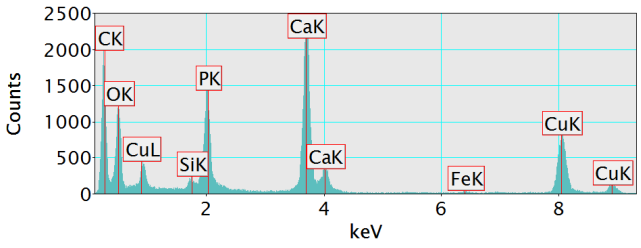

File: EU Infant Formula 3 TEM EDX of Image 1.jpeg

European Infant Formula Sample 4: Impamil

- TEM confirmed the presence of Ca, P, and O containing particles (24 were counted)
    - Primary particles
        - Average Diameter: 57 ± 25 nm
        - 96% of particles below 100 nm
    - Irregular morphology
    - Aggregate particles
        - 936 nm
- XRD did not identify a mineral phase
- ICP-MS found the concentration of:
    - Silicon: 545 µg/g
    - Titanium: 30 µg/g
    - Calcium: 6,460 µg/g
    - Phosphorus: 2,592 µg/g

Figure A25. EU Infant Formula 4

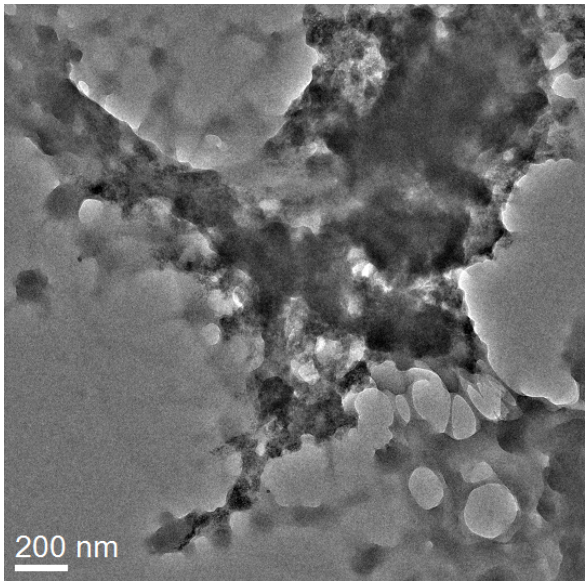

File: EU Infant Formula 4 TEM of Image 1.jpeg

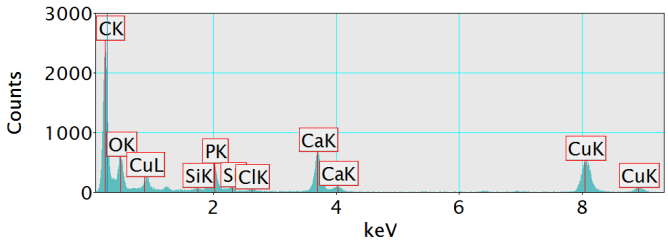

File: EU Infant Formula 4 TEM EDX of Image 1.jpeg

Food Produce Report

- Six food produce procured from Farmer's Market in Washington D.C.
    - Standard Tomato
    - Tomatoes (baby)
    - Apple
    - Cucumber
    - Sweet Pepper
    - Watermelon
- One wax reference material from Friends of the Earth USA
    - Michelman Wax

Sample Preparation

- Two samples were prepared for each food produce
- Air dried
    - Unaltered produce allowed for analysis of the nanomaterials present on the surface of the sample
- Fixation with aldehydes and metal deposition of Osmium
    - Preserve the biological structures of the food produce to analyze the cell structure of the produce

Scanning Electron Microscopy (TEM) paired with Energy Dispersive X-ray Spectroscopy (EDX) Sample Preparation

- SEM is the gold standard method for determine the shape, morphology and size distribution of particles, but cannot be used to determine quantity of nanoparticles in samples.
- Sample preparation involved two samples prepared for each food produce:
    - Air dried
        - Unaltered produce allowed for analysis of the nanomaterials present on the surface of the sample
    - Fixation with aldehydes and metal deposition of Osmium
        - Preserve the biological structures of the food produce to analyze the cell structure of the produce
    - Microscopy was performed on a XL30 scanning electron microscope with energy dispersive X-ray spectroscopy. EDX data is reported in a counts vs. energy (KeV) graph. Peaks report elemental presence at a respective K or L line for each element (CaK or CK refers to calcium or carbon respectively at a Kα emission line). Osmium peaks are a result of the Osmium deposition on the sample.
- Mean particle diameter was measured manually with ImageJ software.

Analysis of Particle Size

- Sizing analysis was performed using ImageJ, a free image processing program available from the National Institute of Health. The number of primary particles was noted and were sized. The scale bar was used to set the scale for calculating each particle's diameter. In the case of high aspect ratio structures both a width and length were measured. Error is reported as +/- 1 standard deviation. Percent of particles below 100nm was calculated based on the primary particles imaged.

Food Produce Sample 1: Standard Tomato

- No uniform nanomaterial coating was found on the surface of the tomato peel
- NaCl particle found on the surface with dimensions of 2.7 micron by 4.3 micron

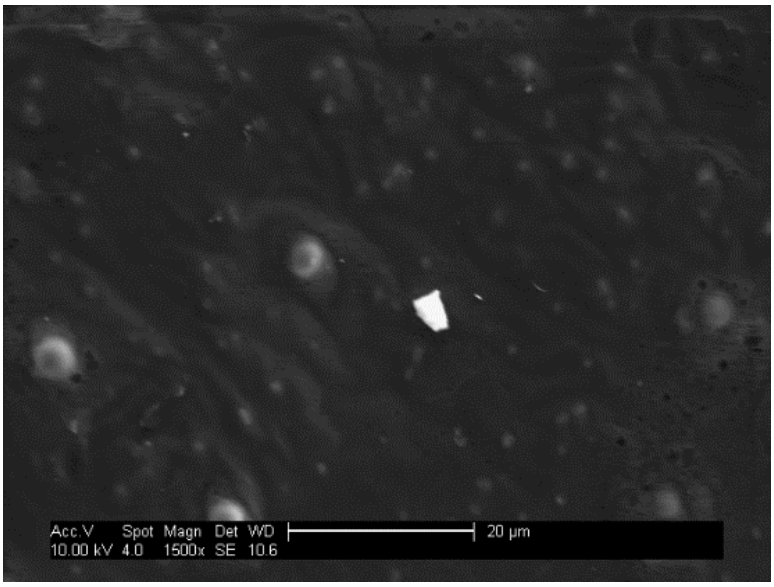

File: Produce 1 SEM of Image 1.jpeg

Element	Wt%	At%
CK	06.83	14.97
OK	00.96	01.59
NaK	37.26	42.65
ClK	54.94	40.79
Matrix	Correction	ZAF

File: Produce 1 SEM EDX of Image 1.jpeg

Food Produce Sample 2: Baby Tomato

- No uniform nanomaterial coating was found on the surface of the baby tomato peel
- Micron size particles present
- KCl found on the surface of the peel with average particle size of 1.3 microns
- No uniform nanomaterial coating found on the surface or peel

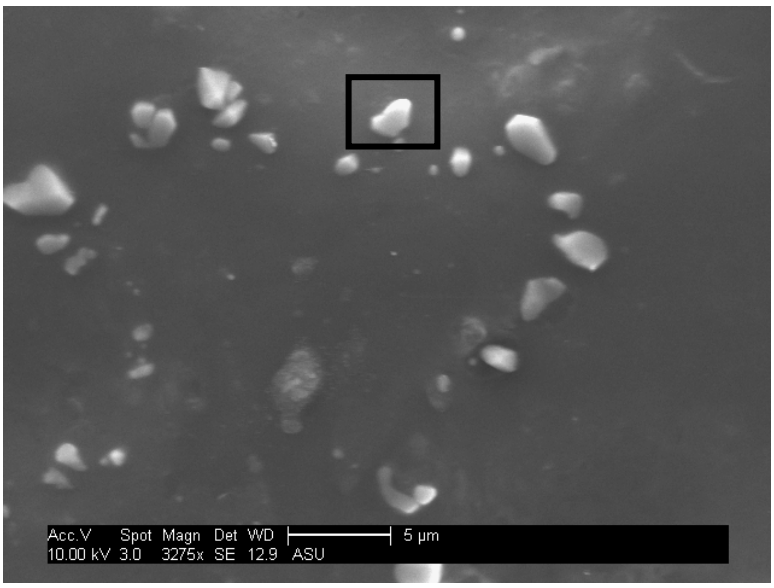

File: Produce 2 SEM of Image 1.jpeg

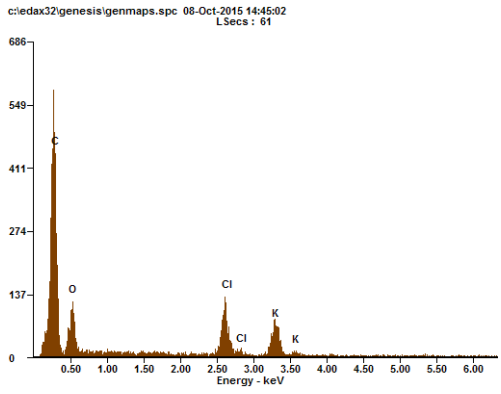

File: Produce 2 SEM EDX of Image 1.jpeg

Food Produce Sample 3: Apple

- No uniform nanomaterial coating was found on the surface of the baby tomato peel

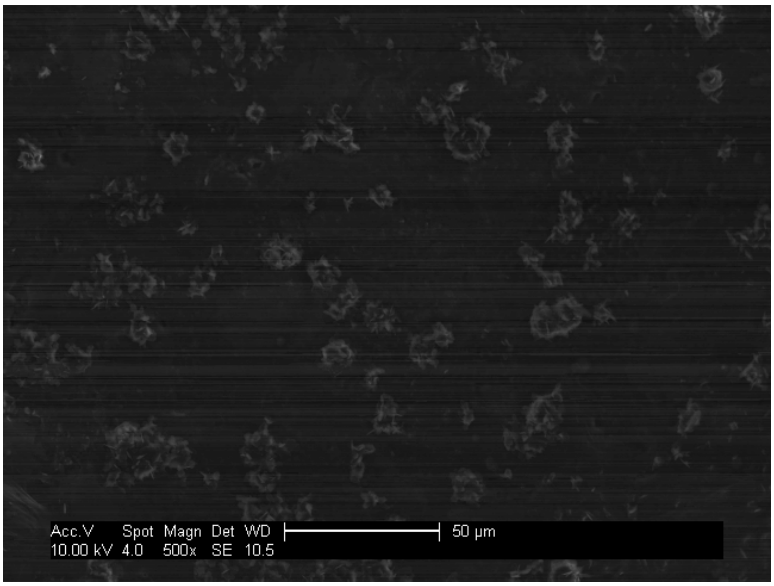

File: Produce 3 SEM of Image 1.jpeg

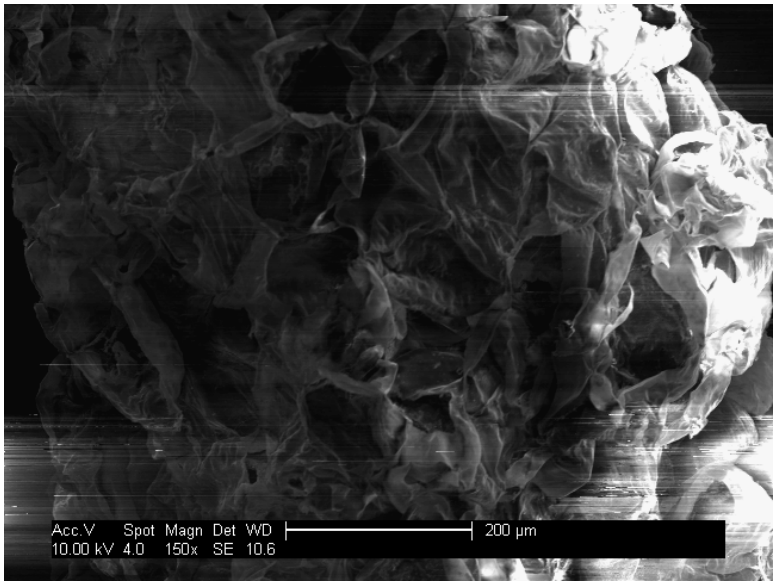

File: Produce 3 SEM of Image 2.jpeg

Food Produce Sample 4: Cucumber

- No uniform nanomaterial coating was found on the surface of the baby tomato peel
- Micron size particles present containing C, O, Si, S, and K
- Particles with compositions consistent of dirt found on samples

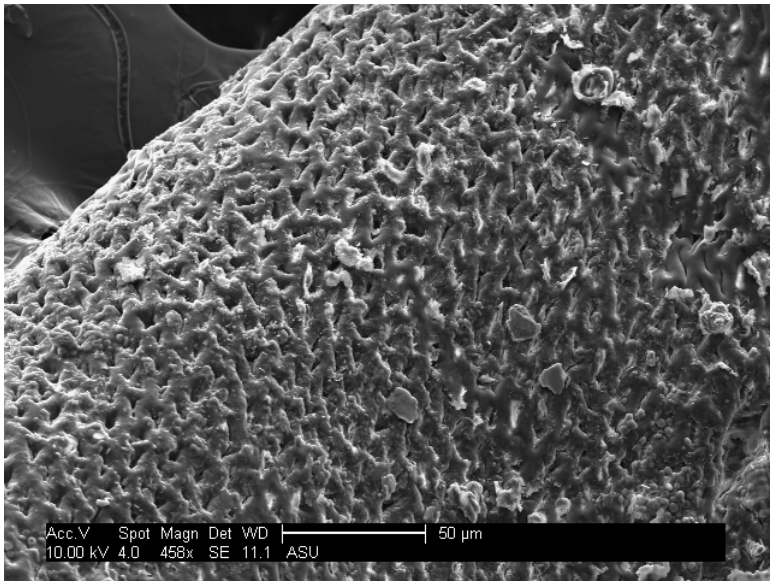

File: Produce 4 SEM Image 1.jpeg

Element	Wt%	At%
CK	64.71	73.38
OK	26.69	22.72
SiK	06.52	03.16
SK	00.22	00.09
KK	01.86	00.65
Matrix	Correction	ZAF

File: Produce 4 SEM EDX of Image 1.jpeg

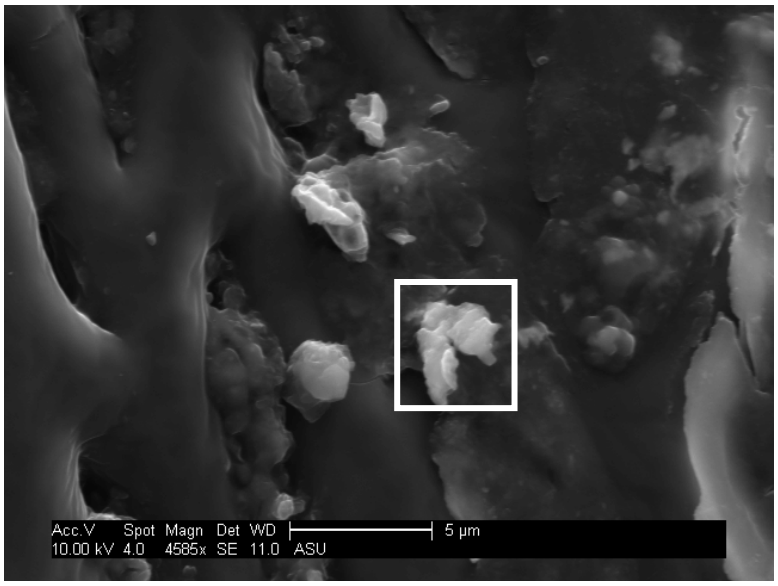

File: Produce 4 SEM Image 2.jpeg

Food Produce Sample 5: Sweet Pepper

- No uniform nanomaterial coating was found on the surface of the baby tomato peel
- Micron sized particles present composed of C, O, Ti, Si, Al, Fe, Mg, K, Co, and Au
- Particles with compositions consistent of dirt found on samples

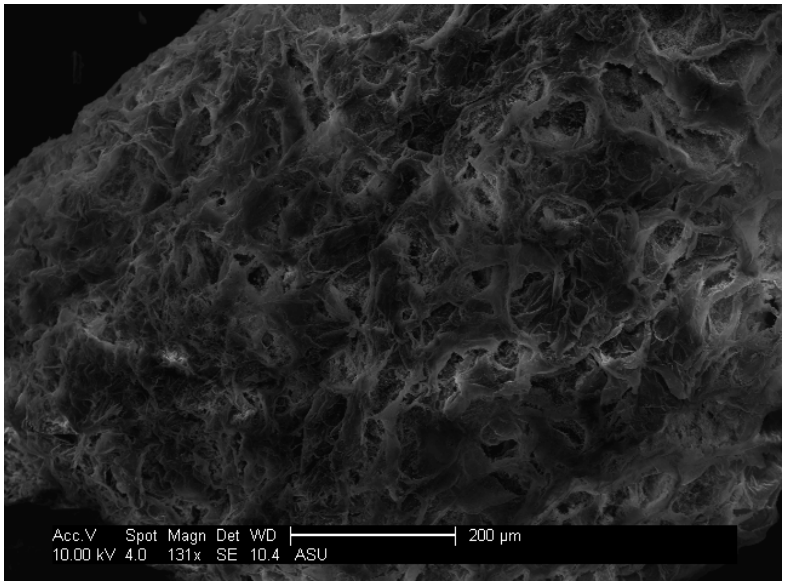

File: Produce 5 SEM Image 1.jpeg

Surface of the peel

- C and O containing particle with Al, Mg, Si, K, Fe, and Co elements with average diameter of 4.3 microns
- No uniform nanomaterials coating present
-

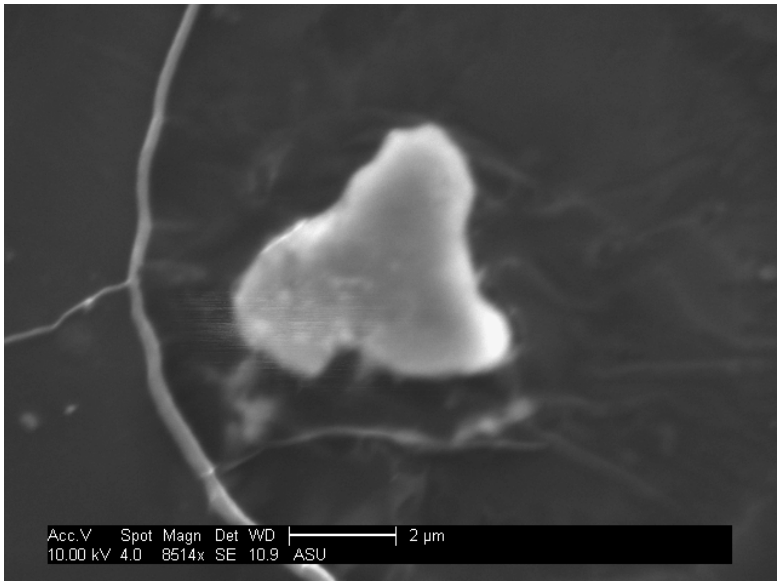

File: Produce 5 SEM Image 2.jpeg

Element	Wt%	At%
CK	22.05	35.06
OK	35.89	42.84
MgK	03.24	02.55
AlK	07.75	05.48
SiK	09.50	06.46
KK	01.97	00.96
FeK	16.61	05.68
CoK	02.99	00.97
Matrix	Correction	ZAF

File: Produce 5 SEM EDX of Image 2.jpeg

- Surface of the peel
- C, O, and Ti containing particle with dimensions of 200 nm by 400 nm

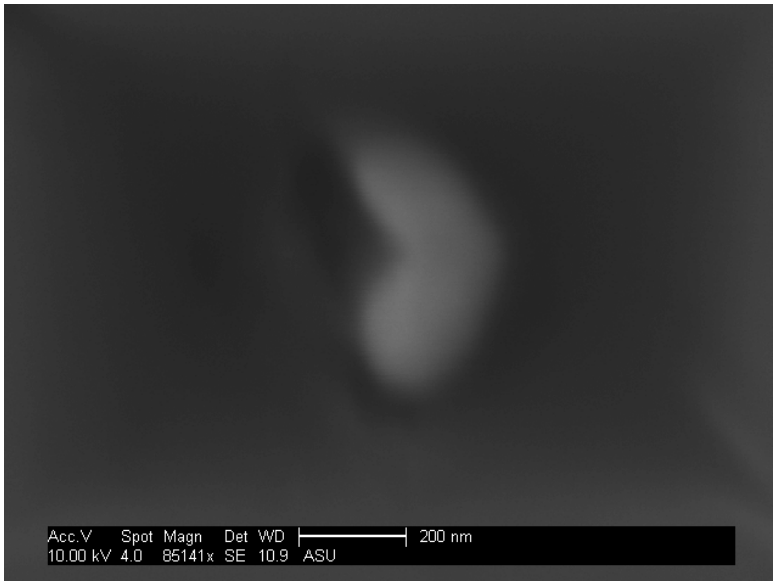

File: Produce 5 SEM Image 3.jpeg

Element	Wt%	At%
CK	54.81	70.92
OK	22.28	21.65
TiK	22.91	07.43
Matrix	Correction	ZAF

File: Produce 5 SEM EDX of Image 3.jpeg

Food Produce Sample 6: Watermelon

- No uniform nanomaterial coating was found on the surface of the baby tomato peel
- Particles with compositions consistent of dirt found on samples
- Surface of watermelon
- Particles containing C, O, Al, and Si with average diameter of 1.0 microns

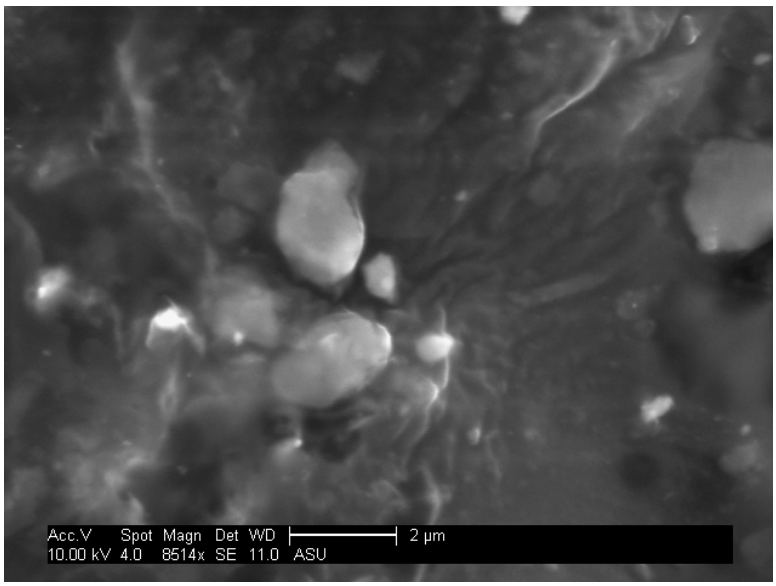

File: Produce 6 SEM Image 1.jpeg

Element	Wt%	At%
CK	65.12	73.07
OK	27.92	23.52
AlK	03.33	01.66
SiK	03.63	01.74
Matrix	Correction	ZAF

File: Produce 6 SEM EDX of Image 1.jpeg

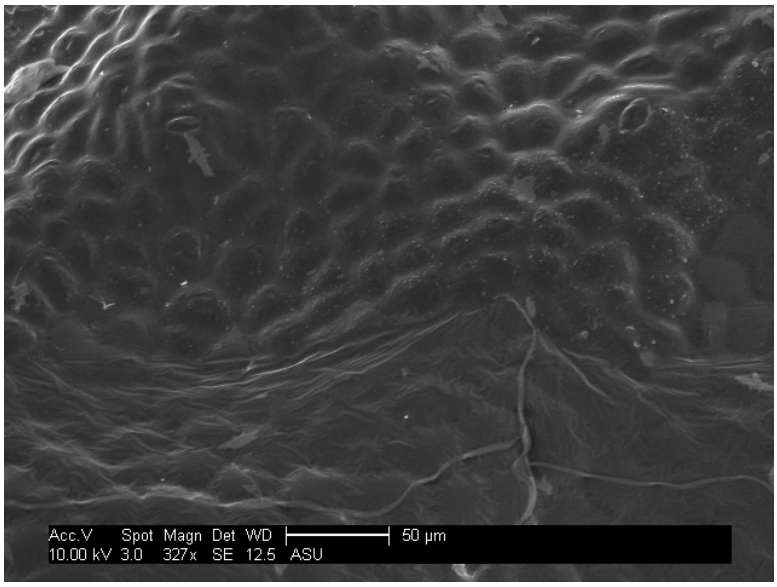

File: Produce 6 SEM Image 2.jpeg

Food Produce Sample 7: Michelman – Standard Wax

- EDX confirmed the presence of Al, Si, O, P, and C in the sample
- No nanoparticles found

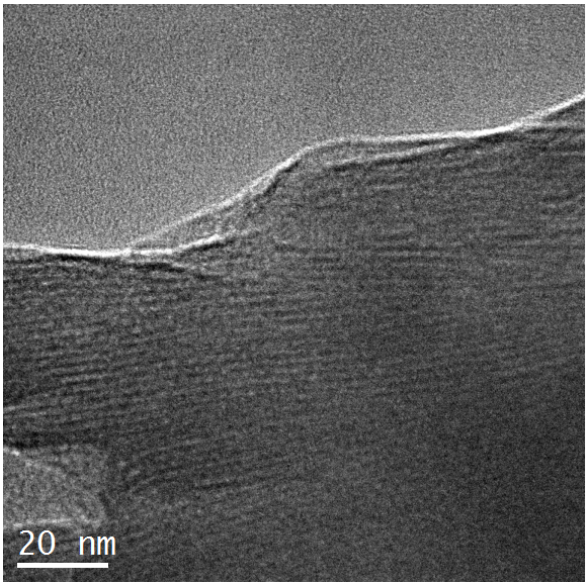

File: Produce 7 SEM Image 1.jpeg

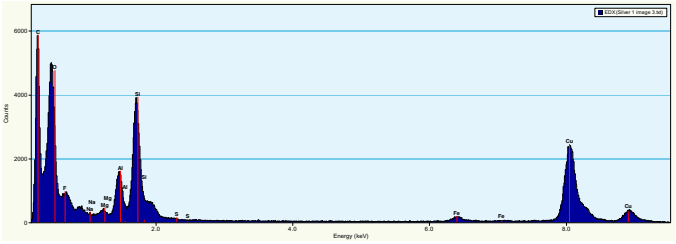

File: Produce 7 SEM EDX of Image 1.jpeg

Conclusion

- Particles consistent with dirt found on samples
- No uniform nanomaterial coating found on any of the six samples analyzed with SEM and EDX